Hierarchy Based Construction of Signature Matrices for Simplified Decoding in Overloaded CDMA

Amiya Singh

Department of Electronics and Communication Engineering
National Institute of Technology Rourkela

Hierarchy Based Construction of Signature Matrices for Simplified Decoding in Overloaded CDMA

Thesis submitted in partial fulfillment

of the requirements of the degree of

Doctor of Philosophy

in

Electronics and Communication Engineering

by

Amiya Singh

(Roll Number: 511EC110)

based on research carried out

under the supervision of

Prof. Poonam Singh

January, 2017

Department of Electronics and Communication Engineering

National Institute of Technology Rourkela

Department of Electronics and Communication Engineering
National Institute of Technology Rourkela

January 07, 2017

Certificate of Examination

Roll Number: *511EC110*

Name: *Amiya Singh*

Title of Dissertation: *Hierarchy Based Construction of Signature Matrices for Simplified Decoding in Overloaded CDMA*

We the below signed, after checking the dissertation mentioned above and the official record book (s) of the student, hereby state our approval of the dissertation submitted in partial fulfillment of the requirements of the degree of Doctor of Philosophy in Department of Electronics and Communication Engineeringat National Institute of Technology Rourkela. We are satisfied with the volume, quality, correctness, and originality of the work.

Poonam Singh Principal Supervisor	Sarat Kumar Patra Member, DSC
Santanu Kumar Behera Member, DSC	Durga Prasad Mohapatra Member, DSC
S M Sameer External Examiner	Sukadev Meher Chairperson, DSC

Kamalakanta Mahapatra
Head of the Department

Department of Electronics and Communication Engineering
National Institute of Technology Rourkela

Prof. Poonam Singh
Associate Professor

January 07, 2017

Supervisor's Certificate

This is to certify that the work presented in the dissertation entitled *Hierarchy Based Construction of Signature Matrices for Simplified Decoding in Overloaded CDMA* submitted by *Amiya Singh*, Roll Number 511EC110, is a record of original research carried out by him under my supervision and guidance in partial fulfillment of the requirements of the degree of *Doctor of Philosophy* in *Department of Electronics and Communication Engineering*. Neither this thesis nor any part of it has been submitted earlier for any degree or diploma to any institute or university in India or abroad.

Poonam Singh

Dedication

Dedicated to each of them,
whom, learnings in this Life have come from,
directly or indirectly.

Signature

Declaration of Originality

I, *Amiya Singh*, Roll Number *511EC110* hereby declare that this dissertation entitled *Hierarchy Based Construction of Signature Matrices for Simplified Decoding in Overloaded CDMA* presents my original work carried out as a doctoral student of NIT Rourkela and, to the best of my knowledge, contains no material previously published or written by another person, nor any material presented by me for the award of any degree or diploma of NIT Rourkela or any other institution. Any contribution made to this research by others, with whom I have worked at NIT Rourkela or elsewhere, is explicitly acknowledged in the dissertation. Works of other authors cited in this dissertation have been duly acknowledged under the sections "Reference" or "Bibliography". I have also submitted my original research records to the scrutiny committee for evaluation of my dissertation.

I am fully aware that in case of any non-compliance detected in future, the Senate of NIT Rourkela may withdraw the degree awarded to me on the basis of the present dissertation.

January 07, 2017
NIT Rourkela

Amiya Singh

Acknowledgment

Living and working in the campus amidst the vibrant serenity of nature, and sensible human beings and resources have offered a lot actually. Right from the day of joining to the time of writing this thesis, every moment has its own unique impact regarding learning. May it be attending the lectures, cordial discussion with professors, friendly interaction with the colleagues, etc., everything has served me in a better sense of self-growth.

Touching upon some personalities whose contribution to me will always be due. First, I want to name Prof. Poonam Singh, my supervisor for her moral support, guidance, encouragement, and friendliness. I am also thankful to Prof. Sarat Kumar Patra and Prof. Santanu Kumar Behera for their soulful direction during the lean period of Prof. Singh. Besides, my gratitude also goes to the other DSC members: Prof Susmita Dash, Prof Durga Prasad Mohapatra for their valuable suggestion towards the thesis. Straight from the heart, I also hold immense respect and appreciation for Prof. Farokh Marvasti and Dr. Arash Amini for offering me the opportunity to work in the Multimedia Laboratory at the Sharif University of Technology, in Iran and facilitating me with a homely environment for the stay.

I am equally proud to share this journey with friends, and well wishers like; the late Venkatesh, Prasanjit, Jyoti, Imtiyaz, Jyotiprasana, Anoop, Sonu, Bijay, Divya, Snigdha, Ravi, Rabi, Rohit, Manas, Mostafa, Mehdi, Hozzat, Nemat, Gyana, Khusboo, Sadananda, Bapun, Bahadur Da. I owe my special acknowledgment to Fateme for her deliberate attempts to nurture the better transformation within me. Lastly, I am highly indebted to my family for their unconditional love and support.

January 9, 2017 — *Amiya Singh*

NIT Rourkela — Roll Number: 511EC110

Abstract

The overloaded CDMA system, as the solution to the capacity limit of its conventional counterpart, has drawn frequent interest of the researchers in the past. While there exists numerous proposals on the construction of uniquely decodable (UD) signature matrices for overloaded CDMA system with very high value of overloading factor, most of them lag the efficient multiuser detector (MUD) for noisy transmission. Here, by efficient, we imply the MUD to have acceptable BER performance and simplified in design. Whereas the lack of efficiency of several MUDs is primarily due to the impact of excess level of multiple access interference (MAI) because of the rise in the number of active users, its random nature prohibits its accurate estimation and elimination. Under such constraints, if the signature matrices can be intelligently constructed so as to generate a defined and controlled pattern (hierarchy) of MAI so that the designed MUD will exploit the knowledge of this hierarchy to remove the MAI completely and attain better error performance at much lower cost of complexity. We consider this as the motivation for research in this thesis.

First, we propose the ternary signature matrix with orthogonal subsets (TSMOS), where the matrix with index-k comprises of k orthogonal subsets with each having different number signatures, and all subsets besides the first (largest) one are of ternary type. The correlation (interference) pattern among the signatures is mapped into a twin tree hierarchy, which is further leveraged to design a simplified MUD using the linear decoding blocks like matched filter (MF) to provide errorfree and better error performance for noiseless and noisy transmission respectively. Next, we generalize the construction of TSMOS to multiple structures i.e.; Type I, Type II, Type III and mixed versions and reveal the complementary feature of 50% signatures of the largest (binary) subset that further results in their optimality. Further, we propose the non-ternary version of SMOS (called as $2k$-SMOS), where the binary alphabets in each of the k subsets are different from each other. With

no complementary feature, 50% signatures of its largest subset are also found to be optimal. The superiority of $2k$-SMOS over TSMOS is also verified for an overloading capacity of 150%. Next, we propose and discuss the hybrid SMOS (HSMOS), where the subsets from TSMOS and $2k$-SMOS are used as the constituents to produce multiple SMOS structures, of which TSMOS and $2k$-SMOS are treated as the special cases. For better understanding of the features of the whole family of SMOS (with an overloading capacity of 200%), the gradual change in the twin tree hierarchy and BER performance of the left and right child of the individual subsets are studied. Similar to SMOS, we also introduce the hierarchy based low density signature (HLDS) matrix, where any UD matrix satisfying particular criterion can be considered as the basis set. For hadamard matrix as the basis set, we design a MUD that uses the MF to implement the decision vector search (DVS) algorithm, which is meant to exploit the advantageous hierarchy of constellation of the transmitted vector to offer errorfree decoding. For noisy channel, the marginal degradation in the level of BER of the MUD (DVS) as compared to the optimum joint maximum likelihood decoder (MLD) is worthy to be overlooked when compared with the significant gain achieved in terms of complexity. For the smallest dimension of the hadamard matrix as the basis, the MUD is further simplified to offer recovery using a comparison driven decision making algorithm, also known as comparison aided decoding (CAD). Despite simplicity, the error performance of the MUD (CAD) is observed to be very close to that of MUD (DVS).

Keywords: CDMA; Overloaded CDMA; Uniquely Decobale Codes; Multiuser Detection; AWGN; Bit Error Rate; Complexity.

Contents

List of Acronyms

Acronym	Description
ADC	analog to digital converter
AWGN	additive white gaussian noise
AMPS	Advanced Mobile phone system
BER	bit error rate
BPSK	binary phase shift keying
CAD	comparison aided decoding
CDMA	code division multiple access
DAMPS	digital AMPS
DVS	decision vector search
ED	euclidean distance
EDP	equivalent delay pair
FDMA	frequency division multiple access
GCO	generalized codes for overloading
GSM	global system for mobile
HLDS	hierarchy based low density signatures
HoS	hierachy of subsets
HSMOS	hybrid signature matrices with orthogonal subsets
IC	interference cancellation
IE	interference estimation
LDPC	low density parity check
LDS	low density signatures
LSM	logical signature matrices
MAI	multiple access interference
MC-CDMA	multi carrier CDMA
MF	matched filter
ML	maximum likelihood
MLD	maximum likelihood decoder
MUD	multi user detector
MMSE	minimum mean square error

continued on the next page

List of Acronyms (*continued*)

Acronym	Description
MPA	message passing algorithm
OFDMA	orthogonal FDMA
PA	peak autocorrelation
PAPR	peak to average power ratio
PIC	parallel interference cancellation
SCDMA	synchronous CDMA
SCMA	sparse code multiple access
SIC	successive interference cancellation
SISO	soft in soft out
SMLD	simplified MLD
SMOS	signature matrices with orthogonal subsets
TDMA	time division multiple access
TPC	total peak cross-correlation
TSC	total square cross-correlation
TSMOS	ternary SMOS
UD	uniquely decodable
UDC	UD codes

List of Notations

Acronym	Description
$\mathbf{C}^k$	Signature matrix of index-k
N_k	Spreading gain or code length of $\mathbf{C}^k$
N_{ef}	Effective spreading gain of a signature in $\mathbf{C}^k$ (where $N_{ef} \leq N_k$)
M_k	Number of signatures in $\mathbf{C}^k$
$\mathbf{C}_i^k$	i^{th} subset in $\mathbf{C}^k$
$\mathbf{C}_{iL}^k$	Left child of subset-i in $\mathbf{C}^k$
$\mathbf{C}_{iR}^k$	Right child of subset-i in $\mathbf{C}^k$
β or β_k or $\beta(k)$	Overloading factor of $\mathbf{C}^k$ i.e.; $\beta = ({}^{M_k}/_{N_k})$
$\mathbf{x}$	Input vector $\in (1, 0, -1)^{M_k}$
$\mathbf{n}$	AWGN vector with zero mean
$\mathbf{r}_k$	Transmitted (noiseless) sum vector for $\mathbf{C}^k$
$\mathbf{r}_{N_a}$	Transmitted (noiseless) sum vector for class or subset-$\mathbf{C}_a^k$
$\mathbf{y}$	Received noisy vector
$\mathbf{y}_{AD}$	Received noisy vector at the output of analog to digital converter
$\mathbf{B}$	Basis Matrix of construction for SMOS
$\mathbf{H}_h$	Hadamard matrix of diemsnsion $(h \times h)$
$\otimes 0$	Tensor or Kronecker product
ρ	Correlation matrix
$\mathbf{z}$	Output of matched filter
$\mathbf{i}$	Estimated interference
P_e^{ij}	Average probability of error for signature-j in class or subset-$\mathbf{C}_i^k$
$S_{mul}^{avg.}$	Average number of multiplications involved in decoding
$S_{add}^{avg.}$	Average number of additions involved in decoding
$S_{cmp}^{avg.}$	Average number of comparisons involved in decoding

List of Figures

List of Tables

Chapter 1
Introduction

The field of multiple access (MA), being an important means of communication for multiple users in wireless systems, has consistently retained its gravity for being in the active zone of research. In many applications e.g.; satellite-based systems and mobile and fixed terrestrial systems, the scope of sharing the limited available communication medium among many active users provide an obvious edge in terms of cost-effective and flexible channel utilization.

1.1 Code Division Multiple Access (CDMA)

In the early 1980's, the first cellular network (i.e.; advanced mobile phone system (AMPS)) using the concept of analog radio transmission was introduced for commercialization. With the advent of this breakthrough approach for mobile voice services, an immense rise was observed in the number of subscribers urging for more air time. Subsequently, the problems in terms of busy network and call droppings became more common. To serve the booming traffic within a radio spectrum of restricted capacity, the concept of time division multiple access (TDMA) was brought forth where multiple users could access the same channel on a time sharing basis. Soon after, the systems like DAMPS (Digital AMPS) and GSM (Global System for Mobile) with three to four times the capacity of AMPS were introduced. Meanwhile, the DAMPS was in its phase of standardization in North America, an improved solution for multiple access made its release i.e.; CDMA technology.

In the 1990s, the first mobile cellular communication standard using CDMA (known as IS-95) was successfully developed by Qualcomm and commercialized in 1995. With a capacity, approximately ten times of AMPS, DAMPS or GSM, the mobile cellular architecture using CDMA has indeed surpassed the expectation concerning its growth over other wireless technologies. Besides the advantage of accommodating more traffic, several other complementary benefits e.g.; stronger security, improved voice quality,

lower average power emission, broader coverage, and smoother evolutionary upgrading of the networks.

Later on, both in theory and practice, the CDMA system using the direct sequence (DS) spreading approach has retained its popularity not only due to its higher bandwidth efficiency over TDMA and frequency division multiple access (FDMA) but also due to other important features e.g.; privacy, low probability of interception, attractive overlay operation with existing radio systems, immunity against multipath interference, etc.. Till date, DS-CDMA technology is considered as a preferable multiple access technology for numerous wireless networks and mobile cellular standards e.g.; cdma2000, W-CDMA, and TD-SCDMA. In third generation (3G) wireless systems, the standards IMT-2000 (cdma2000 and UMTS) support both voice and data services. For fourth-generation (4G) wireless systems, the emphasis is purely on the orthogonal frequency division multiple access (OFDMA). However, the challenge related to the consequences of the unacceptable rise in peak to average power ratio (PAPR) in OFDMA system, and need for enhancement in loading capacity has, very recently, established the foundation of sparse code multiple access (SCMA) [1–3]. The SCMA technology being a non-orthogonal technique of MA leverages the advantages of both OFDMA and CDMA, therefore, is considered as a promising candidate for the fifth generation (5G) wireless architecture [4].

1.2 Overloaded CDMA

The above discussion on CDMA explicitly clarifies about its superiority over the other existing MA schemes like FDMA and TDMA. A radio channel with bandwidth $B_{channel} = NB_{user}$ using FDMA can accommodate a maximum number of N users, each with an available transmission bandwidth of B_{user}. Likewise, the maximum number of allowable users in the same channel for TDMA is also N, provided the each data frame is divided into N time slots. The noteworty point for the systems using TDMA or FDMA is the strict hard limit on their capacity i.e.; the number of users, at no cost, can exceed N. In contrast, this limit is quite soft for systems using CDMA. The system using DS-CDMA assigns each user with a unique code (signature). A signature with N elements (chip) is said to have the processing (spreading) gain of N e.g.; $T_b = NT_c$, where T_b= time duration of each transmitted bit and T_c= time

duration of each chip. Conventionally, the capacity limit for the CDMA system using the codes with spreading gain of N is N. In other words, the maximum achievable loading (overloading) factor β (i.e.; $\beta = {}^{M}/_{N}$) for a CDMA system using the signature matrix $\mathbf{C}_{N\times M}$ $(N \leq M)$ is unity i.e; $\beta \leq 1$. However, according to the practical studies, the limit on the value of β is not hard, which implies that the capacity of the CDMA systems, unlike TDMA and FDMA, can be increased substantially.

1.3 Overview of Literature

1.3.1 Multi User Coding and Detecting Matrices

The motivation for the construction of detecting or uniquely decodable (UD)[1] signature matrices of overloaded dimension actually originated from the coin-weighing problem of Söderberg and Shapiro [5] in the period of early 1960s. The problem statement is defined as follows: provided a positive integer M, what is the minimum value of $f_b(M)$ on N such that the binary detecting matrix of dimension $(N \times M)$ exists? As a combinatorial problem, it became popular among several mathematicians. The binary constructions proposed by Lindström [6], and Cantor and Mills [7] gave explicit recursive constructions of binary detecting matrices with size $(2^k - 1) \times (2^{k-1} - 1)$, which is found to be settled in asymptotic sense i.e.;

$$\lim_{M\to\infty} \frac{f_b(M)\log_2 M}{M} = 2 \tag{1.1}$$

In [6], the construction of bipolar matrices proposed by Lindström has many similarities with that of the binary. In [7], a class of ternary detecting matrices of dimension $2^k \times (2^{k-1}(k+2))$, as an intermediate step to form their binary counterparts, came into picture, where

$$\lim_{M\to\infty} \frac{f_t(M)\log_2 M}{M} \leq 2, \tag{1.2}$$

for f_t being the ternary counterpart of f_b. Unlike the case of binary and bipolar, any explicit lower bound on $f_t(M)$ was hard to find, even though adapting the results of $f_b(M)$ in [6] to this case is not that difficult. However, it is speculated that the problem of formation of ternary matrices was not that popular at that time, which might be due to its less relevance to the context of coin weighing problem.

On an interesting note, the construction of ternary detecting matrices for the

[1] A matrix $\mathbf{C}$ is considered as UD over $\mathbf{x}$, if for $\mathbf{x}_1 \neq \mathbf{x}_2$, the inequality $\mathbf{C}\mathbf{x}_1 \neq \mathbf{C}\mathbf{x}_2$ is true, where $\mathbf{x}_1$ and $\mathbf{x}_2$ denote two different input vectors. In other words, a UD matrix is injective in nature or there exists one-to-one mapping between the input, and output.

issue of multiuser coding is of high importance, even if it has shown its minor role in the coin-weighing problem. Chang and Weldon [8], in the late 1970s, introduced the problem of multiuser coding for the additive channel. In particular, their efforts emphasized on determining the Shannon capacity region and establishing a class of UD signatures, such that

$$\lim_{N\to\infty} \frac{\beta(k)}{S_{sum}(k)} = 1 \text{ (Eq. 4.5, Corollary in [8])}$$

where $\beta(k) = ({}^{M_k}/_{N_k})$ and $S_{sum}(k) = \sum_{f=0}^{M_k} \frac{\binom{M_k}{f}}{2^{M_k}} \log_2 \frac{2^{M_k}}{\binom{M_k}{f}}$ (Theorem 2.1 in [8]) represents the maximum achievable sum capacity. Equivalently, it implies

$$\lim_{M_k\to\infty} \frac{f_t(M_k)\log_2 M_k}{M_k} = 2 \tag{1.3}$$

In the early 1980s, Ferguson [9] introduced a more general class, while attempting to generalize the results of [8]. Later on, Chang [10] improvised their initial construction [8] so as to produce a construction with an arbitrary number of columns (signatures). Subsequently, few more constructions [11, 12] (bipolar and binary respectively) came into literature explicitly mentioning towards the relation between the multi-user coding and coin-weighing problem. More recently, in [13], an in-depth re-examination of the above constructions are discussed by Mow through a unified window of analysis. The role of the ternary UD matrices, fundamentally controlling the construction of the signature sets for multi-user coding over bipolar and binary has also been discussed. Afterward, the synchronous code division multiple access (SCDMA) as the primary application of the detecting matrices was explained by Khachatrian and Martirossian [14], Wu and Chang [15], and Mow [16]. According to them, the system capacity exceeding the conventional limit of SCDMA can be achieved by allocating the columns of the detecting matrices as the signatures for spreading purpose. Even if the above proposals built the foundation of UD matrices for CDMA with asymptotic equality (AE) 1.3 (i.e.; implying a very high value of β), none of them comprised an efficient detection algorithm for noisy transmission. Probably, it is because hardly a long time had passed after the commercialization of CDMA cellular network in 1995 and the capacity of SCDMA with conventional decoders was sufficient enough to address the

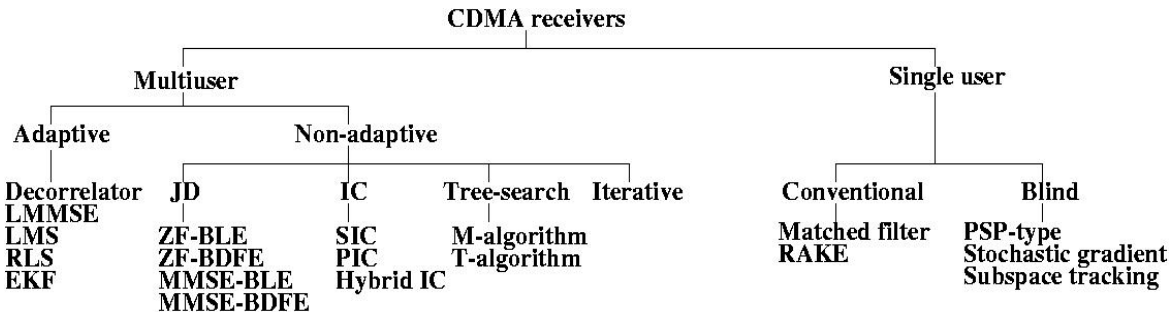

Figure 1.1: Receiver Classification for CDMA

capacity problem efficiently. Gradually, the popularity of CDMA led to the extension of the capacity beyond the expected limit. Since then the demand of the decoder or multi-user detector (MUD) for the signature matrices ($\beta > 1$) jointly offering low complexity and better error performance became an open problem to look into.

1.3.2 Bounds on Total Squared Correlation (TSC)

The noisy transmission being a common scenario in practical communication applications destroys the errorless feature of the UD matrices and the overall error performance of the system is controlled by the cross-correlation property of the code matrices, which is usually defined by the term total squared correlation (TSC). For code matrix $\mathbf{C}$, the TSC can be defined as the sum of the squared magnitudes of all inner products of the elemental codes i.e., $\mathrm{TSC}(\mathbf{C}) \triangleq \sum_{i=1}^{M}\sum_{j=1}^{M}\left|\mathbf{c}_i^H\mathbf{c}_j\right|^2$, where H denotes the conjugate transpose operator. For the real or complex valued matrices, TSC is lower bounded by $\mathrm{TSC}(\mathbf{C}) \geq \left(\frac{MK}{N}\right)$, where $K = \max\{M, N\}$ for M and N representing the number of signatures and spreading gain of the codes respectively. From the study of literature, the optimum sequences for synchronous transmission meet the welch bound equality (WBE), which actually minimizes the variance of the multiple access interference (MAI). While attaining the Welch bound is quite common for the real/complex signature sets [17–25], deviation is observed for the case of finite-alphabet codes. Recently, new operational bounds on TSC have been derived for binary alphabets (1,-1) in conjunction with optimal signature designs [26–28]. In [29–38, 38–40], other binary sets designs have been investigated.

1.3.3 Multi User Detector

Over a decade, the group based approach for the construction of signature matrices for overloaded CDMA has gained the attention, significantly. Be it UD or non-UD,

the usual practice adopted in this method for the formation of the overloaded matrix $\mathbf{C}_{N\times M} = \left[\mathbf{H}_{N\times N}|\mathbf{O}_{N\times(M-N)}\right]$ $(M > N)$ is to add another group (set) of random or quasi-orthogonal signature sequences $\mathbf{O}_{N\times(M-N)}$ to the existing orthogonal matrix (usually Hadamard denoted as $\mathbf{H}_{N\times N}$) and thus achieve suitable gain in the value of β.

Without the prior knowledge of channel information, the effect of MAI can, thence, be eliminated by the use of sophisticated multiuser detectors at the receiver. The optimum joint multiuser detector (also known as joint maximum likelihood decoder (MLD)) [41] yields the best outcome regarding the error performance. But, its computational complexity being exponential to the number of active signatures prohibits it straight from the practical implementation and thus, prompts the researchers to look for the appropriate substitutes. Subsequently, several low-complexity optimal or suboptimal detectors (Figure 1.1) came into literature, where the utmost effort was concentrated on balancing the *performance-complexity trade-off*. Few such instances can be found in [42–45].

When it comes to linear detectors, the decorrelator [46, 47] and minimum mean square error (MMSE) detector [48, 49] performs better with significantly lower complexity in comparison to their optimum equivalent. The MMSE detector executes a linear mapping approach to keep the mean square error between the original input symbol and soft outputs of the decoder at the minimum possible level and thus offers acceptable error performance at much lower complexity than the optimum detector. Likewise, the function of the decorrelator is driven by simple inversion of the channel matrix, but by this action, the impact of noise becomes more pronounced. As an advantage of the decorrelator, no demand for the knowledge of the received power during detection phase is required, thereby avoiding the consequences of the near-far problem. However their performances are not that satisfactory for the case of the overloaded environment as the desired signal subspaces become rank-deficient. Later, group wise multiuser detection involving the decorrelator [50] and MMSE detector [51] strategies came into picture that can also be applied to the overloaded scenario. In an improvised and generalized evaluation of the group based MUD in [52], the decision-feedback detector suggested in [43] and [53] was found to be applicable for grouping strategy.

Among the non-linear decoding approaches, the multi-stage detector [54, 55] came into discussion in the year 2000, where the method of detection is highly complex [56–58] due to the iterative mechanism of the MUD using successive interference cancellation (SIC) [59, 60] and parallel interference cancellation (PIC) [61, 62] stages as the fundamental block of design for interference mitigation. More recently, the method of probabilistic data association (PDA) [63] has been used for the iterative multi user detection. Its error performance shows a rapid degradation for the overloaded scenario. Later on, improvisations has been incorporated in the signature waveforms so as to keep the TSC to the minimum, while achieving improvement in capacity [64] and error performance. The above iterative decoders despite their high complexity fail to eliminate the impact of MAI completely. Therefore, achieving errorfree performance in the absence of noise, becomes impossible. Additionally, the massive complexity of the detectors also makes its implementation doubtful.

Subsequently, the technique of reusing the WBE [65] sequences for different users with different wave forms in [66] leads to the significant maximization in capacity, and simplification of the receiver too. However, its implementation becomes challenging due to the non-scalable [67] nature of the WBE sequences. Among the other reusing techniques, the concept of collaborative coding [68, 69] and superposition coding [70] have contributed towards the substantial expansion of the capacity limit.

In an attempt to construct an optimal set with the hierarchy of subsets (HoS), Learned proposed a tree joint detection algorithm. Even though the detector offers the optimal estimate with reduced complexity as compared to the optimum MLD [41], the relaxation gained regarding complexity is still not fair when compared with that of the linear decoders.

In an approach to propose a two-stage simplified MLD (SMLD) [71, 72], Pad et al., in late 2000, came with the idea of exploiting the Kronecker (or Tensor) product based construction for the UD sets to achieve simplified decoding. First, to generate the matrices of larger dimension from its smaller counterparts (i.e.; $\mathbf{C}_{N\times M}$) simple Kronecker product is used e.g.; $(\mathbf{H}\otimes\mathbf{C})$ is of size $(hN\times hM)$. For decoding, the received (decoding) vector is to be multiplied by $(\mathbf{H}^{-1}\otimes\mathbf{I})$ to split the overall recovery problem into h parallel stages, each of which contributes to the detection of M users. The result shows that the error performance of the system using core matrix of

moderate or larger dimension is found to be better than that of smaller dimension. But, selection of the core matrix with relatively large dimension, on the other hand, also leads to the increase in decoder's complexity due to the rise in the number of secondary users (Hadamard refers to primary users), usually detected through the method of joint MLD. In overall, the decoding using SMLD for the tensor product based constructions has undoubtedly minimized the complexity of the optimum MLD to a large extent. However, the rise in complexity of the decoder as compared to the linear decoders is still not moderate.

From the aspect of implementation for the noisy channel, the additional (excess) users are usually kept to a suitable minimal value to ensure better error performance [71, 73, 74]. It is because, for the noisy transmission, the effect of MAI becomes more prominent even if its impact remains silent for the noiseless case. To overcome this drawback, an attempt has been made in [74], using the genetic algorithms involving multiple distance criteria as the metric for analysis, to optimize the selection of signatures so that the total available MAI in the code space can be notably reduced, and hence, resulting in improvement of the error performance. Besides, a hierarchy criterion is imposed on construction in [32] that minimizes the impact of MAI to a suitable extent and brings improvement in the level of bit error rate (BER). Later, the approach of tensor product based construction followed by decoding using SMLD has been offered a deep insight by Alishahi et al. in [73, 75], where rigorous efforts are invested towards the evaluation of the lower and upper bounds of the construction for different sets of alphabets of the input vector and signature matrix as well. Further improvisations concerning generalization of the similar type of construction can also be found in [76].

1.3.4 Low Density Signatures (LDS) Matrices

For conventional CDMA architecture using binary signature matrices, each chip of the received vector carries the transmitted bit from all the active users. Equivalently, at every received chip, each user sees the contribution from all other users. When it comes to the case of overloaded CDMA, the situation becomes worse as the level of MAI on each user at a particular chip shows an abrupt rise. Under such conditions, optimum MUD can be engaged with lower complexity as compared to the optimum

joint MLD [41], provided the overall correlation matrix follows a specific hierarchy [77]. However, the outcome of the system regarding complexity of the MUD lies much higher over the linear detectors [46–49]. Now, recalling the result from [77–79], we reckon that the necessary condition for each user to transmit the nonzero values to all of its signature chips can also be skipped. Further investigations have emphasized on creating an intelligent pattern or arrangement among the signature elements of the whole matrix, such that, the MAI on each user can be advantageously aligned to render satisfactory improvement in BER performance.

In pursuit of the above idea, over the past few years, the research on LDS [80] matrices have shown its popularity towards the problem of design of the low complex MUD. Recently, a new recurrent LDS construction [81] with $\beta = 2$ has been proposed, where the priority drives straight towards the design of the highly simplified decoder for the noisy channel, at the cost of sacrifice in asymptotic equality unlike the case of the ternary constructions in [8–10, 13]. In [80], the authors exploit the pattern of the low-density parity check (LDPC) matrices to design simplified MUD for overloaded CDMA applications. Note that, the LDPC sets, as an efficient construction for error correcting, has consistently retained its popularity so far. However, in recent literature [80, 82], researchers being attracted by its overloaded dimension has attempted to propose some low complex design of the MUD for CDMA application.

While the LDS based DS-CDMA is considered as a promising candidate bringing up solutions to the problem of efficient MUD designs for overloaded CDMA, its exposure to orthogonal frequency division multiplexing (OFDM) [3, 80, 83–85] technique can be an efficient approach towards the substantial reduction in peak to average power ratio (PAPR), which is yet considered as a crucial problem with the networks based on OFDM system. Systems using OFDM and multi-carrier code division multiple access (MC-CDMA) being referred as highly efficient techniques to provide high data rate services have been embraced as the core technologies for the several mobile communication architectures e.g.; the Worldwide Interoperability for Microwave Access (WiMAX) and 3rd Generation Partnership Project Long Term Evolution (3GPP-LTE). More recently, the SCMA [1, 2, 86–91] being a collaborative embodiment of OFDM and LDS-CDMA is being provisionally considered as an efficient prospective MA technique for the fifth generation (5G) architecture [4].

1.4 Motivation

The possibility of successful implementation of any communication system including CDMA is determined by the two factors: (a) the feasibility of practical realization of the transmitter and receiver design, and (b) the error performance of the receiver over the noisy and fading channel. Besides, the criterion of selection of the transmission mode (synchronous and asynchronous) also supplements to the decision making towards its application (downlink and uplink) in the cellular architecture.

As a matter of fact, the concept of overloading in CDMA being a solution to the capacity limit of its conventional counterpart has drawn the frequent interest of the researchers and continuously evolved through several phases. The extensive research in this field can be broadly classified into problems like: (a) design of the signature matrices and study of their maximum achievable capacity bounds, (b) development of techniques to reuse the existing non-overloaded matrices, (c) design of MUD, (d) proposing spreading strategy for improved error performance, and (e) study of the error performance for different channel and input conditions, both for synchronous and asynchronous transmission etc. Importantly, design of an efficient MUD being a crucial problem in this area depends on the following criteria.

1.4.1 Better Alternative to TSC

From the earlier discussion on TSC, a WBE code set is supposed to have the minimum TSC and the level of correlation for each signature is not taken into count. As a result, it is possible that some signatures, under the effect of very high level of MAI, will go through severe decoding failure. Therefore, for underloaded ($M \leq N$) CDMA, although TSC is a suitable parameter to evaluate the performance, it does not hold valid for the overloaded ($M > N$) CDMA system. It is because, TSC being a complete measure of the correlation lags attention to the individual users. While within a particular code set, the net level of peak cross-correlation among the signatures shows random variation, their decoding also gets affected non-uniformly. Therefore, for more accurate analysis of the error performance, considering the study of the correlation level of signatures individually or group-wise should be of significant priority.

1.4.2 Defined Correlation Hierarchy

Most of the proposed systems in literature deal with a type of MAI pattern, which is completely random in nature. Due to the unpredictability and non-uniformity in its distribution among the signatures, it's accurate estimation (for each signature) for the purpose of elimination, in the absence of noise, becomes almost impossible despite the complex iterative structures of the MUD involving linear detection blocks like MF. Irrespective of the type of detection (linear or non-linear), the quality of recovery is directly associated with the impact of MAI, which for a particular signature is the sum of its *peak level* of cross-correlation on other active signatures. Therefore, having a known or defined pattern of MAI will be of high advantage towards its complete elimination, further resulting in the improvement in BER performance.

1.4.3 Sacrificing the Asymptotic Equality

The initial discussion in the field of overloaded CDMA started from the design of the UD matrices, which are found to project asymptotic equality 1.3 (i.e.; having large capacity). In fact, the literature is crowded with the kind of approaches where the whole attention is diverted to construct matrices satisfying the criterion of AE only. Hardly any reasonable efforts have been made to propose useful MUD for their full-fledged practical implementation. In other words, very obviously, construction of the signature matrices with a very high value of β can hardly be a practical solution, unless it is integrated by a fast, efficient encoder, and decoder. Over a decade, the problem of design an efficient MUD has drawn the significant attention of the researchers and evolved through multiple phases. From their approach of attempting the problem, it is evident that sacrificing the AE for the reduction in MAI is, in fact, a compromise worthy to be considered towards the design of an efficient MUD.

1.4.4 Embodiment of MF in MUD

From the discussion so far, a crucial point that has caught our immediate attention is that hardly any MUD using matched filter (MF) as the fundamental block of decoding exist which offers errorless performance in the absence of noise. In fact, MF decoding (see Figure 1.2) being the most simplified and conventional form of decoding if spaced in the design of the MUD, generate the scope of achieving a rich simplicity

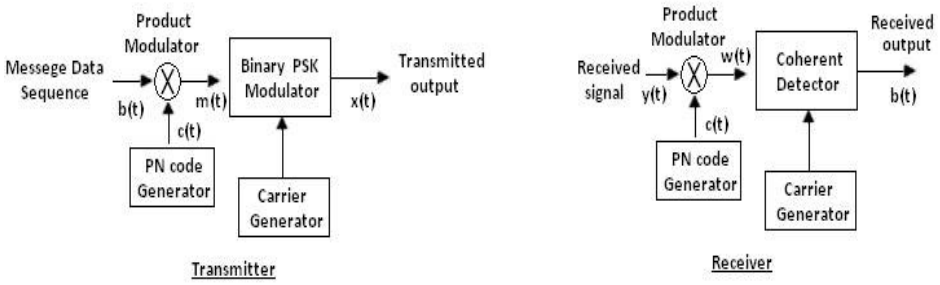

Figure 1.2: CDMA Receiver using Matched Filtering

in overall design. Additionally, implementing the MUD with MF blocks also imbibes further scope in terms of realizing its feasibility for the improvised architectures like rake receiver, meant for the detection over multi-path fading channels. Within such priorities, the crucial criterion that needs to be satisfied for the MF decoding of a particular signature to be errorless is: the level of its peak autocorrelation (PA) must be greater than that of the level of total peak cross-correlation (TPC) on it from other active signatures in the code space. However, fulfillment of this criterion for all the signatures in an overloaded code set, so far, has not been possible. Achieving this critical objective is not impossible if a firm control can be established over the correlation pattern.

1.5 Problem Statement and Research Objectives

By and large, the above important motivations if summarized on a unified frame work can be easily defined in a single problem statement i.e.; the literature still lags the system design for overloaded CDMA, where the construction of the signature matrices with significant value of β can be tactically controlled to produce an advantageous and regularized correlation pattern so as to capacitate the MUD using MF to leverage it to offer errorfree and better error performance for the noiseless and noisy channel respectively. In this thesis, we consider this gap as the motivation for research. The overall contribution can be split into the following meaningful objectives.

- To design new sets of UD signature matrices with the significant value of β, such that they will reflect a specific hierarchy of correlation pattern.

- To identify the available pattern of correlation among the signatures and exploit it to propose an efficient sub-optimal MUDs offering errorfree performance in the absence of noise.

• To present sufficient mathematical proof to validate the UD and errorless nature of the signature matrix and MUD respectively.

• To look for the scope of existence of the optimal users, either fully or partially.

• To classify the study of error performance of the whole signature matrix into multiple subsets (subgroups) based on their difference in the level of total MAI.

• To formulate the suitable expression for evaluation of the theoretical error performance and complexity of the MUD for noisy transmission.

• To analyze the simulation results for cross-verification in correspondence with the study of the MAI followed by the logical explanation.

• To provide appropriate validations of the counter-intuitive deviations observed in the performance behavior of the different subsets.

• To present suitable performance (error performance and complexity) comparison concerning the existing literature.

1.6 Thesis Overview

Besides introduction, the thesis has five chapters, which demonstrates our approaches and their novelty towards proposing the hierarchy based construction of the signature matrices followed by extensive analysis of the MUD design and performance study.

In **Chapter 2**, we introduce the ternary signature matrix with orthogonal subsets (SMOS) where the number of subsets in the matrix with index-k is k, for the number of signatures in one subset to be different than the other. Primarily, we describe how its twin tree structured correlation hierarchy facilitates an advantageous balance between the PA and TPC for the signatures in each subset to offer errorless recovery using MF, in the absence of noise. For noisy transmission, the BER performance of the system is studied through analytical modeling and simulation results. With the use of MF as the basic design block, the overall low complexity of the MUD is guaranteed. Also, the complementary feature of the specific signatures of the largest subset for quasi-synchronous transmission leading to optimality is discussed.

In **Chapter 3**, we feature the non-ternary version of SMOS where the binary alphabets in each of the k constituent subsets are unique. Due to the participation of $2k$ number of alphabets in the formation of the matrix, we call it $2k$-ary SMOS. Despite the similarity in twin tree hierarchy of interference, its non-uniformity brings

noticeable contrast in the overall analysis, and outcome including the existence of optimal signatures. For the maximization in user capacity to be 50%, the BER performance of $2k$-ary outsmarts that of the ternary SMOS (TSMOS), but beyond that, it becomes a conditional entity. To validate the counter-intuitive deviations in the simulation results, suitable logical explanation involving the actual operational metrics are presented.

In **Chapter 4**, we show that further extension of the SMOS architecture, beyond TSMOS and $2k$-SMOS, in the hybrid form (a combination of TSMOS and $2k$-SMOS, called as hybrid SMOS (HSMOS)) is also possible. For construction, either $bottom - to - top$ or $top - to - bottom$ approach can be adopted. Looking at the unified structure of construction involving the non-uniform tree hierarchy, we study the variation observed in the error performance of each subset for noisy channel. The whole discussion elaborates the translation of the SMOS architecture in detail: from TSMOS to $2k$-SMOS through the intermediate structures of HSMOS.

In **Chapter 5**, we propose a novel hierarchy based LDS (HLDS) matrix for overloaded CDMA where multiple advantages i.e.; fast construction, generalization to other existing UD sets, feasibility to arbitrary dimensions, fast decoding, and satisfactory error performance for noisy transmission, all, can be attained. Unlike existing approaches, our construction of the larger matrices from, the smaller counterparts (basis sets) is driven by a simply overlapped hierarchy. For Hadamard matrix as the basis, the construction poses a unique cross-correlation pattern that is further leveraged by the decision vector search (DVS) algorithm to propose a simplified MUD than the optimum MLD. For noisy case, the degradation in BER can be overlooked in contrast to the prominent advantage gained in complexity. Our efforts, to further simplify the MUD, results in the comparison aided decoding, where the input symbols can be directly predicted from the constellation values through simple comparisons.

Finally, in **Chapter 6**, we summarize the conclusions, limitations of the proposed system models and present the scope for further research.

Chapter 2
Generalized TSMOS

2.1 Introduction

In this chapter, we explore the design of a new set of UD Codes (UDC) for overloaded CDMA that addresses three crucial problems. The first one concerns, if the existence of *multiple orthogonal subsets* within a single UD set is feasible, and if so, what general criterion is to be followed by its recursive construction. The second one is about the design of the *simplified* MUD. The third one is about the scope to achieve optimality for the resultant UDC set, either wholly or partially.

In response to the first problem, we identify the unique fundamental matrix ($\mathbf{C}^1$ i.e., for $k = 1$) of construction from the existing literature [8–10, 81], develop a new perspective for the recurrent design of the proposed matrices, and mathematically validate its UD nature. The proposed construction being recursive results in a UD matrix of dimension (M_k, N_k) for $M_k > N_k$, which can further be split into $k = \log_2 N_k$ number of orthogonal subsets (one binary (Hadamard) and $(k-1)$ ternary) of varied dimension.

In response to the second problem, a uniform *twin-tree structured* hierarchy of cross-correlation is realized for the whole matrix due to the *linear dependency* existing in the formation of the larger subsets from, the smaller counterparts. Later, this opportunity is leveraged by the proposed MUD, where the simple logic of MF serves as the primary block of design and recovers each subset with no error in the absence of noise, given that the detector has a *priori knowledge of the user's status (active or inactive)*. Also, we prove the errorfree nature of the decoder for noiseless transmission. The logic of MF serving as the core design block of the decoder provides an enormous saving over the complexity of optimum joint MLD [41]. Following the twin tree hierarchy of correlation, each subset is exposed to a different level of MAI. Subsequently, expecting the variation in their error performance is evident. For the

noisy channel, we derive the theoretical expression of the average BER for each subset.

In response to the third problem, we discover the complementary feature of the specific signatures of the largest (i.e.; binary) subset, which, with no significant modification added at the MUD end, leads to their optimality in error performance. For error performance analysis, we emphasize on the role of the two factors (cardinality of the subset, and net level of MAI) for being responsible for the non-uniformity in the order of their error performance.

Based on the discussion from literature in Section 1.4.1, we have already invalidated the appropriateness of choosing the TSC as the metric to evaluate the impact of MAI in the available code space. Therefore, throughout this thesis, it is logical to consider the TPC and PA as the important metrics to assess the impact of MAI on each individual user, where $\text{TPC}(\mathbf{c}_a) \triangleq \sum_{i\neq a, i=1}^{M-1} \sum_{n=1}^{N} c_{an}c_{in}$ and $\text{PA}(\mathbf{c}_a) \triangleq \sum_{n=1}^{N} c_{an}c_{an}$, for $\mathbf{C}_{N\times M} = [\mathbf{c}_1\mathbf{c}_2\cdots\mathbf{c}_M]$ and $\mathbf{c}_a = [c_{a1}c_{a2}\cdots c_{aN}]$. In the existing literature, deploying these metrics for analysis is highly critical due to the randomness prevailing in the level of TPC, even if the level of PA remains the same for all the signatures (i.e.; assuming the matrix to be binary). In contrast, due to the predictable hierarchical pattern of our proposed construction, dealing with these metrics for scrutinizing becomes simpler. Moreover, these two metrics playing the actual role for the recovery in the MF approach of decoding will offer a more accurate statistics to explain the error performance of the system.

Rest of this chapter is arranged as follows. Section 2.2 describes the system model with particular attention towards the role and features of the basis (fundamental) matrix of the construction. Section 2.3 emphasizes on the recursive construction of the proposed matrices followed by its generalization. The hierarchy of MAI including the complementary feature is presented in Section 2.4 followed by design of the MUD in Section 2.5. In Section 2.6, the analytical error performance of the system is discussed focusing more towards the explanation of the error performance of the individual subset. Section 2.7 presents the overview of simulation results. Finally, the conclusion is presented in Section 2.8.

Table 2.1: Recursive Consruction of the UDC Sets (Binary or Ternary) with $\mathbf{C}^1 = \mathbf{B}$ in (2.2) , where $B(2^k) = 2^{k-1}k$ ((3), [13]), Y, N, NL, NY, Ter., and Bin. denote "Yes", "No", "Noiseless", and "Noisy", "Ternary", and "Binary" respectively.

Yr./Publication	Type	N_k	M_k	$\beta(k) \sim S_{sum}(k)$	Decoding
1979 / [7]	Ter.	2^k	$2^{k-1}(k+1)$	Y	NL
1982 /[9]	Ter.	2^k	$2^{k-1}(k+2)$	Y	NL
1984/ [10]	Ter.	k	$\leq B(k)+k$	Y	NL
1995/ [14]	Ter.	2^k	$k2^{k-1}+1$	Y	NL
1997/ [15]	Bin.	k	$\geq k\left(\frac{\log_2 k-2}{2\log_2 3}\right)+\frac{1}{\log_2 3}$	Y	NL
1998/ [92]	Bin.	2^k	$2^{k-1}(k+1)+i$	Y	NL
2012 /[81]	Ter.	2^k	$2^{k+1}-1$	N	NY

2.2 System Model

The synchronous CDMA system (synchronization corresponding to both bit and chip) using the ternary UDC matrix with index-k (i.e.; $\mathbf{C}^k$ or $\mathbf{C}_{N_k \times M_k}$) for $k \in \mathbf{Z}^+$ can be modeled as

$$\mathbf{y} = \mathbf{r} + \mathbf{n} \tag{2.1}$$

where $\mathbf{r} = \mathbf{C}^k\mathbf{R}\mathbf{x}$ is the noiseless received vector with $\mathbf{R} = \mathbf{I}_{M_k \times M_k}$ = Identity Matrix with diagonal elements representing the amplitudes assuming the system to be perfectly power controlled. Here, $\mathbf{x} \in \{\pm 1, 0\}^{M_k}$ is the input column vector, and $\mathbf{n}$ denotes the vector corresponding to the AWGN channel with zero mean and variance σ^2. In an effort to provide an unified approach of analysis, let us concentrate on the recursive constructions (mentioned in Table 2.1), for which $\mathbf{C}^1 = \mathbf{B} = \frac{1}{\sqrt{2}}\left[\begin{array}{c|c} \mathbf{H}_2 & \begin{array}{c} + \\ 0 \end{array} \end{array}\right]$ = basis matrix. Our intention is to study the varied interpretations of $\mathbf{B}$ existing in different approaches towards the formation of the matrices with larger dimension. Therefore, we focus on the basis matrix $\mathbf{B}$ and derive the perspective of our method of construction.

2.2.1 Root of Construction: the Basis Matrix

Before proceeding further, it is important to note that, the fundamental (basis) matrix of our construction ($\mathbf{B}$ in (2.2)) also delivers the same requisites for the construction methods presented in Table 2.1. More appropriately, for the recursive design of the matrices in [8–10, 14, 81], $\mathbf{C}^1 = \mathbf{B}$ and the researchers, based on the structure of $\mathbf{B}$, have established different interpretations to form the matrices of larger dimensions.

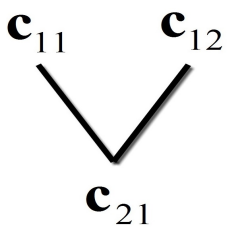

Figure 2.1: Uniform Twin Tree Hierarchy for $\mathbf{B} = [\mathbf{c}_{11}\mathbf{c}_{12}|\mathbf{c}_{21}]$

In this work, we propose a new approach towards the interpretation of $\mathbf{B}$, not only in the method of construction but also to simplify the process of decoding. For our proposed construction, the inequality $\mathbf{C}^1 \neq \mathbf{B}$ is easy to track. However, the so-called fundamental matrix $\mathbf{B}$ appears in the intermediate stage during the recursive formation of $\mathbf{C}^2$ from $\mathbf{C}^1$, and hence serves the purpose of providing an underlaying structure to the design, where

$$\mathbf{B} = \frac{1}{\sqrt{2}} \left[\begin{array}{c|c} \mathbf{H}_2 & \begin{array}{c} + \\ 0 \end{array} \end{array} \right] = \frac{1}{\sqrt{2}} \begin{bmatrix} + & + & + \\ + & - & 0 \end{bmatrix} = [\mathbf{c}_{11}\mathbf{c}_{12}|\mathbf{c}_{21}]\,. \tag{2.2}$$

and "|" in $\mathbf{B}$ indicates its partitioning into two subsets i.e.; $\mathbf{H}_2 = [\mathbf{c}_{11}\mathbf{c}_{12}]$ and $\mathbf{c}_{21}$.

2.2.2 Correlation Pattern of the Basis Matrix

First, we analyze the pattern of the cross-correlation matrix ($\boldsymbol{\rho}$), associated i.e.;

$$\boldsymbol{\rho} = \mathbf{B}^T\mathbf{B} = \begin{bmatrix} 1 & 0 & 1/2 \\ 0 & 1 & 1/2 \\ 1/2 & 1/2 & 1/2 \end{bmatrix} \tag{2.3}$$

In (2.3), the first, second, and third row of $\boldsymbol{\rho}$ denote the cross-correlation coefficient corresponding to the signature in first, second and third column of $\mathbf{B}$ respectively. On further evaluation, it is easy to decipher $\mathrm{Det}(\boldsymbol{\rho}) = 0$, where Det( ) denotes the determinant of the matrix. Equivalently, the first two columns of $\mathbf{B}$ are correlated to the third one, since the last row of $\boldsymbol{\rho}$ can be interpreted as the linear combination of the scalar-multiplied version of the first two rows. Hence, it is logical to present their correlation in the form of a tree structure, as shown in Figure 2.1.

2.2.3 Decoding the Basis Matrix

The decoding of $\mathbf{B}$ from the noisefree received vector $\mathbf{r}$ in (2.1), if subjected to the logic of MF is not fully errorless, which is due to the presence of interference from an additional user beyond $\mathbf{H}_2$. So, let us split $\mathbf{B}$ into two subsets (i.e.; $\mathbf{H}_2 = [\mathbf{c}_{11}\mathbf{c}_{12}]$

and $\mathbf{c}_{21}$) as described in correspondence to (2.2). Accordingly, the input vector $\mathbf{x}$ can be defined as $\mathbf{x} = [\mathbf{x}_1\mathbf{x}_2]$, where $\mathbf{x}_1 = [x_{11}x_{12}]$ and $\mathbf{x}_2 = [x_{21}]$. According to the logic of MF, the decoding of $\hat{\mathbf{x}}_1$ can be achieved with no error (i.e.; $\hat{\mathbf{x}}_1 = \mathbf{x}_1$), where as that of $\hat{\mathbf{x}}_2$ gets erroneous (i.e.; $\hat{\mathbf{x}}_2 \neq \mathbf{x}_2$). This can be verified from the expression of $\mathbf{z} = [z_{11}z_{12}z_{21}]$ for $\mathbf{x} = [x_{11}x_{12}x_{21}]$, where $\hat{\mathbf{x}} = \text{sign}(\mathbf{z}) = \text{sign}(\boldsymbol{\rho}\mathbf{x})$, such that:

$$z_{11} = 2x_{11} + x_{21},\ z_{12} = 2x_{12} + x_{21},\ z_{21} = x_{11} + x_{12} + x_{21}.$$

From the above expression,

$$\hat{x}_{11} = \text{sign}(z_{11}) = x_{11}, \quad \hat{x}_{12} = \text{sign}(z_{12}) = x_{12}$$

holds true irrespective of the value of x_{21} (interfering user of second subset). Conversely, for all the 2^3 combinations of $\mathbf{x}$, the similar outcome is not visible for the decoding of $\hat{x}_{21}$ i.e., $\hat{x}_{21} \neq x_{21}$.

So, as a possible approach towards the errorless recovery of $\mathbf{B}$, the whole process of decoding can be split into two stages. First, the orthogonal matrix $\mathbf{H}_2$ is decoded. Second, we estimate its interference on the additional user and remove it completely so that decoding of $\hat{x}_{21}$ can be achieved with no error. In Section 2.5, we exploit the similar logic to devise a MUD for the errorless recovery of multiple subsets within the proposed matrices of larger dimension.

2.2.4 Complementary Feature of the Basis Matrix

In the above sections, the pattern of the correlation matrix ($\boldsymbol{\rho}$) of the basis matrix, and the respective layout of decoder leading to errorless recovery has been clearly illustrated. Now again, let us consider $\mathbf{B} = \left[\begin{array}{c|c} \mathbf{H}_2 & \mathbf{p} \end{array}\right] = [\mathbf{c}_{11}\mathbf{c}_{12}|\mathbf{c}_{21}]$ to explain the *complementary* feature of different types of SMOS, shown in Table 2.2. Addition of suitable timing delay (t_d) in transmission of $\mathbf{p}$ with respect to that of $\mathbf{H}_2$ reduces the net level of peak cross-correlation on a specific signature i.e.; $\mathbf{c}_{12} = [1\ -1]$, whereas no such deviation is observed for the signature $\mathbf{c}_{11} = [1\ 1]$. For the purpose of comparison, the value of $\boldsymbol{\rho}$ for both the cases ($t_d = 0$, and $t_d = {}^{T_c}/_4$) are presented below.

$$\boldsymbol{\rho}_{t_d=0} = \left(\mathbf{B}^T\mathbf{B}\right)_{t_d=0} = \begin{bmatrix} 1 & 0 & {}^1/_2 \\ 0 & 1 & {}^1/_2 \\ {}^1/_2 & {}^1/_2 & {}^1/_2 \end{bmatrix},\ \boldsymbol{\rho}_{t_d={}^{T_c}/_4} = \left(\mathbf{B}^T\mathbf{B}\right)_{t_d={}^{T_c}/_4} = \begin{bmatrix} 1 & 0 & {}^1/_2 \\ 0 & 1 & {}^1/_4 \\ {}^1/_2 & {}^1/_4 & {}^1/_2 \end{bmatrix} \tag{2.4}$$

Table 2.2: Construction of TSMOS matrices for $k = 1, 2, 3$ i.e.; $\mathbf{C}^1 = [\mathbf{C}_1^1]$, $\mathbf{C}^2 = [\mathbf{C}_1^2|\mathbf{C}_2^2]$, $\mathbf{C}^3 = [\mathbf{C}_1^3|\mathbf{C}_2^3|\mathbf{C}_3^3]$

$\mathrm{C}_1^1 = \frac{1}{\sqrt{2}}[\mathrm{H}_2]$

$\mathrm{C}_1^1 = \frac{1}{\sqrt{4}}[\mathrm{H}_4]$, $\mathrm{C}_2^1 = \begin{bmatrix} + & + \\ 0 & 0 \\ + & - \\ 0 & 0 \end{bmatrix}$

$\mathrm{C}_1^1 = \frac{1}{\sqrt{8}}[\mathrm{H}_8]$, $\mathrm{C}_2^1 = \frac{1}{\sqrt{8}} \begin{bmatrix} + & + & + & + \\ 0 & 0 & 0 & 0 \\ + & - & + & - \\ 0 & 0 & 0 & 0 \\ + & + & - & - \\ 0 & 0 & 0 & 0 \\ + & - & - & + \\ 0 & 0 & 0 & 0 \end{bmatrix}$, $\mathrm{C}_3^1 = \frac{1}{\sqrt{8}} \begin{bmatrix} + & + \\ 0 & 0 \\ 0 & 0 \\ 0 & 0 \\ + & - \\ 0 & 0 \\ 0 & 0 \\ 0 & 0 \end{bmatrix}$

According to (2.4), it is easily understandable that the peak level of cross-correlation on $\mathbf{C}_{12}$ reduces by 50% for $t_d = {}^{T_c}/_2$, which definitely approves for its improved error performance in noisy channel. We call this progressive reduction of the MAI as the *complementary* feature. In Section 2.4, we discuss the implication of this property, in details.

2.3 Construction of TSMOS

2.3.1 Recursive Construction

We introduce the following recursive mechanism for the construction of TSMOS $\mathbf{C}_{N_k \times M_k}$ for $N_k = 2^k$, where $k \in \mathbf{Z}^+$.

- Initialize $\mathbf{C}^0 = [1]$ and find $\mathbf{C}^1 = \left(\frac{1}{\sqrt{2}}\mathbf{H}_{2\times 2} \otimes \mathbf{C}^0\right) = \frac{1}{\sqrt{2}}\mathbf{H}_2$
- For $k > 1$, $\mathbf{C}^k = \left(\frac{1}{\sqrt{2}}\mathbf{H}_{2\times 2} \otimes \mathbf{A}\right)$, where $\mathbf{A} = \left[\mathbf{C}^{k-1}|[1\ 0\ 0\ \cdots\ 0]^T{}_{1\times 2^{k-1}}\right]$.

According to the above approach, for $k = 2$, we have $\mathbf{A} = \mathbf{B}$. In [8], for the recursive design of the matrices with higher dimension, the authors interpret the element '1' in the vector $\{1\ 0\}$ in $\mathbf{B}$ as the simple (1×1) *Identity Matrix* and continue the same for the next iterations too. On the contrary, for the proposed construction, we consider the sequence $\mathbf{c}_{21} = [1\ 0]$ as a one dimensional vector *with one element as 1 and the rest as* 0. From Table 2.2, the proposed matrices with index-k has k orthogonal subsets i.e.; $\mathbf{C}^k = \left[\mathbf{C}_1^k|\mathbf{C}_2^k|\cdots|\mathbf{C}_k^k\right]$, where the value of k is in the logarithmic with

the spreading gain i.e.; $k = \log_2 N_k$ and the subset $\mathbf{C}_i^k$ for $i = 1, 2, \ldots, k$ owns 2^{k-i+1} number of signatures with the *effective spreading gain* (N_{ef}) of $N_{ef_i} = \frac{N_k}{2^{i-1}}$. In the present context, the effective spreading gain of a signature can be defined as its total number of non-zero elements (1,-1). Below, we present Theorem 1 to prove the UD nature of TSMOS.

Theorem 1: The k^{th} indexed version of the TSMOS $\mathbf{C}^k$ with M_k signatures and spreading gain of N_k being classified into k orthogonal subsets is uniquely decodable.

Proof : To prove $\mathbf{C}^k$, in general, to be UD over $\mathbf{x}_k \in \{1, 0, -1\}^{M_k}$, let us start with $\mathbf{C}^1$. Following Table 2.2, $\mathbf{C}^1 = \mathbf{H}_2$ is orthogonal, which by default also assures for its UD nature. For $\mathbf{C}^1$ being UD, $\mathbf{B} = \left[\mathbf{C}^1 | [1\ 0]^T\right]$ can be shown to be of UD type (Theorem 1 in [92]). Now, let us extend this logic to a generalized sense.

If $\mathbf{C}^{k-1}$ is UD over $\mathbf{x}_{k-1} \in \{1, 0, -1\}^{M_{k-1}}$ i.e.; $\mathbf{C}^{k-1}\mathbf{x}_{k-1(1)} \neq \mathbf{C}^{k-1}\mathbf{x}_{k-1(2)}$, then for $\mathbf{A} = \left[\mathbf{C}^{k-1} | [1\ 0\ 0\ \cdots\ 0]^T{}_{1\times 2^{k-1}}\right]$, the relation $\mathbf{A}\left(\mathbf{x}_{k-1(1)}\ x_1\right) \neq \mathbf{A}\left(\mathbf{x}_{k-1(2)}\ x_2\right)$ always holds true when $x_1 \neq x_2$, for $\mathbf{x}_{k-1(2)}, \mathbf{x}_{k-1(2)} \in \{1, 0, -1\}^{M_{k-1}}$ and $x_1, x_2 \in \{1, 0, -1\}$. Following the steps of recursive construction of TSMOS, as the remaining part, now, all we need to prove is the UD nature of $\mathbf{C}^k = \left(\frac{1}{\sqrt{2}}\mathbf{H}_{2\times 2} \otimes \mathbf{A}\right)$ that is explained below.

For $\mathbf{C}^k = \left(\frac{1}{\sqrt{2}}\mathbf{H}_2 \otimes \mathbf{A}\right) = \begin{bmatrix} \mathbf{A} & \mathbf{A} \\ \mathbf{A} & -\mathbf{A} \end{bmatrix}$ to be injective over $\{1, 0, -1\}^{M_k}$, all sums of the term $\mathbf{C}^k\mathbf{x}_k$ need to be distinct. In other words, $\mathbf{C}^k\mathbf{x}_{k(1)} = \mathbf{C}^k\mathbf{x}_{k(2)}$ must be true, if and only if $\mathbf{x}_{k(1)} = \mathbf{x}_{k(2)}$. To prove this, let us split the input vectors: $\mathbf{x}_{k(1)} = \left[\mathbf{x}_{k(11)}\mathbf{x}_{k(12)}\right]^T$ and $\mathbf{x}_{k(2)} = \left[\mathbf{x}_{k(21)}\mathbf{x}_{k(22)}\right]^T$, so that

$$\mathbf{A}(\mathbf{x}_{k(11)} + \mathbf{x}_{k(12)}) = \mathbf{A}(\mathbf{x}_{k(21)} + \mathbf{x}_{k(22)}) \text{ and } \mathbf{A}(\mathbf{x}_{k(11)} - \mathbf{x}_{k(12)}) = \mathbf{A}(\mathbf{x}_{k(21)} - \mathbf{x}_{k(22)})$$

Further, addition and subtraction of the above two equations results in $\mathbf{A}\mathbf{x}_{k(11)} = \mathbf{A}\mathbf{x}_{k(21)}$ and $\mathbf{A}\mathbf{x}_{k(12)} = \mathbf{A}\mathbf{x}_{k(22)}$ respectively. This in turn implies $\mathbf{x}_{k(1)} = \mathbf{x}_{k(2)}$ and hence, proves $\mathbf{C}^k$ to be uniquely decodable. ■

Under the above developments in analysis, now, let us define the TSMOS.

Definition 1: The matrix $\mathbf{C}_{N_k \times M_k}$ is said to be TSMOS over the input $\{0, 1, -1\}$, if the following conditions are satisfied.

- $\mathbf{C}^k$ is uniquely decodable over $\{0, 1, -1\}^{M_k}$.
- $\mathbf{C}^k$ comprises of k orthogonal subsets, such that $\mathbf{C}^k = \left[\mathbf{C}_1^k | \mathbf{C}_2^k | \cdots | \mathbf{C}_k^k\right]$, where the number of signatures in $\mathbf{C}_i^k$ are $\frac{N_k}{2^{i-1}}$

• $\text{Det}(\boldsymbol{\rho}) = 0$, for $\boldsymbol{\rho} = (\mathbf{C}^k)^T\mathbf{C}^k$

• The level of PA of an arbitrary signature in subset-$\mathbf{C}_i^k$ must be greater than the level of TPC, due to the $(k-i)$ successive subsets: $\mathbf{C}_{i+1}^k, \mathbf{C}_{i+2}^k, \ldots, \mathbf{C}_k^k$. Mathematically, it can be described by the expression:

$$\rho_{ii}(u,u) > \sum_{j=i+1}^{k} \sum_{v=1}^{\frac{N_k}{2^{j-1}}} \rho_{ij}(u,v). \tag{2.5}$$

where

$$\boldsymbol{\rho}_{ii} = \left(\mathbf{C}_i^k\right)^T \mathbf{C}_i^k = \begin{bmatrix} \rho_{ii}(1,1) & \rho_{ii}(1,2) & \cdots & \rho_{ii}(1,2^{k-i+1}) \\ \rho_{ii}(2,1) & \rho_{ii}(2,2) & \cdots & \rho_{ii}(2,2^{k-i+1}) \\ \vdots & \vdots & \vdots & \vdots \\ \rho_{ii}(2^{k-i+1},1) & \rho_{ii}(2^{k-i+1},2) & \cdots & \rho_{ii}(2^{k-i+1},2^{k-i+1}) \end{bmatrix}$$

and

$$\boldsymbol{\rho}_{ij} = \left(\mathbf{C}_i^k\right)^T \mathbf{C}_j^k = \begin{bmatrix} \rho_{ij}(1,1) & \rho_{ij}(1,2) & \cdots & \rho_{ij}(1,2^{k-j+1}) \\ \rho_{ij}(2,1) & \rho_{ij}(2,2) & \cdots & \rho_{ij}(2,2^{k-j+1}) \\ \vdots & \vdots & \vdots & \vdots \\ \rho_{ij}(2^{k-i+1},1) & \rho_{ij}(2^{k-i+1},2) & \cdots & \rho_{ij}(2^{k-i+1},2^{k-j+1}) \end{bmatrix}$$

2.3.2 Construction Generalization

The method of construction of TSMOS, as discussed in the previous section follows a recursive approach. Our further observation reveals that other similar ternary structures can also be realized, while still satisfying the conditions in Definition 1. We classify them into different types e.g.; Type I, II, and III, Mixed (Type I), Mixed (Type II), Mixed (Type III). In order to generalize their methods of formation, we define the transformation function $f(\ )$, which is unique to each type and summarized in Table 2.3.

Theorem 2: For $\mathbf{C}^{k-1} \in \{0,1,-1\}^{M_{k-1}}$ being the TSMOS, the newly formed matrix $\mathbf{C}^k = f(\mathbf{A})$ is also TSMOS, where $f(\ )$ represents the transformation function (see Table 2.3) and $\mathbf{A} = \left[\mathbf{C}^{k-1}|\mathbf{p}\right]$ or $\left[\mathbf{C}^{k-1}|\mathbf{q}\right]$ for $\mathbf{p} = [1\ 0\ 0\ \cdots\ 0]_{1\times 2^{k-1}}$, $\mathbf{q} = [0\ \cdots\ 0\ 0\ 1]_{1\times 2^{k-1}}$.

Proof: From Section 2.2, the basis matrix being considered as the root of the whole ternary construction is $\mathbf{B}$ (2.2), and the proof to its UD nature can be found in

(Theorem 1 in [92]). Equating $\mathbf{B}$ to $\mathbf{A}$, we have $\mathbf{C}^1 = \mathbf{H}_2$, and $\mathbf{p} = [1 \;\; 0]$. Likewise, $[\mathbf{H}_2|\mathbf{q}]$ can also be logically considered as another set of basis matrix, where $\mathbf{q} = [0 \;\; 1]$.

To provide an unified approach of analysis, assume $f(\,)$ to be the desired transformation function, such that: $\mathbf{C}^k = f(\mathbf{A})$ is UD for $\mathbf{A}$ being UD, then it is trivial to show that

$$f(\mathbf{A}) = \left[f\left(\mathbf{C}^{k-1}\right)|f(\mathbf{p})\right] \quad or \quad \left[f\left(\mathbf{C}^{k-1}\right)|f(\mathbf{q})\right], \tag{2.6}$$

for $\mathbf{A} = \left[\mathbf{C}^{k-1}|\mathbf{p}\right]$ and $\left[\mathbf{C}^{k-1}|\mathbf{q}\right]$ respectively. Let us define $f(\mathrm{A}) = \begin{bmatrix} g_{11}(\mathbf{A}) & g_{12}(\mathbf{A}) \\ g_{21}(\mathbf{A}) & g_{22}(\mathbf{A}) \end{bmatrix}$. In order to show $f(\mathbf{A})$ to be injective over the input vector $\{1, 0, -1\}^{M_k}$, all sums of the term $f(\mathbf{A})\mathbf{x}_k$ need to be distinct i.e.; $f(\mathbf{A})\mathbf{x}_{k(1)} = f(\mathbf{A})\mathbf{x}_{k(2)}$ is true for $\mathbf{x}_{k(1)} = \mathbf{x}_{k(2)}$. In other words, if $\mathbf{x}_{k(1)} = \left[\mathbf{x}_{k(11)}\mathbf{x}_{k(12)}\right]^T$ and $\mathbf{x}_{k(2)} = \left[\mathbf{x}_{k(21)}\mathbf{x}_{k(22)}\right]^T$, then

$$g_{11}(\mathbf{A})\mathbf{x}_{k(11)} + g_{12}(\mathbf{A})\mathbf{x}_{k(12)} = g_{11}(\mathbf{A})\mathbf{x}_{k(21)} + g_{12}(\mathbf{A})\mathbf{x}_{k(22)} \tag{2.7}$$

$$g_{21}(\mathbf{A})\mathbf{x}_{k(11)} + g_{22}(\mathbf{A})\mathbf{x}_{k(12)} = g_{21}(\mathbf{A})\mathbf{x}_{k(21)} + g_{22}(\mathbf{A})\mathbf{x}_{k(22)} \tag{2.8}$$

Further addition and subtraction of (2.7) and (2.8) result in the following expressions

$$\begin{aligned}(g_{11}(\mathbf{A}) + g_{21}(\mathbf{A}))\,\mathbf{x}_{k(11)} + (g_{12}(\mathbf{A}) + g_{22}(\mathbf{A}))\,\mathbf{x}_{k(12)} = \\ (g_{11}(\mathbf{A}) + g_{21}(\mathbf{A}))\,\mathbf{x}_{k(21)} + (g_{12}(\mathbf{A}) + g_{22}(\mathbf{A}))\,\mathbf{x}_{k(22)}\end{aligned} \tag{2.9}$$

$$\begin{aligned}(g_{11}(\mathbf{A}) - g_{21}(\mathbf{A}))\,\mathbf{x}_{k(11)} + (g_{12}(\mathbf{A}) - g_{22}(\mathbf{A}))\,\mathbf{x}_{k(12)} = \\ (g_{11}(\mathbf{A}) - g_{21}(\mathbf{A}))\,\mathbf{x}_{k(21)} - (g_{12}(\mathbf{A}) + g_{22}(\mathbf{A}))\,\mathbf{x}_{k(22)}\end{aligned} \tag{2.10}$$

To make the equality in (2.9) and (2.10) hold true irrespective of the values of $\mathbf{x}_{k(1)}$, and $\mathbf{x}_{k(2)}$, the condition which needs to be satisfied is

$$g_{11}(\mathbf{A}) + g_{21}(\mathbf{A}) \neq g_{12}(\mathbf{A}) + g_{22}(\mathbf{A}) \quad or \quad g_{11}(\mathbf{A}) - g_{21}(\mathbf{A}) \neq g_{12}(\mathbf{A}) - g_{22}(\mathbf{A}) \tag{2.11}$$

Subjected to the fact that the conditions in (2.11) are to be met for $f(\mathbf{A})$ to be UD, following possible relations between the co-efficients of $f(\mathbf{A})$ can be derived:

$$g_{12}(\mathbf{A}) = g_{11}(\mathbf{A}), g_{22}(\mathbf{A}) = -g_{21}(\mathbf{A}) \text{ and } \; g_{11}(\mathbf{A}) = g_{21}(\mathbf{A}) \;\; \text{(TSMOS Type I)}, \tag{2.12}$$

$$g_{12}(\mathbf{A}) = \mathrm{rot}(g_{11}(\mathbf{A})), g_{22}(\mathbf{A}) = -\mathrm{rot}(g_{21}(\mathbf{A})) \text{ and } g_{11}(\mathbf{A}) = g_{21}(\mathbf{A}) \;\; \text{(TSMOS Type III)} \tag{2.13}$$

Table 2.3: Defining $f(\mathbf{A})$ for different types of TSMOS and their mixed counterparts in terms of $\mathbf{p} = [100\cdots0]_{1\times 2^{k-1}}$ and $\mathbf{q} = [0\cdots001]_{1\times 2^{k-1}}$

$f(\ )$	TSMOS (Type I)	TSMOS (Type II)	TSMOS (Type III)
$f(\mathbf{p})$	$\begin{bmatrix} \mathbf{p} & \mathbf{p} \\ \mathbf{p} & -\mathbf{p} \end{bmatrix}$	$\left[\begin{array}{cc\|cc} \mathbf{p}_{NZ} & \mathbf{p}_{NZ} & \mathbf{p}_Z & \mathbf{p}_Z \\ \mathbf{p}_{NZ} & -\mathbf{p}_{NZ} & \mathbf{p}_Z & -\mathbf{p}_Z \end{array}\right]$	$\begin{bmatrix} \text{rot}(\mathbf{p}) & \text{rot}(\mathbf{p}) \\ \text{rot}(\mathbf{p}) & -\text{rot}(\mathbf{p}) \end{bmatrix}$
$f(\mathbf{q})$	$\begin{bmatrix} \mathbf{q} & \mathbf{q} \\ \mathbf{q} & -\mathbf{q} \end{bmatrix}$	$\left[\begin{array}{cc\|cc} \mathbf{q}_{NZ} & \mathbf{q}_{NZ} & \mathbf{q}_Z & \mathbf{q}_Z \\ \mathbf{q}_{NZ} & -\mathbf{q}_{NZ} & \mathbf{q}_Z & -\mathbf{q}_Z \end{array}\right]$	$\begin{bmatrix} \text{rot}(\mathbf{q}) & \text{rot}(\mathbf{q}) \\ \text{rot}(\mathbf{q}) & -\text{rot}(\mathbf{q}) \end{bmatrix}$
$f(\mathbf{p},\mathbf{q})$	$\begin{bmatrix} \mathbf{p} & \mathbf{p} \\ \mathbf{q} & -\mathbf{q} \end{bmatrix}$	$\left[\begin{array}{cc\|cc} \mathbf{p}_{NZ} & \mathbf{p}_{NZ} & \mathbf{p}_Z & \mathbf{p}_Z \\ \mathbf{q}_Z & -\mathbf{q}_Z & \mathbf{q}_{NZ} & -\mathbf{q}_{NZ} \end{array}\right]$	$\begin{bmatrix} \text{rot}(\mathbf{p}) & \text{rot}(\mathbf{p}) \\ \text{rot}(\mathbf{q}) & -\text{rot}(\mathbf{q}) \end{bmatrix}$
$f(\mathbf{q},\mathbf{p})$	$\begin{bmatrix} \mathbf{q} & \mathbf{q} \\ \mathbf{p} & -\mathbf{p} \end{bmatrix}$	$\left[\begin{array}{cc\|cc} \mathbf{q}_Z & \mathbf{q}_Z & \mathbf{q}_{NZ} & \mathbf{q}_{NZ} \\ \mathbf{p}_{NZ} & -\mathbf{p}_{NZ} & \mathbf{p}_Z & -\mathbf{p}_Z \end{array}\right]$	$\begin{bmatrix} \text{rot}(\mathbf{q}) & \text{rot}(\mathbf{q}) \\ \text{rot}(\mathbf{p}) & -\text{rot}(\mathbf{p}) \end{bmatrix}$

where $\text{rot}(\mathbf{A})$ indicates the rotated version of $\mathbf{A}$ e.g.; if $\mathbf{A} = \begin{bmatrix} a & b \\ c & d \end{bmatrix}$, then $\text{rot}(\mathbf{A}) = \begin{bmatrix} b & a \\ d & c \end{bmatrix}$. Likewise, if $\mathbf{A}$ can be split into two adjacent matrices e.g.; $\mathbf{A} = [\mathbf{A}_{NZ}|\mathbf{A}_Z]$, then application of either (2.12) or (2.13) generates a new group of TSMOS, which is termed as of Type II. Since the relation among the coefficients from (2.12) and (2.13) essentially approves for the UD nature of $f(\mathbf{A})$, following (2.6), they are also applicable to $f\left(\mathbf{C}^{k-1}\right)$ and $f\left(\mathbf{p}\right)$ separately. Similar realization is also applicable for $f\left(\mathbf{C}^{k-1}\right)$ and $f\left(\mathbf{q}\right)$. So, we consider it logical to use either of them to define $f(\ )$ in Table 2.3. Also, it is realized that corresponding to each of these constructions (Type I, II, III), we can also define $f(\mathbf{p},\mathbf{q})$, which will also result in TSMOS, but with different structures. We call them *mixed* TSMOS. For a comparative overview, all the structures of $f(\ )$ and $\mathbf{C}^3 = \left[\mathbf{C}_1^3\mathbf{C}_2^3|\mathbf{C}_3^3\right]$ for each variant of TSMOS are presented in Table 2.3 and Table 2.6 respectively.

2.4 Hierarchy of MAI

2.4.1 Correlation hierarchy for $t_d = 0$: $(\mathbf{Det}(\rho_{t_d=0}) = 0)$

The design and performance of any detection algorithm in CDMA is driven by the level of MAI on its users. For further explanation, the system model in (2.1) corresponding

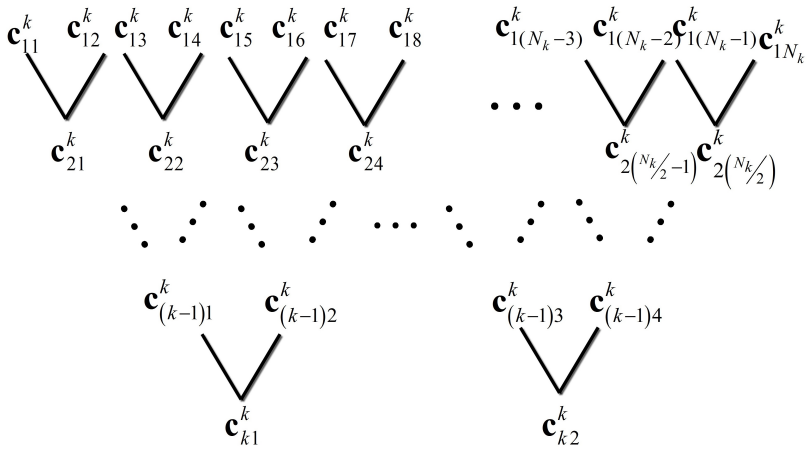

Figure 2.2: Uniform Twin Tree Hierarchy for TSMOS (TYpe I): $\mathbf{C}^k = \left[\mathbf{C}_1^k|\mathbf{C}_2^k|\cdots|\mathbf{C}_k^k\right]$

to $\mathbf{C}^k = \left[\mathbf{C}_1^k|\mathbf{C}_2^k|\cdots|\mathbf{C}_k^k\right]$ can be redefined as

$$\mathbf{y} = \sum_{i=1}^{k} \mathbf{C}_i^k \mathbf{x}_i + \mathbf{n} \tag{2.14}$$

In this section, we intend to analyze the correlation structure of TSMOS.

The geometric pattern of the subsets in $\mathbf{C}^k$ can be shown to have a *uniform twin tree structured cross-correlation* as shown in Figure 2.2. The nodes of the tree at a particular level (depth) $l = 1, 2, \ldots, k$ (i.e., $l = k-i+1$) collectively represent a specific subset. The following facts can be summarized from the pictorial representation.

• There exist two identical (twin) trees, each of which has its origin or root from the smallest orthogonal subset (i.e.; $\mathbf{C}_k^k$ at the lowest level of the tree, $l = 1$). The nodes at the highest level of the tree (i.e., $l = k$) represent the largest subset: $\mathbf{C}_1^k$.

• Each node (parent) at a level-l generates two nodes (child) for its next higher level $(l + 1)$.

• All the 2^l nodes at level-l collectively form an orthogonal set and each node at a particular level is correlated to its child and parent nodes only. For node-j at level-l (i.e.; $\mathbf{c}_{lj}^k$), the two child nodes emanated at level-$(l + 1)$ (i.e.; $\mathbf{c}_{(l+1)(2j-1)}^k$ and $\mathbf{c}_{(l+1)(2j)}^k$) are considered as *linear combination* on $\mathbf{c}_{lj}^k$, which can be expressed either following the bottom-to-top or top-to-bottom approach, as described below.

Bottom-to-Top Approach: For node-j at level-l of the tree (denoted as $\mathbf{c}_{lj}^k$), the two child nodes emanated in level-$(l + 1)$ ($\mathbf{c}_{(l+1)(2j-1)}^k$ and $\mathbf{c}_{(l+1)(2j)}^k$) can be expressed

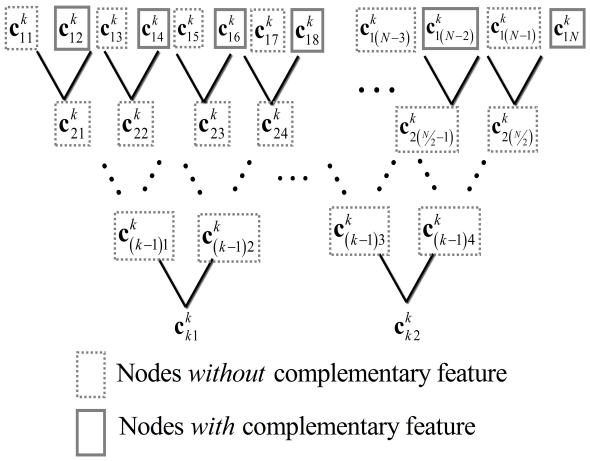

Figure 2.3: Twin Tree Hierarchy for TSMOS (Type I) $\mathbf{C}^k$ showing complementary nodes.

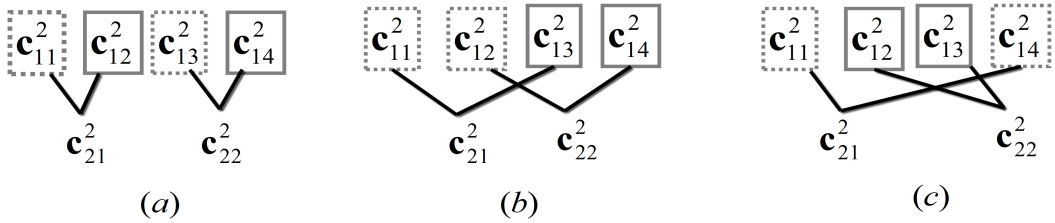

Figure 2.4: Twin Tree Structure for $\mathbf{C}^2$ indicating the nodes with complementary feature for (a) TSMOS (Type I), (b) TSMOS (Type II), and (c) TSMOS (Type III).

as the *linear combination* on $\mathbf{c}_{lj}^k$ e.g.,

$$\mathbf{c}_{(l+1)(2j-1)}^k = \mathbf{c}_{lj}^k + \mathbf{c}_{lj}^k \left(t \pm (N/2^{l+1})\, T_c\right) \tag{2.15}$$

$$\mathbf{c}_{(l+1)\ (2j)}^k \quad = \mathbf{c}_{lj}^k - \mathbf{c}_{lj}^k \left(t \pm (N/2^{l+1})\, T_c\right) \tag{2.16}$$

Top-to-Bottom Approach: For node-$(2j-1)$ and $2j$ at level-$(l+1)$, denoted by $\mathbf{c}_{(l+1)(2j-1)}^k$ and $\mathbf{c}_{(l+1)(2j)}^k$ respectively, the new node generated at level-l can be defined as

$$\mathbf{c}_{lj}^k = 1/2 \left(\mathbf{c}_{(l+1)(2j-1)}^k + \mathbf{c}_{(l+1)(2j)}^k\right)$$

Note that, similar logic can also be considered for explaining the correlation among the subsets in TSMOS (Type II and III), but with a variation in selection of the nodes from the higher level.

2.4.2 Correlation hierarchy for $t_d \neq 0$: $(\mathbf{Det}(\rho_{t_d \neq 0}) \neq 0)$

Complementary Feature of TSMOS: In order to demonstrate the complementary nature of the users of $\mathbf{C}^k$ (in fact of $\mathbf{C}_1^k$), let us analyze its

correlation property with respect to Figure 2.3. Consider splitting of $\mathbf{C}_1^k$ into two binary subsets $\mathbf{C}_{1L}^k$ and $\mathbf{C}_{1R}^k$ depending on the linearity involved in its generation as defined by (2.15) and (2.16) respectively, where "L" and "R" indicates the "Left" and "Right" child respectively. In other words, $\mathbf{C}_1^k = \left[\mathbf{C}_{1L}^k | \mathbf{C}_{1R}^k\right]$ where each subset has ${}^{N_k}\!/_2$ number of signatures i.e.; $\mathbf{C}_{1L}^k = \left[\mathbf{c}_{1L_1}^k \mathbf{c}_{1L_2}^k \cdots \mathbf{c}_{1L_{\frac{N_k}{2}}}^k\right] = \left[\mathbf{c}_{11}^k \mathbf{c}_{13}^k \cdots \mathbf{c}_{1(N_k-1)}^k\right]$, and $\mathbf{C}_{1R}^k = \left[\mathbf{c}_{1R_1}^k \mathbf{c}_{1R_2}^k \cdots \mathbf{c}_{1R_{\frac{N_k}{2}}}^k\right] = \left[\mathbf{c}_{12}^k \mathbf{c}_{14}^k \cdots \mathbf{c}_{1N_k}^k\right]$. Figure 2.4 shows the structural variation in the twin tree hierarchy for different sets of TSMOS: Type I, Type II, Type III. Note that afterwards, for the purpose of explanation, we consider TSMOS (Type I) only, and it is trivial to expect the identical behavior to be noticed for other types.

As per the observations so far, for $t_d = 0$, for each root signature in $\mathbf{C}_i^k = \left[\mathbf{c}_{i1}^k \mathbf{c}_{i2}^k \cdots \mathbf{c}_{i2^{k-i+1}}^k\right]$ $(2 \leq i \leq k)$, level of MAI on the child signatures in $\mathbf{C}_1^k$ i.e., $\mathbf{c}_{1L_j}^k$ and $\mathbf{c}_{1R_j}^k$ remain the same. For $0 < t_d < T_c$, where the level of MAI on $\mathbf{c}_{1L_j}^k$ bears the same value as that of $t_d = 0$, a reduction in its level is observed for $\mathbf{c}_{1R_j}^k$. To verify this, the generalized expression for the *periodic* cross-correlation between signature-j of $\mathbf{C}_1^k$ (i.e., $\mathbf{c}_{1j}^k$) and its root signature-r in $\mathbf{C}_i^k$ (i.e., $\mathbf{c}_{ir}^k$), denoted by $\rho_p(\mathbf{c}_{1j}, \mathbf{c}_{ir}, {}^m\!/_n)$ have the following discrete form of presentation.

$$\rho_p(\mathbf{c}_{1j}, \mathbf{c}_{ir}, {}^m\!/_n) = {}^1\!/_\eta \left[\sum_{q=1}^{Nn-m} \mathbf{c}_{ir}(q)\mathbf{c}_{1j}(q+m) + \sum_{q=1}^{m} \mathbf{c}_{ir}(N-m+q)\mathbf{c}_{1j}(q)\right] \tag{2.17}$$

In (2.17), $({}^m\!/_n)$ represents the discrete domain equivalent of the fractional delay t_d, such that $t_d = ({}^m\!/_n)\, T_c$, where n = total number discrete fractional intervals within one chip duration T_c and m = number of fractional intervals within t_d. In particular, $m = 0$ and n corresponds to the case of synchronous and one chip delayed transmission respectively. On further simplification, the expression in (2.17) becomes

$$\rho_p(\mathbf{c}_{1j}, \mathbf{c}_{ir}, {}^m\!/_n) = \frac{2^{k-i+1}}{n}\left[(n-m)\,(b_1) + m(b_2)\right] \tag{2.18}$$

where $(b_1, b_2) = ({}^1\!/_N, {}^1\!/_N)$ and $({}^1\!/_N, {}^{-1}\!/_N)$ for $\mathbf{c}_{1j}^k \in \mathbf{C}_{1L}^k$ and $\mathbf{C}_{1R}^k$ respectively.

Equivalent Delay Pair (EDP) (t_{d_1}, t_{d_2}): Consider $\rho_p(\mathbf{c}_{1j}, \mathbf{c}_{ir}, {}^m\!/_n)$ in (2.18) for two different values of time delays: $t_{d1} = ({}^{m_1}\!/_n)\, T_c$ and $t_{d2} = ({}^{m_2}\!/_n)\, T_c$, where $t_{d1}, t_{d2} \leq T_c$. For both the cases, the level of MAI will be equal, if and only if

$$\rho_p(\mathbf{c}_{1j}, \mathbf{c}_{ir}, {}^{m_1}\!/_n) = -\rho_p(\mathbf{c}_{1j}, \mathbf{c}_{ir}, {}^{m_2}\!/_n).$$

According to (2.18), the above expression can also be written as

$$\tfrac{2^{k-i+1}}{n}\left[n-2m_1\right] = -\left(\tfrac{2^{k-i+1}}{n}\left[n-2m_2\right]\right),$$

which implies $(m_1 + m_2) = n$. This can be approved as the condition for equal level of MAI and hence, for identical error performance for two different values of t_d. So, we call them equivalent delay pair . ■

Optimality Criterion for $\mathbf{C}_{1R}^k \in \mathbf{C}_1^k$: From (2.18), for $(b_1, b_2) = (1/N, -1/N)$, value of $\rho_p(\mathbf{c}_{1j}, \mathbf{c}_{ir}, m/n)$ will be minimum (zero), when $m/n = 1/2$ and it corresponds to a time delay of $t_d = (0.5)T_c$. Under such conditions, the $N_k/2$ users of $\mathbf{C}_1^k$ (i.e., $\mathbf{C}_{1R}^k$) transmits under no MAI despite being a part of the same number of users that exists for $t_d = 0$. In other words, for $t_d = (0.5)T_c$ there prevails two different levels of optimality in $\mathbf{C}^k$: optimal for $\mathbf{C}_{1R}^k$ and sub-optimal for rest: $\mathbf{C}_{1L}^k$, $\mathbf{C}_2^k$, $\mathbf{C}_3^k$,..., $\mathbf{C}_k^k$. ■

Please note that, for TSMOS (Type I, II, III), the number of optimal signatures for $\mathbf{C}^k$ remains $N_k/2$. Similar behavior is also recorded for the hybrid counterparts.

Note 1: On further analysis, it is observed that the optimality criterion of $\mathbf{C}_{1e}^k \in \mathbf{C}_1^k$ not only occurs for $t_d = 0.5T_c$ but also for $t_d = 2.5T_c, 4.5T_c, 6.5T_c, \ldots$. Therefore, it is logical to state that the occurrence of this property is periodic at an interval of $2T_c$, starting from $t_d = 0.5T_c$.

2.5 Design of MUD

From the tree hierarchy in Figure 2.2, considering the existence of k multiple subsets in $\mathbf{C}^k$, a signature in subset $\mathbf{C}_i^k$ (or $\mathbf{C}_{(k-l+1)}^k$) is correlated to each of its root sequence in previous $(k-i)$ (or $l-1$) subsets: $\mathbf{C}_{i+1}^k, \mathbf{C}_{i+1}^k, \cdots, \mathbf{C}_k^k$. Along with, the correlation also prevails with $(2^i - 2)$ number of child signatures existing in next $(i-1)$ orthogonal subsets. In particular, corresponding to each of the code sequence in $\mathbf{C}_i^k$, the subsets $\mathbf{C}_{i-1}^k, \mathbf{C}_{i-2}^k, \cdots, \mathbf{C}_1^k$ carry $2^1, 2^2, \ldots, 2^{i-1}$ number of child signatures respectively. Therefore, major part of the MAI (or intergroup MAI) on a particular signature in a subset is due to the child signatures. Since the number of child signatures is usually decided by the level of the subset, a subset with lower level (low value of l or high value of i) has comparatively more number of child signatures and hence, is

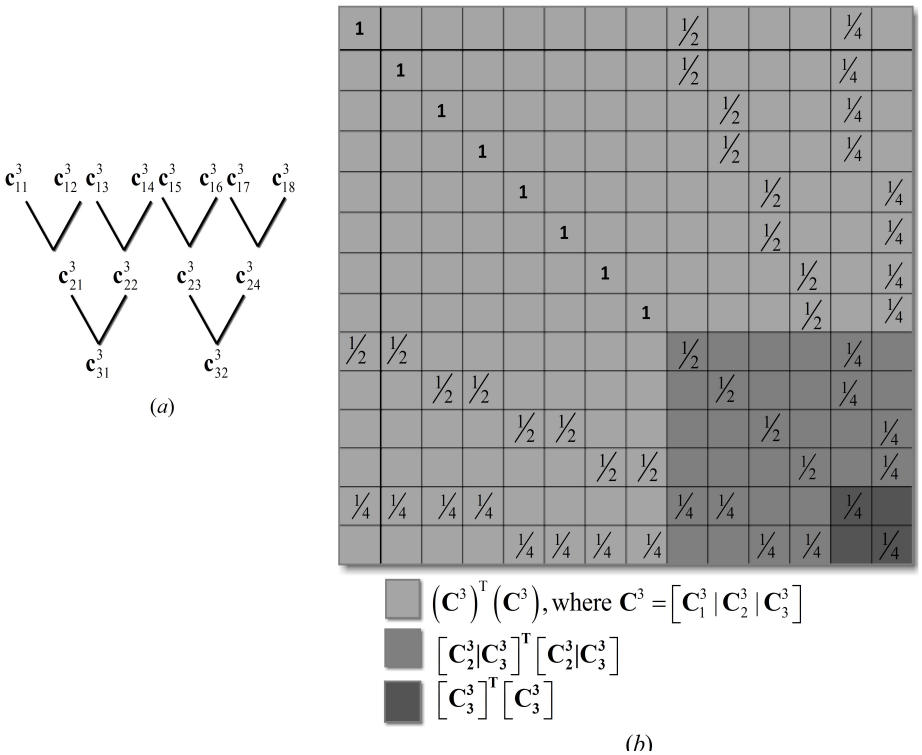

Figure 2.5: (a) Twin tree hierarchy for TSMOS (Type I) $\mathbf{C}^3$ (b) Correlation Matrix for $\mathbf{C}^3$: $\boldsymbol{\rho}_3 = \left(\mathbf{C}^3\right)^T\mathbf{C}^3$

subjected to the higher level of MAI. Equivalently, the following relation summarizes the effect of MAI on different subsets.

$$\mathrm{MAI}_{\mathbf{C}^k_1} < \mathrm{MAI}_{\mathbf{C}^k_2} < \cdots < \mathrm{MAI}_{\mathbf{C}^k_k} \tag{2.19}$$

According to the expression in (2.19), each signature in the orthogonal subset at the highest level (of largest size) is subjected to the least level of MAI. Hence, the corresponding subset validates its candidature to be decoded first.

For example: Figure 2.5 (b) shows the overall cross-correlation matrix associated with that of $\mathbf{C}^3$ i.e., $\boldsymbol{\rho}_3 = \left(\mathbf{C}^3\right)^T\mathbf{C}^3$, where the matrix and its respective tree structure are shown by Table 2.2 and Figure 2.5 (a) respectively. The row-a or column-a in Figure 2.5 (b) presents the correlation coefficients for user-a for $1 \leq a \leq 14$. While the *non-zero entry* in a cell indicates the presence of correlation among the particular signatures, the cells with *no entries* implies the orthogonal nature of the signatures involved.

Now, we attempt to justify the errorless nature of the proposed decoder. First, we present Lemma 1 which further guides to the proof of Theorem 3.

Lemma 1: For $\mathbf{C}^k \in \{\pm 1, 0\}^{N_k \times M_k}$ denoting the fully loaded TSMOS (Type I), the decoding of the subset with the least MAI using MF detection is always errofree.

Proof: According to (2.19), the subset with the least MAI in TSMOS $\mathbf{C}^k$ is $\mathbf{C}_1^k$. Adopting the logic of MF (in Section 2.2.3), the decision of sign($\mathbf{z}_1$) corresponding to $\mathbf{x}_1$ will be errorless, if and only if $\hat{\mathbf{x}_1} = \text{sign}(\mathbf{z}_1) = \mathbf{x}_1$ where

$$\mathbf{z}_1 = \mathbf{r}\left(\mathbf{C}_1^k\right)^T = \sum_{i=1}^{k} \rho_{1i}\mathbf{x}_i \tag{2.20}$$

for $\boldsymbol{\rho}_1 = [\boldsymbol{\rho}_{11}|\boldsymbol{\rho}_{12}|\cdots|\boldsymbol{\rho}_{1k}]$ denoting the matrix representing the cross-correlation coefficients of all the subsets with respect to $\mathbf{C}_1^k$, such that $\boldsymbol{\rho}_{11} = \left(\mathbf{C}_1^k\right)^T\mathbf{C}_1^k$, $\boldsymbol{\rho}_{12} = \left(\mathbf{C}_1^k\right)^T\mathbf{C}_2^k$, ..., $\boldsymbol{\rho}_{1k} = \left(\mathbf{C}_1^k\right)^T\mathbf{C}_k^k$. So, for any signature in $\mathbf{C}_1^k$ (say signature-u), the relation $\hat{x}_{1u} = x_{1u}$, is true, only if the following expression on $\boldsymbol{\rho}_1$ holds valid.

$$\rho_{11}(u,u) > \sum_{i=2}^{k}\sum_{v=1}^{\frac{N_k}{2^{i-1}}} \rho_{1i}\,(u,v) \tag{2.21}$$

Note that the expression in (2.21) fully complies with the attribute of TSMOS cited in (2.5), where the fundamental logic of decoding is governed by the fact that the errorless recovery of the input data in the multi-user environment in CDMA is feasible, if the level of its PA exceeds that of the TPC on it.

For better apprehension, let us take a look at the correlation matrix for $\mathbf{C}^3$ ($\boldsymbol{\rho}_3$ in Figure 2.5). The first 8 rows or columns indicate the cross-correlation entries for the users of $\mathbf{C}_1^3$, which can be denoted individually as $\mathbf{C}_{1a}^3$ for $1 \leq a \leq 8$. For an arbitrary user in $\mathbf{C}_1^3$, the *correlation vector* presenting the non-zero correlation coefficients is found to be $\{1, 1/2^1, 1/2^2\}$, where the first and the rest indicate the level of auto and peak cross-correlations respectively. Extending the analysis to the general case of $\mathbf{C}^k$, the correlation vector of any user in $\mathbf{C}_1^k$ becomes $\{1/2^0, 1/2^1, 1/2^2, \cdots, 1/2^{k-1}\}$, which also approves the relation in (2.21), since $1 > (1/2^1 + 1/2^2 + \cdots + 1/2^k)$. Now, if we remove $\mathbf{C}_1^k$ from $\mathbf{C}^k$ indicating the successful detection of $\hat{\mathbf{x}}_1$, then following (2.19), $\mathbf{C}_2^k$ is to be counted as the subset with the least MAI and the correlation vector for any user in $\mathbf{C}_2^k$ becomes $\{1/2^1, 1/2^2, \cdots, 1/2^{k-1}\}$ and qualifies the logic associated in (2.21) too, as $1/2^1 > (1/2^2 + 1/2^3 + \cdots + 1/2^k)$. Thus, with the similar approach considered for removing a series of subsets from the higher level of the tree (say p subsets: $\mathbf{C}_1^k$, $\mathbf{C}_2^k$ ..., $\mathbf{C}_p^k$), it is easy to show the decoding of subset $\mathbf{C}_{p+1}^k$ to be errorfree. Therefore,

for the proposed code design, it is possible to decode the subset with the least MAI with no error. ■

Theorem 3: For $\mathbf{C}^k \in \{\pm 1, 0\}^{N_k \times M_k}$ being the fully loaded TSMOS (Type I), there exists a feasible model low complex MUD for the error less detection of the input vector $\mathbf{x} \in \{1, -1\}^{M_k}$.

Proof: The proof is guided by the outcome from Lemma 1, adopting which the subset of $\mathbf{C}^k$ with the least MAI (i.e., $\mathbf{C}_1^k$) can be decoded with no error. This can be considered as the first stage of the MUD. After it is correctly decoded (i.e., $\hat{\mathbf{x}}_1 = \mathbf{x}_1$), it is possible to accurately estimate its level of MAI on other $(k-1)$ subsets i.e., $\mathbf{i}_1 = \mathbf{C}_1^k \hat{\mathbf{x}}_1$. Now, subtraction of $\mathbf{i}_1$ from $\mathbf{r}$ (also call $\mathbf{r}_1$) generates $\mathbf{r}_2$, such that,

$$\mathbf{r}_2 = \mathbf{r}_1 - \mathbf{i}_1 = \sum_{i=2}^{k} \mathbf{C}_i^k \mathbf{x}_i \tag{2.22}$$

is the summed transmitted signal of the matrix with remaining $(k-1)$ subsets still left to be decoded: $\left[\mathbf{C}_2^k | \mathbf{C}_3^k | \cdots | \mathbf{C}_k^k\right]$. According to (2.19), $\mathbf{C}_2^k$ then becomes the subset under the least MAI. With reference to Figure 2.5 (b), for each of the $(N_k/2)$ users of $\mathbf{C}_2^k$, the correlation vector becomes $\{1/2^1, 1/2^2, \cdots, 1/2^{k-1}\}$ and validates the relation in (2.21). Hence, the input vector corresponding to $\mathbf{C}_2^k$ is also detectable with no error (i.e., $\hat{\mathbf{x}}_2 = \mathbf{x}_2$) and this becomes the second stage of MUD. On a recurrent mode, similar interpretation of Lemma 1 is to be carried out in sequence till stage-k, so as to validate the errorfree decoding of $\hat{\mathbf{x}}_3, \hat{\mathbf{x}}_4, \ldots, \hat{\mathbf{x}}_k$ corresponding to $\mathbf{C}_3^k, \mathbf{C}_4^k, \ldots, \mathbf{C}_k^k$ from $\mathbf{r}_3$, $\mathbf{r}_4$, ..., $\mathbf{r}_k$ denoting the summed data vector for $\left[\mathbf{C}_3^k | \mathbf{C}_4^k | \cdots | \mathbf{C}_k^k\right]$, $\left[\mathbf{C}_4^k | \cdots | \mathbf{C}_k^k\right]$, ..., $\left[\mathbf{C}_k^k\right]$ respectively. This completes the proof. ■

Now, we present a practically implementable design of the decoder for noisy transmission in Table 2.4. The only deviation that needs to be noted in the following steps is the substitution of $\mathbf{r}$ (noiseless received vector) by $\mathbf{y}$ (the noisy received vector in (2.1)).

Note 2: Observation reveals that the proposed code set $\mathbf{C}^k$ is a subset of the UD matrix generated at the k^{th} iteration of the construction proposed in [10, 92]. This implies that for these matrices, all the features of the proposed system can be realized, if and only if the transmission of the specific signatures (besides $\mathbf{C}^k$) remain inactive. In other words, the system in [10, 92] can have a low complex MUD for noisy

Table 2.4: Detection Algorithm for $\mathbf{C}^k$

MUD for Noisy Channel
For stage-i $(1 \leq i \leq k)$, estimate • $\mathbf{i}_i = \mathbf{C}^k_{i-1}\hat{\mathbf{x}}_{i-1}$ • $\mathbf{y}_i = \mathbf{y}_{i-1} - \mathbf{i}_{i-1}$ (where $\mathbf{y}_1 = \mathbf{y}$, and $\mathbf{i}_1 = \mathbf{0}_{N_k \times 1}$) • $\mathbf{z}_i = \mathbf{y}_i \mathbf{C}^k_i$ • $\hat{\mathbf{x}}_i = \text{sign}(\mathbf{z}_i)$ Finally, $\hat{\mathbf{x}} = \{\hat{\mathbf{x}}_1, \hat{\mathbf{x}}_2, \cdots, \hat{\mathbf{x}}_k\}$ is the decoded vector.

transmission at the cost of sacrificing the asymptotic equality of $\beta(k)$ with $S_{sum}(k)$, as per our discussion in Section 1.4.3.

2.6 Performance Analysis

2.6.1 Bit Error Rate

While for the noisefree transmission, the proposed MUD guarantees unique detectability, existence of error in the recovery of $\mathbf{x}_k$ is inevitable, when the channel gets noisy. From Table 2.4, the elaborated expression of $\mathbf{z}_i$ corresponding to the subset $\mathbf{C}^k_i$ can be written as

$$\mathbf{z}_i = \left(\frac{N_{ef_i}}{N_k}\right)\mathbf{I}\mathbf{x}_i + \sum_{u=(i+1)}^{k} \boldsymbol{\rho}_{iu}\mathbf{x}_u + \sum_{v=1}^{i-1} \boldsymbol{\rho}_{iv}(\mathbf{x}_v - \hat{\mathbf{x}}_v) + \mathbf{n}_i \tag{2.23}$$

where $\mathbf{x}_i$ is the desired input vector, $\boldsymbol{\rho}_{iu}$ and $\boldsymbol{\rho}_{iv}$ denote the cross-correlation matrix of the desired subset $(\mathbf{C}^k_i)$ with respect to the child subsets (already detected, and denoted as $\mathbf{C}^k_v$) and the root subsets (to be detected, and denoted as $\mathbf{C}^k_u$). In (2.23) the terms involving $\boldsymbol{\rho}_{iu}$ and $\boldsymbol{\rho}_{iv}$ represent the sources of MAI where $(\mathbf{x}_v - \hat{\mathbf{x}}_v)$ indicates the error introduced during decoding in previous $(i-1)$ iterations and $\mathbf{n}_i = \left(\mathbf{C}^k_i\right)^T\mathbf{n} =$ AWGN vector with zero mean.

To determine the probability of error for the j^{th} user of $\mathbf{C}^k_i$, let us rewrite the expression in (2.23) as

$$z_{ij} = \left(\frac{N_{ef_i}}{N_k}\right) x_{ij} + \sum_{u=(i+1)}^{k} \rho_{iu(j)}\mathbf{x}_u + \sum_{v=1}^{i-1} \rho_{iv(j)}(\mathbf{x}_v - \hat{\mathbf{x}}_v) + n_{i(j)} \tag{2.24}$$

where $\mathbf{x}_i = \left[x_{i1}x_{i2}\cdots x_{i\frac{N_k}{2^{i-1}}}\right]$, $\mathbf{z}_i = \left[z_{i1}z_{i2}\cdots z_{i\frac{N_k}{2^{i-1}}}\right]$, and $\mathbf{n}_i = \left[n_{i(1)}n_{i(2)}\cdots n_{i(N_k)}\right]$.

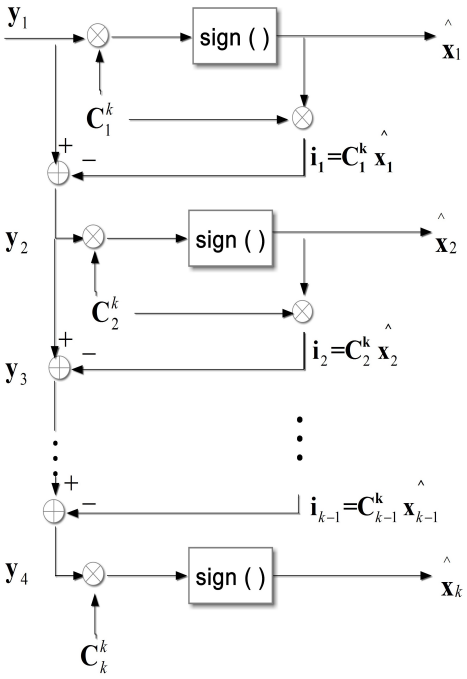

Figure 2.6: Block Digram of proposed MUD (Table 2.4, 1.3.3)

Following the central limit theorem, the terms (second and third) contributing to MAI in (2.24) can be considered as the secondary source of noise. Hence, this is logical to simplify the expression in (2.24) as

$$z_{ij} = \left(\frac{N_{ef_i}}{N_k}\right) x_{ij} + \eta_{ij}. \tag{2.25}$$

With the expression in (2.25) representing the communication system model for a single user BPSK system, we can write the probability of error of the user-j in subset-i as

$$P_e^{ij} = \frac{1}{\sqrt{2\pi}\sigma} \int_{\frac{N_{ef_i}}{N} x_{ij}}^{\infty} e^{-\left(\eta_{ij}^2/\sigma^2\right)} d\eta_{ij} \tag{2.26}$$

which on further modification can also be written as

$$P_e^{ij} = \frac{1}{2} erfc\left(\frac{\frac{N_{ef_i}}{N} x_{ij}}{\sqrt{2}\sigma}\right) = Q\left(\sqrt{\frac{\left(\frac{N_{ef_i}}{N}\right)^2 \mathrm{E}\left(x_{ij}^2\right)}{\sigma^2}}\right). \tag{2.27}$$

For better accuracy, the value of σ^2 in (2.27) is estimated to be

$$\mathrm{E}\left(\eta_{ij}{}^2\right) = \sum_{u=(i+1)}^{k} \rho_{iu(j)}^2 \mathrm{E}\left(\mathbf{x}_u{}^2\right) + \sum_{v=1}^{i-1} \rho_{iv(j)}^2 \mathrm{E}\left(\left(\mathbf{x}_v - \hat{\mathbf{x}}_v\right)^2\right) + \mathrm{E}\left(n_{i(j)}{}^2\right) \tag{2.28}$$

In (2.28),

$$\mathrm{E}\left(\left(\mathbf{x}_v - \hat{\mathbf{x}}_v\right)^2\right) = 0P_c{}^v + 4P_e{}^v$$

where P_c^v and P_e^v denote the probability of correctness and error in decoding,

corresponding to the binary input. Therefore, the resultant expression for P_e^{ij} is derived to be

$$P_e^{ij} = Q\left(\sqrt{\frac{\left(\frac{N_{ef_i}}{N}\right)^2 \mathrm{E}\left(x_{ij}^2\right)}{\sum_{u=i+1}^{k} \rho_{iu(j)}^2 + 4\sum_{v=1}^{i-1} \rho_{iu(j)}^2 P_e^v + \mathrm{E}\left(n_{i(j)}^2\right)}}\right), \tag{2.29}$$

where $\mathrm{E}\left({n_{i(j)}}^2\right) = ({}^{N_o}\!/_2)$.

2.6.2 Error Performance of Individual Subsets

For CDMA system employing the ternary matrices, error performance of a user or group of users using MF decoding is primarily influenced by two crucial metrics i.e.; the net level of MAI and the available diversity (spreading gain). Therefore, we may expect the hierarchy of MAI in (2.19) and the order of N_{ef} defined as

$$N_{ef_1} > N_{ef_2} > \cdots > N_{ef_k} \tag{2.30}$$

to jointly approve for the following order in BER among the k subsets.

$$\mathrm{BER}_{\mathbf{C}_1^k} < \mathrm{BER}_{\mathbf{C}_2^k} < \cdots < \mathrm{BER}_{\mathbf{C}_k^k}, \tag{2.31}$$

In the above expressions, N_{ef_i} and $\mathrm{BER}_{\mathbf{C}_i^k}$ denote the effective spreading gain and the average BER for subset $\mathbf{C}_i^k$ respectively. It is important to realize that the value of N_{ef_i} is directly proportional to the transmitted power associated with a signature in subset-i. Now, it is worthy to follow the derived expression in (2.29) and explain behavior of the curves representing the average BER of the individual subsets.

For lower values of E_b/N_o (or higher values of $\mathrm{E}\left(n_{i(j)}^2\right)$ in the denominator in (2.29)), when the level of MAI is constant, the order of available diversity (N_{ef_i} in the numerator) dominates and results in the order of error performance of the subsets, as shown in (2.31). On a closer investigation of the MUD, the flow of the algorithm appears to be sequential i.e.; the subset with lower value of N_{ef} or at lower level of the tree is recovered only after the decoding of that with higher value of N_{ef} or at higher level. Consequently, the BER performance of the latter being improved than that of the former is perceptible. Nevertheless, for the higher values of E_b/N_o, there exists the possibility of *unusual variation* in the order of their BER. Therefore, the analysis takes a different turn with the following elaboration.

For higher values of E_b/N_o (or lower values of $\mathrm{E}\left(n_{i(j)}^2\right)$ in the denominator in (2.29)), the factor that crucially controls the quality of recovery of the immediate next

subset ($\mathbf{C}_{i+1}^k$) is the net level of MAI, due to the remaining subsets ($\mathbf{C}_{i+2}^k, \ldots \mathbf{C}_k^k$). From Lemma 1, this is already clear that for $\left[\mathbf{C}_{i+1}^k|\mathbf{C}_{i+2}^k|\ldots|\mathbf{C}_k^k\right]$ being the decoding matrix, the net level of MAI on $\mathbf{C}_{i+1}^k$ is always less than that on $\mathbf{C}_i^k$ corresponding to the decoding matrix of $\left[\mathbf{C}_i^k|\mathbf{C}_{i+1}^k|\ldots|\mathbf{C}_k^k\right]$. So, the lowering in level of BER for $\mathbf{C}_{i+1}^k$ (lowering of first term in denominator in (2.29)), as compared to $\mathbf{C}_i^k$ is expected over a certain higher range of E_b/N_o, even if it carries a low order diversity. This indicates that there exists a high probability that the impact of MAI will dominate over that of the diversity. As a result, the subsets spaced at the bottom level of the tree will perform better than that of the top level. The value of E_b/N_o at which the fall in BER with respect to that of the subsets at higher level will start, is influenced by its level in the tree hierarchy (hence, the total level of intergroup MAI) and the value of N_{ef}. This is reflected in the simulation results in Figure 2.9.

2.6.3 Complexity

The proposed MUD deciphers all the k orthogonal subsets of $\mathbf{C}^k$ in k sequential stages. The detection of a particular subset at a specific stage is achieved by the simple logic of matched filtering. Furthermore, each stage is followed by an intermediate stage meant for the estimation and cancellation of the interference due the subsets, already detected. However, the complexity rise, if compared with that of the iterative cancellation techniques involved in [35, 58, 64, 82, 93, 94] is found to be marginal. Moreover, the massive saving in complexity as compared to that of the optimum MLD [41] is easy to realize due to no use of the maximum likelihood (ML) approach. We recall that the method of detection using optimum MLD strictly demands the calculation of 2^{M_k} euclidean distance (ED) vectors of length N_k, adopting which the rise in complexity behaves exponentially with the value of N_k. To compare with other simplified MUD design available in the literature, we derive the following mathematical expression for the average number of multiplications (i.e.; S_{mul}^{avg}) and additions (i.e.; S_{add}^{avg}) required to decipher all the M_k input symbols.

$$S_{mul}^{avg} = \underbrace{M_k N_k}_{\text{MF}} + \underbrace{N_k^2 \left(\frac{1 - \left(\frac{1}{2}\right)^{k-1}}{1 - \left(\frac{1}{2}\right)} \right)}_{\text{IE}} \tag{2.32}$$

Table 2.5: Comparison of Complexity: TSMOS (Proposed MUD) versus GCO (SMLD) [71]

Type	Parameter	Size of the Matrix		
		64 x 96	64 x 112	64 x 120
SMOS (Proposed MUD)	S_{mul}^{avg}	10240	13312	14848
	S_{add}^{avg}	10144	13200	14728
GCO (SMLD)	S_{mul}^{avg}	21248	66432	132032
	S_{add}^{avg}	20032	62144	123648

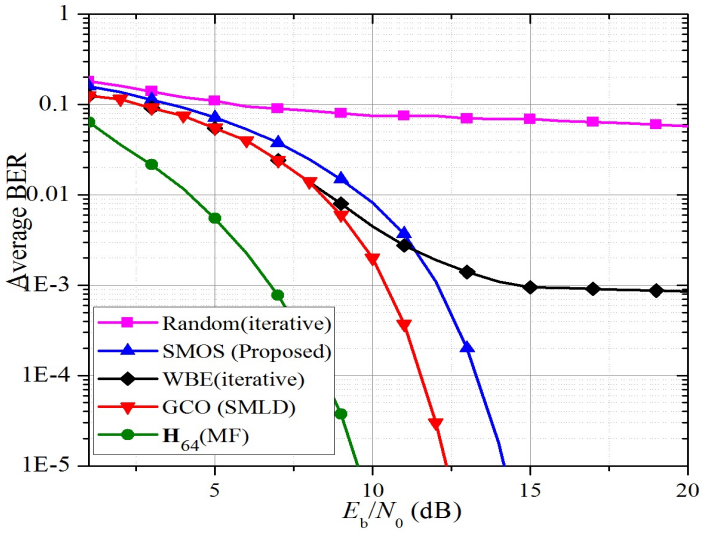

Figure 2.7: BER versus E_b/N_o performance for three different systems of dimension (64×96): TSMOS (proposed MUD), binary random and BWBE (iterative decoder [95]) and binary GCO (SMLD [71]).

$$S_{add}^{avg} = \underbrace{M_k\left(N_k-1\right)}_{\text{MF}} + \underbrace{N_k\left(N_k\left(\frac{1-\left(\frac{1}{2}\right)^{k-1}}{1-\left(\frac{1}{2}\right)}\right)-(k-1)\right)}_{\text{IE}} + \underbrace{N_k(k-1)}_{\text{IC}} \tag{2.33}$$

According to Figure 2.6, the design of the MUD in each stage can be divided into three different stages i.e.; matched filtering, interference estimation (IE), and interference cancellation (IC). Accordingly, we have pointed out the corresponding terms in the expressions in (2.32) and (2.33). As an example, the comparison study with respect to the generalized codes for overloaded (GCO) CDMA using SMLD is presented in Table 2.5.

2.7 Simulation Results

In this section, we focus on the BER versus (E_b/N_0) performance of the proposed system, assuming the channel to be additive white gaussian noise (AWGN). The system is supposed to be BPSK modulated and perfectly power controlled. For simulation

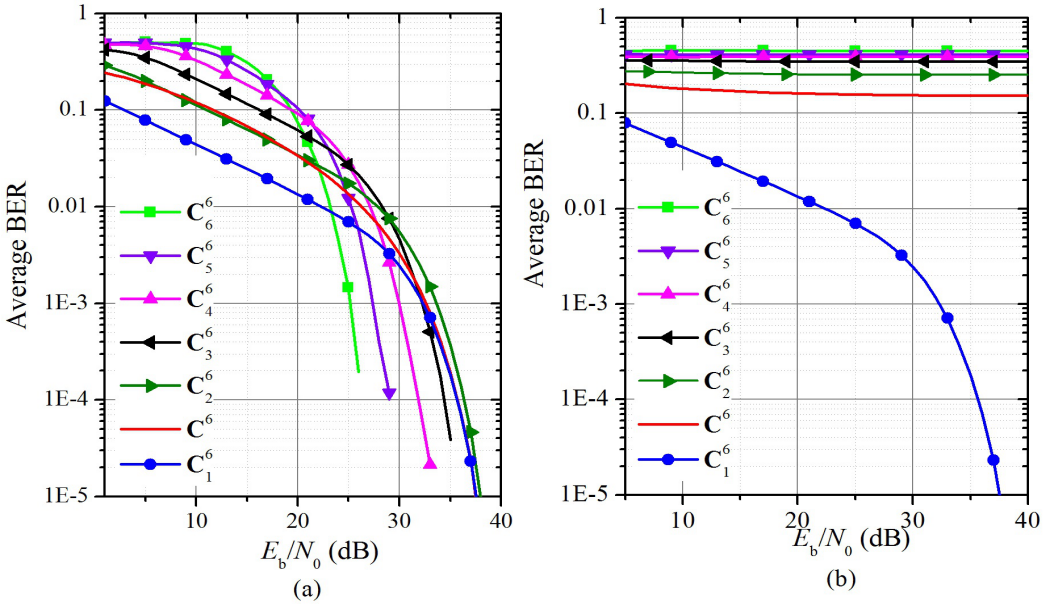

Figure 2.8: BER versus E_b/N_o performance for individual subsets of TSMOS (Type I) $\mathbf{C}_{64\times126} = [\mathbf{C}_1^6|\mathbf{C}_2^6|\mathbf{C}_3^6|\mathbf{C}_4^6|\mathbf{C}_5^6|\mathbf{C}_6^6]$ for (a) proposed MUD (b) MF.

throughout this thesis, we have used the MATLAB 2014 platform installed on a personal computer (hp, 32 bit OS, 2GB RAM, Intel (R), Core (TM) i7 processor, CPU @ 3.40 GHz).

Figure 2.7 is meant to offer an insight of the efficiency of TSMOS as compared to two other class of codes: binary random and WBE sequences. For SMOS, we consider the proposed MUD (as shown in Table 2.4), an iterative decoder with soft limiting [95] is preferred for the random and WBE sequences. To have the uniformity in analysis, the matrix dimension for all is kept at (64×96) leading to $\beta = 1.5$. Simulation of conventional CDMA using Hadamard matrix of dimension (64×64) is also included as the performance benchmark. As evident, for $E_b/N_o < 11$ dB, a marginal improvement in BER of the WBE codes as compared to SMOS is observed. But, for $E_b/N_o > 11$ dB, the level of BER of WBE saturates, which is because the mapping of binary WBE codes, unlike the UD matrices, lags the invertible characteristic. Therefore, by no means, it is possible to reduce the BER below the error floor, even not by enhancing the E_b/N_o to infinite. Conversely, for SMOS, the gradual approach of the BER level to zero with the increase in E_b/N_o is justified. When compared with the BER performance of binary GCO [73] matrices using SMLD [71], the superiority of the TSMOS does not exist. However, the notable advantage gained regarding complexity reduction (as shown in Table 2.5) of the proposed MUD using MF over SMLD yet

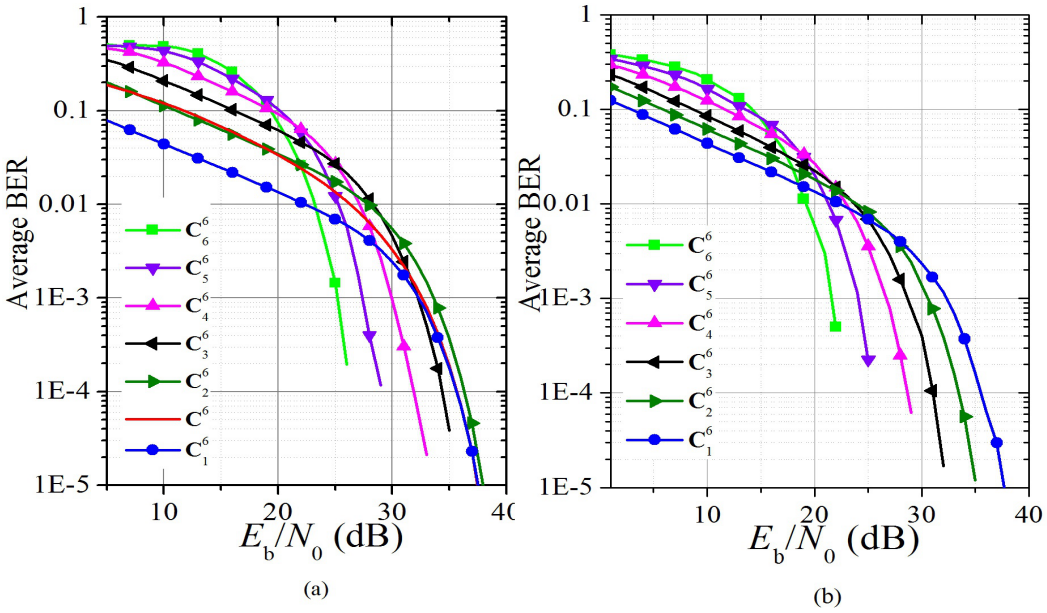

Figure 2.9: For individual subsets of TSMOS (Type I) $\mathbf{C}_{64\times126}$: (a) average BER versus E_b/N_o (b) minimum BER versus E_b/N_o

retains its priority.

Figure 2.8 (a) and (b) illustrates the error performance of the individual subsets of $\mathbf{C}^6 = \mathbf{C}_{64\times126} = \left[\mathbf{C}_1^6|\mathbf{C}_2^6|\mathbf{C}_3^6|\mathbf{C}_4^6|\mathbf{C}_5^6|\mathbf{C}_6^6\right]$, when the detection is achieved by the proposed MUD and the conventional MF decoder respectively. While the curves in Figure 2.8 (b) validates the expression in (2.19), their behavior in Figure 2.8 (a) shows an unprecedented variation over the range of E_b/N_o. This is already explained in detail in Section 2.6. In Figure 2.8 (b), the dramatic lowering in the level of BER of $\mathbf{C}_1^6$ is best explained by Lemma 1.

Figure 2.9 illustrates the impact of the detection error introduced at one stage of the MUD in affecting the average error performance of the subsequent stages. In Figure 2.9 (a) and (b), we show the average and the minimum level of the BER performance for the individual subsets respectively. To validate the tendency of the curves for the minimum level of BER, we follow the statement of Lemma 1. It is just because Lemma 1 serves as the fundamental layout towards the design of the proposed MUD, following whose extrapolation for the noisy transmission, the subset under the least MAI can be efficiently decoded with the minimum probability of error. In order to plot for the subsets $\mathbf{C}_1^6$, $\mathbf{C}_2^6$, $\mathbf{C}_3^6$, $\mathbf{C}_4^6$, $\mathbf{C}_5^6$, and $\mathbf{C}_6^6$, we select the decoding matrices $\left[\mathbf{C}_1^6|\mathbf{C}_2^6|\mathbf{C}_3^6|\mathbf{C}_4^6|\mathbf{C}_5^6|\mathbf{C}_6^6\right]$, $\left[\mathbf{C}_2^6|\mathbf{C}_3^6|\mathbf{C}_4^6|\mathbf{C}_5^6|\mathbf{C}_6^6\right]$, $\left[\mathbf{C}_3^6|\mathbf{C}_4^6|\mathbf{C}_5^6|\boldsymbol{C}_6^6\right]$, $\left[\mathbf{C}_4^6|\mathbf{C}_5^6|\mathbf{C}_6^6\right]$, $\left[\mathbf{C}_5^6|\mathbf{C}_6^6\right]$, $\left[\mathbf{C}_6^6\right]$ respectively, such that each subset following the tree

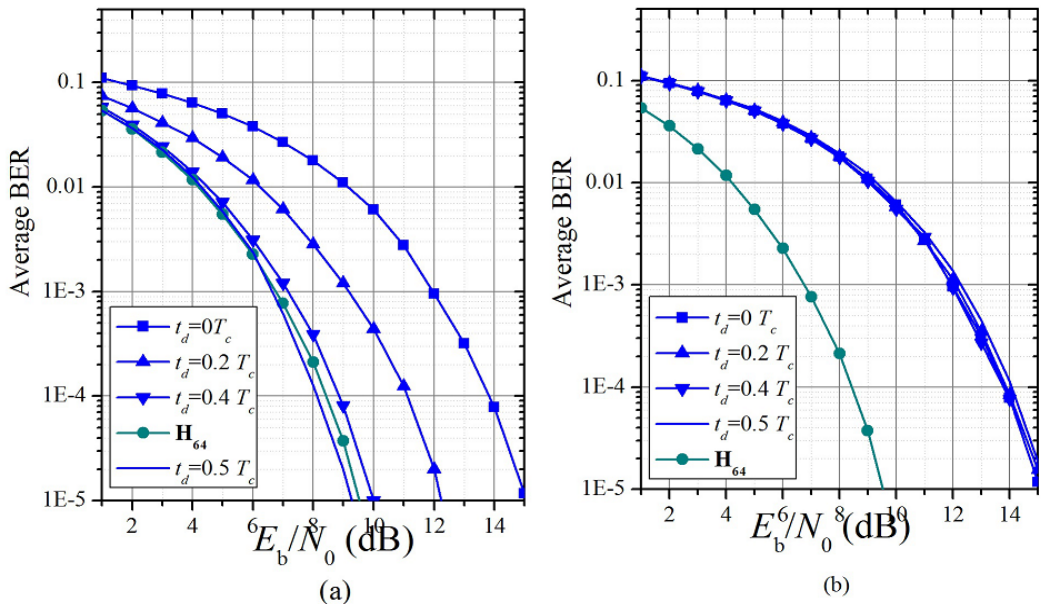

Figure 2.10: BER versus E_b/N_o performance comparison between (a) $\mathbf{C}_{1L}$, (b) $\mathbf{C}_{1R}$ with change in value of t_d.

hierarchy of the corresponding matrix is under the least level of MAI. It further implies that in order to plot the minimum level of BER of a particular subset of $\mathbf{C}_{64\times126}$, we assume the subsets at the higher levels of the tree structure (if any) to be inactive (not transmitting). With this approach, our intention is to neglect the effect of MAI on the subsequent stages of MUD due to the detection error induced in previous stages (second term in the denominator in (2.29). Still, in both the cases, the behavior of the subsets hardly shows any noticeable deviation as far as their order among the BER is concerned over a fixed span of E_b/N_o. Indirectly, this confirms that for the lower and higher values E_b/N_o, it is the two factors only: the value of N_{ef} and the net level of MAI on the subset, which controls this order. On the other hand, it also validates the fact that the propagation error from one stage to next hardly has any command over this order, even though it has a marginal impact on the overall error performance of the subsets.

In Figure 2.10 (a), we show the improvement achieved in error performance of the $\frac{N_k}{2}$ users of $\mathbf{C}_1^k$ (denoted as $\mathbf{C}_{1R}^k$ in Section 2.4.2, where $\mathbf{C}_1^k = \left[\mathbf{C}_{1L}^k|\mathbf{C}_{1R}^k\right]$), due to its complementary nature, as already explained in the previous section. For simulation, we consider $\mathbf{C}_{64\times96}$ (with two subsets $\mathbf{C}_1^k$ and $\mathbf{C}_2^k$). Four different values of t_d : 0(synchronous), $0.2T_c, 0.4T_c$, and, $0.5T_c$ are selected. With increase in the value of t_d, significant lowering in the level of BER is observed. Interestingly, for $t_d = 0.5T_c$

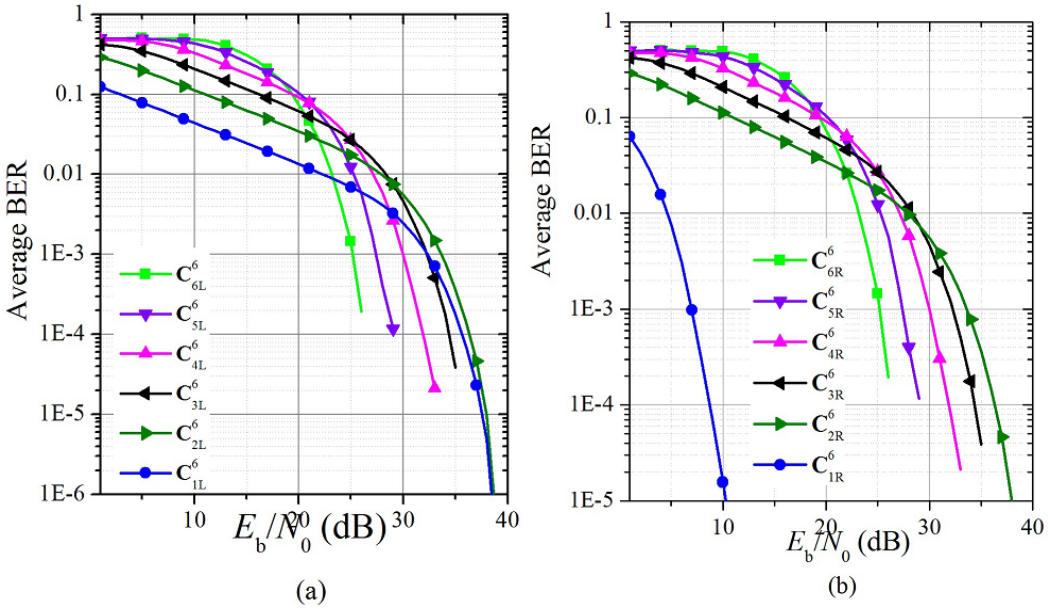

Figure 2.11: BER versus E_b/N_o performance comparison for $t_d = 0.5T_c$, for $\mathbf{C}_{64\times126} = [\mathbf{C}^6_1|\mathbf{C}^6_2|\mathbf{C}^6_3|\mathbf{C}^6_4|\mathbf{C}^6_5|\mathbf{C}^6_6]$, between (a) $\mathbf{C}_{1L}$, (b) $\mathbf{C}_{1R}$.

the curve defining the average BER of $\mathbf{C}^k_{1R}$ overlaps with that of the optimum error performance (of $\mathbf{H}_{64}$). This confirms the outcome of corollary 2. Figure 2.10 (b), similar to Figure 2.10 (a) presents the BER performance of the rest $\frac{N_k}{2}$ users of $\mathbf{C}^k_1$ (denoted as $\mathbf{C}^k_{1L}$). Unlike $\mathbf{C}^k_{1R}$, the level of BER for $\mathbf{C}^k_{1L}$ subjected to the increase in t_d remains undeviated from that of the synchronous case.

Figure 2.11 (a) and (b) corresponds to the error performance of left and right child of the individual subsets in $\mathbf{C}^6_{64\times126}$, for $t_d = 0.5T_c$ respectively. While for synchronous transmission ($t_d = 0$), the behavior of the left and right child of $\mathbf{C}^k_1$ is fully identical (shown in Section Figure 2.10), significant deviation can be recorded for $t_d = 0.5T_c$. For $t_d = 0.5T_c$ in Figure 2.11 (b), the only variation with respect to in Figure 2.11 (a) observed is the optimal error performance of $\mathbf{C}^6_{1R}$, which is due to the complementary feature as discussed in Corollary 2.

In Figure 2.12, the average error performance of the system is subjected to comparison under different loading conditions for $t_d = 0$ and $0.5T_c$ respectively. For $t_d = 0.5T_c$, the optimal error performance of $\mathbf{C}^6_{1L}$, as a whole, reduces the average error performance of $\mathbf{C}^6_1$, which sequentially reduces the average BER associated with the subsets detected in later stages of detection. Thus, the average level of BER for the overall SMOS, at a particular loading condition for $t_d = 0.5T_c$, always stands lower than that of $t_d = 0$. The variation in error performance subjected to the rise in the value of β

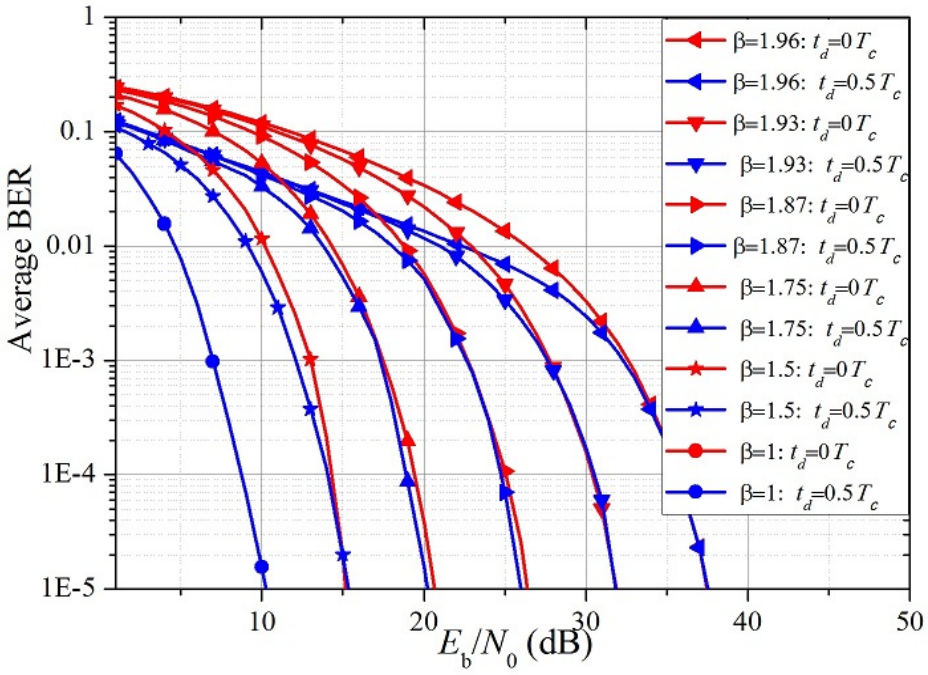

Figure 2.12: BER versus E_b/N_o performance comparison with increase in matrix dimension for $N_k = 64$ i.e.; $\mathbf{C}_{64\times64} = [\mathbf{C}_1^6]$, $\mathbf{C}_{64\times96} = [\mathbf{C}_1^6|\mathbf{C}_2^6]$, $\mathbf{C}_{64\times112} = [\mathbf{C}_1^6|\mathbf{C}_2^6|\mathbf{C}_3^6]$, $\mathbf{C}_{64\times120} = [\mathbf{C}_1^6|\mathbf{C}_2^6|\mathbf{C}_3^6|\mathbf{C}_4^6]$, $\mathbf{C}_{64\times124} = [\mathbf{C}_1^6|\mathbf{C}_2^6|\mathbf{C}_3^6|\mathbf{C}_4^6|\mathbf{C}_5^6]$, $\mathbf{C}_{64\times126} = [\mathbf{C}_1^6|\mathbf{C}_2^6|\mathbf{C}_3^6|\mathbf{C}_4^6|\mathbf{C}_5^6|\mathbf{C}_6^6]$ corresponding to $\beta = 1, 1.5, 1.75, 1.875, 1.94, 1.97$ (a) for $t_d = 0$ and (b) for $t_d = 0.5T_c$.

(for $k = 6$ or $N_k = 64$) is presented. To increase β, we continuously added the subsets one by one, following the tree hierarchy. We start with the largest subset of $\mathbf{C}_{64\times126}^6$ (i.e., $\mathbf{C}_1^6$) and subsequently, smaller subsets ($\mathbf{C}_2^6$, $\mathbf{C}_3^6$, $\mathbf{C}_4^6$, $\mathbf{C}_5^6$, $\mathbf{C}_6^6$) are added one-by-one in order to realize six different loading conditions: $\beta = 1.5, 1.75, 1.875, 1.94, 1.97$. For $\mathbf{C}_1^6$, having error performance identical to that of $\mathbf{H}_{64}$ is obvious, since according to construction of SMOS, $\mathbf{C}_1^6 = \mathbf{H}_{64}$. The degradation in level of BER with increase in β is due to the increase in the level of MAI and serial propagation of error from one stage to the next stage.

Figure 2.13, in overall, illustrates the periodic nature of the optimality criterion, as described in *Note 1*. Unlike $t_d = 0.5T_c$ in Figure 2.13 (a), the optimality nature of $\mathbf{C}_{1R}^k$ does not exist for $t_d = 1.5T_c$, which is quite evident from Figure 2.13 (b). However, for $t_d = 2.5T_c$, the optimal nature of $\mathbf{C}_{1R}^k$ again becomes prominent, as shown in Figure 2.13 (c).

Figure 2.14 validates the existence of an equivalent delay pair (t_{d1}, t_{d2}), e.g., $t_{d_1} = T_c - t_{d_2}$, for which similar level of BER is achievable. For simulation, we selected few such pairs: $(0, T_c), (0.2T_c, 0.8T_c), (0.4T_c, 0.6T_c)$. From the plots, it is easy to realize that for each set of EDP, the BER curves show complete overlapping over the scale of

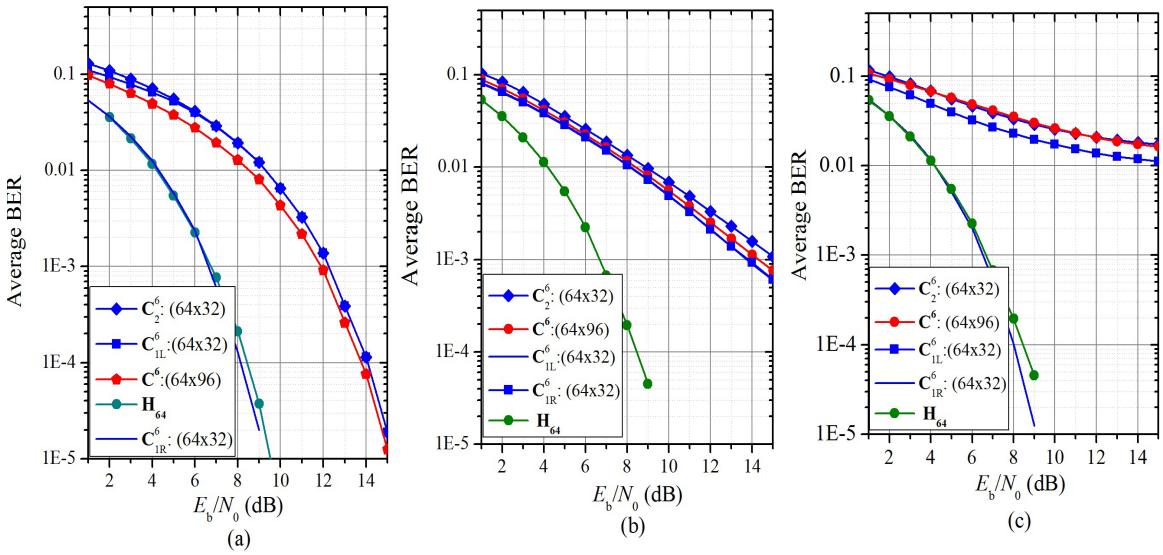

Figure 2.13: BER versus E_b/N_o performance comparison for TSMOS (Type I) $\mathbf{C}_{64\times96}$ for (a) $t_d = 0.5T_c$, (b) $t_d = 1.5T_c$, (c) $t_d = 2.5T_c$.

E_b/N_o and thus, proves its equivalence.

2.8 Summary

We investigated the problem of design a new set of UD matrices (i.e.; TSMOS) for overloaded CDMA system, which carries multiple orthogonal subsets (i.e.; first one binary Hadamard, and rest ternary). Based on the study of literature, first, we identified the basis matrix and built up a unique perspective towards the construction of the proposed matrix. While the orthogonality of each subset ensured for the zero intra-group MAI, the existing inter-group MAI among the subsets is balanced by the advantageous pattern of the twin-tree structured cross-correlation hierarchy. As a result, the linear decoding logic of MF became efficient to support as the fundamental block of the decoder for the errorfree recovery for the noiseless channel and consistently retained its simplicity in design even for the noisy case. For analyzing the error performance, we emphasized more on the individual subsets than that of the overall matrix and observed sheer non-uniformity in their order. The impact of the spreading diversity and MAI being jointly responsible for such unusual behavior of the BER curves was clearly explained concerning the derived expression of the average BER. The superiority in BER of SMOS over the binary random and WBE sequences was verified through simulation. On the other side, the superiority of the binary GCO matrices using SMLD over TSMOS was achieved at the cost of noticeable gain in the

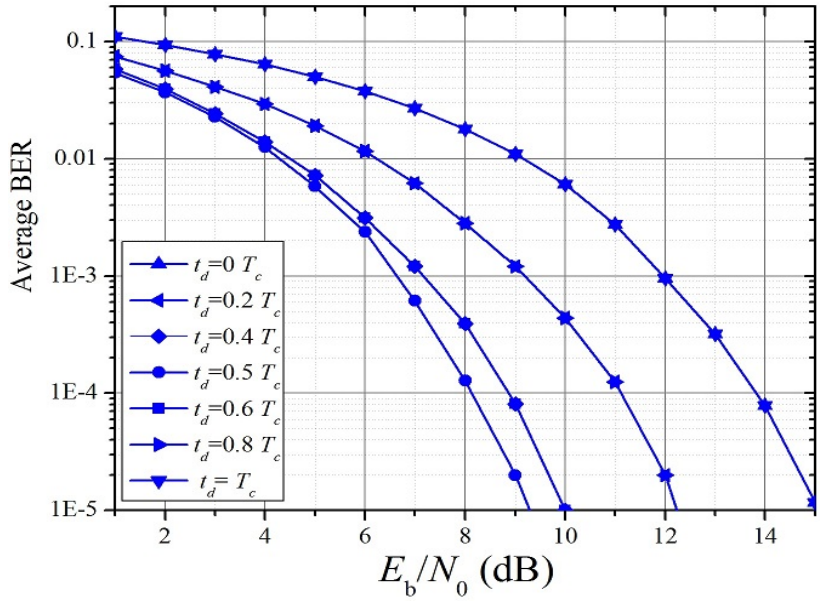

Figure 2.14: BER versus E_b/N_o performance comparison of $\mathbf{C}_{1R}$ of TSMOS (Type I) $\mathbf{C}_{64\times96}$ explaining the EDP.

complexity of SMLD over the proposed MUD. For synchronous noisy transmission, the average error performance of all the subsets was found to be sub-optimal. However, providing a timing delay ($0 < t_d < T_c$) in the transmission of any ternary subset with the binary (Hadamard) led to dramatic reduction in the level of MAI on the complementary signatures, due to that subset only, and thus improving their average error performance. Accordingly, having $t_d = 0.5T_c$ for all ternary subsets further facilitated the complementary signatures to attain optimality, where no deviation was reported about the sub-optimal nature of the rest. Later, we also discovered the periodic nature of occurrence of the optimal behavior, and presence of equivalent delay pair.

Table 2.6: Construction of multiple structures of TSMOS (shown in Table 2.3): $\mathbf{C}^3 = \left[\mathbf{C}_1^3|\mathbf{C}_2^3|\mathbf{C}_3^3\right]$ of Type II, Type III, Mixed Type I, Mixed Type II, and Mixed Type III. (For Type I, see Table 2.1).

Type II:

$$\mathbf{C}_1^3 = \tfrac{1}{\sqrt{8}}\left[\mathbf{H}_8\right], \mathbf{C}_2^3 = \tfrac{1}{\sqrt{8}}\begin{bmatrix} + & + & + & + \\ + & - & + & - \\ + & + & - & - \\ + & - & - & + \\ 0 & 0 & 0 & 0 \\ 0 & 0 & 0 & 0 \\ 0 & 0 & 0 & 0 \\ 0 & 0 & 0 & 0 \end{bmatrix} \quad \mathbf{C}_3^3 = \tfrac{1}{\sqrt{8}}\begin{bmatrix} + & + \\ + & - \\ 0 & 0 \\ 0 & 0 \\ 0 & 0 \\ 0 & 0 \\ 0 & 0 \\ 0 & 0 \end{bmatrix}$$

Type III

$$\mathrm{C}_1^3 = \tfrac{1}{\sqrt{8}}\left[\mathbf{H}_8\right], \mathbf{C}_2^3 = \tfrac{1}{\sqrt{8}}\begin{bmatrix} + & + & + & + \\ 0 & 0 & 0 & 0 \\ 0 & 0 & 0 & 0 \\ + & - & + & - \\ + & + & - & - \\ 0 & 0 & 0 & 0 \\ 0 & 0 & 0 & 0 \\ + & - & - & + \end{bmatrix} \quad \mathbf{C}_3^3 = \tfrac{1}{\sqrt{8}}\begin{bmatrix} + & + \\ 0 & 0 \\ 0 & 0 \\ 0 & 0 \\ 0 & 0 \\ 0 & 0 \\ 0 & 0 \\ + & - \end{bmatrix}$$

Mixed Type I:

$$\mathbf{C}_1^3 = \tfrac{1}{\sqrt{8}}\left[\mathbf{H}_8\right] \ \mathbf{C}_2^3 = \tfrac{1}{\sqrt{8}}\begin{bmatrix} + & + & 0 & 0 \\ 0 & 0 & + & + \\ + & - & 0 & 0 \\ 0 & 0 & + & - \\ + & + & 0 & 0 \\ 0 & 0 & - & - \\ + & - & 0 & 0 \\ 0 & 0 & - & + \end{bmatrix} \quad \mathbf{C}_1^3 = \tfrac{1}{\sqrt{8}}\begin{bmatrix} + & 0 \\ 0 & 0 \\ 0 & 0 \\ 0 & + \\ + & 0 \\ 0 & 0 \\ 0 & 0 \\ 0 & - \end{bmatrix}$$

Mixed Type II:

$$\mathbf{C}_1^3 = \tfrac{1}{\sqrt{8}}\left[\mathbf{H}_8\right], \ \mathbf{C}_2^3 = \tfrac{1}{\sqrt{8}}\begin{bmatrix} + & + & 0 & 0 \\ + & - & 0 & 0 \\ + & + & 0 & 0 \\ + & - & 0 & 0 \\ 0 & 0 & + & + \\ 0 & 0 & + & - \\ 0 & 0 & - & - \\ 0 & 0 & - & + \end{bmatrix} \quad \mathbf{C}_3^3 = \tfrac{1}{\sqrt{8}}\begin{bmatrix} + & 0 \\ + & 0 \\ 0 & 0 \\ 0 & 0 \\ 0 & 0 \\ 0 & 0 \\ 0 & + \\ 0 & - \end{bmatrix}$$

Mixed Type III:

$$\mathbf{C}_1^3 = \tfrac{1}{\sqrt{8}}\left[\mathbf{H}_8\right], \ \mathbf{C}_2^3 = \tfrac{1}{\sqrt{8}}\begin{bmatrix} + & + & 0 & 0 \\ 0 & 0 & + & + \\ 0 & 0 & + & - \\ + & - & 0 & 0 \\ + & + & 0 & 0 \\ 0 & 0 & - & - \\ 0 & 0 & - & + \\ + & - & 0 & 0 \end{bmatrix} \quad \mathbf{C}_3^3 = \tfrac{1}{\sqrt{8}}\begin{bmatrix} + & 0 \\ 0 & 0 \\ 0 & 0 \\ 0 & + \\ 0 & - \\ 0 & 0 \\ 0 & 0 \\ + & 0 \end{bmatrix}$$

Chapter 3
$2k$-ary SMOS: Extending the Scope beyond TSMOS

3.1 Introduction

In Chapter 2, the introductory discussion on SMOS is limited to the construction of ternary matrices, the illustration of their *twin tree hierarchy* of correlation pattern, the design of the simplified MUD followed by the validation of its errorless decoding, and above all, the performance analysis for noisy transmission. Furthermore, TSMOS being a subset to the matrices in literature [8–10, 92] implies that their efficient decoding for noisy channel is also possible, but at the cost of the sacrifice concerning the loss in asymptotic equality. As a noticeable observation, the unusual behavior of the error performance of the individual orthogonal subsets is recorded, for which the progressive variation in cardinality and pattern of MAI are shown to be responsible. However, the relevant queries those have remained unanswered and hence, become our source of encouragement for further research in this paper are:

- if the existence of non-ternary version of SMOS is realizable,
- if yes, then how the approach of construction is going to vary from the ternary,
- what difference will be observed in the error performance of its individual subsets for noisy channel,
- whether there prevails any scope to achieve optimality as in the case of TSMOS, either wholly or partially, and
- lastly, which of them (ternary or non-ternary) has the overall superiority in error performance.

In this chapter, we address the above queries chronologically. First, we propose the non-ternary version of SMOS, where the elements used in the construction of each subset are binary, and the set of binary alphabets in each subset are unique. In total, $2k$ number of alphabets are involved in the construction of the SMOS with index-k (i.e.;

$\mathbf{C}^k$). So, we call it $2k$-ary SMOS. For synchronous transmission, 50% signatures of its largest subset (binary) are recognized to be optimal. While both types of constructions (ternary and $2k$-ary), in overall, replicate a twin tree structured correlation among the signatures, notable difference in the value and pattern of their correlation coefficients is recorded. Hence, expecting the proportional deviation in error performance of their individual subsets as compared to ternary is easily predictable and verified through simulation. The fact that makes this contribution more productive is its approach of analysis of the error performance. Here, we firmly emphasize on the overall study of error performance to be partitioned into that of the smaller subsets, rather than just accepting the average BER of the whole SMOS for evaluation. While for ternary, this classification results in k separate subsets, that for the $2k$-ary, to validate the current non-uniformity in MAI split it further into two smaller counterparts, and thus, produces $2k$ number of subsets, in total. With this extensive segregation, the objective to compare the error performance between $2k$-ary and ternary demands a significant number of simulations to be accomplished. Moreover, due to multiple abnormalities and non-uniformity captured in the simulation results, the extraction of a concrete decision about the superiority (ternary versus $2k$-ary) also gets complex. To offer a simplified explanation, we introduce few logical anomalies and trade-off that collectively bring sufficient insight towards the apprehension of their overall performance. By and large, the rigorous analysis of the MAI hierarchy, comparative elaboration of the error performance under different loading conditions, the interesting outcomes and above all, their logical validations imbibe further gravity into the whole discussion, in this chapter.

We organize the remaining part of this chapter as follows. Section 3.2 describes the brief review to the construction of TSMOS. In Section 3.3, we focus on the structure and correlation of the basis set followed by the recursive construction. Section 3.4 deals with the explanation of the correlation hierarchy. Section 3.5 describes about the MUD. Section 3.6, being an important section, emphasizes on the error performance of $2k$-ary and its significant deviation from that of ternary followed by the appropriate explanation. In Section 3.7, the simulation results are logically analyzed. Finally, the conclusion is presented in Section 3.8.

3.2 Review of TSMOS

Let us start from the introductory literature on TSMOS in Chapter 2. Based on its definition from Section 2.3, the matrix $\mathbf{C}_{N_k \times M_k}$ is said to be SMOS over the input $\{0, 1, -1\}$, if the following conditions are satisfied.

- $\mathbf{C}^k$ is UD over $\{0, 1, -1\}^{M_k}$.
- $\mathbf{C}^k$ comprises of k orthogonal subsets, such that $\mathbf{C}^k = \left[\mathbf{C}_1^k | \mathbf{C}_2^k | \cdots | \mathbf{C}_k^k\right]$, where the number of signatures in subset-$\mathbf{C}_i^k$ is $\frac{N_k}{2^{i-1}}$.
- $\mathbf{Det}(\rho) = 0$, for $\rho = (\mathbf{C}^k)^T \mathbf{C}^k$
- The level of PA of an arbitrary signature in subset-$\mathbf{C}_i^k$ must be greater than the TPC from $(k - i)$ successive subsets: $\mathbf{C}_{i+1}^k, \mathbf{C}_{i+2}^k, \ldots, \mathbf{C}_k^k$, which is the sufficient condition for the MF decoding of each subset to be errorless. Mathematically, it is described by the relation:

$$\rho_{ii}(u, u) > \sum_{j=i+1}^{k} \sum_{v=1}^{\frac{N_k}{2^{j-1}}} \rho_{ij}(u, v). \tag{3.1}$$

In the next section and onwards, our objective not only just lies in proposing the non-ternary version of SMOS, but also in presenting a comparative overview of the features of the new construction in contrast to its existing counterpart (i.e.; TSMOS in Chapter 2). Apart from refining the concepts of SMOS through a generalized perspective, our approach also provides an opportunity to reveal about, which of them carries the ultimate superiority in error performance for noisy transmission.

3.3 Construction of 2k-ary SMOS

3.3.1 Correlation Structure of the Basis Matrix

In Section 2.2, the role of the basis matrix $\mathbf{B} = \begin{bmatrix} + & + & | & + \\ + & - & | & 0 \end{bmatrix} = [\mathbf{c}_{11}\mathbf{c}_{21} | \mathbf{c}_{21}]$ in recursively driving the construction and decoding of SMOS has been explained in detail. So, prior to proposing the 2k-ary SMOS, investing equal emphasis on analysis of the structure of the its basis matrix $\mathbf{B}'$ is of high importance, where

$$\mathbf{B}' = \begin{bmatrix} + & + & | & 1/2 \\ + & - & | & 1/2 \end{bmatrix} \tag{3.2}$$

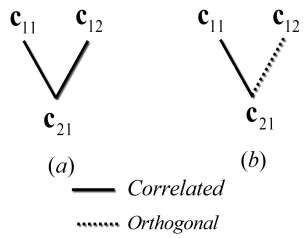

Figure 3.1: Comparison of Tree hierarchy of Basis sets: (a) for $\mathbf{B}$ (Ternary), (b) for $\mathbf{B}'$ ($2k$-ary).

First, let us draw a comparison of the correlation matrices (ρ and $\rho\prime$) of the respective basis sets i.e.; $\mathbf{B}$ and $\mathbf{B}'$, where both

$$\boldsymbol{\rho} = \mathbf{B}^T\mathbf{B} = \begin{bmatrix} 1 & 0 & 1/2 \\ 0 & 1 & 1/2 \\ 1/2 & 1/2 & 1/2 \end{bmatrix} = \begin{bmatrix} \rho_{11} & \rho_{12} & \rho_{13} \\ \rho_{21} & \rho_{22} & \rho_{23} \\ \rho_{31} & \rho_{32} & \rho_{33} \end{bmatrix} \text{ and} \tag{3.3}$$

$$\boldsymbol{\rho}' = (\mathbf{B})^T\mathbf{B} = \begin{bmatrix} 1 & 0 & 1/2 \\ 0 & 1 & 0 \\ 1/2 & 0 & 1/4 \end{bmatrix} = \begin{bmatrix} \rho'_{11} & \rho'_{12} & \rho'_{13} \\ \rho'_{21} & \rho'_{22} & \rho'_{23} \\ \rho'_{31} & \rho'_{32} & \rho'_{33} \end{bmatrix} \tag{3.4}$$

carrying an organized correlation pattern, can be translated to a meaningful two level tree hierarchy, as shown in Figure 3.1. Below, we arrange its important outcomes.

• The node (signature) $\mathbf{c}_{21}$ at the bottom level can be interpreted as the root to two signatures (i.e.; $\mathbf{c}_{11}$: left child, $\mathbf{c}_{12}$: right child) of the top level.

• For $\mathbf{B}$, there exists equal level of correlation between $\mathbf{c}_{11}$, $\mathbf{c}_{21}$, and $\mathbf{c}_{12}$, $\mathbf{c}_{21}$ i.e.; $\rho_{13} = \rho_{23} = 1/2$ (uniform). In contrast, the correlation is not equal for $\mathbf{B}'$ i.e.; $\rho\prime_{13} = 1/2$, $\rho\prime_{23} = 0$ (non-uniform)

• Unlike $\mathbf{B}$, the right child ($\mathbf{c}_{12}$) available in the topmost level is always *optimal* due to its complete orthogonality i.e.; $\rho\prime_{23} = 0$

• Besides cross-correlation, the difference in the level of PA is also noteworthy e.g; $\rho_{11} = \rho_{22} = \rho\prime_{11} = \rho\prime_{22} = 1$ (i.e.; $\rho\prime_{11} = \rho_{11}, \rho\prime_{22} = \rho_{22}$), where as $\rho_{33} = 1/2$, $\rho\prime_{33} = 1/4$ (i.e.; $\rho\prime_{33} \neq \rho_{33}$). It distinctly indicates the mismatch persisting in the level of PA for the signature that is not a part of the largest subset (binary Hadamard matrix).

• Despite the above variation from TSMOS, the criterion for the errorless decoding (2.21) remains valid for each signature of $2k$-ary SMOS.

Table 3.1: Construction of $2k$-ary SMOS Matrices for $k = 1, 2, 3$ e.g., $\mathbf{C}^1 = [\mathbf{C}_1^1]$, $\mathbf{C}^2 = [\mathbf{C}_1^2|\mathbf{C}_2^2]$, $\mathbf{C}^3 = [\mathbf{C}_1^3|\mathbf{C}_2^3|\mathbf{C}_3^3]$

$$\mathrm{C}_1^1 = \tfrac{1}{\sqrt{2}}\left[\mathbf{H}_2\right]$$

$$\mathbf{C}_1^2 = \tfrac{1}{\sqrt{4}}\left[\mathbf{H}_8\right], \mathbf{C}_2^2 = \tfrac{1}{\sqrt{4}}\begin{bmatrix} 1/2 & 1/2 \\ 1/2 & 1/2 \\ 1/2 & -1/2 \\ 1/2 & -1/2 \end{bmatrix}$$

$$\mathbf{C}_1^3 = \tfrac{1}{\sqrt{8}}\left[\mathbf{H}_8\right], \mathbf{C}_2^3 = \tfrac{1}{\sqrt{8}}\begin{bmatrix} 1/2 & 1/2 & 1/2 & 1/2 \\ 1/2 & 1/2 & 1/2 & 1/2 \\ 1/2 & -1/2 & 1/2 & -1/2 \\ 1/2 & -1/2 & 1/2 & -1/2 \\ 1/2 & 1/2 & -1/2 & -1/2 \\ 1/2 & 1/2 & -1/2 & -1/2 \\ 1/2 & -1/2 & -1/2 & 1/2 \\ 1/2 & -1/2 & -1/2 & 1/2 \end{bmatrix} \mathbf{C}_1^3 = \tfrac{1}{\sqrt{8}}\begin{bmatrix} 1/2^2 & 1/2^2 \\ 1/2^2 & 1/2^2 \\ 1/2^2 & 1/2^2 \\ 1/2^2 & 1/2^2 \\ 1/2^2 & -1/2^2 \\ 1/2^2 & -1/2^2 \\ 1/2^2 & -1/2^2 \\ 1/2^2 & -1/2^2 \end{bmatrix}$$

3.3.2 Recursive Construction

Based on the above developments in the structure of $\mathbf{B}'$, we propose the following recurrent approach for the construction of the matrices with larger dimension i.e.; $\mathbf{C}_{N_k \times M_k}$ for $N_k = 2^k$ where $k \in \mathbf{Z}^+$, such that

- Initialize $\mathbf{C}^0 = [1]$ and find $\mathbf{C}^1 = \left(\frac{1}{\sqrt{2}}\mathbf{H}_{2\times 2} \otimes \mathbf{C}^0\right) = \frac{1}{\sqrt{2}}\mathbf{H}_2$
- For $k > 1$, $\mathbf{C}^k = \left(\frac{1}{\sqrt{2}}\mathbf{H}_{2\times 2} \otimes \mathbf{A}\right)$, where

$$\mathbf{A} = \begin{bmatrix} \mathbf{C}^{k-1} & | & \begin{bmatrix} 1/2^{k-1} & 1/2^{k-1} & \cdots & 1/2^{k-1} \end{bmatrix}^T_{1\times 2^{k-1}} \end{bmatrix}$$

Table 3.1 illustrates the construction of $2k$-ary SMOS for $k = 1, 2, 3$. As evident, for $\mathbf{C}^3 = \left[\mathbf{C}_1^3|\mathbf{C}_2^3|\mathbf{C}_3^3\right]$, the elements of each subset are binary and these binary elements (alphabets or symbols) differ from one subset to other e.g.; $\mathbf{C}_1^3 \in \{1, -1\}^8$, $\mathbf{C}_2^3 \in \{1/2, -1/2\}^4$,$\mathbf{C}_3^3 \in \{1/2^2, -1/2^2\}^2$. Also, we may define it as $\mathbf{C}^3 \in \{1, 1/2, 1/2^2, -1/2^2, -1/2, -1\}^{14}$. In general, the matrix $\mathbf{C}^k \in \{1, 1/2, 1/2^2, 1/2^3, \cdots, -1/2^3, -1/2^2, -1/2, -1\}^{M_k}$ for its construction, requires $2k$ number of elements, where the nature of each subset, individually, is binary e.g.; $\mathbf{C}_1^k \in \{1, -1\}^{N_k}, \mathbf{C}_2^k \in \{1/2, -1/2\}^{N_k/2}, \mathbf{C}_3^k \in \{1/2^2, -1/2^2\}^{N_k/2^2}, \cdots, \mathbf{C}_k^k \in \{1/2^{k-1}, -1/2^{k-1}\}^2$. The steps to prove the UD nature of the above construction are similar to that of the proof in 2.3. Without loss in generality of the construction approach, the relation $M_k = (2N_k - 2)$ is maintained for each value of k, thereby allowing a maximum achievable value of β to approach 2 i.e.; $\lim_{N_k \to \infty} \beta_k = \lim_{N_k \to \infty} \left(\frac{M_k}{N_k}\right) = 2$.

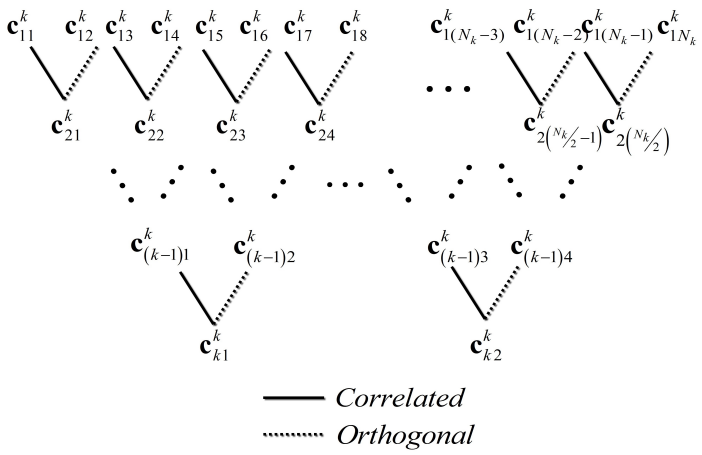

Figure 3.2: Twin Tree Hierarchy for $\mathbf{C}^k$ ($2k$-ary SMOS)

3.4 Hierarchy of MAI

As an important inference from the discussion of the basis matrices (in Section 3.3), the *two level* tree hierarchy of $\mathbf{B}'$ in comparison to that of $\mathbf{B}$ is found to be non-uniform. To have a broader vision of the statistics involved in the correlation pattern, let us look upon the *multi level* hierarchy of $2k$-ary SMOS $\mathbf{C}^k$, where the nodes of the tree at a particular level (depth) $l = 1, 2, \ldots, k$ (i.e., $l = k-i+1$ for $1 \leq i \leq k$) collectively form the subset-$\mathbf{C}^k_{k-l+1}$. The following observations collaboratively provide an appropriate summarization.

• There exist two identical (twin) trees, each of which has its origin or root from the smallest orthogonal subset (i.e.; $\mathbf{C}^k_k$ at the lowest level of the tree, $l = 1$). The nodes at the highest level of the tree ($l = k$) represent the largest subset: $\mathbf{C}^k_1$.

• Each node (parent) at level-l can be interpreted to generate two child nodes for its next higher level i.e.; level-$(l+1)$, of which, the *left child* (connected by *solid lines* in Figure 3.2) is correlated to the parent node, where as no such correlation exists for the *right child* (connected by *dotted lines*).

• Each left child at level-l is correlated to its left child in the subsequent upper levels (i.e.; level-$(l+1)$ to k) and lower levels (i.e.; level-$(l-1)$ to 1) e.g.;

$$\mathbf{c}^k_{(k)(2j-1)} = 2\mathbf{c}^k_{(k-1)(j)},\ \ldots,\ \mathbf{c}^k_{(l+1)(2j-1)} = 2\mathbf{c}^k_{(l)(j)},\ \mathbf{c}^k_{(l)(2j-1)} = 2\mathbf{c}^k_{(l-1)(j)},\ \ldots,$$
$$\mathbf{c}^k_{(l-(l-2))(2j-1)} = 2\mathbf{c}^k_{(l-(l-1))(j)} \text{ for } 1 \leq j \leq 2^l$$

and *orthogonal* (zero correlation) to all its right child lying in the subsequent upper levels.

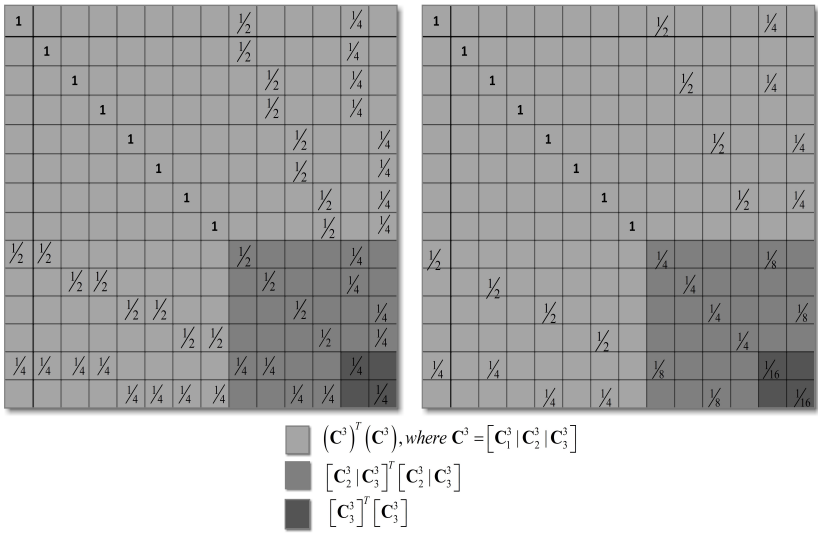

Figure 3.3: Correlation Matrix corresponding to $\mathbf{C}^3$ for (a) SMOS (ternary), (b) SMOS (2k-ary)

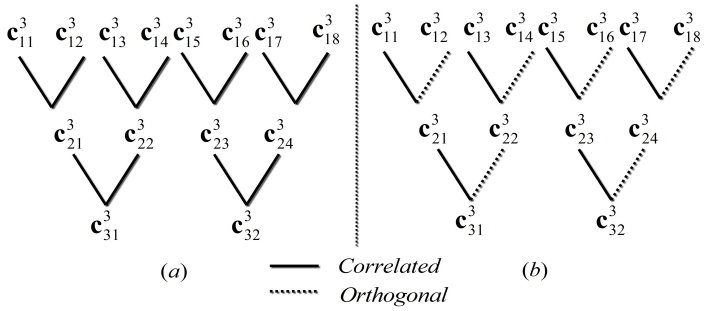

Figure 3.4: Twin Tree Hierarchy corresponding to $\mathbf{C}^3$ for (a) SMOS (ternary), (b) SMOS (2k-ary)

• On the other hand, each right child at level-l is correlated to its left child in the subsequent upper levels only. To all other nodes of the whole tree, it is fully orthogonal. Therefore, the left child at each level confronts a relatively high level of MAI over the right and subsequently for $l = k$, the right child corresponding to each root node in $l = (k-1)$ is under *zero MAI* and hence, justifies its *optimality*.

With an aim to offer better insight to the differences existing in the correlation pattern, between the ternary and $2k$-ary, we present the correlation matrices for $\mathbf{C}^3 = [\mathbf{C}_1^3|\mathbf{C}_2^3|\mathbf{C}_3^3]$ and the corresponding twin tree structured hierarchy in Figure 3.3 and 3.4 respectively. From the perspective of the basis matrix, it is important to note that simply substituting $\mathbf{c}_{21} = [1/2 \ \ -1/2]^T$ in (3.2) also retains the power of $\mathbf{B}'$ to generate the desired SMOS, with the only variation added in the form of switching of the behavior between the left and right child. In other words, the pattern of MAI related to the left and right child corresponding to the present construction (Table 3.1) will be conveyed by the right and left child of the newly produced one.

3.5 Design of MUD

In Section 2.5, the proof of the errorfree decoding of the ternary SMOS is already explained in Lemma 1, where the criterion in (3.1) primarily regularizes the errorfree validation at each stage of detection. Due to the resemblance in construction and pattern of MAI, an analogous approach can also be adopted to justify the errorless decoding of $2k$-ary. Equivalently, the design of MUD proposed for TSMOS (shown by in Figure 2.6) is also applicable for the decoding of $2k$-ary. Therefore, the advantage in terms of MUD's simplicity is also available for $2k$-ary SMOS.

3.6 Error Performance Analysis

3.6.1 Expression for Average BER

Based on the discussion from the previous section, let us first rewrite the expression in (2.1) so as to support our analysis involving the left and right child in each subset of $2k$-ary i.e.;

$$\mathbf{y} = \sum_{u=1}^{k} \mathbf{C}_{uL}^{k} \mathbf{x}_{uL} + \sum_{v=1}^{k} \mathbf{C}_{vR}^{k} \mathbf{x}_{vR} + \mathbf{n}. \tag{3.5}$$

To have the expression for the average BER of the left and right child of subset-$\mathbf{C}_i^k$, it is logical to modify the expression of BER for the individual subsets of TSMOS, presented in (2.29). Finally, we present the corresponding expressions in Table 3.2, which indicates the difference existing in the average error performance of different smaller subsets, thereby embracing the existing outcomes related to their non-uniformity in MAI. Afterwards, regardless of the type, our approach to analyze the behavior of each subset (say $\mathbf{C}_i^k$) is, therefore, divided in terms of its constituents subsets (i.e.; $\mathbf{C}_{iL}^k$ and $\mathbf{C}_{iR}^k$).

3.6.2 Analysis involving fundamental metrics: A Closer Overview

Before we switch to the error performance analysis in next section, it is highly imperative to consider the variation in the behavior of the basic metrics (i.e.; TPC and PA) controlling the quality of recovery of the MUD. According to Figure 2.6, for the errorless MF detection of different subsets (i.e.; $\mathbf{C}_1^k, \mathbf{C}_2^k, \mathbf{C}_3^k, \ldots, \mathbf{C}_k^k$) from the respective received vectors (i.e.; $\mathbf{y}_1$, $\mathbf{y}_2$, $\mathbf{y}_3$, $\ldots$, $\mathbf{y}_k$.), the inequality in (3.1) is to be satisfied. In Table 3.3, we describe the statistics involving these metrics for the

Table 3.2: Expression for the Average BER of different subsets in SMOS ($2k$-ary)

Subset	Average BER
$\mathbf{C}_{1R}^{k}$	$Q\left(\sqrt{\frac{\mathrm{E}\left(\mathrm{x}_{1\mathrm{R_j}}^2\right)}{\mathrm{E}\left(\mathrm{n}_{\mathrm{i(j)}}^2\right)}}\right)$
$\mathbf{C}_{iR}^{k}\ (2 \leq i \leq k)$	$Q\left(\sqrt{\frac{\left(\frac{1}{4^{i-1}}\right)^2 \mathrm{E}\left(\mathrm{x}_{1\mathrm{R_j}}^2\right)}{4\sum_{v=1}^{i-1}\left(\rho'_{iRv(j)}\right)^2+\mathrm{E}\left(\mathrm{n}_{\mathrm{i(j)}}^2\right)}}\right)$
$\mathbf{C}_{iL}^{k}\ (1 \leq i \leq k)$	$Q\left(\sqrt{\frac{\left(\frac{1}{4^{i-1}}\right)^2 \mathrm{E}\left(\mathrm{x}_{\mathrm{iL_j}}^2\right)}{\sum_{u=i+1}^{k}\left(\rho_{iLu(j)}^2\right)^2+4\sum_{v=1}^{i-1}\rho_{iLv(j)}^2 P_e^v+\mathrm{E}\left(\mathrm{n}_{\mathrm{i(j)}}^2\right)}}\right)$

Table 3.3: Comparison of the inequality $\rho_{ii}(u,u) > \sum_{j=i+1}^{k}\sum_{v=1}^{\frac{N_k}{2^{j-1}}}\rho_{ij}(u,v)$ for each subset in $\mathbf{C}_{64\times126}^{6} = \left[\mathbf{C}_{1L}^{6}|\mathbf{C}_{1R}^{6}|\mathbf{C}_{2L}^{6}|\mathbf{C}_{2R}^{6}|\mathbf{C}_{3L}^{6}|\mathbf{C}_{3R}^{6}|\mathbf{C}_{4L}^{6}|\mathbf{C}_{4R}^{6}|\mathbf{C}_{5L}^{6}|\mathbf{C}_{5R}^{6}|\mathbf{C}_{6L}^{6}|\mathbf{C}_{6R}^{6}\right]$ (ternary and $2k$-ary), prior to applying the MF decoding in the respective stages (see Figure 2.6)

Subset ($\downarrow$)	Ternary SMOS	$2k$-ary SMOS
$\mathbf{C}_{1L}^{6}$	$1 > \left(\frac{1}{2}+\frac{1}{2^2}+\frac{1}{2^3}+\frac{1}{2^4}+\frac{1}{2^5}\right)$	$1 > \left(\frac{1}{2}+\frac{1}{2^2}+\frac{1}{2^3}+\frac{1}{2^4}+\frac{1}{2^5}\right)$
$\mathbf{C}_{1R}^{6}$	$1 > \left(\frac{1}{2}+\frac{1}{2^2}+\frac{1}{2^3}+\frac{1}{2^4}+\frac{1}{2^5}\right)$	$1 > 0$
$\mathbf{C}_{2L}^{6}$	$\frac{1}{2} > \left(\frac{1}{2^2}+\frac{1}{2^3}+\frac{1}{2^4}+\frac{1}{2^5}\right)$	$\frac{1}{2^2} > \left(\frac{1}{2^3}+\frac{1}{2^4}+\frac{1}{2^5}+\frac{1}{2^6}\right)$
$\mathbf{C}_{2R}^{6}$	$\frac{1}{2} > \left(\frac{1}{2^2}+\frac{1}{2^3}+\frac{1}{2^4}+\frac{1}{2^5}\right)$	$\frac{1}{2^2} > 0$
$\mathbf{C}_{3L}^{6}$	$\frac{1}{2^2} > \left(\frac{1}{2^3}+\frac{1}{2^4}+\frac{1}{2^5}\right)$	$\frac{1}{2^4} > \left(\frac{1}{2^5}+\frac{1}{2^6}+\frac{1}{2^7}\right)$
$\mathbf{C}_{3R}^{6}$	$\frac{1}{2^2} > \left(\frac{1}{2^3}+\frac{1}{2^4}+\frac{1}{2^5}\right)$	$\frac{1}{2^4} > 0$
$\mathbf{C}_{4L}^{6}$	$\frac{1}{2^3} > \left(\frac{1}{2^4}+\frac{1}{2^5}\right)$	$\frac{1}{2^6} > \left(\frac{1}{2^7}+\frac{1}{2^8}\right)$
$\mathbf{C}_{4R}^{6}$	$\frac{1}{2^3} > \left(\frac{1}{2^4}+\frac{1}{2^5}\right)$	$\frac{1}{2^6} > 0$
$\mathbf{C}_{5L}^{6}$	$\frac{1}{2^4} > \left(\frac{1}{2^5}\right)$	$\frac{1}{2^8} > \left(\frac{1}{2^9}\right)$
$\mathbf{C}_{5R}^{6}$	$\frac{1}{2^4} > \left(\frac{1}{2^5}\right)$	$\frac{1}{2^8} > 0$
$\mathbf{C}_{6L}^{6}$	$\frac{1}{2^5} > 0$	$\frac{1}{2^{10}} > 0$
$\mathbf{C}_{6R}^{6}$	$\frac{1}{2^5} > 0$	$\frac{1}{2^{10}} > 0$

decoding of $\mathbf{C}^6 = \left[\mathbf{C}_1^6|\mathbf{C}_2^6|\mathbf{C}_3^6|\mathbf{C}_4^6|\mathbf{C}_5^6|\mathbf{C}_6^6\right]$ (i.e.; N_k=64 and M_k=126). We position them separately for both ternary and $2k$-ary SMOS, so that the transition in their values can be carefully scrutinized. Even if the smaller subsets ($\mathbf{C}_{iL}^6, \mathbf{C}_{iR}^6$) comprising the left and right child of subset-$\mathbf{C}_i^6$ (e.g.; $\mathbf{C}_i^6 = \left[\mathbf{C}_{iL}^6|\mathbf{C}_{iR}^6\right]$) are detected in the same stage of the decoder (stage-i), they are presented in separate (consecutive) rows, only to vindicate the difference in their pattern of MAI, as already discussed in Section 3.3. Below, we list the crucial remarks extracted from Table 3.3.

TPC and PA: (Left Child versus Right Child) For Ternary, both the left and right child in a subset (i.e.; $\mathbf{C}_{iL}^6$ and $\mathbf{C}_{iR}^6$) confronts identical level of TPC and PA. Consequently, for $2k$-ary, the level of TPC on the right child is always lower than that

of the left. Nevertheless, no such mismatch is reported in the level of PA.

TPC and PA: (Ternary versus $2k$-ary) Except $\mathbf{C}^6_{1L}$ and $\mathbf{C}^6_{1R}$, the level of PA and TPC for all other subsets of $2k$-ary lies lower than that of the ternary i.e.; $\sqrt{(\text{PA})_{2k-ary}} = (\text{PA})_{ternary}$ and $(\text{TPC})_{2k-ary} << (\text{TPC})_{ternary}$. For $\mathbf{C}^6_{1L}$ and $\mathbf{C}^6_{1R}$, the corresponding values are fully equal i.e.; $(\text{PA})_{2k-ary} = (\text{PA})_{ternary}$ and $(\text{TPC})_{2k-ary} = (\text{TPC})_{ternary}$.

(PA−TPC): (Ternary versus $2k$-ary) For $2k$-ary, first, the difference (PA − TPC) for the left and right child is significant for the larger subsets (i.e.; the higher level of the tree) and it shows a continuous fall as we proceed towards the smaller subsets (i.e.; lower level of the tree). Secondly, the gap between the difference of the left and right child (i.e.; $d = ((\text{PA} - \text{TPC})_L - (\text{PA} - \text{TPC})_R)$ is also more for the larger subset and gradually decreases towards the smaller ones. For the smallest subset (the bottommost level of the tree), the value of d becomes zero, thus implying the equality in the level of (PA − TPC), for both left and right child.

After the above description on the behavior of the metrics, an immediate retrospection may yield multiple estimations about their error performance. But, hardly any of them leads to a concrete projection of the reality. So, for a clear-cut summarization, we present the following inferences to provide an appropriate explanation towards the match between the theory (so far) and observations (simulation results in Section 3.7).

3.6.3 Trade-off: PA versus TPC

Consider the explanation in Section 3.6.2. In the context of $2k$-ary SMOS, it actually points to the trade-off associated with the level of PA and TPC for an arbitrary signature (left or right child) in a subset (except $\mathbf{C}^k_{1L}$). In fact, the structure of construction of $2k$-ary openly allows the TPC on its signature in any subset to remain always lower than that of ternary. So, for noisy transmission, the level of BER of the former becoming lower than that of the later is expected. But, at the same time, significant fall in the level of PA for the same signature of $2k$-ary is also discovered, which on the other hand indicates the rise in BER level. Therefore, leading

to a firm conclusion about their superiority becomes practically infeasible since, for a particular value of the SNR, realization of both the outcomes are considered as mutually exclusive. Purposefully, we leave it to be addressed in the simulation section.

3.6.4 Anomaly 1: Impact of Effective Peak Correlation (ρ_{ef})

According to Table 3.3, regardless of being the left or right child ($\mathbf{C}^6_{iL}$ or $\mathbf{C}^6_{iR}$), the level of PA and TPC on a signature in a subset of $2k$-ary SMOS (except $\mathbf{C}^6_{1L}$) always remains lower than that of ternary. For $\mathbf{C}^6_{1L}$, the deviation regarding the equality of the level of the corresponding metrics is realized and hence, anticipating their error performance to be identical is quite apparent. However, keeping in mind about the variation of the signature alphabets and their positioning across each subset, the probability of our expectation turning into a counter-intuitive outcome can not be fully overlooked. The following explanation offers a logical validation to this inference.

Assume two different signatures belonging to two different code sets (not necessarily SMOS) e.g.; $\mathbf{c}_{a1} \in \mathbf{C}_a \triangleq [\mathbf{c}_{a1}, \mathbf{c}_{a2}, \cdots, \mathbf{c}_{aN}]$ and $\mathbf{c}_{b1} \in \mathbf{C}_b \triangleq [\mathbf{c}_{b1}, \mathbf{c}_{b2}, \cdots, \mathbf{c}_{bN}]$, where $\mathbf{C}_a$, $\mathbf{C}_b \in \{1, -1, 0\}^N$. Also, assume the net level of MAI on $\mathbf{c}_{a1}$ and $\mathbf{c}_{b1}$ (due to the non-zero cross-correlation from remaining $(N-1)$ signatures) to be equal. While for $\mathbf{C}_a$ and $\mathbf{C}_b$ to be binary i.e.; $\mathbf{C}_a$, $\mathbf{C}_b \in \{1, -1\}^N$, the expression $\rho_{ij} = \sum_{n=1}^{N} c_{in}c_{jn}$ should be considered to measure the peak cross-correlation level between any two signatures ($\mathbf{c}_i = [c_{i1}, c_{i2}, \cdots, c_{iN}]$ and $\mathbf{c}_j = [c_{j1}, c_{j2}, \cdots, c_{jN}]$) of length N (for binary code set, $N_{ef_i} = N$ for $1 \leq i \leq N$), its importance looses its precision, if the code domain translates to ternary. This is because, for a ternary code space, the net peak cross-correlation on a signature is due to the non-zero elements (only) of other active signature sequences. Therefore, a more accurate tool of analysis is to define a new metric i.e.; *effective peak cross-correlation*, which is nothing but the normalized version of the peak cross-correlation. For instance, the effective peak-cross correlation due to c_j on c_i can be expressed as

$$\begin{aligned}\rho_{ef_{ij}} &= \left(\tfrac{1}{N_{ef_i}}\right) \sum_{n=1}^{N} c_{in}c_{jn} \ (\text{ for } N_{ef_i} < N_{ef_j}) \\ &= \left(\tfrac{1}{N_{ef_j}}\right) \sum_{n=1}^{N} c_{in}c_{jn} \ (\text{ for } N_{ef_i} > N_{ef_i}).\end{aligned}$$

Equivalently, the expression for the level of TPC on $\mathbf{c}_{a1}$ and $\mathbf{c}_{b1}$ can be expressed as $\rho_{ef_{a1}} = \sum_{i=1}^{N-1} \rho_{ef_{a1i}}$ and $\rho_{ef_{b1}} = \sum_{i=1}^{N-1} \rho_{ef_{b1i}}$ respectively. Without loss of generality, if the

concept of ρ_{ef} is imposed on $\mathbf{C}_{1L}^{6}$, the existing equality based on the concept of peak cross-correlation i.e.;

$$\left(\sum_{j=2}^{k}\sum_{v=1}^{\frac{N_k}{2^{j-1}}}\rho_{1j}(u,v)\right)_{ternary} = \left(\sum_{j=2}^{k}\sum_{v=1}^{\frac{N_k}{2^{j-1}}}\rho_{1j}(u,v)\right)_{2k-ary} \tag{3.6}$$

gets modified to the following inequality.

$$\left(\sum_{j=2}^{k}\sum_{v=1}^{\frac{N_k}{2^{j-1}}}\frac{\rho_{1j}(u,v)}{N_{ef_i}}\right)_{ternary} > \left(\sum_{j=2}^{k}\sum_{v=1}^{\frac{N_k}{2^{j-1}}}\frac{\rho_{1j}(u,v)}{N_{ef_i}}\right)_{2k-ary}. \tag{3.7}$$

Surprisingly enough, the expression in (3.7) now breaks its ambiguity in (3.6) related to superiority between the ternary and $2k$-ary for $\mathbf{C}_{1L}^{6}$, as the above inequality favors for the better error performance of $2k$-ary. Also, it can be clarified from the simulation results (in Figure 3.7 (a)). Please note that, for the left child in all other subsets (say $\mathbf{C}_i^k$ for $2 \leq i \leq k$), the relationship

$$\left(\sum_{j=i}^{k}\sum_{v=1}^{\frac{N_k}{2^{j-1}}}\rho_{ij}(u,v)\right)_{ternary} > \left(\sum_{j=2}^{k}\sum_{v=1}^{\frac{N_k}{2^{j-1}}}\rho_{1j}(u,v)\right)_{2k-ary} \tag{3.8}$$

always holds true, thus always satisfying the equivalent relation of (3.7), in default.

3.6.5 Anomaly 2: Impact of Free Diversity ($N_{fd_i} = \frac{N_{ef_i}}{2}$)

Let us revisit the structure of the ternary SMOS in Table 2.2. With reference to the expression of $\mathbf{y}$ for $\mathbf{C}^k = \left[\mathbf{C}_1^k|\mathbf{C}_2^k|\ldots|\mathbf{C}_k^k\right]$ in (2.1), for subset-$\mathbf{C}_i^k$ with effective spreading[1] gain N_{ef_i}, there exists $\frac{N_{ef_i}}{2}$ number of elements (chips) in $\mathbf{y}_i$ (see Figure 2.6) that carries the spread data of $\mathbf{C}_i^k$ with no MAI, *provided* the previous $(i-1)$ subsets are decoded with no error. The existence of such chips can be considered as the outcome of the tactical placement of the zero elements throughout the ternary structure. We call it *MAI free diversity* or simply *free diversity* for $\mathbf{C}_i^k$. Even if, the detection of the previous subsets go erroneous (for transmission to be noisy) leading to the inaccuracy in interference cancellation, the level of MAI in these chips still continues to be significantly lower than that of its remaining counterparts. As a result, having 50% of the transmitted diversities (chips) with zero or reduced MAI level, indeed, becomes an open scope for improving the BER of ternary SMOS. On a

[1]From Chapter 2, recall that the effective spreading gain N_{ef} for a signature is equal to its number of non-zero elements or cardinality.

note, no such advantage is spotted for the case of $2k$-ary due to the absence of the zero element in the available chips.

With the alleviation of loading condition by subsequent removal of the smaller subsets (lower level of tree hierarchy) in $\mathbf{C}^k$ (ternary or $2k$-ary), the level of MAI on an arbitrary signature of each active subset (based on the concept of ρ_{ef} in Anomaly-1) also decreases. While following *Anomaly-1*, for the left child, the superiority of $2k$-ary over ternary should prevail for noisy transmission, deflection in this regard may be perceived for relatively low loading condition. This translation is evidently due to the impact of free diversity that empowers the ternary to dominate. We call this transition of superiority (from $2k$-ary to ternary) as the *superiority crossover*. An elaborate picture of this transformation can be tracked in Table 3.4 presenting a comparative overview of the outcomes of Figure 3.10 and Figure 3.11.

3.7 Simulation Results

In this Section, we concentrate on the BER versus (E_b/N_0) performance of the system, assuming the channel to be AWGN. The system is supposed to be BPSK modulated, perfectly power controlled, and operated under synchronous transmission. Each figure illustrates the comparison between ternary and $2k$-ary with a specific purpose. Finally, we assimilate their outcomes in Table 3.4 so as to reach a conclusion about the superiority.

Figure 3.5 (a) and (b) presents the comparison of the average BER of the left child. For simulation, we choose $\mathbf{C}^6 = \mathbf{C}_{64\times126} = \left[\mathbf{C}_1^6|\mathbf{C}_2^6|\mathbf{C}_3^6|\mathbf{C}_4^6|\mathbf{C}_5^6|\mathbf{C}_6^6\right]$ as the encoding matrix. The decoder shown in Figure 2.6 is selected for detection. In Section 2.6, the role of N_{ef} and net MAI (or TPC) being responsible for the non-uniformity in response of the error performance of the individual subsets has already been explained, following which a dramatic lowering in the level of BER is observed for the smaller subsets (with lower N_{ef} or detected in the later stages of decoder) over the larger ones (higher N_{ef} or detected in the earlier stages), at higher values of E_b/N_o (see Fig 3.5 (a)). As the reason of this irregularity, the gradual reduction in the level of TPC with the progress of the decoding stages is reported to be accountable.

On the other hand, similar behavior is not observed for the $2k$-ary (Fig 3.5 (b)), even if the effect of reduced level of TPC on the subsequent smaller subsets (similar to

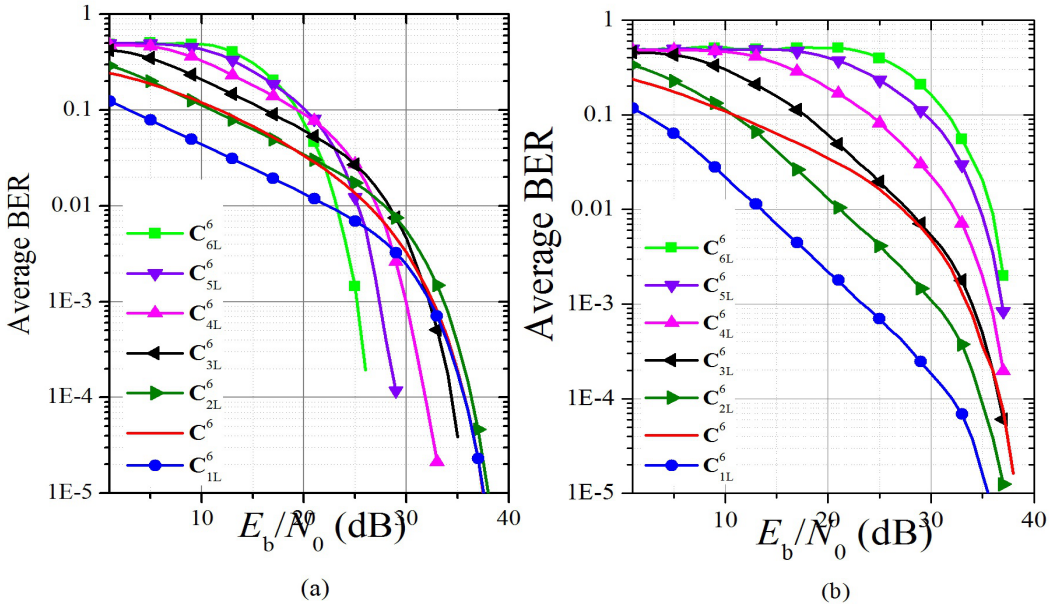

Figure 3.5: BER versus E_b/N_o performance comparison of the *Left* child in each subset of $\mathbf{C}^6_{64\times126} = [\mathbf{C}^6_{1L}|\mathbf{C}^6_{1R}|\mathbf{C}^6_{2L}|\mathbf{C}^6_{2R}|\mathbf{C}^6_{3L}|\mathbf{C}^6_{3R}|\mathbf{C}^6_{4L}|\mathbf{C}^6_{4R}|\mathbf{C}^6_{5L}|\mathbf{C}^6_{5R}|\mathbf{C}^6_{6L}|\mathbf{C}^6_{6R}]$ for (a) SMOS (ternary) (b) SMOS ($2k$-ary).

ternary) can still be found to exist. For this contrast, the effect of significant reduction in the level of PA for each subset (except $\mathbf{C}^6_1$) (e.g.; $\sqrt{(\rho_{ii})_{2k-ary}} = (\rho_{ii})_{ternary}$, see Section 3.6.2) is to be held responsible. Furthermore, for higher values of E_b/N_o, the convergence of the curves of different subsets is also captured, which is intrinsically due to the UD nature of construction that allows them to approach to the errorfree performance.

Figure 3.6 (a) and (b), being the right counterpart of Figure 3.5 (a) and (b), present the BER performance of the right child for ternary and $2k$-ary SMOS respectively. While for ternary, the behavior of the right child is fully identical to that of the left, observing a dramatic variation for $2k$-ary is well precedented. In fact, the explanation to this difference is straight i.e.; before MF detection, the level of TPC on the right child is notably less than that of the left (Section 3.6.2). The explanation to the noticeable degradation in BER performance of the smaller subsets is same as that of the left child in Figure 3.5 (a) i.e.; significant lowering of the level of PA.

Figure 3.7 being the distributed version of Fig 3.5, projects a one-to-one comparison of the performance of the left child. Our intention is to study the variation in their (ternary versus $2k$-ary) performance more vividly, followed by appropriate rationalization. Fig 3.7 (a) to (f) chronologically correspond to $\mathbf{C}^6_{1L}$,$\mathbf{C}^6_{2L}$, $\mathbf{C}^6_{3L}$,$\mathbf{C}^6_{4L}$, $\mathbf{C}^6_{5L}$, and $\mathbf{C}^6_{6L}$ respectively. Where for $\mathbf{C}^6_{1L}$, the superiority of the $2k$-ary is due to

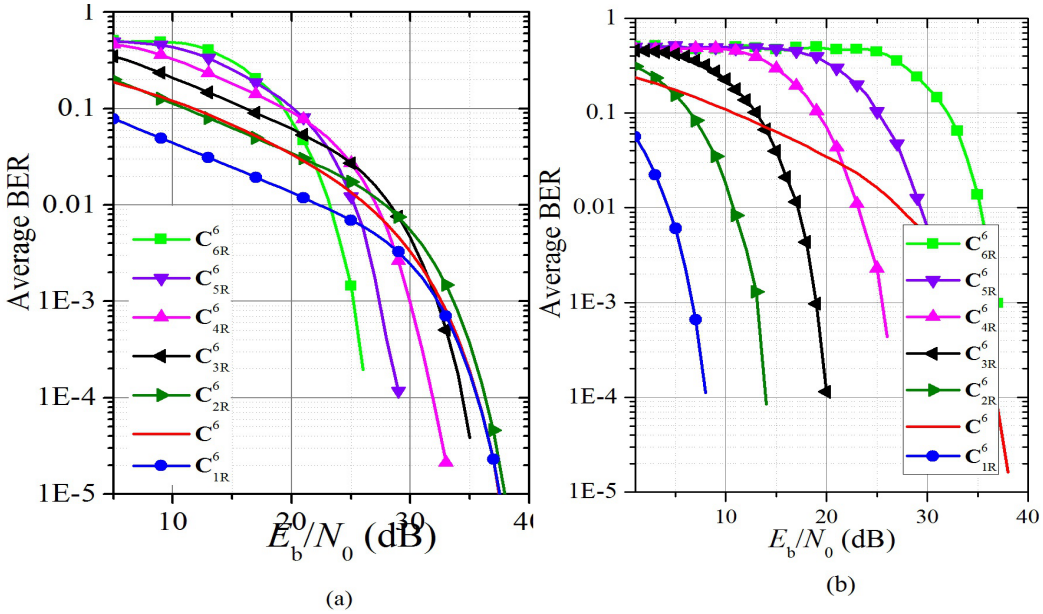

Figure 3.6: BER versus E_b/N_o comparison of the *Right* child in each subset of $\mathbf{C}^6_{64\times126} = [\mathbf{C}^6_{1L}|\mathbf{C}^6_{1R}|\mathbf{C}^6_{2L}|\mathbf{C}^6_{2R}|\mathbf{C}^6_{3L}|\mathbf{C}^6_{3R}|\mathbf{C}^6_{4L}|\mathbf{C}^6_{4R}|\mathbf{C}^6_{5L}|\mathbf{C}^6_{5R}|\mathbf{C}^6_{6L}|\mathbf{C}^6_{6R}]$ for (a) SMOS (ternary) (b) SMOS ($2k$-ary).

the impact of low level of ρ_{ef} (3.7) (Anomaly-1, Section 3.6), its influence on the subsequent subsets gradually gets suppressed due to the substantial fall in the level of PA (Trade-off, Section 3.6). As a result, the edge in the level of BER over the moderate range of E_b/N_o starts to fall and finally attends the equality with ternary for $\mathbf{C}^6_{3L}$. Eventually, from $\mathbf{C}^6_{4L}$ onwards, the level of BER of the ternary dominates and the difference continuously grows, from $\mathbf{C}^6_{4L}$ to $\mathbf{C}^6_{6L}$.

Figure 3.8 being the distributed version of Figure 3.6 illustrates the one-to-one comparison of the BER for the right child. Figure 3.8 (a) to (f), in sequence, correspond to $\mathbf{C}^6_{1R}$,$\mathbf{C}^6_{2R}$, $\mathbf{C}^6_{3R}$,$\mathbf{C}^6_{4R}$, $\mathbf{C}^6_{5R}$, and $\mathbf{C}^6_{6R}$ respectively. The explanation to the non-uniformity in their superiority is same as that of the left and hence, needs no further detailing. However, as a crucial observation, the optimality of $\mathbf{C}^6_{1R}$ must be highlighted.

In Figure 3.10, we extend the comparison of the left child (in Figure 3.5 and Figure 3.7), a step further. While Figure 3.5 and 3.7 illustrates the comparison for the left child at maximum loading condition (i.e.; $\mathbf{C}^6_{64\times126}$ or $\beta = 1.97$), the study of their performance for different (reduced) loading condition will further supplement our analysis. So, we start with $\mathbf{C}^6_{64\times126}$ (see Figure 3.7) and subsequently, smaller subsets ($\mathbf{C}^6_6$, $\mathbf{C}^6_5$, $\mathbf{C}^6_4$, $\mathbf{C}^6_3$, and $\mathbf{C}^6_2$) are removed one-by-one to realize five different loading conditions: $\mathbf{C}^6_{64\times124}$, $\mathbf{C}^6_{64\times120}$, $\mathbf{C}^6_{64\times112}$, $\mathbf{C}^6_{64\times96}$. While *each column* of the grid

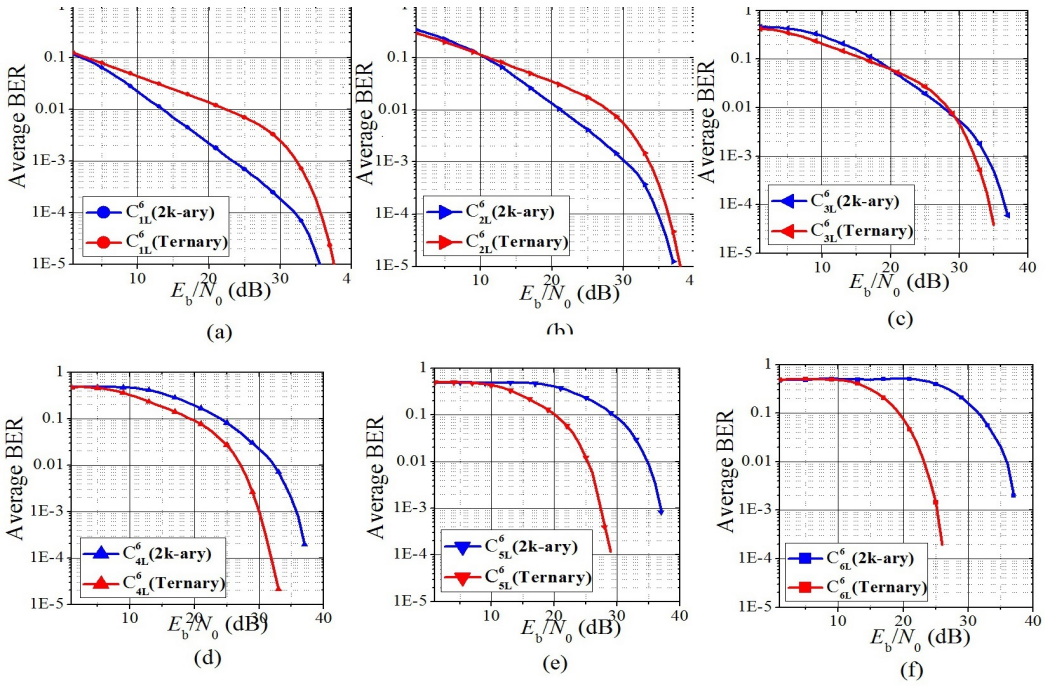

Figure 3.7: BER versus E_b/N_o performance: SMOS (Ternary) versus SMOS ($2k$-ary) for $\mathbf{C}^6_{64\times126} = [\mathbf{C}^6_{1L}|\mathbf{C}^6_{1R}|\mathbf{C}^6_{2L}|\mathbf{C}^6_{2R}|\mathbf{C}^6_{3L}|\mathbf{C}^6_{3R}|\mathbf{C}^6_{4L}|\mathbf{C}^6_{4R}|\mathbf{C}^6_{5L}|\mathbf{C}^6_{5R}|\mathbf{C}^6_{6L}|\mathbf{C}^6_{6R}]$: for (a) $\mathbf{C}^6_{1L}$, (b) $\mathbf{C}^6_{2L}$, (c) $\mathbf{C}^6_{3L}$, (d) $\mathbf{C}^6_{4L}$, (e) $\mathbf{C}^6_{5L}$, (f) $\mathbf{C}^6_{6L}$.

(Figure 3.10 and 3.11) corresponds to the available subsets for a particular loading condition, *each row* corresponds to a specific subset under different loading. The size of the subset decreases from top to bottom e.g.; Figure 3.10 (a1) and (a6) represents the BER of $\mathbf{C}^6_{1L}$ and $\mathbf{C}^6_{6L}$ respectively. Likewise, (b1) to (b5), (c1) to (c4), (d1) to (d3), and (e1) to (e2) illustrate for $\mathbf{C}^6_{1L}$ to $\mathbf{C}^6_{5L}$, $\mathbf{C}^6_{1L}$ to $\mathbf{C}^6_{4L}$, $\mathbf{C}^6_{1L}$ to $\mathbf{C}^6_{3L}$, $\mathbf{C}^6_{1L}$ to $\mathbf{C}^6_{2L}$ respectively. For better perception of this grid structure, its replication in Figure 3.9 briefing the description about the change in the behavior of different operational metrics can be referred. From the observation, for a fixed loading condition (column wise), for the larger subsets the performance of $2k$-ary outsmarts that of ternary and it has already been explained in the context of Figure 3.7, for $\mathbf{C}^6_{64\times126}$ (the first column in Figure 3.10). Therefore, identical reasoning also suffices to understand the behavior of the other columns. However, with the reduction in loading (or level of TPC), the deviation is noticed in the order of their superiority. To explain this, let us shift our perspective of analysis to row-wise, since the level of MAI shows a continuous fall along a row (see Figure 3.10). For example, take the case of the first row (Figure 3.10 (a1), (b1), (c1), (d1), (e1)), where the superiority of the $2k$-ary can be found to have gradual degradation (from left to right). In particular, while for Figure 3.10 (a1) and

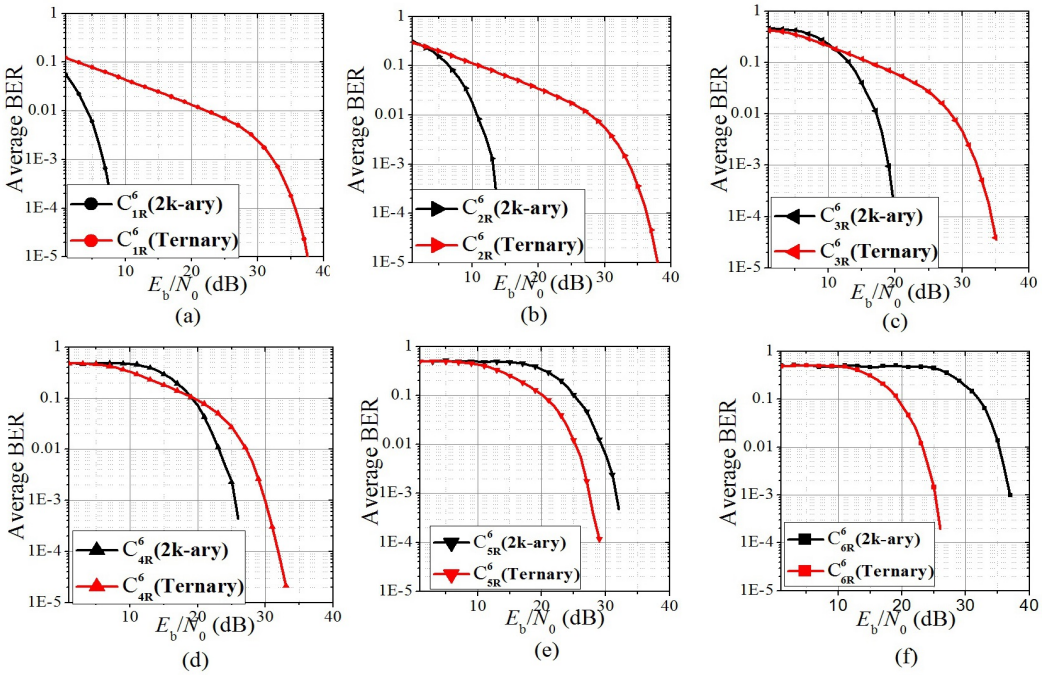

Figure 3.8: BER versus E_b/N_o performance: SMOS (Ternary) versus SMOS ($2k$-ary) for $\mathbf{C}^6_{64\times126} = [\mathbf{C}^6_{1L}|\mathbf{C}^6_{1R}|\mathbf{C}^6_{2L}|\mathbf{C}^6_{2R}|\mathbf{C}^6_{3L}|\mathbf{C}^6_{3R}|\mathbf{C}^6_{4L}|\mathbf{C}^6_{4R}|\mathbf{C}^6_{5L}|\mathbf{C}^6_{5R}|\mathbf{C}^6_{6L}|\mathbf{C}^6_{6R}]$, for (a) $\mathbf{C}^6_{1R}$, (b) $\mathbf{C}^6_{2R}$, (c) $\mathbf{C}^6_{3R}$, (d) $\mathbf{C}^6_{4R}$, (e) $\mathbf{C}^6_{5R}$, (f) $\mathbf{C}^6_{6R}$.

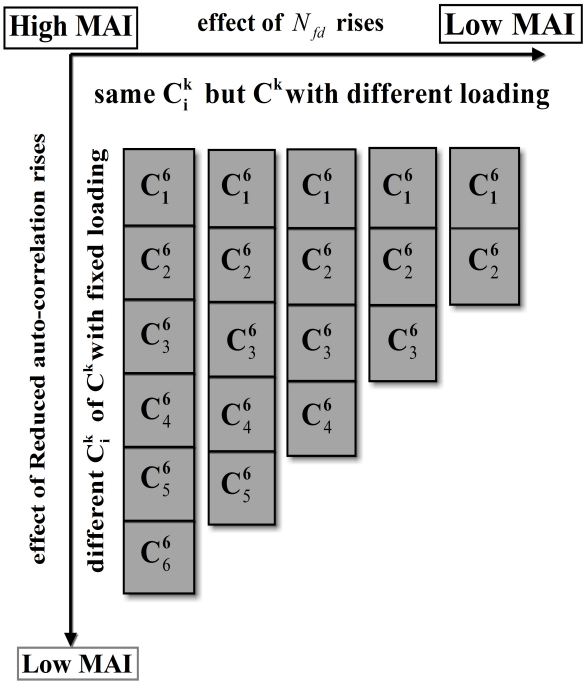

Figure 3.9: Behavior of the operational metrics across the grid structure of figures in Figure 3.10 and Figure 3.11.

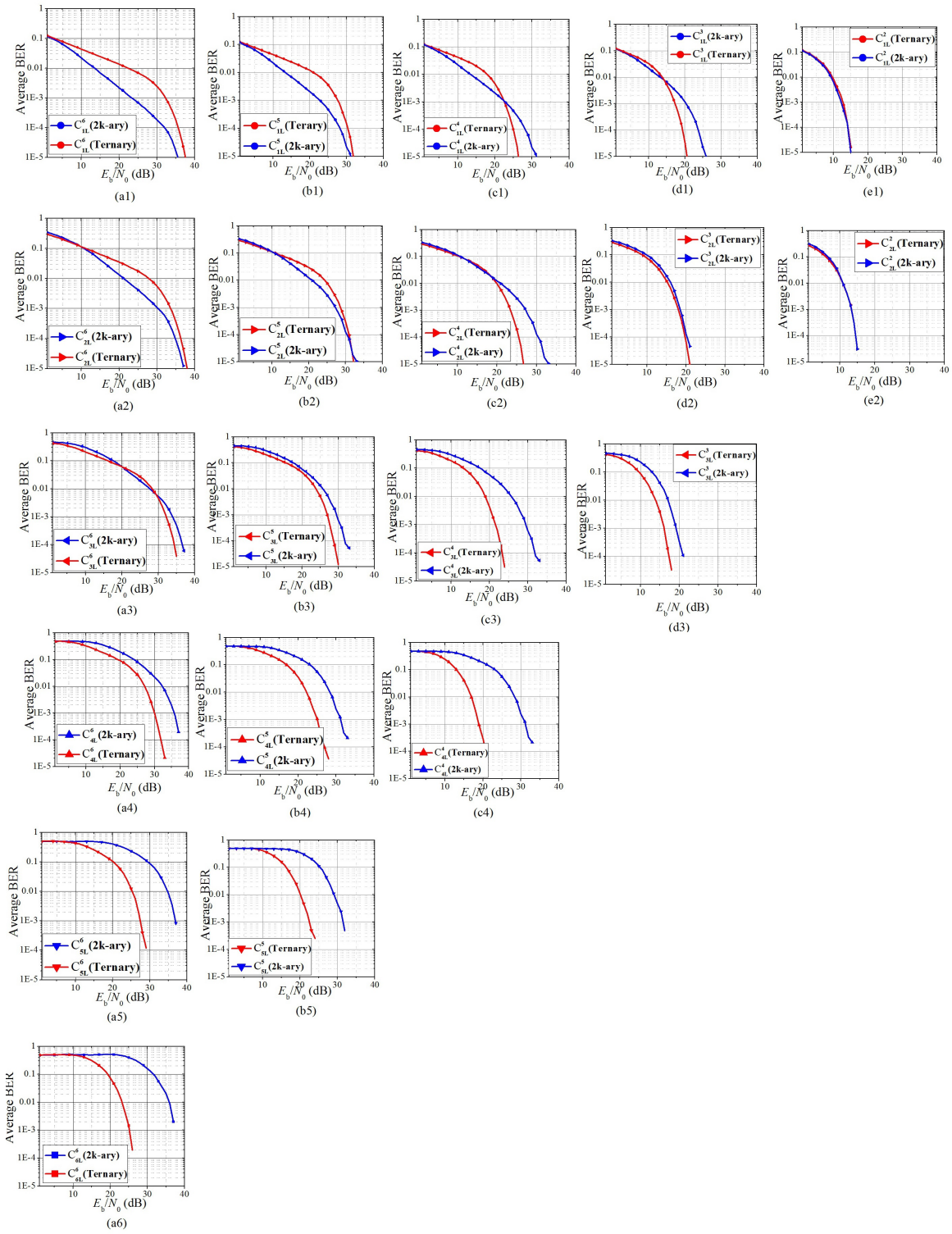

Figure 3.10: BER versus E_b/N_o performance of left child: SMOS (Ternary) versus SMOS ($2k$-ary) at different loading conditions: i.e.; (a1) to (a6): $\mathbf{C}^6_{1L}$ to $\mathbf{C}^6_{6L}$ for $\mathbf{C}^6_{64\times126}$, (b1) to (b5): $\mathbf{C}^6_{1L}$ to $\mathbf{C}^6_{5L}$ for $\mathbf{C}^6_{64\times124}$, (c1) to (b4): $\mathbf{C}^6_{1L}$ to $\mathbf{C}^6_{4L}$ for $\mathbf{C}^6_{64\times120}$, (d1) to (d4): $\mathbf{C}^6_{1L}$ to $\mathbf{C}^6_{3L}$ for $\mathbf{C}^6_{64\times112}$, (e1) to (e4): $\mathbf{C}^6_{1L}$ to $\mathbf{C}^6_{2L}$ for $\mathbf{C}^6_{64\times96}$.

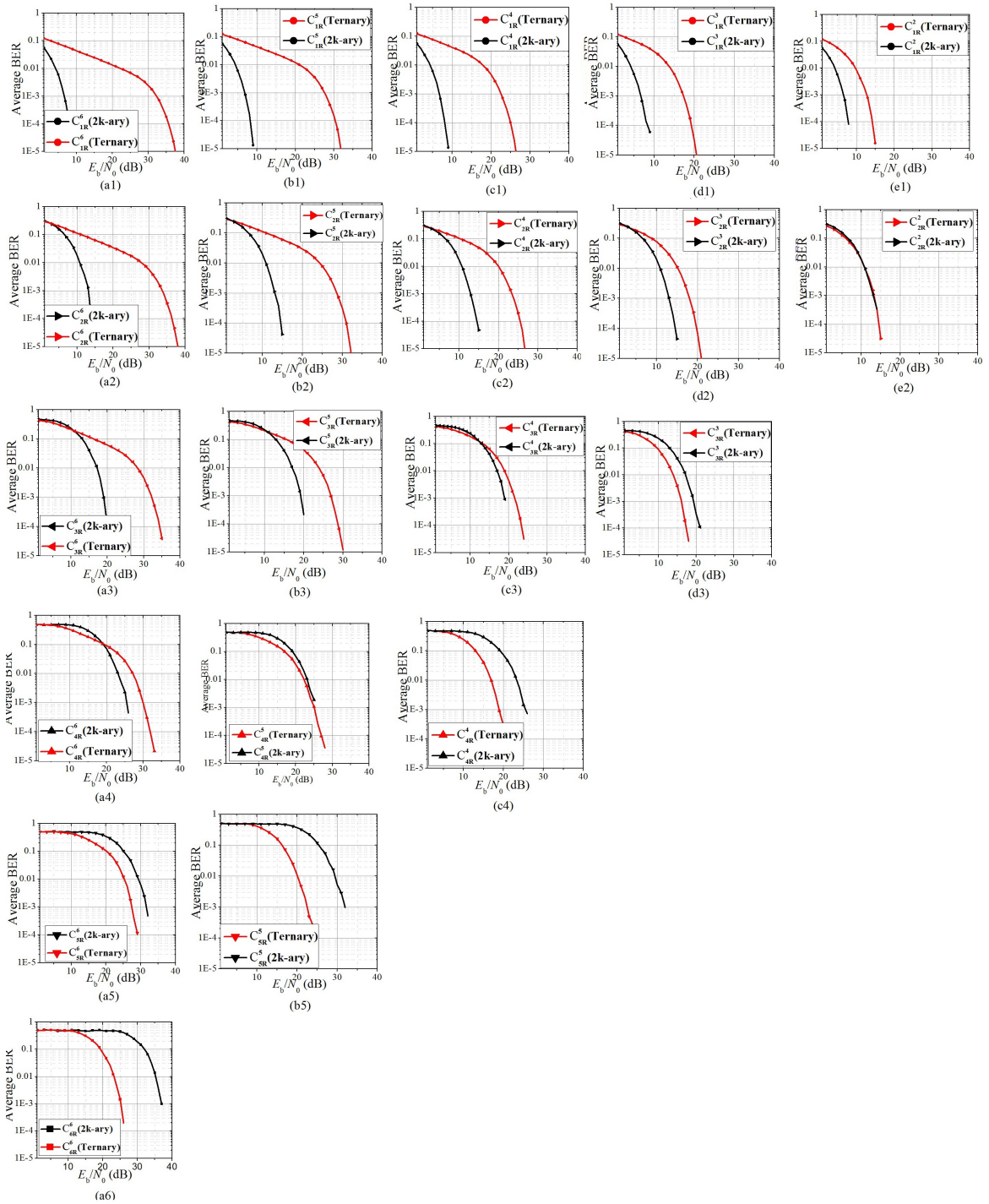

Figure 3.11: BER versus E_b/N_o performance of right child: SMOS (Ternary) versus SMOS (2k-ary) at different loading conditions i.e.; (a1) to (a6): $\mathbf{C}^6_{1R}$ to $\mathbf{C}^6_{6R}$ for $\mathbf{C}^6_{64\times126}$, (b1) to (b5): $\mathbf{C}^6_{1R}$ to $\mathbf{C}^6_{5R}$ for $\mathbf{C}^6_{64\times124}$, (c1) to (b4): $\mathbf{C}^6_{1R}$ to $\mathbf{C}^6_{4R}$ for $\mathbf{C}^6_{64\times120}$, (d1) to (d4): $\mathbf{C}^6_{1R}$ to $\mathbf{C}^6_{3R}$ for $\mathbf{C}^6_{64\times112}$ (e1) to (e4): $\mathbf{C}^6_{1R}$ to $\mathbf{C}^6_{2R}$ for $\mathbf{C}^6_{64\times96}$.

Table 3.4: Comparison of Superioty in average BER: $2k$-ary versus Ternary, where '$\times$','$\approx$', and '$-$' denote the "superiority crossover", "approximate equality", and "Not Applicable" respectively.

Loading ($\rightarrow$)	$\mathbf{C}^6_{64\times126}$		$\mathbf{C}^6_{64\times124}$		$\mathbf{C}^6_{64\times120}$		$\mathbf{C}^6_{64\times112}$		$\mathbf{C}^6_{64\times96}$	
i ($\downarrow$)	$\mathbf{C}^6_{iL}$	$\mathbf{C}^6_{iR}$	$\mathbf{C}^6_{iL}$	$\mathbf{C}^6_{iR}$	$\mathbf{C}^6_{iL}$	$\mathbf{C}^6_{iR}$	$\mathbf{C}^6_{iL}$	$\mathbf{C}^6_{iR}$	$\mathbf{C}^6_{iL}$	$\mathbf{C}^6_{iL}$
1	$2k$	$2k$	$2k$	$2k$	$\times$	$2k$	$\times$	$2k$	$\approx$	$2k$
2	$2k$	$2k$	$2k$	$2k$	Ter.	$2k$	Ter.	$2k$	$\approx$	$\approx$
3	$\times$	$2k$	Ter.	$2k$	Ter.	Ter.	Ter.	Ter.	-	-
4	Ter.	$2k$	Ter.	Ter.	Ter.	Ter.	-	-	-	-
5	Ter.	Ter.	Ter.	Ter.	-	-	-	-	-	-
6	Ter.	Ter.	-	-	-	-	-	-	-	-

(b1) the superiority is traced for the $2k$-ary SMOS, a transition to the ternary in terms of the superiority cross-over is captured in Figure 3.10 (c1), and for Figure 3.10 (d1) onwards, the ternary finally dominates. Without any variation, similar tendency can be recorded for other rows too.

Figure 3.11 is the extrapolation to Figure 3.6, in the same way, Figure 3.10 is meant to Figure 3.5. Therefore, it is logical to expect a similar apprehension towards the demonstration of their behavior across the grid structure. On a note, the description of various metrics in Figure 3.9, controlling the BER performance of the left child in Figure 3.10 is also applicable to this case.

After the relative analysis of the BER for the left and right child under different loading conditions in Figure 3.10 and 3.11, now, it is essential to collect their outcome in a single frame so as to attain a firm conclusion of the superiority. So, we present Table 3.4. Following its observation, at a particular loading condition, concluding any of them as superior, in overall, is contradictory due to mixed nature of their outcomes. Nonetheless, as the only difference, for $\mathbf{C}^2_{64\times96}$ (last column in Table 3.4) (i.e.; $\beta = 1.5$) it is no more illogical to consider $2k$-ary as superior.

In Figure 3.12 (a) to (f), the comparison lies in between the left and right child for the individual subsets of $2k$-ary. For an arbitrary signature in CDMA, to gain better (optimal) error performance, the most coveted criterion to be satisfied is the higher value of PA (≈ 1) in conjunction with the lower value of TPC (≈ 0). Since the importance of PA serves exactly opposite to that of the TPC, it is clearly acceptable to treat their difference as a suitable metric for the analysis of error performance. For this difference to be higher for a signature, the better performance is expected and vice versa. For a system using $2k$-ary SMOS, it can be defined as

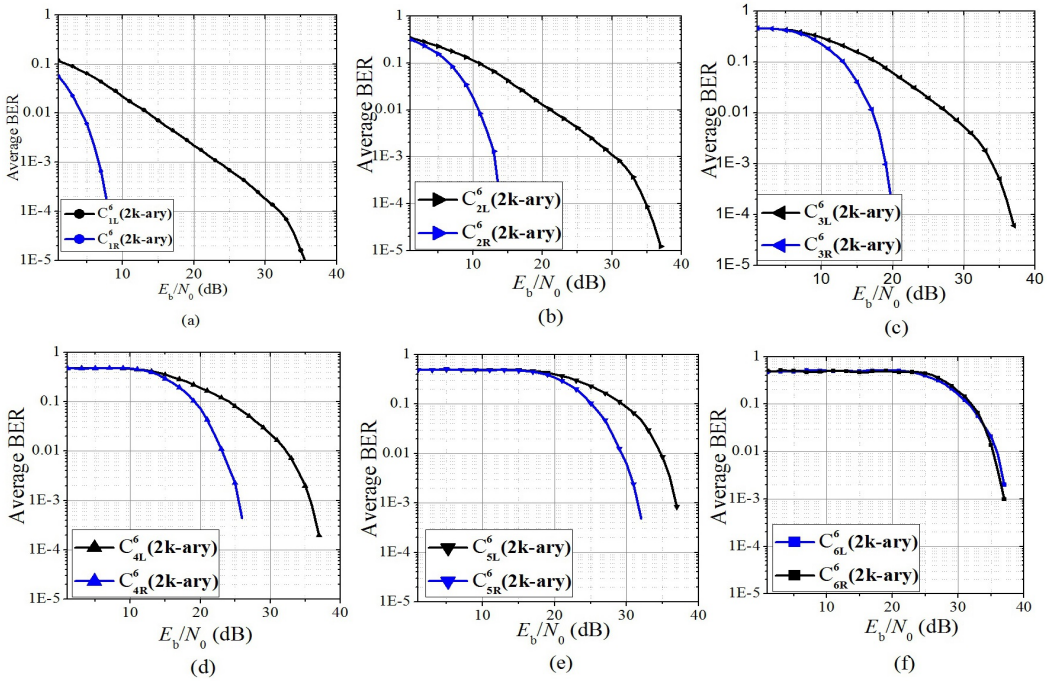

Figure 3.12: BER versus E_b/N_o performance for SMOS (2k-ary) for $\mathbf{C}^6_{64\times126} = [\mathbf{C}^6_{1L}|\mathbf{C}^6_{1R}|\mathbf{C}^6_{2L}|\mathbf{C}^6_{2R}|\mathbf{C}^6_{3L}|\mathbf{C}^6_{3R}|\mathbf{C}^6_{4L}|\mathbf{C}^6_{4R}|\mathbf{C}^6_{5L}|\mathbf{C}^6_{5R}|\mathbf{C}^6_{6L}|\mathbf{C}^6_{6R}]$, where (a) $\mathbf{C}^6_{1L}$ versus $\mathbf{C}^6_{1R}$, (b) $\mathbf{C}^6_{2L}$ versus $\mathbf{C}^6_{2R}$, (c) $\mathbf{C}^6_{3L}$ versus $\mathbf{C}^6_{3R}$, (d) $\mathbf{C}^6_{4L}$ versus $\mathbf{C}^6_{4R}$, (e) $\mathbf{C}^6_{5L}$ versus $\mathbf{C}^6_{5R}$, (f) $\mathbf{C}^6_{6L}$ versus $\mathbf{C}^6_{6R}$.

$d_i = \frac{\rho_{ii}(u,v)}{N_{ef_i}} - \sum_{j=i+1}^{k} \sum_{v=1}^{\frac{N_k}{2^{j-1}}} \frac{\rho_{ij}(u,v)}{N_{ef_i}}$, where d_i indicates the difference corresponding to an arbitrary signature in subset $\mathbf{C}^k_i$. Now, based on the change in the magnitude of d_i (see Table 3.3), two crucial observations are spotted. First, for each subset, the value of d_i for the right child (d_{iR}) is always higher than that of the left (d_{iL}) and its value gradually decreases as we move from top ($\mathbf{C}_1$) to bottom ($\mathbf{C}_6$) of the tree hierarchy. As a result, the level of BER for the right child always remains lower than that of the left. Second, the difference in its magnitude (i.e.; $(d_i)_L - (d_i)_R$) also manifests a continuous reduction, as we move from $\mathbf{C}_1$ to $\mathbf{C}_6$ (i.e.; from Figure 3.12 (a) to (f)). Finally, for $\mathbf{C}_6$, the value of $((d_i)_L - (d_i)_R)$ almost gets to zero that results in the overlapping of the curves in Figure 3.12 (f).

3.8 Summary

In this chapter, our attempt to extend the domain of SMOS beyond ternary (or TSMOS) culminated in a new set of SMOS i.e.; 2k-ary SMOS. Besides the similarity with ternary SMOS existing in the method of construction and maximized capacity of 200%, the difference was also observed regarding the non-uniformity of the twin

tree hierarchy and the existence of optimal users for the largest subset. In contrast to TSMOS, where the level of MAI within a subset was found to be uniform, the deviation in this regard was discovered for $2k$-ary regarding two separate levels of MAI (based on the left or right child generated). Subsequently, the error performance analysis of the individual subsets was split into two sections, and the simulation results also confirmed this difference. By the selection of appropriate metrics, we reasonably validated the distinction between the performance of the ternary and $2k$-ary in terms of suitable anomalies and trade-off. Despite the prominent edge concerning optimality of the specific users, proclaiming the $2k$-ary to be superior over ternary appeared to be illogical, since the outcome of our attempt for recognizing either of them as superior was later found not to be mutually exclusive. This inference became more vivid from our observations when for a fixed loading condition, the superiority of any of them was found not to preserve the uniformity for the constituent subsets. Therefore, evidently enough, superiority in this context, became a conditional entity. However, with a difference, for the maximization in loading capacity to be 150% ($\beta = 1.5$ i.e.; the first two subsets being active), the superiority was found to be exclusively possessed by the $2k$-ary. In overall, the demonstration, so far, concentrating on the multiple attributes and aspects related to each and every individual signature (of the smallest possible subset), rather than taking into account their average statistics, was truly profound towards the better understanding of the $2k$-ary SMOS, relative to its ternary counterpart.

Chapter 4
Hybrid SMOS: A Unified Approach to Construction of SMOS

4.1 Introduction

The discussion on SMOS, in this thesis, starts with the proposal of its ternary version (i.e.; TSMOS in Chapter 2) posing the twin tree hierarchy of MAI. Later, in Chapter 3, we show that further extrapolation of the SMOS architecture to realize the whole construction as the combination of binary subsets is also possible. Due to the involvement of $2k$ number of alphabets in construction of SMOS with k subsets it's called $2k$-ary SMOS. Over the discussion in Chapter 3, the comparative explanation of $2k$-ary SMOS considering the TSMOS as the reference is highly comprehensive. While the introductory concept of SMOS in its ternary form (in chaper 2) builds the layout for further research, its extension in the $2k$-ary form explains, in more detail, the role of the metrics like: PA, TPC, (PA-TPC), free diversity in controlling the error performance of the individual subsets. Furthermore, the existence of multiple relational phenomena e.g.; PA versus TPC trade-off, anomaly due to TPC, anomaly due to free diversity, as a whole, have vividly presented the features of the $2k$-ary SMOS. Also, the superiority of the $2k$-ary over ternary for 150% maximization in loading capacity has been reported. However, the important queries those have yet to be answered and hence, motivated us for further research in this chapter are:

- if there exist any other variants of SMOS, besides the TSMOS and $2k$-ary SMOS (or $2k$-SMSOS),
- if yes, what kind of approach is considered for its construction,
- is it feasible to have an unified approach to interpret and analyze all types of SMOS, and
- lastly, how the performance of their individual subsets are going to differ as compared to TSMOS and $2k$-SMOS.

In this chapter, the above queries have been sequentially addressed. First, the construction of multiple SMOS structures other than TSMOS and $2k$-SMOS is possible and can be realized through two approaches: bottom-to-top and top-to-bottom. Considering TSMOS with k subsets as the origin of the evolution of SMOS structures, in the bottom-to-top approach, $(k-g)$ ternary subsets from the bottom level of the tree can be replaced by the equivalent binary counterparts from the $2k$-SMOS, where as no such replacement is imposed on the g subsets, in the top level of the tree. Likewise, in top-to-bottom approach, the g subsets from the top level of the tree can be replaced by the equivalent binary counterparts from the $2k$-SMOS, where as no such replacement is required for the rest of the $(k-g)$ subsets, existing in the bottom level of the tree. Due to the mixed (hybrid) nature of the overall structure (few ternary and rest binary), we call then hybrid SMOS (HSMOS). For $1 \leq g \leq k$, using either of the two approaches, k different HSMOS structures can be constructed. Interestingly, for $g = 1$ and $g = k$, the resulting HSMOS corresponds to the case of T-SMOS and $2k$-SMOS respectively, thus, justifying the unified feature of the construction. For decoding, even if the MUD used for the detection of TSMOS and $2k$-SMOS can also be applied to the HSMOS structures, expecting dramatic variation in their error performance of the later from the former ones is inevitable. For each of the $2k$ possible sets of HSMOS, we analyze the non-uniform tree structure to identify the variation in the status of the inequality (PA $>$ TPC) for both the left and right child. Next, using the statistics of these inequalities, we discuss to reach the appropriate validation to the error performance of the individual subsets. In overall, the comprehensive approach to analyze all the $2k$ possible sets of HSMOS in a correlated perspective offers better understanding into the overall architecture of SMOS.

4.2 Construction of SMOS: A Unified Approach

4.2.1 Structure Formulation

In Section 2.3 and 3.3, the role of the basis matrices $\mathbf{B} = \left[\begin{array}{cc|c} + & + & + \\ + & - & 0 \end{array}\right]$ and $\mathbf{B}' = \left[\begin{array}{cc|c} + & + & 1/2 \\ + & - & 1/2 \end{array}\right]$ in recursively driving the construction of ternary and $2k-ary$ SMOS has been explained respectively. However, our further study shows that formation of several other sets of SMOS is also feasible by allowing the

overall structure of the construction to be hybrid i.e.; the avaibale subsets becomes a combination of *ternary* and *binary*. If we denote an arbitrary ternary subset by $\mathbf{T}$ and binary subset by $\mathbf{V}$ then the hybrid structure of SMOS $\mathbf{C}_{N_k \times M_k}$ for $N_k = 2^k$ can be expressed as $\mathbf{C}^k = \left[\mathbf{T}^g | \mathbf{V}^{k-g}\right]$, for

$$\mathbf{T}^g = \left[\mathbf{C}^k_{1V} | \mathbf{C}^k_{2T} | \cdots | \mathbf{C}^k_{gT}\right], \quad \mathbf{V}^{k-g} = \left[\mathbf{C}^k_{(g+1)V} | \mathbf{C}^k_{(g+2)V} | \cdots | \mathbf{C}^k_{kV}\right], \text{ and}$$

$\mathbf{C}^k = \left[\mathbf{V}^g | \mathbf{T}^{k-g}\right]$, for

$$\mathbf{V}^g = \left[\mathbf{C}^k_{1V} | \mathbf{C}^k_{2V} | \cdots | \mathbf{C}^k_{gV}\right], \quad \mathbf{T}^{k-g} = \left[\mathbf{C}^k_{(g+1)T} | \mathbf{C}^k_{(g+2)T} | \cdots | \mathbf{C}^k_{kT}\right].$$

It is important to note that the above approach of hybridization, at a certain point, leads to the formation of TSMOS and $2k$-SMOS, which can be represented as

- $\mathbf{C}^k = \left[\mathbf{T}^k\right] = \left[\mathbf{C}^k_1 | \mathbf{C}^k_2 | \cdots | \mathbf{C}^k_k\right] = \left[\mathbf{C}^k_{1V} | \mathbf{C}^k_{2T} | \cdots | \mathbf{C}^k_{kT}\right]$

  and

- $\mathbf{C}^k = \left[\mathbf{V}^k\right] = \left[\mathbf{C}^k_1 | \mathbf{C}^k_2 | \cdots | \mathbf{C}^k_k\right] = \left[\mathbf{C}^k_{1V} | \mathbf{C}^k_{2V} | \cdots | \mathbf{C}^k_{kV}\right]$ respectively.

So, keeping in view of the *inclusive* nature of the current construction, it is logical to cite the overall approach as *unified*. Table 4.1 presents the structure of $\mathbf{C}^3 = \left[\mathbf{C}^3_1 | \mathbf{C}^3_2 | \mathbf{C}^3_3\right]$ for four different types of HSMOS configurations.

4.2.2 Method of Construction

Below, we describe the recurrent approach for the construction of all possible HSMOS structures.

4.2.2.1 TSMOS

To construct $\mathbf{C}^k = \left[\mathbf{T}^k\right] = \left[\mathbf{C}^k_1 | \mathbf{C}^k_2 | \cdots | \mathbf{C}^k_k\right]$

- Initialize $\mathbf{C}^0 = [1]$ and find $\mathbf{C}^1 = \left(\frac{1}{\sqrt{2}}\mathbf{H}_{2\times 2} \otimes \mathbf{C}^0\right) = \frac{1}{\sqrt{2}}\mathbf{H}_2$
- For $1 \leq a \leq k$, $\mathbf{C}^a = \left(\frac{1}{\sqrt{2}}\mathbf{H}_{2\times 2} \otimes \mathbf{A}\right)$, where

$$\mathbf{A} = \left[\mathbf{C}^{a-1} | [1\ 0\ 0\ \cdots\ 0]^T{}_{1\times 2^{a-1}}\right]$$

4.2.2.2 HSMOS ($\mathbf{C}^k = \left[\mathbf{T}^g | \mathbf{V}^{k-g}\right]$)

To construct $\mathbf{C}^k = \left[\mathbf{T}^g | \mathbf{V}^{k-g}\right] = \left[\mathbf{C}^k_1 | \mathbf{C}^k_2 | \cdots | \mathbf{C}^k_k\right]$

- Initialize $\mathbf{C}^0 = [1]$ and find $\mathbf{C}^1 = \left(\frac{1}{\sqrt{2}}\mathbf{H}_{2\times 2} \otimes \mathbf{C}^0\right) = \frac{1}{\sqrt{2}}\mathbf{H}_2$
- For $1 \leq a \leq g$, $\mathbf{C}^a = \left(\frac{1}{\sqrt{2}}\mathbf{H}_{2\times 2} \otimes \mathbf{A}\right)$, where

$$\mathbf{A} = \left[\mathbf{C}^{a-1} | [1\ 0\ 0\ \cdots\ 0]^T{}_{1\times 2^{a-1}}\right]$$

Table 4.1: Structure of SMOS $\mathbf{C}^3 = \left[\mathbf{C}_1^3|\mathbf{C}_2^3|\mathbf{C}_3^3\right]$: (a) $\left[\mathbf{T}^3\right]$ (TSMOS) (b) $\left[\mathbf{T}^2|\mathbf{V}^1\right]$ (HSMOS) (c) $\left[\mathbf{T}^1|\mathbf{V}^2\right]$ (HSMOS) (d) $\left[\mathbf{V}^3\right]$ ($2k$-SMOS)

TSMOS

$$\mathbf{C}_{1V}^3 = \tfrac{1}{\sqrt{8}}\left[\mathbf{H}_8\right], \mathbf{C}_{2T}^3 = \tfrac{1}{\sqrt{8}}\begin{bmatrix} + & + & + & + \\ 0 & 0 & 0 & 0 \\ + & - & + & - \\ 0 & 0 & 0 & 0 \\ + & + & - & - \\ 0 & 0 & 0 & 0 \\ + & - & - & + \\ 0 & 0 & 0 & 0 \end{bmatrix} \mathbf{C}_{3T}^3 = \tfrac{1}{\sqrt{8}}\begin{bmatrix} + & + \\ 0 & 0 \\ 0 & 0 \\ 0 & 0 \\ + & - \\ 0 & 0 \\ 0 & 0 \\ 0 & 0 \end{bmatrix}$$

HSMOS ($\left[\mathbf{T}^g|\mathbf{V}^{k-g}\right]$)

$$\mathbf{C}_{1V}^3 = \tfrac{1}{\sqrt{8}}\left[\mathbf{H}_8\right]\mathbf{C}_{2T}^3 = \tfrac{1}{\sqrt{8}}\begin{bmatrix} + & + & + & + \\ 0 & 0 & 0 & 0 \\ + & - & + & - \\ 0 & 0 & 0 & 0 \\ + & + & - & - \\ 0 & 0 & 0 & 0 \\ + & - & - & + \\ 0 & 0 & 0 & 0 \end{bmatrix} \mathbf{C}_{3V}^3 = \tfrac{1}{\sqrt{8}}\begin{bmatrix} 1/2^2 & 1/2^2 \\ 1/2^2 & 1/2^2 \\ 1/2^2 & 1/2^2 \\ 1/2^2 & 1/2^2 \\ 1/2^2 & -1/2^2 \\ 1/2^2 & -1/2^2 \\ 1/2^2 & -1/2^2 \\ 1/2^2 & -1/2^2 \end{bmatrix}$$

HSMOS($\left[\mathbf{V}^g|\mathbf{T}^{k-g}\right]$)

$$\mathbf{C}_{1V}^3 = \tfrac{1}{\sqrt{8}}\left[\mathbf{H}_8\right], \mathbf{C}_{2V}^3 = \tfrac{1}{\sqrt{8}}\begin{bmatrix} 1/2 & 1/2 & 1/2 & 1/2 \\ 1/2 & 1/2 & 1/2 & 1/2 \\ 1/2 & -1/2 & 1/2 & -1/2 \\ 1/2 & -1/2 & 1/2 & -1/2 \\ 1/2 & 1/2 & -1/2 & -1/2 \\ 1/2 & 1/2 & -1/2 & -1/2 \\ 1/2 & -1/2 & -1/2 & 1/2 \\ 1/2 & -1/2 & -1/2 & 1/2 \end{bmatrix}, \mathbf{C}_{3T}^3 = \tfrac{1}{\sqrt{8}}\begin{bmatrix} + & + \\ 0 & 0 \\ 0 & 0 \\ 0 & 0 \\ + & - \\ 0 & 0 \\ 0 & 0 \\ 0 & 0 \end{bmatrix}$$

$2k$-SMOS

$$\mathbf{C}_{1V}^3 = \tfrac{1}{\sqrt{8}}\left[\mathbf{H}_8\right], \mathbf{C}_{2V}^3 = \tfrac{1}{\sqrt{8}}\begin{bmatrix} 1/2 & 1/2 & 1/2 & 1/2 \\ 1/2 & 1/2 & 1/2 & 1/2 \\ 1/2 & -1/2 & 1/2 & -1/2 \\ 1/2 & -1/2 & 1/2 & -1/2 \\ 1/2 & 1/2 & -1/2 & -1/2 \\ 1/2 & 1/2 & -1/2 & -1/2 \\ 1/2 & -1/2 & -1/2 & 1/2 \\ 1/2 & -1/2 & -1/2 & 1/2 \end{bmatrix}, \mathbf{C}_{3V}^3 = \tfrac{1}{\sqrt{8}}\begin{bmatrix} 1/2^2 & 1/2^2 \\ 1/2^2 & 1/2^2 \\ 1/2^2 & 1/2^2 \\ 1/2^2 & 1/2^2 \\ 1/2^2 & -1/2^2 \\ 1/2^2 & -1/2^2 \\ 1/2^2 & -1/2^2 \\ 1/2^2 & -1/2^2 \end{bmatrix}$$

- For $(g+1) \leq a \leq k$, $\mathbf{C}^a = \left(\frac{1}{\sqrt{2}}\mathbf{H}_{2\times 2} \otimes \mathbf{A}\right)$, where

$$\mathbf{A} = \begin{bmatrix} \mathbf{C}^{a-1} & | & \begin{bmatrix} 1/2^{a-1} & 1/2^{a-1} & \cdots & 1/2^{a-1} \end{bmatrix}^T_{1\times 2^{a-1}} \end{bmatrix}$$

4.2.2.3 HSMOS ($\mathbf{C}^k = \left[\mathbf{V}^g|\mathbf{T}^{k-g}\right]$)

To construct $\mathbf{C}^k = \left[\mathbf{V}^i|\mathbf{T}^{k-i}\right] = \left[\mathbf{C}_1^k|\mathbf{C}_2^k|\cdots|\mathbf{C}_k^k\right]$

- Initialize $\mathbf{C}^0 = [1]$ and find $\mathbf{C}^1 = \left(\frac{1}{\sqrt{2}}\mathbf{H}_{2\times 2} \otimes \mathbf{C}^0\right) = \frac{1}{\sqrt{2}}\mathbf{H}_2$
- For $1 \leq a \leq g$, $\mathbf{C}^a = \left(\frac{1}{\sqrt{2}}\mathbf{H}_{2\times 2} \otimes \mathbf{A}\right)$, where

$$\mathbf{A} = \begin{bmatrix} \mathbf{C}^{a-1} & | & \begin{bmatrix} 1/2^{a-1} & 1/2^{a-1} & \cdots & 1/2^{a-1} \end{bmatrix}^T_{1\times 2^{a-1}} \end{bmatrix}$$

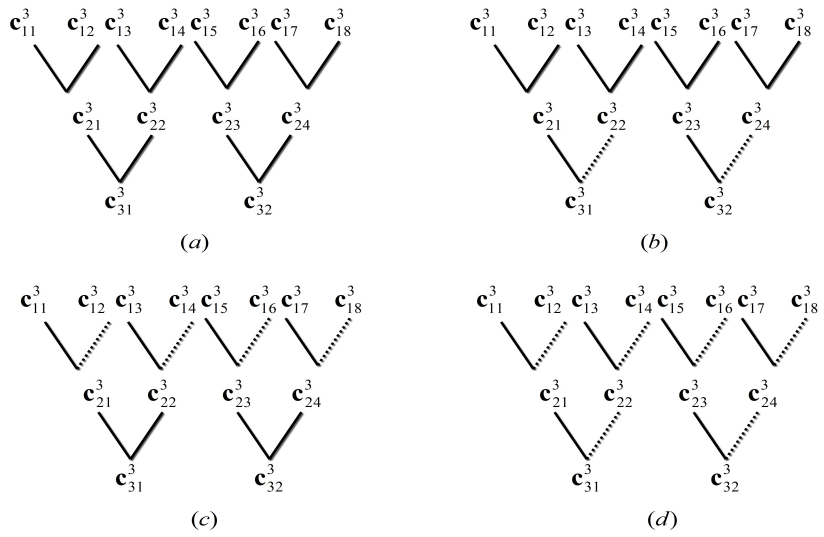

Figure 4.1: Twin Tree hierarchy for the matrices in Table 4.1: (a) $[\mathbf{T}^3]$ (b) $[\mathbf{T}^2|\mathbf{V}^1]$ (c) $[\mathbf{T}^1|\mathbf{V}^2]$ (d) $[\mathbf{V}^3]$.

- For $(g+1) \leq a \leq k$, $\mathbf{C}^a = \left(\frac{1}{\sqrt{2}}\mathbf{H}_{2\times 2} \otimes \mathbf{A}\right)$, where

$$\mathbf{A} = \left[\mathbf{C}^{a-1} | [1\ 0\ 0\ \cdots\ 0]^T{}_{1\times 2^{a-1}}\right]$$

4.2.2.4 2k-SMOS

To construct $\mathbf{C}^k = \left[\mathbf{V}^k\right] = \left[\mathbf{C}_1^k | \mathbf{C}_2^k | \cdots | \mathbf{C}_k^k\right]$

- Initialize $\mathbf{C}^0 = [1]$ and find $\mathbf{C}^1 = \left(\frac{1}{\sqrt{2}}\mathbf{H}_{2\times 2} \otimes \mathbf{C}^0\right) = \frac{1}{\sqrt{2}}\mathbf{H}_2$
- For $1 \leq a \leq k$, $\mathbf{C}^a = \left(\frac{1}{\sqrt{2}}\mathbf{H}_{2\times 2} \otimes \mathbf{A}\right)$, where

$$\mathbf{A} = \left[\ \mathbf{C}^{a-1}\ \ |\ \ \left[\ 1/2^{a-1}\ \ 1/2^{a-1}\ \ \cdots\ \ 1/2^{a-1}\ \right]^T_{1\times 2^{a-1}}\ \right]$$

4.3 Hierarchy of MAI

As per the discussion of the correlation pattern of TSMOS and $2k$-SMOS, the orthogonal subsets projects a *twin tree multi level* hierarchy, where the nodes of the tree at a particular level (depth) $l = 1, 2, \ldots, k$ (i.e., $l = k - i + 1$ for $1 \leq i \leq k$) collectively form the subset-$\mathbf{C}_{k-l+1}^k$. There exist two identical (twin) trees, each of which has its origin or root from the smallest orthogonal subset (i.e.; $\mathbf{C}_k^k$ at the lowest level of the tree, $l = 1$). The nodes at the highest level of the tree ($l = k$) represent the largest subset: $\mathbf{C}_1^k$. The observations from TSMOS and $2k$-SMOS collaboratively provide the summarization, presented in Table 4.2. Figure 4.1 illustrates the twin tree hierarchy for the matrices of HSMOS, shown in Table 4.1.

Table 4.2: Comparative Review: of the correlation pattern: TSMOS versus $2k$-SMOS

Ternary SMOS
• Each parent node is correlated to both the $left$ and $right$ child
• A node ($left$ or $right$) at level-l is correlated to: - its parent nodes in the $(l-1)$ lower levels, - its child nodes in the $(k-l)$ upper levels, such that: $\mathbf{c}^k_{lj} = \frac{1}{2}\left(\mathbf{c}^k_{(l+1)(2j-1)} + \mathbf{c}^k_{(l+1)(2j)}\right)$. (Section 2.4)
$2k$-SMOS
• Each parent node is correlated to the $left$ child only.
• A $left$ node at level-l is correlated to: - all its left child, in the subsequent upper levels (i.e.; level-$(l+1)$ to k) - all its parent nodes in the lower levels (i.e.; level-$(l-1)$ to 1) i.e.; $\mathbf{c}^k_{(k)(2j-1)} = 2\mathbf{c}^k_{(k-1)(j)}$, ..., $\mathbf{c}^k_{(l+1)(2j-1)} = 2\mathbf{c}^k_{(l)(j)}$, $\mathbf{c}^k_{(l)(2j-1)} = 2\mathbf{c}^k_{(l-1)(j)}$, ..., $\mathbf{c}^k_{(l-(l-2))(2j-1)} = 2\mathbf{c}^k_{(l-(l-1))(j)}$ for $1 \leq j \leq 2^l$ (Section 3.4)
• A $right$ node at level-l is correlated to all its $left$ child in the subsequent upper levels (i.e.; level-$(l+1)$ to k)

4.3.1 Review of the MAI Hierachy of TSMOS and $2k$-SMOS

Following the discussion in Section 2.3 and 3.6, the role of the variation in the values of the metrics like, PA and TPC in controlling the error performance of the left and right child of the subsets is of foremost priority. In fact, in Section 3.6, the fall in the significant level of PA and TPC for the subsets with binary signatures over the ternary and its direct impact on their error performance has been illustrated, in detail. While being with the concept of HSMOS introduces a greater degree of non-uniformity in terms of having two different types of subsets (i.e.; binary and ternary), anticipating significant differences in the behavior of their PA and TPC is inevitable. Hence, sufficient focus needs to be directed for their analysis, so that appropriate explanations can be delivered towards the match or mismatch between the theory (so far) and observations in the simulation results.

For further understanding, we present the status of the inequality (PA > TPC) for both type of transformations i.e.; TSMOS to $2k$-SMOS through HSMOS $\left[\mathbf{T}^g|\mathbf{V}^{k-g}\right]$

subset (↓)		(PA > TPC) *for* C^6_{iL}	(PA > TPC) *for* C^6_{iR}
type	index		
V	$\mathbf{C}^1_1$	$1>\left(\frac{1}{2^1}+\frac{1}{2^2}+\frac{1}{2^3}+\frac{1}{2^4}+\frac{1}{2^5}\right)$	$1>\left(\frac{1}{2^1}+\frac{1}{2^2}+\frac{1}{2^3}+\frac{1}{2^4}+\frac{1}{2^5}\right)$
T	$\mathbf{C}^1_2$	$\frac{1}{2}>\left(\frac{1}{2^2}+\frac{1}{2^3}+\frac{1}{2^4}+\frac{1}{2^5}\right)$	$\frac{1}{2}>\left(\frac{1}{2^2}+\frac{1}{2^3}+\frac{1}{2^4}+\frac{1}{2^5}\right)$
T	$\mathbf{C}^1_3$	$\frac{1}{2^2}>\left(\frac{1}{2^3}+\frac{1}{2^4}+\frac{1}{2^5}\right)$	$\frac{1}{2^2}>\left(\frac{1}{2^3}+\frac{1}{2^4}+\frac{1}{2^5}\right)$
T	$\mathbf{C}^1_4$	$\frac{1}{2^3}>\left(\frac{1}{2^4}+\frac{1}{2^5}\right)$	$\frac{1}{2^3}>\left(\frac{1}{2^4}+\frac{1}{2^5}\right)$
T	$\mathbf{C}^1_5$	$\frac{1}{2^4}>\left(\frac{1}{2^5}\right)$	$\frac{1}{2^4}>\left(\frac{1}{2^5}\right)$
T	$\mathbf{C}^1_6$	$\frac{1}{2^5}>0$	$\frac{1}{2^5}>0$

(a)

subset (↓)		(PA > TPC) *for* C^6_{iL}	(PA > TPC) *for* C^6_{iR}
type	index		
V	$\mathbf{C}^1_1$	$1>\left(\frac{1}{2^1}+\frac{1}{2^2}+\frac{1}{2^3}+\frac{1}{2^4}+\frac{1}{2^5}\right)$	$1>\left(\frac{1}{2^1}+\frac{1}{2^2}+\frac{1}{2^3}+\frac{1}{2^4}+0\right)$
T	$\mathbf{C}^1_2$	$\frac{1}{2}>\left(\frac{1}{2^2}+\frac{1}{2^3}+\frac{1}{2^4}+\frac{1}{2^6}\right)$	$\frac{1}{2}>\left(\frac{1}{2^2}+\frac{1}{2^3}+\frac{1}{2^4}+0\right)$
T	$\mathbf{C}^1_3$	$\frac{1}{2^2}>\left(\frac{1}{2^3}+\frac{1}{2^4}+\frac{1}{2^7}\right)$	$\frac{1}{2^2}>\left(\frac{1}{2^3}+\frac{1}{2^4}+0\right)$
T	$\mathbf{C}^1_4$	$\frac{1}{2^3}>\left(\frac{1}{2^4}+\frac{1}{2^8}\right)$	$\frac{1}{2^3}>\left(\frac{1}{2^4}+0\right)$
T	$\mathbf{C}^1_5$	$\frac{1}{2^4}>\left(\frac{1}{2^9}\right)$	$\frac{1}{2^4}>(0)$
V	$\mathbf{C}^1_6$	$\frac{1}{2^{10}}>0$	$\frac{1}{2^{10}}>0$

(b)

subset (↓)		(PA > TPC) *for* C^6_{iL}	(PA > TPC) *for* C^6_{iR}
type	index		
V	$\mathbf{C}^1_1$	$1>\left(\frac{1}{2^1}+\frac{1}{2^2}+\frac{1}{2^3}+\frac{1}{2^4}+\frac{1}{2^5}\right)$	$1>\left(\frac{1}{2^1}+\frac{1}{2^2}+\frac{1}{2^3}+0+0\right)$
T	$\mathbf{C}^1_2$	$\frac{1}{2}>\left(\frac{1}{2^2}+\frac{1}{2^3}+\frac{1}{2^4}+\frac{1}{2^6}\right)$	$\frac{1}{2}>\left(\frac{1}{2^2}+\frac{1}{2^3}+0+0\right)$
T	$\mathbf{C}^1_3$	$\frac{1}{2^2}>\left(\frac{1}{2^3}+\frac{1}{2^4}+\frac{1}{2^7}\right)$	$\frac{1}{2^2}>\left(\frac{1}{2^3}+0+0\right)$
T	$\mathbf{C}^1_4$	$\frac{1}{2^3}>\left(\frac{1}{2^4}+\frac{1}{2^8}\right)$	$\frac{1}{2^3}>(0+0)$
T	$\mathbf{C}^1_5$	$\frac{1}{2^4}>\left(\frac{1}{2^9}\right)$	$\frac{1}{2^8}>(0)$
V	$\mathbf{C}^1_6$	$\frac{1}{2^{10}}>0$	$\frac{1}{2^{10}}>0$

(c)

subset (↓)		(PA > TPC) *for* C^6_{iL}	(PA > TPC) *for* C^6_{iR}
type	index		
V	$\mathbf{C}^1_1$	$1>\left(\frac{1}{2^1}+\frac{1}{2^2}+\frac{1}{2^3}+\frac{1}{2^4}+\frac{1}{2^5}\right)$	$1>\left(\frac{1}{2^1}+0+0+0+0\right)$
T	$\mathbf{C}^1_2$	$\frac{1}{2}>\left(\frac{1}{2^2}+\frac{1}{2^3}+\frac{1}{2^4}+\frac{1}{2^5}+\frac{1}{2^6}\right)$	$\frac{1}{2}>(0+0+0+0)$
T	$\mathbf{C}^1_3$	$\frac{1}{2^2}>\left(\frac{1}{2^3}+\frac{1}{2^4}+\frac{1}{2^5}+\frac{1}{2^7}\right)$	$\frac{1}{2^2}>(0+0+0)$
T	$\mathbf{C}^1_4$	$\frac{1}{2^3}>\left(\frac{1}{2^4}+\frac{1}{2^5}+\frac{1}{2^8}\right)$	$\frac{1}{2^3}>(0+0)$
T	$\mathbf{C}^1_5$	$\frac{1}{2^4}>\left(\frac{1}{2^5}+\frac{1}{2^9}\right)$	$\frac{1}{2^4}>(0)$
V	$\mathbf{C}^1_6$	$\frac{1}{2^5}>0$	$\frac{1}{2^5}>0$

(d)

subset (↓)		(PA > TPC) *for* C^6_{iL}	(PA > TPC) *for* C^6_{iR}
type	index		
V	$\mathbf{C}^1_1$	$1>\left(\frac{1}{2^1}+\frac{1}{2^2}+\frac{1}{2^3}+\frac{1}{2^4}+\frac{1}{2^5}\right)$	$1>\left(\frac{1}{2^1}+0+0+0+0\right)$
T	$\mathbf{C}^1_2$	$\frac{1}{2}>\left(\frac{1}{2^2}+\frac{1}{2^3}+\frac{1}{2^4}+\frac{1}{2^5}+\frac{1}{2^6}\right)$	$\frac{1}{2}>(0+0+0+0)$
V	$\mathbf{C}^1_3$	$\frac{1}{2^4}>\left(\frac{1}{2^5}+\frac{1}{2^6}+\frac{1}{2^7}\right)$	$\frac{1}{2^4}>(0+0+0)$
V	$\mathbf{C}^1_4$	$\frac{1}{2^6}>\left(\frac{1}{2^7}+\frac{1}{2^8}\right)$	$\frac{1}{2^6}>(0+0)$
V	$\mathbf{C}^1_5$	$\frac{1}{2^8}>\left(\frac{1}{2^9}\right)$	$\frac{1}{2^8}>(0)$
V	$\mathbf{C}^1_6$	$\frac{1}{2^{10}}>0$	$\frac{1}{2^{10}}>0$

(e)

subset (↓)		(PA > TPC) *for* C^6_{iL}	(PA > TPC) *for* C^6_{iR}
type	index		
V	$\mathbf{C}^1_1$	$1>\left(\frac{1}{2^1}+\frac{1}{2^2}+\frac{1}{2^3}+\frac{1}{2^4}+\frac{1}{2^5}\right)$	$1>(0+0+0+0+0)$
V	$\mathbf{C}^1_2$	$\frac{1}{2^2}>\left(\frac{1}{2^3}+\frac{1}{2^4}+\frac{1}{2^5}+\frac{1}{2^6}\right)$	$\frac{1}{2^2}>(0+0+0+0)$
V	$\mathbf{C}^1_3$	$\frac{1}{2^4}>\left(\frac{1}{2^5}+\frac{1}{2^6}+\frac{1}{2^7}\right)$	$\frac{1}{2^4}>(0+0+0)$
V	$\mathbf{C}^1_4$	$\frac{1}{2^6}>\left(\frac{1}{2^7}+\frac{1}{2^8}\right)$	$\frac{1}{2^6}>(0+0)$
V	$\mathbf{C}^1_5$	$\frac{1}{2^8}>\left(\frac{1}{2^9}\right)$	$\frac{1}{2^8}>(0)$
V	$\mathbf{C}^1_6$	$\frac{1}{2^{10}}>0$	$\frac{1}{2^{10}}>0$

(f)

Figure 4.2: Status of (PA > TPC) for (a) TSMOS ($\mathbf{T}^6$), (b) HSMOS ($[\mathbf{T}^5|\mathbf{V}^1]$), (c) HSMOS ($[\mathbf{T}^4|\mathbf{V}^2]$), (d) HSMOS ($[\mathbf{T}^3|\mathbf{V}^3]$), (e) HSMOS ($[\mathbf{T}^2|\mathbf{V}^4]$), (f) $2k$-SMOS ($\mathbf{V}^6$).

subset (↓)		(PA > TPC) *for* C^6_{iL}	(PA > TPC) *for* C^6_{iR}
type	index		
V	$\mathbf{C}^1_1$	$1>\left(\frac{1}{2^1}+\frac{1}{2^2}+\frac{1}{2^3}+\frac{1}{2^4}+\frac{1}{2^5}\right)$	$1>\left(\frac{1}{2^1}+\frac{1}{2^2}+\frac{1}{2^3}+\frac{1}{2^4}+\frac{1}{2^5}\right)$
T	$\mathbf{C}^1_2$	$\frac{1}{2^2}>\left(\frac{1}{2^3}+\frac{1}{2^4}+\frac{1}{2^5}\right)$	$\frac{1}{2^2}>\left(\frac{1}{2^3}+\frac{1}{2^4}+\frac{1}{2^5}\right)$
T	$\mathbf{C}^1_3$	$\frac{1}{2^2}>\left(\frac{1}{2^3}+\frac{1}{2^4}+\frac{1}{2^5}\right)$	$\frac{1}{2^2}>\left(\frac{1}{2^3}+\frac{1}{2^4}+\frac{1}{2^5}\right)$
T	$\mathbf{C}^1_4$	$\frac{1}{2^3}>\left(\frac{1}{2^4}+\frac{1}{2^5}\right)$	$\frac{1}{2^3}>\left(\frac{1}{2^4}+\frac{1}{2^5}\right)$
T	$\mathbf{C}^1_5$	$\frac{1}{2^4}>\left(\frac{1}{2^5}\right)$	$\frac{1}{2^4}>\left(\frac{1}{2^5}\right)$
T	$\mathbf{C}^1_6$	$\frac{1}{2^5}>0$	$\frac{1}{2^5}>0$

(*a*)

subset (↓)		(PA > TPC) *for* C^6_{iL}	(PA > TPC) *for* C^6_{iR}
type	index		
V	$\mathbf{C}^1_1$	$1>\left(\frac{1}{2^1}+\frac{1}{2^2}+\frac{1}{2^3}+\frac{1}{2^4}+\frac{1}{2^5}\right)$	$1>\left(0+\frac{1}{2^2}+\frac{1}{2^3}+\frac{1}{2^4}+\frac{1}{2^5}\right)$
V	$\mathbf{C}^1_2$	$\frac{1}{2^2}>\left(\frac{1}{2^3}+\frac{1}{2^4}+\frac{1}{2^5}+\frac{1}{2^6}\right)$	$\frac{1}{2^2}>\left(\frac{1}{2^3}+\frac{1}{2^4}+\frac{1}{2^5}+\frac{1}{2^6}\right)$
T	$\mathbf{C}^1_3$	$\frac{1}{2^2}>\left(\frac{1}{2^3}+\frac{1}{2^4}+\frac{1}{2^5}\right)$	$\frac{1}{2^2}>\left(\frac{1}{2^3}+\frac{1}{2^4}+\frac{1}{2^5}\right)$
T	$\mathbf{C}^1_4$	$\frac{1}{2^3}>\left(\frac{1}{2^4}+\frac{1}{2^5}\right)$	$\frac{1}{2^3}>\left(\frac{1}{2^4}+\frac{1}{2^5}\right)$
T	$\mathbf{C}^1_5$	$\frac{1}{2^4}>\left(\frac{1}{2^5}\right)$	$\frac{1}{2^4}>\left(\frac{1}{2^5}\right)$
T	$\mathbf{C}^1_6$	$\frac{1}{2^5}>0$	$\frac{1}{2^5}>0$

(*b*)

subset (↓)		(PA > TPC) *for* C^6_{iL}	(PA > TPC) *for* C^6_{iR}
type	index		
V	$\mathbf{C}^1_1$	$1>\left(\frac{1}{2^1}+\frac{1}{2^2}+\frac{1}{2^3}+\frac{1}{2^4}+\frac{1}{2^5}\right)$	$1>\left(\frac{1}{2^1}+\frac{1}{2^2}+\frac{1}{2^3}+\frac{1}{2^4}+\frac{1}{2^5}\right)$
V	$\mathbf{C}^1_2$	$\frac{1}{2^2}>\left(\frac{1}{2^3}+\frac{1}{2^4}+\frac{1}{2^5}+\frac{1}{2^6}\right)$	$\frac{1}{2^2}>\left(0+\frac{1}{2^4}+\frac{1}{2^5}+\frac{1}{2^6}\right)$
V	$\mathbf{C}^1_3$	$\frac{1}{2^4}>\left(\frac{1}{2^5}+\frac{1}{2^6}+\frac{1}{2^7}\right)$	$\frac{1}{2^4}>\left(\frac{1}{2^5}+\frac{1}{2^6}+\frac{1}{2^7}\right)$
T	$\mathbf{C}^1_4$	$\frac{1}{2^3}>\left(\frac{1}{2^4}+\frac{1}{2^5}\right)$	$\frac{1}{2^3}>\left(\frac{1}{2^4}+\frac{1}{2^5}\right)$
T	$\mathbf{C}^1_5$	$\frac{1}{2^4}>\left(\frac{1}{2^5}\right)$	$\frac{1}{2^4}>\left(\frac{1}{2^5}\right)$
T	$\mathbf{C}^1_6$	$\frac{1}{2^5}>0$	$\frac{1}{2^5}>0$

(*c*)

subset (↓)		(PA > TPC) *for* C^6_{iL}	(PA > TPC) *for* C^6_{iR}
type	index		
V	$\mathbf{C}^1_1$	$1>\left(\frac{1}{2^1}+\frac{1}{2^2}+\frac{1}{2^3}+\frac{1}{2^4}+\frac{1}{2^5}\right)$	$1>\left(\frac{1}{2^1}+\frac{1}{2^2}+\frac{1}{2^3}+\frac{1}{2^4}+\frac{1}{2^5}\right)$
V	$\mathbf{C}^1_2$	$\frac{1}{2^2}>\left(\frac{1}{2^3}+\frac{1}{2^4}+\frac{1}{2^5}+\frac{1}{2^6}\right)$	$\frac{1}{2^2}>\left(0+\frac{1}{2^4}+\frac{1}{2^5}+\frac{1}{2^6}\right)$
V	$\mathbf{C}^1_3$	$\frac{1}{2^4}>\left(\frac{1}{2^5}+\frac{1}{2^6}+\frac{1}{2^7}\right)$	$\frac{1}{2^4}>\left(\frac{1}{2^5}+\frac{1}{2^6}+\frac{1}{2^7}\right)$
T	$\mathbf{C}^1_4$	$\frac{1}{2^3}>\left(\frac{1}{2^4}+\frac{1}{2^5}\right)$	$\frac{1}{2^3}>\left(\frac{1}{2^4}+\frac{1}{2^5}\right)$
T	$\mathbf{C}^1_5$	$\frac{1}{2^4}>\left(\frac{1}{2^5}\right)$	$\frac{1}{2^4}>\left(\frac{1}{2^5}\right)$
T	$\mathbf{C}^1_6$	$\frac{1}{2^5}>0$	$\frac{1}{2^5}>0$

(*f*)

subset (↓)		(PA > TPC) *for* C^6_{iL}	(PA > TPC) *for* C^6_{iR}
type	index		
V	$\mathbf{C}^1_1$	$1>\left(\frac{1}{2^1}+\frac{1}{2^2}+\frac{1}{2^3}+\frac{1}{2^4}+\frac{1}{2^5}\right)$	$1>\left(0+0+0+\frac{1}{2^4}+\frac{1}{2^5}\right)$
V	$\mathbf{C}^1_2$	$\frac{1}{2^2}>\left(\frac{1}{2^3}+\frac{1}{2^4}+\frac{1}{2^5}+\frac{1}{2^6}\right)$	$\frac{1}{2^2}>\left(0+0+\frac{1}{2^4}+\frac{1}{2^5}\right)$
V	$\mathbf{C}^1_3$	$\frac{1}{2^4}>\left(\frac{1}{2^5}+\frac{1}{2^6}+\frac{1}{2^7}\right)$	$\frac{1}{2^4}>\left(\frac{1}{2^5}+\frac{1}{2^6}+\frac{1}{2^7}\right)$
T	$\mathbf{C}^1_4$	$\frac{1}{2^3}>\left(\frac{1}{2^4}+\frac{1}{2^5}\right)$	$\frac{1}{2^3}>\left(\frac{1}{2^4}+\frac{1}{2^5}\right)$
T	$\mathbf{C}^1_5$	$\frac{1}{2^4}>\left(\frac{1}{2^5}\right)$	$\frac{1}{2^4}>\left(\frac{1}{2^5}\right)$
T	$\mathbf{C}^1_6$	$\frac{1}{2^5}>0$	$\frac{1}{2^5}>0$

(*d*)

subset (↓)		(PA > TPC) *for* C^6_{iL}	(PA > TPC) *for* C^6_{iR}
type	index		
V	$\mathbf{C}^1_1$	$1>\left(\frac{1}{2^1}+\frac{1}{2^2}+\frac{1}{2^3}+\frac{1}{2^4}+\frac{1}{2^5}\right)$	$1>\left(0+0+0+0+\frac{1}{2^5}\right)$
V	$\mathbf{C}^1_2$	$\frac{1}{2^2}>\left(\frac{1}{2^3}+\frac{1}{2^4}+\frac{1}{2^5}+\frac{1}{2^6}\right)$	$\frac{1}{2^2}>\left(0+0+0+\frac{1}{2^6}\right)$
V	$\mathbf{C}^1_3$	$\frac{1}{2^4}>\left(\frac{1}{2^5}+\frac{1}{2^6}+\frac{1}{2^7}\right)$	$\frac{1}{2^4}>\left(0+0+\frac{1}{2^7}\right)$
V	$\mathbf{C}^1_4$	$\frac{1}{2^6}>\left(\frac{1}{2^7}+\frac{1}{2^8}\right)$	$\frac{1}{2^6}>\left(0+\frac{1}{2^8}\right)$
V	$\mathbf{C}^1_5$	$\frac{1}{2^8}>\left(\frac{1}{2^9}\right)$	$\frac{1}{2^8}>\left(0\right)$
V	$\mathbf{C}^1_6$	$\frac{1}{2^5}>0$	$\frac{1}{2^{10}}>0$

(*e*)

Figure 4.3: Status of (PA > TPC) for (a) TSMOS ($\mathbf{T}^6$), (b) HSMOS ($\left[\mathbf{V}^2|\mathbf{T}^4\right]$), (c) HSMOS ($\left[\mathbf{V}^3|\mathbf{T}^3\right]$), (d) HSMOS ($\left[\mathbf{V}^4|\mathbf{T}^2\right]$), (e) HSMOS ($\left[\mathbf{V}^5|\mathbf{T}^1\right]$), (f) $2k$-SMOS ($\mathbf{V}^6$).

and TSMOS to $2k$-SMOS through HSMOS $\left[\mathbf{V}^g|\mathbf{T}^{k-g}\right]$, in Figure 4.2 and 4.3 respectively. Recall that for the errorless MF detection of different subsets (i.e.; $\mathbf{C}_1^k, \mathbf{C}_2^k, \mathbf{C}_3^k, \ldots, \mathbf{C}_k^k$) from the respective received vectors (i.e.; $\mathbf{y}_1$, $\mathbf{y}_2$, $\mathbf{y}_3$, $\ldots$, $\mathbf{y}_k$.), the inequality in (3.1) is the only necessary condition to be satisfied. Note that, in Figure 4.2 and 4.3, the presentation of the statistics are for $\mathbf{C}^6$ (N_k=64 and M_k=126, i.e.; k=6) and for simulation, we have considered the matrices of similar dimension so as to tally the simulation results with the theoretical observations.

Each figure contains $k = 6$ sub-figures presenting the behavior of all $k = 6$ possible structures, out of which, the first and last one always replicate the ternary and $2k$-ary type. In other words, our intention lies in illustrating the behavioral transition in the structure of the inequality (PA > TPC), when the TSMOS is interpreted to be transformed to $2k$-SMOS using the two possible approaches: gradual (one-by-one) replacement of the binary subsets ($\mathbf{V}$) (a) from the *closing end* of the matrix, and (b) from the *starting end* of the matrix. For each case, the analysis is carried out for the left and right child, separately in two separate columns, with a purpose to identify the difference in their pattern of PA and TPC. Below, we discuss the crucial remarks extracted from Figure 4.2 and 4.3

Figure 4.4 illustrates the overall change in the behavior of the basic metrics (i.e.; TPC and PA) within the family of SMOS i.e.; TSMOS, HSMOS ($\left[\mathbf{T}^g|\mathbf{V}^{k-g}\right]$, $\left[\mathbf{V}^g|\mathbf{T}^{k-g}\right]$), and $2k$-SMOS. In particular, for HSMOS, the TPC on a particular signature in a subset can be characterized into two types: TPC (intra.) and TPC (inter.). Where TPC (intra.) and TPC (inter.) indicates the level of TPC due to the subsets of similar (between $\mathbf{T}$, $\mathbf{T}$, or $\mathbf{V}$, $\mathbf{V}$) and different (between $\mathbf{T}$, $\mathbf{V}$) types respectively. *For example*: Take the case of a ternary subset in HSMOS $\left[\mathbf{T}^g|\mathbf{V}^{k-g}\right]$. Here, TPC (intra.) and TPC (inter.) implies to the TPC from the other ternary subsets of $\mathbf{T}$, and all $(k-g)$ binary subsets of $\mathbf{V}$ respectively. The explanation, in this figure, is with reference to the TSMOS, considering it as the origin of the SMOS family. In other words, in the figure, the variation in the level of PA, TPC (intra.), TPC (inter.) for HSMOS and $2k$-SMOS are noted down with reference to that of the TSMOS, which facilitates with a relative approach to analyze and realize the gradual transformation in their overall behavior.

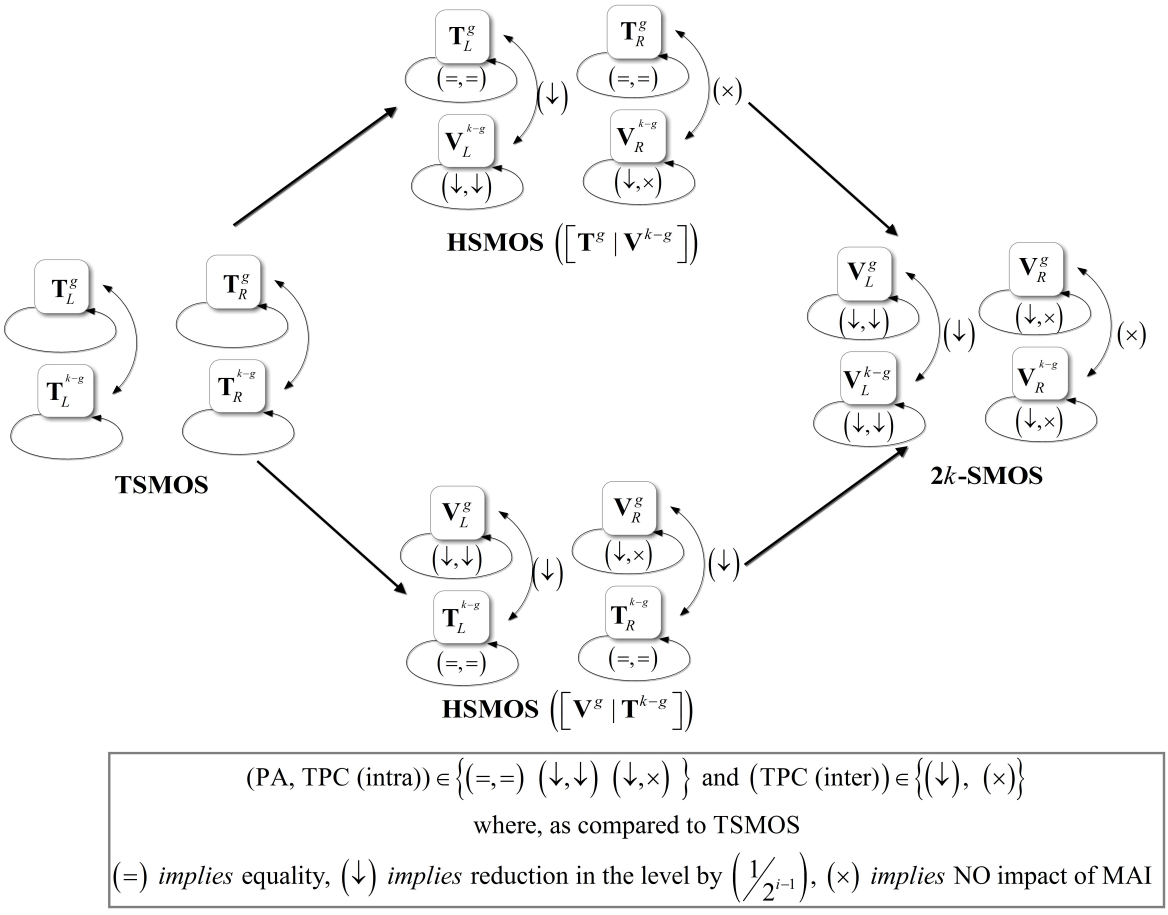

(PA, TPC (intra)) $\in \{(=,=)\ (\downarrow,\downarrow)\ (\downarrow,\times)\}$ and (TPC (inter)) $\in \{(\downarrow),\ (\times)\}$
where, as compared to TSMOS
$(=)$ *implies* equality, $(\downarrow)$ *implies* reduction in the level by $\left(1/2^{i-1}\right)$, $(\times)$ *implies* NO impact of MAI

Figure 4.4: Explanation of the transition within different variants within HSMOS

4.3.2 For HSMOS $\mathbf{C}^k = \left[\mathbf{T}^g|\mathbf{V}^{k-g}\right]$

Figure 4.2 presents the variation in the inequality (PA > TPC), when the TSMOS is transformed to 2k-SMOS by the gradual (one-by-one) replacement of the binary subsets ($\mathbf{V}$) from the *closing end* of the matrix. Thus, for $k = 6$, six different structures are realized i.e.; $\left[\mathbf{C}^6_{1V}|\mathbf{C}^6_{2T}|\mathbf{C}^6_{3T}|\mathbf{C}^6_{4T}|\mathbf{C}^6_{5T}|\mathbf{C}^6_{6V}\right]$, $\left[\mathbf{C}^6_{1V}|\mathbf{C}^6_{2T}|\mathbf{C}^6_{3T}|\mathbf{C}^6_{4T}|\mathbf{C}^6_{5V}|\mathbf{C}^6_{6V}\right]$, $\left[\mathbf{C}^6_{1V}|\mathbf{C}^6_{2T}|\mathbf{C}^6_{3T}|\mathbf{C}^6_{4V}|\mathbf{C}^6_{5V}|\mathbf{C}^6_{6V}\right]$, $\left[\mathbf{C}^6_{1V}|\mathbf{C}^6_{2T}|\mathbf{C}^6_{3V}|\mathbf{C}^6_{4V}|\mathbf{C}^6_{5V}|\mathbf{C}^6_{6V}\right]$, $\left[\mathbf{C}^6_{1V}|\mathbf{C}^6_{2V}|\mathbf{C}^6_{3V}|\mathbf{C}^6_{4V}|\mathbf{C}^6_{5V}|\mathbf{C}^6_{6V}\right]$, and they are illustrated in Figure 4.2 (a), 4.2 (b), 4.2 (c), 4.2 (d), 4.2 (e), and 4.2 (f) respectively.

According to Figure 4.4, the metrics required to be subjected to analysis are: PA on both types of subsets ($\mathbf{T}$ and $\mathbf{V}$), TPC (inter.) and TPC (intra.) on the left and right child of each subset.

$$\left(\mathrm{PA}_{\left[\mathbf{T}^g\mathbf{V}^{k-g}\right]}\right)_{\mathbf{C}^k_{iV}} = \frac{\left(\mathrm{PA}_{[\mathbf{T}^k]}\right)_{\mathbf{C}^k_i (for\ g+1\ \leq\ i\ \leq\ k)}}{2^{i-1}}, \tag{4.1}$$

Table 4.3: Analaysis of metrics for HSMOS ($\mathbf{C}^k = \left[\mathbf{T}^g|\mathbf{V}^{k-g}\right]$).

Metrics	$\mathbf{T}^g$ / $\mathbf{V}^{k-g}$	L / R	Status of the Metrics	Symbol
PA	$\mathbf{T}^g$	L	Remains unchanged	=
		R	Remains unchanged	=
	$\mathbf{V}^{k-g}$	L	Reduces by $1/2^{i-1}$ (4.1)	↓
		R	Reduces by $1/2^{i-1}$ (4.1)	↓
TPC (inter.)	$\mathbf{T}^g$	L	Reduces by $1/2^{i-1}$ (4.2)	×
		R	Reduces to Zero	↓
TPC (intra.)	$\mathbf{T}^g$	L	Remains unchanged	=
		R	Remains unchanged	=
	$\mathbf{V}^{k-g}$	L	Reduces by $1/2^{i-1}$ (4.3)	↓
		R	Reduces to Zero	×

$$\left(\text{TPC}_{[\mathbf{T}^g\mathbf{V}^{k-g}]}\right)_{\mathbf{C}^k_{iT}} = \frac{\left(\text{TPC}_{[\mathbf{T}^k]}\right)_{\mathbf{C}^k_i (for\ g+1 \le i \le k)}}{2^{i-1}}, \tag{4.2}$$

$$\left(\text{TPC}_{[\mathbf{T}^g\mathbf{V}^{k-g}]}\right)_{\mathbf{C}^k_{iV}} = \frac{\left(\text{TPC}_{[\mathbf{T}^k]}\right)_{\mathbf{C}^k_i (for\ g+1 \le i \le k)}}{2^{i-1}}, \tag{4.3}$$

Table 4.4: Analaysis of metrics for HSMOS ($\mathbf{C}^k = [\mathbf{V}^g|\mathbf{T}^{k-g}]$).

Metrics	$\mathbf{V}^g$ $\mathbf{T}^{k-g}$	L / R	Status of the Metrics	Symbol
PA	$\mathbf{V}^g$	L	Reduces by $1/2^{i-1}$ (4.4)	↓
		R	Reduces by $1/2^{i-1}$ (4.4)	↓
	$\mathbf{T}^{k-g}$	L	Remains unchanged	=
		R	Remains unchanged	=
TPC (inter.)	$\mathbf{V}^g$	L	Reduces by $1/2^{i-1}$ (4.5)	↓
		R	Reduces by $1/2^{i-1}$ (4.5)	↓
TPC (intra.)	$\mathbf{V}^g$	L	Reduces by $1/2^{i-1}$ (4.6)	↓
		R	Reduces to Zero	×
	$\mathbf{T}^{k-g}$	L	Remains unchanged	=
		R	Remains unchanged	=

Remark: In Table 4.3, unlike the other metrics (i.e.; PA and TPC (intra.)), we have limited the analysis for TPC (inter.) to the first g subsets (i.e.; $\mathbf{V}^g$) only. This difference is because of our current approach of decoding which recovers the top g layers of the tree prior to the bottom $(k-g)$ layers. As a result, by the time the bottom $(k-g)$ layers (i.e.; $\mathbf{V}$) get subjected to decoding, the top layers (i.e.; $\mathbf{T}$) are already decoded with no error for noisefree transmission. So, including the interference of $\mathbf{T}$ on $\mathbf{V}$ in analysis is of no significance. Even if there exists few error in decoding of top layers, its impact on the bottom layers, in terms of TPC (inter.), can be logically

considered to be marginal only. Identical apprehension can also be applied to the case of HSMOS ($\mathbf{C}^k = \left[\mathbf{V}^g|\mathbf{T}^{k-g}\right]$), explained below. Similar apprehension is also applicable to Table 4.4.

4.3.3 For HSMOS $\mathbf{C}^k = \left[\mathbf{V}^g|\mathbf{T}^{k-g}\right]$

Figure 4.3 illustrates the variation of the inequality (PA > TPC), when TSMOS is transformed to $2k$-SMOS by the gradual (one-by-one) replacement of the binary subsets ($\mathbf{V}$) from the *starting end* of the matrix. Thus, for $k = 6$, six different structures are realized i.e.; $\left[\mathbf{C}^6_{1V}|\mathbf{C}^6_{2T}|\mathbf{C}^6_{3T}|\mathbf{C}^6_{4T}|\mathbf{C}^6_{5T}|\mathbf{C}^6_{6T}\right]$, $\left[\mathbf{C}^6_{1V}|\mathbf{C}^6_{2V}|\mathbf{C}^6_{3T}|\mathbf{C}^6_{4T}|\mathbf{C}^6_{5T}|\mathbf{C}^6_{6T}\right]$, $\left[\mathbf{C}^6_{1V}|\mathbf{C}^6_{2V}|\mathbf{C}^6_{3V}|\mathbf{C}^6_{4T}|\mathbf{C}^6_{5V}|\mathbf{C}^6_{6V}\right]$, $\left[\mathbf{C}^6_{1V}|\mathbf{C}^6_{2V}|\mathbf{C}^6_{3V}|\mathbf{C}^6_{4V}|\mathbf{C}^6_{5T}|\mathbf{C}^6_{6T}\right]$, $\left[\mathbf{C}^6_{1V}|\mathbf{C}^6_{2V}|\mathbf{C}^6_{3V}|\mathbf{C}^6_{4V}|\mathbf{C}^6_{5V}|\mathbf{C}^6_{6T}\right]$, $\left[\mathbf{C}^6_{1V}|\mathbf{C}^6_{2V}|\mathbf{C}^6_{3V}|\mathbf{C}^6_{4V}|\mathbf{C}^6_{5V}|\mathbf{C}^6_{6V}\right]$, and they are illustrated in Figure 4.3 (a), 4.3 (b), 4.3 (c), 4.3 (d), 4.3 (e), and 4.3 (f) respectively.

$$\left(\mathrm{PA}_{\left[\mathbf{V}^g\mathbf{T}^{k-g}\right]}\right)_{\mathbf{C}^k_{iV}} = \frac{(\mathrm{PA}_{[\mathbf{T}^g]})_{\mathbf{C}^k_i (for\ 2 \le i \le g)}}{2^{i-1}} \tag{4.4}$$

$$\left(\mathrm{TPC}_{\left[\mathbf{V}^g\mathbf{T}^{k-g}\right]}\right)_{\mathbf{C}^k_{iV} (for\ 2<i<g)} = \frac{\left(\mathrm{TPC}_{[\mathbf{T}^g]}\right)_{\mathbf{C}^k_i (for\ g+1 \le i \le k)}}{2^{i-1}}, \tag{4.5}$$

$$\left(\mathrm{TPC}_{\left[\mathbf{V}^g\mathbf{T}^{k-g}\right]}\right)_{\mathbf{C}^k_{iV} (for\ 2<i<g)} = \frac{\left(\mathrm{TPC}_{[\mathbf{T}^g]}\right)_{\mathbf{C}^k_i\ (for\ 2 \le i \le g)}}{2^{i-1}}, \tag{4.6}$$

4.4 Expression for Average BER

In Section 2.5, the proof to the errorfree decoding of the TSMOS is already explained in Lemma 1, where the inequality criterion in (3.1) can be found to regularize the errorfree validation at each stage of detection. Due to the resemblance in construction and pattern of MAI, an analogous approach can also be adopted to justify the errorless decoding of $2k$-SMOS. Equivalently, the design of MUD (Figure 2.6) proposed for TSMOS and $2k$-SMOS is applicable for the decoding of HSMOS. Therefore, the advantage in terms of MUD's simplicity is also available for HSMOS.

Now, based on the discussion from the previous section, let us first rewrite the expression in (2.1) so as to support our analysis of error performance involving the left and right child, existing in each subset of $\mathbf{C}^k = \left[\mathbf{T}^g|\mathbf{V}^{k-g}\right]$ and $\mathbf{C}^k = \left[\mathbf{V}^g|\mathbf{T}^{k-g}\right]$

respectively, such that

$$\mathbf{y} = \sum_{u=1}^{g} \mathbf{C}^{k}_{(uT)L}\mathbf{x}_{(uT)L} + \sum_{v=1}^{g} \mathbf{C}^{k}_{(uT)R}\mathbf{x}_{(uT)R} + \sum_{u=(g+1)}^{k} \mathbf{C}^{k}_{(vV)L}\mathbf{x}_{(vV)L} + \sum_{v=(g+1)}^{k} \mathbf{C}^{k}_{(vV)R}\mathbf{x}_{(vV)R} + \mathbf{n}, \tag{4.7}$$

$$\mathbf{y} = \sum_{u=1}^{g} \mathbf{C}^{k}_{(uV)L}\mathbf{x}_{(uV)L} + \sum_{v=1}^{g} \mathbf{C}^{k}_{(uV)R}\mathbf{x}_{(uV)R} + \sum_{u=(g+1)}^{k} \mathbf{C}^{k}_{(vT)L}\mathbf{x}_{(vT)L} + \sum_{v=(g+1)}^{k} \mathbf{C}^{k}_{(vT)R}\mathbf{x}_{(vT)R} + \mathbf{n}. \tag{4.8}$$

The expression in (4.7) and (4.8) represents the received noisy vector for $\left[\mathbf{T}^{g}|\mathbf{V}^{k-g}\right]$ and $\left[\mathbf{V}^{g}|\mathbf{T}^{k-g}\right]$, in terms of the left and right child. Now, in correspondence with the above expressions, the generalized expression of the probability of average error for the *ternary* and *binary* subsets in either $\left[\mathbf{T}^{g}|\mathbf{V}^{k-g}\right]$ or $\left[\mathbf{V}^{g}|\mathbf{T}^{k-g}\right]$ can be written as:

$$P^{ij}_{eT} = Q\left(\sqrt{\frac{\left(\frac{N_{ef_i}}{N}\right)^{2}\mathrm{E}\left(x^{2}_{ij}\right)}{\sum_{u=i+1}^{k}\rho^{2}_{iu(j)} + 4\sum_{v=1}^{i-1}\rho^{2}_{iu(j)}P^{v}_{e} + \mathrm{E}\left(n^{2}_{i(j)}\right)}}\right), \tag{4.9}$$

$$P^{ij}_{eV} = Q\left(\sqrt{\frac{\left(\frac{1}{4^{i-1}}\right)^{2}\mathrm{E}\left(\mathrm{x}^{2}_{\mathrm{iL_j}}\right)}{\sum_{u=i+1}^{k}\left(\rho^{2}_{iLu(j)}\right)^{2} + 4\sum_{v=1}^{i-1}\rho^{2}_{iLv(j)}P^{v}_{e} + \mathrm{E}\left(\mathrm{n}^{2}_{\mathrm{i(j)}}\right)}}\right). \tag{4.10}$$

Note that the aforementioned expression of the average BER are nothing but the expression for average BER of the individual subsets for TSMOS (2.29) and $2k$-SMOS (Table 3.2).

4.5 Simulation Results

In this Section, we discuss the BER versus (E_b/N_0) performance of the system, assuming the channel to be AWGN. The system is supposed to be BPSK modulated, perfectly power controlled, and operated for synchronous transmission. The MUD shown in Figure 2.6 is selected for detection and the matrices of dimension (64×126) are considered for simulation.

In order to trace the gradual variation in the behavior of the BER of the individual subsets of SMOS of different structures, we follow the chronology of presentation: from Ternary to $2k$-ary SMOS through HSMOS structures ($\left[\mathbf{T}^{g}|\mathbf{V}^{k-g}\right]$ and $\left[\mathbf{V}^{g}|\mathbf{T}^{k-g}\right]$). for both the cases, the description of the subsequent transitions observed in the BER

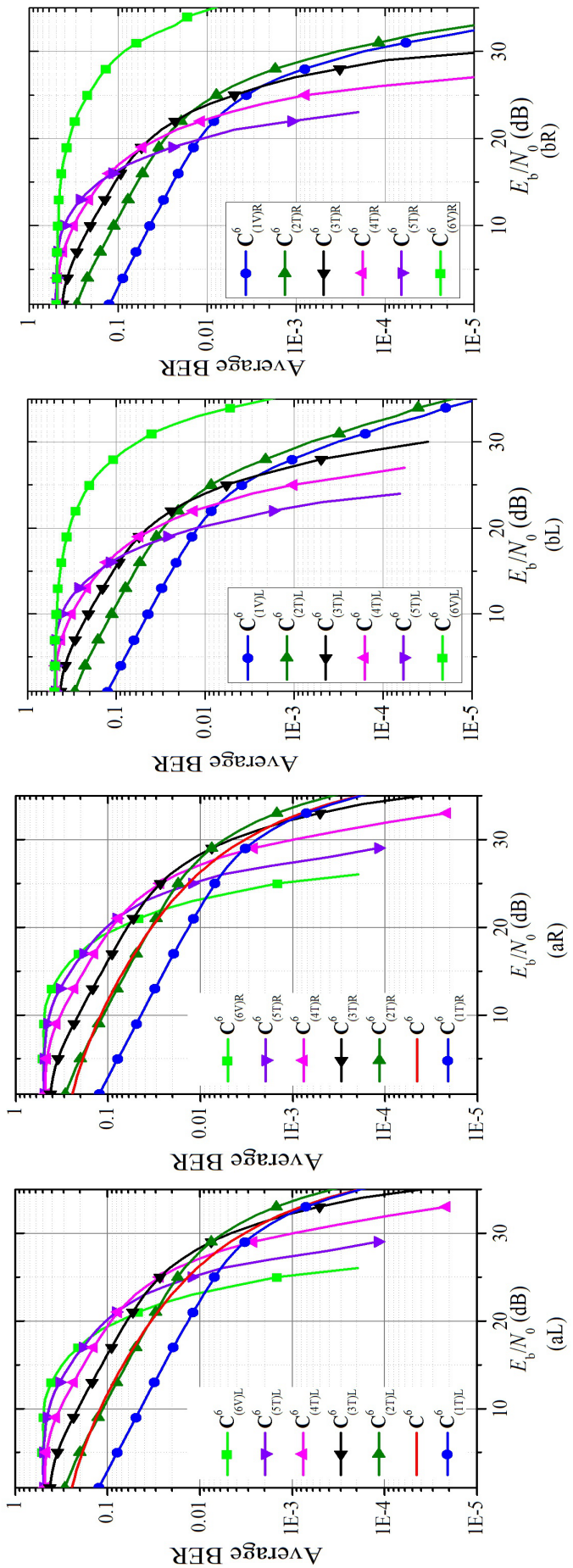

Figure 4.5: BER performance of TSMOS ($\mathbf{T}^6$): (aL) Left child and (aR) Right child, HSMOS ($[\mathbf{T}^5|\mathbf{V}^1]$): (bL) Left child and (bR) Right child.

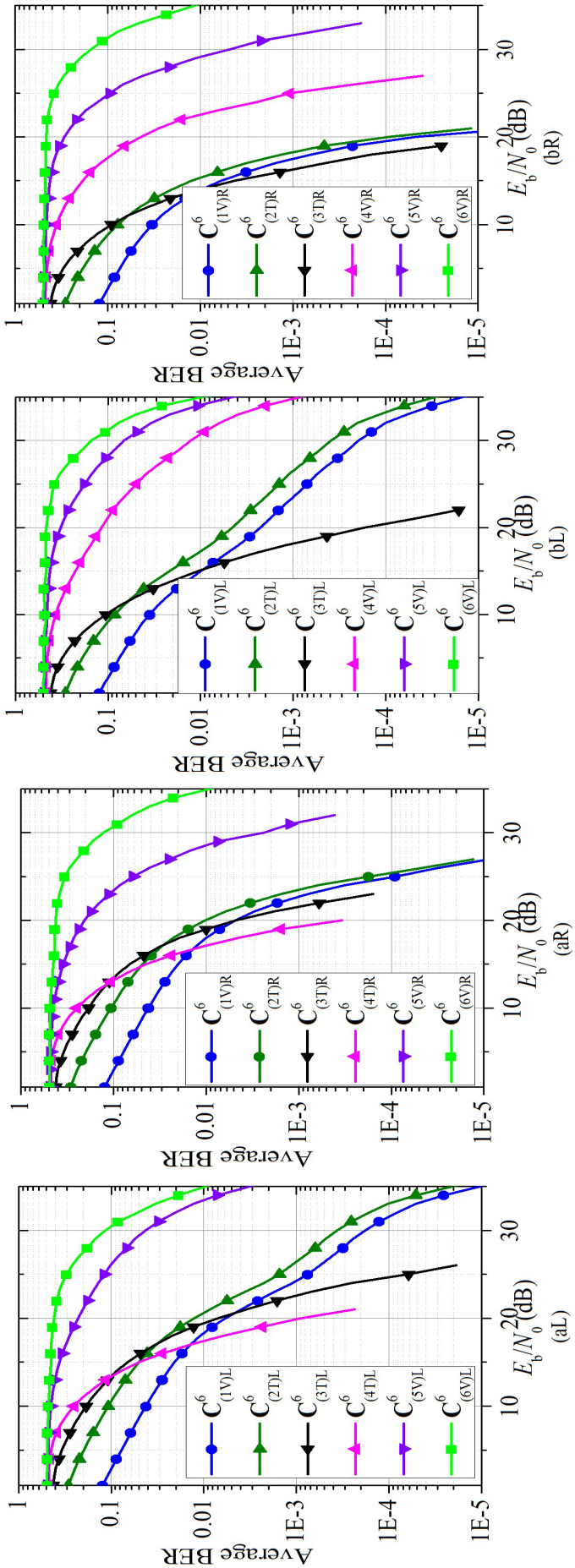

Figure 4.6: BER performance of HSMOS ($[\mathbf{T}^4|\mathbf{V}^2]$): (aL) Left child and (aR) Right child, HSMOS ($[\mathbf{T}^3|\mathbf{V}^3]$) (bL) Left child and (bR) Right child.

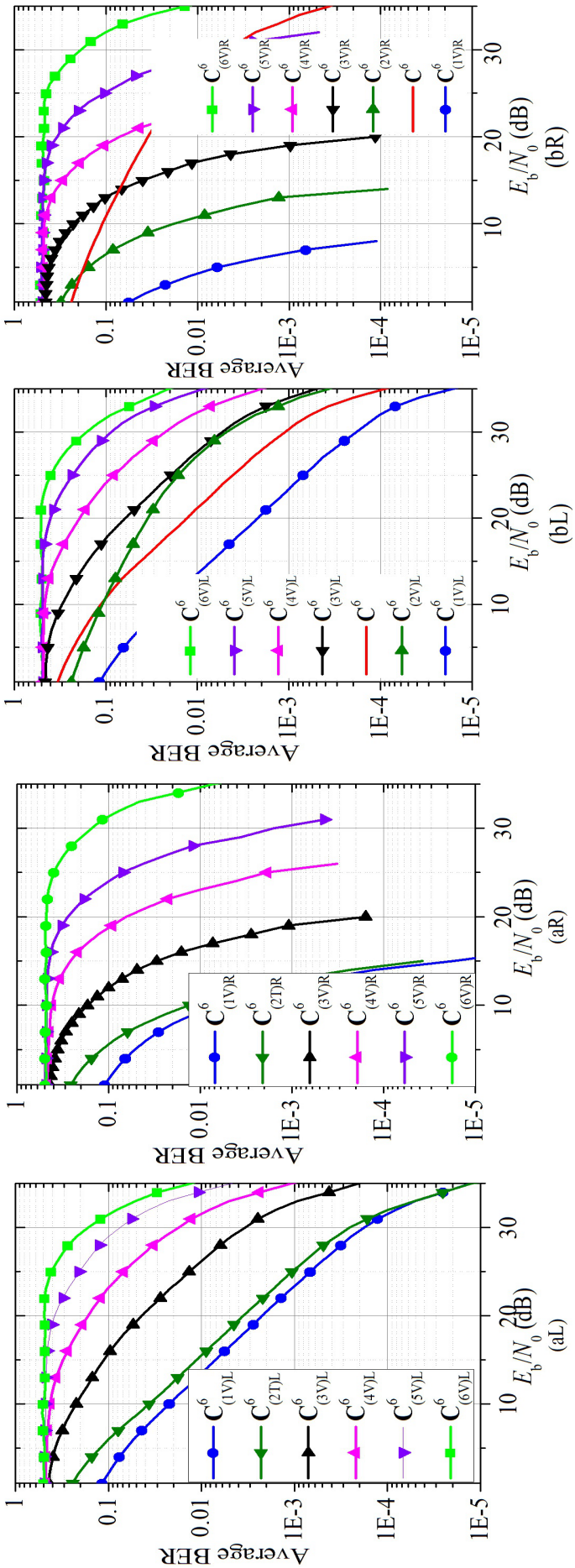

Figure 4.7: BER performance of HSMOS ($[\mathbf{T}^2|\mathbf{V}^4]$) (aL) Left child and (aR) Right child, $2k$-SMOS ($\mathbf{V}^6$): (bL) Left child and (bR) Right child.

curves is discussed with respect to the respective change registered in the status of the inequality (in Figure 4.2 and 4.3).

4.5.1 Explanation to Figure 4.5, 4.6, 4.7

Figure 4.5: (aL), (bL), Figure 4.6: (aL), (bL), Figure 4.7: (aL), (bL), and Figure 4.5: (aR),(bR), Figure 4.6: (aR), (bR), Figure 4.7: (aR), (bR) correspond to the BER performance of the left and right child of HSMOS ($\left[\mathbf{T}^g|\mathbf{V}^{k-g}\right]$) architecture: $\left[\mathbf{C}^6_{1V}|\mathbf{C}^6_{2T}|\mathbf{C}^6_{3T}|\mathbf{C}^6_{4T}|\mathbf{C}^6_{5T}|\mathbf{C}^6_{6T}\right]$, $\left[\mathbf{C}^6_{1V}|\mathbf{C}^6_{2T}|\mathbf{C}^6_{3T}|\mathbf{C}^6_{4T}|\mathbf{C}^6_{5T}|\mathbf{C}^6_{6V}\right]$, $\left[\mathbf{C}^6_{1V}|\mathbf{C}^6_{2T}|\mathbf{C}^6_{3T}|\mathbf{C}^6_{4T}|\mathbf{C}^6_{5V}|\mathbf{C}^6_{6V}\right]$, $\left[\mathbf{C}^6_{1V}|\mathbf{C}^6_{2T}|\mathbf{C}^6_{3T}|\mathbf{C}^6_{4V}|\mathbf{C}^6_{5V}|\mathbf{C}^6_{6V}\right]$, $\left[\mathbf{C}^6_{1V}|\mathbf{C}^6_{2T}|\mathbf{C}^6_{3V}|\mathbf{C}^6_{4V}|\mathbf{C}^6_{5V}|\mathbf{C}^6_{6V}\right]$, $\left[\mathbf{C}^6_{1V}|\mathbf{C}^6_{2V}|\mathbf{C}^6_{3V}|\mathbf{C}^6_{4V}|\mathbf{C}^6_{5V}|\mathbf{C}^6_{6V}\right]$ respectively, whose status of inequality (PA > TPC) are presented in Figure 4.2 (a) to (f). Prior to proceeding further, the summary of the outcome of Figure 4.5 listed in Table 4.3 must be referred for better understanding.

Starting with Figure 4.5 (aL) and (aR), it illustrates the BER performance of the TSMOS, where the role of N_{ef} and net MAI (or TPC) being responsible for the non-uniformity in response of the error performance of the individual subsets has already been explained in the previous section. Following this, a dramatic lowering in the level of BER is observed for the smaller subsets (with lower N_{ef} or detected in the later stages of decoder) over the larger ones (higher N_{ef} or detected in the earlier stages), at higher values of E_b/N_o (already explained for Fig 3.5 (a)). As the reason of this non-uniformity, the gradual reduction in the level of TPC with the progress of the decoding stages has been reported to be responsible.

For $\mathbf{V}^{k-g}$: With the replacement of the binary subsets to form $\left[\mathbf{T}^g|\mathbf{V}^{k-g}\right]$, the *equal* fall in the level of their PA (4.1) allows the level of BER of the left and right child of the $(k-g)$ subsets to rise, as compared to that of the ternary SMOS. However, at the same time, due to the presence of *unequal* level of TPC (intra.) on the decoded subset, performance variation is observed. In particular, the level of TPC (intra.) on the left and right child is found to be non-zero (4.3) and zero respectively, which ultimately leads to the rise in the value of the metric (PA-TPC) for the right child over the left. As a result, the level of BER that is considered to be inversely proportional to (PA-TPC), as already discussed in Section 3.6, improves significantly for the right child.

Example 1 : For HSMOS ($\left[\mathbf{T}^3|\mathbf{V}^3\right]$), the error performance of $\mathbf{C}^6_{(4V)_R}$ (in Figure 4.6 (bL)) is better over $\mathbf{C}^6_{(4V)_L}$ (in Figure 4.6 (bR)).

For $\mathbf{T}^g$: Where the above variations is for the binary subsets, the left and right child of rest of the g subsets (one binary and rest ternary) also get subjected to transitions in their BER behavior. The variation is due to the change in the level of TPC, even if the level of PA remains same as that of the TSMOS. According to Table 4.3, the *right* child of these subsets at a particular level, is exposed to zero and non-zero level of TPC (inter.) and TPC (intra.) respectively. In contrast, the $left$ child is exposed to non-zero level of TPC (inter.) (4.2) and TPC (intra.) (4.3) respectively. Therefore, for the g subsets at the top level of the tree, the right child at a particular level should show superiority in error performance over the left.

Example 2 : For HSMOS ($\left[\mathbf{T}^3|\mathbf{V}^3\right]$), the error performance of $\mathbf{C}^6_{(2V)_R}$ (in Figure 4.6 (bL)) is better over $\mathbf{C}^6_{(2V)_L}$ (in Figure 4.6 (bR)).

In Overall: For a particular subset remaining ternary, with the decrease in the value of g (while approaching from TSMOS to $2k$-SMOS), the level of TPC on its left and right child shows a continuous fall. The fall is because, with the lowering of the value of g, the number of (binary) subsets (i.e.; $k-g$), producing zero MAI and reduced MAI on the right and left child, respectively, increases. With the rise in the $(k-g)$ number of binary subsets, the fall is observed in the level of effective TPC (ETPC)[1] on the left child, as mentioned in Section 3.6. Therefore, with the increase in value of g, the level of BER of the left and right child of a particular subsets falls continuously.

Example 3 : The error performance of $\mathbf{C}^6_{2T}$ for all six scenarios can be referred, where the fall in the BER level of the left and right child can be found to be continuously improving in Figure 4.5 (bL), Figure 4.6 (aL), (bL) and 4.5 (bR), Figure 4.6 (aR), (bR) for the lowering of g from 5 to 2.

4.5.2 Explanation to Figure 4.8, 4.9, 4.10

Figure 4.8: (aL), (bL), Figure 4.9: (aL), (bL), Figure 4.10: (aL), (bL), and Figure 4.8: (aR),(bR), Figure 4.9: (aR), (bR), Figure 4.10: (aR), (bR) correspond to the BER performance of the left and right child of HSMOS ($\left[\mathbf{V}^g|\mathbf{T}^{k-g}\right]$)

[1]Recall from Section 3.6.4 that for matrices with ternary signature, effective peak-cross-correlation 3.7 is considered as a more accurate metric for analysis of the MAI

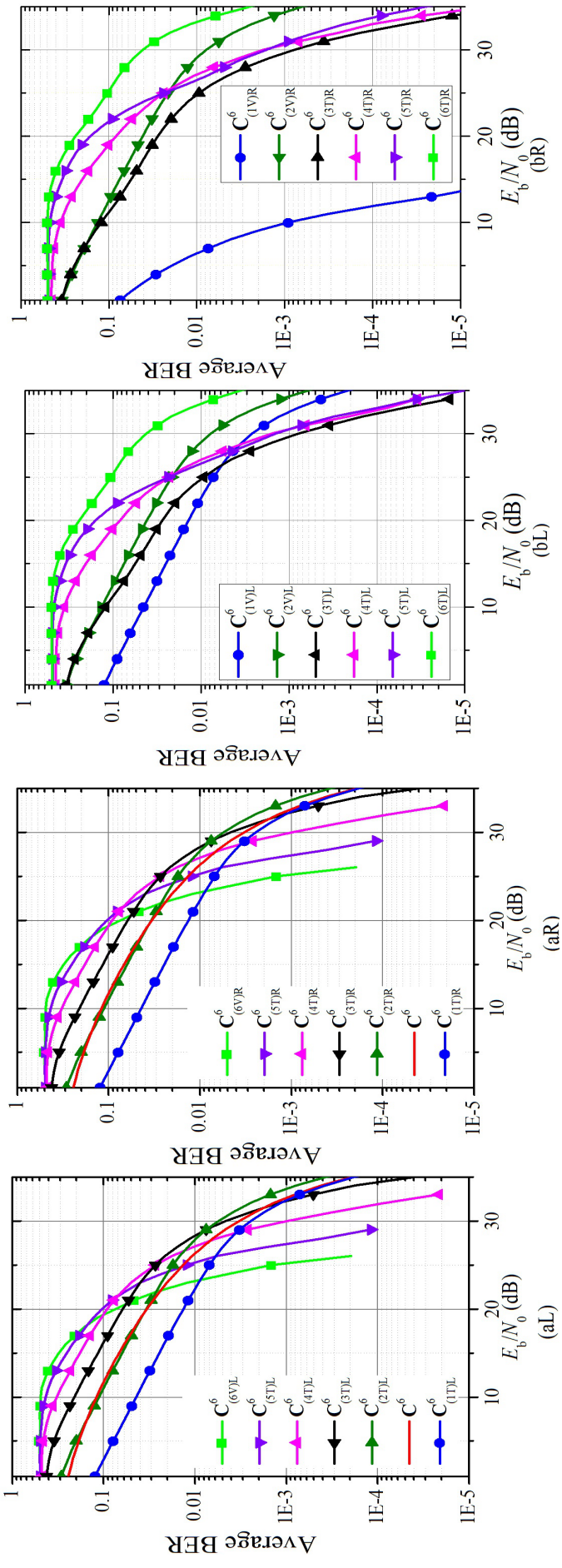

Figure 4.8: BER performance of TSMOS ($\mathbf{T}^6$): (aL) Left child and (aR) Right child, HSMOS ($[\mathbf{V}^2|\mathbf{T}^4]$): (bL) Left child and (bR) Right child.

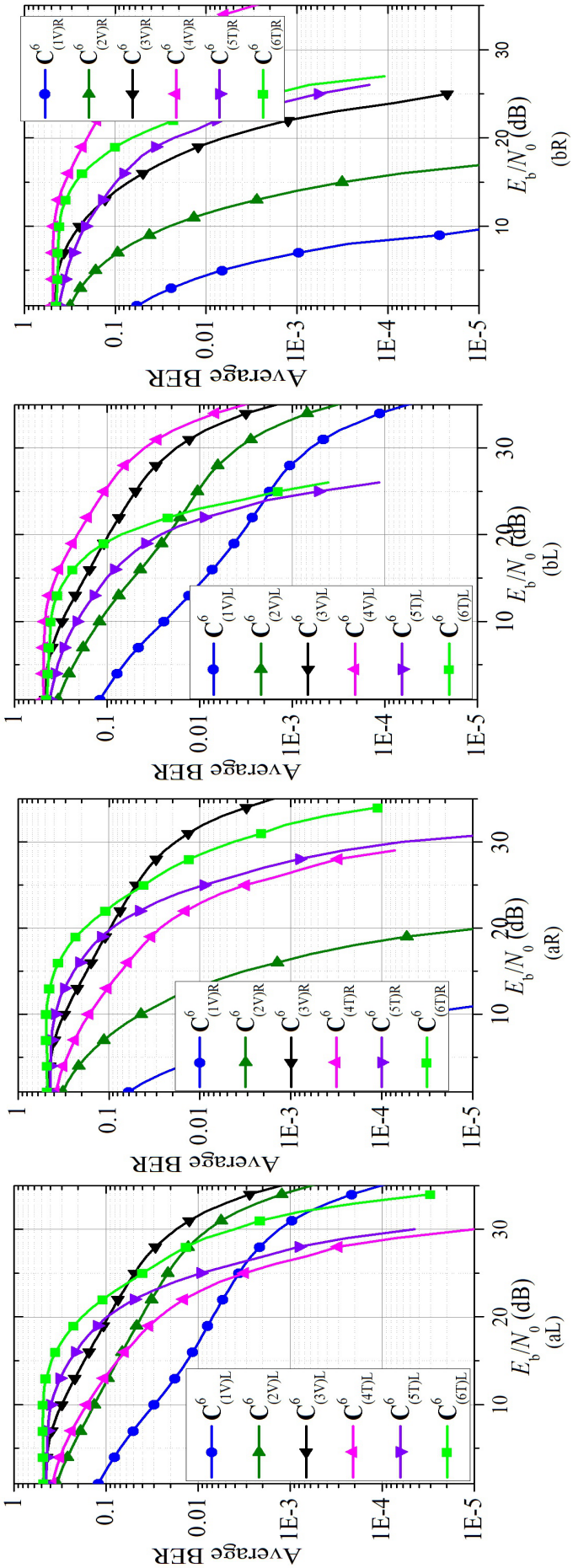

Figure 4.9: BER performance of HSMOS ($[\mathbf{V}^3|\mathbf{T}^3]$): (aL) Left child and (aR) Right child, HSMOS ($[\mathbf{V}^4|\mathbf{T}^2]$) (bL) Left child and (bR) Right child.

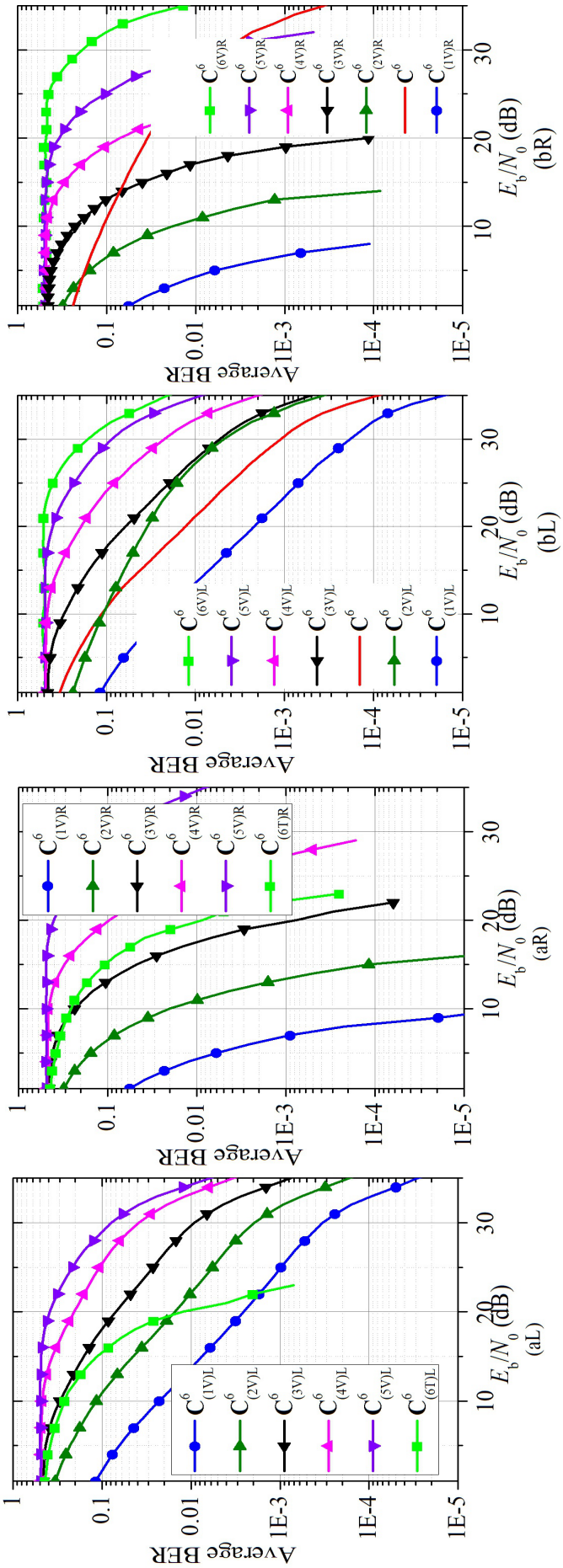

Figure 4.10: BER performance of HSMOS ($[\mathbf{V}^5|\mathbf{T}^1]$) (eL) Left child and (eR) Right child, 2k-SMOS ($\mathbf{V}^6$): (fL) Left child and (fR) Right child.

architecture: $\left[\mathbf{C}^6_{1V}|\mathbf{C}^6_{2T}|\mathbf{C}^6_{3T}|\mathbf{C}^6_{4T}|\mathbf{C}^6_{5T}|\mathbf{C}^6_{6T}\right]$, $\left[\mathbf{C}^6_{1V}|\mathbf{C}^6_{2V}|\mathbf{C}^6_{3T}|\mathbf{C}^6_{4T}|\mathbf{C}^6_{5T}|\mathbf{C}^6_{6T}\right]$, $\left[\mathbf{C}^6_{1V}|\mathbf{C}^6_{2V}|\mathbf{C}^6_{3V}|\mathbf{C}^6_{4T}|\mathbf{C}^6_{5V}|\mathbf{C}^6_{6V}\right]$, $\left[\mathbf{C}^6_{1V}|\mathbf{C}^6_{2V}|\mathbf{C}^6_{3V}|\mathbf{C}^6_{4V}|\mathbf{C}^6_{5T}|\mathbf{C}^6_{6T}\right]$, $\left[\mathbf{C}^6_{1V}|\mathbf{C}^6_{2V}|\mathbf{C}^6_{3V}|\mathbf{C}^6_{4V}|\mathbf{C}^6_{5V}|\mathbf{C}^6_{6T}\right]$, $\left[\mathbf{C}^6_{1V}|\mathbf{C}^6_{2V}|\mathbf{C}^6_{3V}|\mathbf{C}^6_{4V}|\mathbf{C}^6_{5V}|\mathbf{C}^6_{6V}\right]$ respectively, whose status of inequality (PA > TPC) are presented in Figure 4.3 (a) to (f). Prior to proceeding further, the summary of the outcome in Table 4.5 must be referred.

For $\mathbf{V}^g$: With the replacement of the binary subsets to form $\left[\mathbf{V}^g|\mathbf{T}^{k-g}\right]$, the *equal* fall in the level of their PA (4.4) allows the level of BER of the left and right child of the $(g-1)$ subsets (following $\mathbf{C}^6_{1V}$) to rise, as compared to those of the TSMOS. However, at the same time, due to the presence of completely *unequal* level of TPC on the decoded subset, performance variation is observed. With the increase of g, the number of ternary subsets (i.e.; $k-g$) existing at the bottom layers of the tree decreases. Subsequently, it results in the gradual fall in level of TPC (inter.) (4.5) on both the left and right child of any of the binary subsets, whereas the reduced level of PA (4.4) of these subsets remains uniform.

Example 4: Consider the case of the left child in $\mathbf{C}^6_{1V}$. With the increase in value of g from 2 (in Figure 4.8 (bL)) to 6 (in Figure 4.10 (bL)), the level of BER shows continuous improvement. Whereas the level of TPC on the left child of a binary subset remains $uniform$ with the increase in value of g, that on the right child is continuously subjected to significant fall. As a result, the fall in the level of BER (despite the uniformity in the value of PA) becomes more prominent. Similar explanation is also applicable for the improvement in BER performance of the right child in $\mathbf{C}^6_{1V}$, with the increase in value of g from 2 (in Figure 4.8 (bR)) to 6 (in Figure 4.10 (fR)).

For $\mathbf{T}^{k-g}$: For a particular subset remaining ternary, with the increase in the value of g, the level of BER on the left or right child lowers despite the uniformity in the status of (PA > TPC). For the left and right child, this anomaly is because of the fall in the level of BER of the binary subsets in the upper layers of the tree, which consequently leads to the alleviation in the level of BER of the ternary due to the sequential nature of detection of the MUD.

Example 5: Consider the case of the left and right child in C^6_{5V}. With the increase in value of g from 2 (in Figure 4.8 (bL)) to 4 (in Figure 4.8 (dL)), the level of BER improves noticeably.

In Overall: For a particular subset remaining binary, with the *increase* in the value of g (while approaching from TSMOS to $2k$-SMOS), the level of TPC on its left and right child shows a continuous fall, which is because, with the rise in the value of g, the number of (binary) subsets (i.e.; $g-1$), producing no MAI and reduced MAI on the right and left child, respectively, increases. With more number of binary subsets (in the bottom layers), the fall is observed in the level ETPC leading to the improvement of the level of BER.

Example 6: The error performance of the left and right child in $\mathbf{C}_{2T}^{6}$, where their BER level can be found to be continuously improving in Figure 4.8 (cL) to (fL) and 4.8 (cR) to (fR), for the increase of g from 3 to 6.

4.6 Summary

In this chapter, our attempt to extend the domain of SMOS beyond TSMOS and $2k$-SMOS culminated in the proposal of HSMOS. The construction feature of HSMOS is designed in such a way that it includes all possible SMOS structures including the TSMOS and $2k$-SMOS as the special cases. We discussed two possible approaches of construction: $top-to-bottom$ and $bottom-to-top$. Also, the variation in the behavior of the metrics (PA, TPC (intra.), TPC (inter.)) with the transformation in the structure of HSMOS was given analyzed comprehensively. While for each of the cases, there exist k different structures of HSMOS, each of them projects a different level of BER for the individual subsets. Such variation is straight due to the change in the status of the inequality (PA $>$ TPC) controlling the quality of detection using MF approach. To have a clear-cut illustration, we studied the variation in the status the inequality for the left and right child for each configuration. Simulation results validated our observation from the analysis of the inequality to be closely matched with that of the simulation results.

Chapter 5
HLDS Matrix for Overloaded CDMA

5.1 Introduction

In chapter 1, the developments on LDS matrices, as a favorable candidate to low complex decoding for overloaded CDMA, has drawn our attention in Section 1.3.4. Recently, their implication using the OFDM architecture has evolved in a new form of non-orthogonal MA, known as SCMA [1, 2, 87, 88]. SCMA being considered as one of the prospective candidate for the 5G cellular architecture has added further encouragement to propose new sets of LDS with efficient MUD.

More recently, the frequent attempt by the researchers [80, 82] to use the LDPC codes [96] as a prospective signature matrix for overloaded CDMA is due to two primary reasons: (a) the structure with higher number of columns over the rows offers a significant value of β, and (b) the low density nature of construction generates the scope for detection using message passing algorithm (MPA) to deliver the error performance close to the optimum MUD. Among the other detection algorithms meant for the LDPC codes for SCMA, the soft-in-soft-out (SISO) MUD in [80] and iterative MUD in [3, 89–91] has also come to our notice. Within several efforts concentrated towards the design of efficient MUD for LDPC matrix for CDMA application, an important question strikes to our mind i.e.; does there exist any other set of LDS to address the same problem. Among the few such proposals existing in literature, the availability of sufficient sparsity in the UDC set proposed in [81] is the one, where proposed MUD is recognized as one of the highly simplified decoder for overloaded CDMA, offering $\beta \approx 2$. Table 5.1 illustrates a clear overview of the important constructions proposed so far, for overloaded CDMA. It is important to note that in our discussion throughout this chapter, we have not included the cases of LDPC [96], even if few of the current proposals [80, 84] on MUD design for LDS based CDMA are intrinsically meant for the

Table 5.1: A brief review of the literature on overloaded CDMA systems, where UD-"Uniquely Decodable", NUD- "Non UD", R-"Recursive", NR-"Non R", B-"Binary", T-"Ternary", G-"Generalised", L- "Limited", A-"Arbitrary", D-"Discrete", AE- "Assymptotic Equality", NAE-"Non AE", F-"Fast", S-"Simplified", C-"Complex", HC-"Highly Complex", NL-"Noise Less", N-"Noisy".

Year	Pub.	Construction of Signature Matrix						Decoding	
		UD/NUD	R/NR	B/T	G/L	A/D	AE/NAE	F/S/C/HC	NL/N
2015	[32]	UD	NR	B	L	D	NAE	S	N
2014	[76]	UD	NR	B	L	D	NAE	S	N
2014	[58]	NUD	NR	B	L	D	NAE	C	N
2013	[74]	UD	NR	B	L	D	NAE	S	N
2012	[81]	UD	R	T	L	D	NAE	F	N
2012	[73]	UD	NR	B	L	D	NAE	C	N
2012	[97]	UD	NR	B	L	D	NAE	S	N
2009	[71]	UD	NR	B	G	D	NAE	S	N
2006	[35]	NUD	NR	B	L	D	NAE	HC	N
2005	[66]	NUD	NR	B	L	D	NAE	S	N
2004	[64]	NUD	NR	B	L	D	NAE	HC	N
2002	[98]	NUD	NR	B	L	D	NAE	HC	N
2000	[93]	NUD	NR	B	L	D	AE	HC	N
1998	[92]	UD	R	B	L	D	AE	C	NL
1997	[15]	UD	R	B	L	D	AE	C	NL
1995	[14]	UD	R	T	L	D	AE	C	NL
1984	[10]	UD	R	T	L	A	AE	C	NL
1982	[9]	UD	R	T	L	D	AE	C	NL
1979	[8]	UD	R	T	L	D	AE	C	NL

LDPC matrix. This is just because of our priority to emphasize on the constructions meant for the purpose of multiple access only. Conversely, LDPC codes being actually designed for the purpose of error correction has recently gained the attention towards its application for overloaded CDMA. However, further exploration on LDPC codes to design more efficient MUD is a part of our priority for future work.

According to the illustration in Table 5.1, several proposals have already been explored on the present topic. Nevertheless, the design of the system comprising all the favorable features i.e.; fast construction, its generalization to other existing UD sets [71], construction feasibility to arbitrary values of code length [10], design of a fast [81], efficient, and practically implementable MUD for noisy transmission still appears an interesting open problem. In other words, our aim to propose a system with attributes: UD-R-G-A-F-N (according to Table 5.1).

We consider the design of a new set of ternary matrices for overloaded CDMA, where for the formation of its k^{th} indexed version $\mathbf{C}_{N_k \times M_k}$ (for $M_k > N_k$), the

Table 5.2: Important notations from Table 5.1, and their significance.

Notation	Significance
"R-Recursive"	Method of construction is usually faster than that of NR
"B-Binary"	$\in \{1, -1\}$
"T-Ternary"	$\in \{1, -1, 0\}$
"G-Generalized"	Construction method applicable to a broad range of matrices
"L-Limited"	Construction method applicable to a specific matrices
"A-Arbitrary"	Construction is feasible for any value of code length
"D-Discrete"	Construction is feasible for specific values of code length
"F-Fast"	Complexity order:
	Fast << Simplified << Complex << Highly Complex

orthogonal Hadamard matrices of smaller dimensions ($\mathbf{H}_h$ for $h < N_k$ e.g.; $\mathbf{H}^T\mathbf{H} = h\mathbf{I}$) with antipodal binary elements are selected as the basis set. All the proposals in literature, to achieve overloading, relies on either the method of addition of new signature columns to the orthogonal set [54], or the tensor product rule subjected to the smaller optimal sets [73]. In contrast, the proposed construction is governed by a simple *overlapped hierarchy* involving the selected basis (optimal or sub-optimal) set. With no mathematical operations, the construction is easy to realize. We mathematically prove its UD nature, and derive the generalized criterion for selection of the basis sets. Interestingly enough, we find that most of the existing UD sets from literature qualify to be selected as the basis, which further makes our approach more generalized. For the basis set of smallest dimension ($\mathbf{H}_2$), the maximum value of $\beta \approx 2$ is achievable. A low complex k-stage decoder is proposed for $\mathbf{H}_h$ as the basis set, where the decoding of h users in each stage is based on the decision vector search (DVS) algorithm. The algorithm exploiting the unique hierarchy of the available cross-correlation relies on the logic of MF, followed by few comparisons (if necessary), and guarantees for the unique detectability as well as low complex nature of the decoder. For noisy transmission, the degradation in BER is worthy to be overlooked in contrast to the prominent advantage gained in complexity over the optimum MLD. With an aim to come up with a m ore simplified substitute of DVS algorithm, we propose the comparison aided decoding (CAD) approach. Observation shows that the MUD using CAD despite its relative simplicity performs close to that of the MUD using DVS technique. Simulation results illustrate the superiority of the proposed system in BER over other ternary constructions. The expressions to estimate the complexity, and BER upper bound are also derived for analysis.

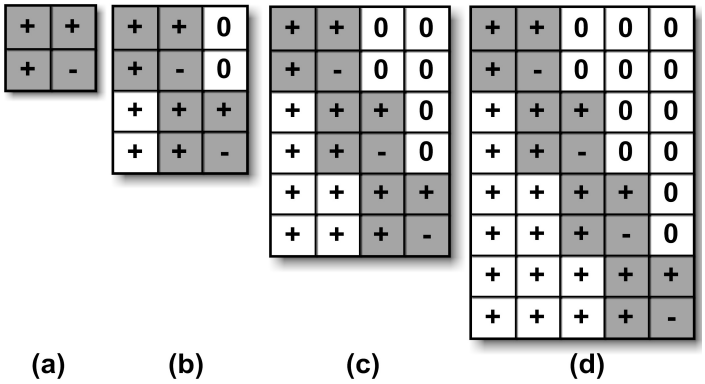

Figure 5.1: Proposed matrices for $\mathbf{H}_2$ as the basis set (a) $(\mathbf{C}^1)^T$ (β=1) (b) $(\mathbf{C}^2)^T$ (β=1.33) (c) $(\mathbf{C}^3)^T$ (β=1.5) (d) $(\mathbf{C}^4)^T$ (β=1.6).

Rest of the chapter is organized as follows. Section 5.2 describes the method of construction of the signature matrix followed by generalization. In Section 5.3, we study the pattern of MAI, design the MUD using MF as the basis block, and derive the analytical expression for average BER and complexity. In Section 5.4, the design of a more simplified MUD using the comparison driven logic is discussed. Section 5.5 covers the discussion on simulation results. Lastly, the conclusions are presented in Section 5.6.

5.2 HLDS Matrix Design

5.2.1 Method of Construction and Features

Following the system model in (2.1), the synchronous (synchronization corresponding to both bit and chip) CDMA system model using the proposed ternary UD matrix with index-k ($\mathbf{C}^k$ or $\mathbf{C}_{N_k \times M_k}$ or $\mathbf{C}\left(N_k, M_k, \mathbf{H}_h\right) \in \{\pm 1, 0\}^{N_k \times M_k}$) for $k \in \mathbf{Z}^+$ can be redefined as

$$\mathbf{y} = \mathbf{r}_k + \mathbf{n}$$

where $\mathbf{r}_k = \mathbf{C}^k \mathbf{A} \mathbf{x}$ is the noiseless received vector for $\mathbf{x} \in \{\pm 1, 0\}^{M_k}$ as the input column vector. The proposed detecting matrix $\mathbf{C}^k$ using $\mathbf{H}_h$ as its basis can be

presented as

$$\left(\mathbf{C}^k\right)^T = \begin{bmatrix} \mathbf{H}_h & & \mathbf{0}_{(N_k-h)\times h} \\ \mathbf{1}_{(h-1)\times h} & \mathbf{H}_{h\times h} & \mathbf{0}_{(N_k-2h+1)\times h} \\ \mathbf{1}_{(2h-1)\times h} & \mathbf{H}_{h\times h} & \mathbf{0}_{(N_k-3h+1)\times h} \\ \vdots & \vdots & \vdots \\ \mathbf{1}_{(N_k-h)\times h} & & \mathbf{H}_{h\times h} \end{bmatrix} \tag{5.1}$$

where $(\mathbf{C}^1)^T = \mathbf{H}_{h\times h}$ e.g., $h \in \{2, 4r\}$ for $r \in \boldsymbol{Z}^+$ and

$$N_k = 1 + (h-1)k \quad \text{and} \quad M_k = hk \tag{5.2}$$

Figure 5.1 comprises of the proposed set of matrices with $\mathbf{H}_2$ as the basis for $k = 1, 2, 3, 4$, where '+' and '-' denotes for 1 and -1 respectively. Subsequently, it is logical to classify all the M_k signatures in $\mathbf{C}^k$ into k uniform classes (each with h codes), based on their identical value of N_{ef} (for $N_{ef} \leq N_k$) i.e.;

$$\mathbf{C}^k = \left[\ \mathbf{C}_1^k \mid \mathbf{C}_2^k \mid \cdots \mid \mathbf{C}_k^k\ \right]. \tag{5.3}$$

In (5.3), $\mathbf{C}_a^k$ denotes the class with $N_{ef} = N_a$ and $N_a = 1 + a(h-1)$, for $a = 1, 2, ..., k$. For example, in Figure 5.1 (c), there are three distinguished classes in $\mathbf{C}^3$: $\mathbf{C}_1^3, \mathbf{C}_2^3, \mathbf{C}_3^3$ with $N_{ef} = 2, 3, 4$ respectively. If $\mathbf{C}^k$ and $\mathbf{C}^{k-1}$ denote the two consecutive versions of the proposed matrix with M_k and M_{k-1} number of signatures respectively ($M_k > M_{k-1}\ \forall N_k > N_{k-1}$), then the *recursive mechanism* leading the formation of $\mathbf{C}^k$ from $\mathbf{C}^{k-1} = \left[\mathbf{C}_1^{k-1} | \mathbf{C}_2^{k-1} | \cdots | \mathbf{C}_{k-1}^{k-1}\right]$ can be described as

$$\mathbf{C}^k = \left[\left[\mathbf{C}^{k-1}\ \mathbf{0}_{(N_k-N_{k-1})\times M_{k-1}}\right]\ \mid \mathbf{C}_k^k\right] \tag{5.4}$$

From (5.4) and (5.5), the average transmission power of all the users in a class are equal, and it decreases in the order: from $\mathbf{C}_k^k$ to $\mathbf{C}_1^k$. Other important points about the construction can be assimilated from Note-1.

Note 1:

• For fixed value of h, the higher value of k results in higher magnitude of N_k, M_k, and $\beta = \beta_k = (M_k/N_k)$. For $\mathbf{H}_2$, $\mathbf{H}_4$, $\mathbf{H}_8$, $\mathbf{H}_{16}$ as the basis, value of β approaches to 2, 1.33, 1.14 and 1.06 respectively, as k *tends to infinity.*

• $\mathbf{C}^k$ with lower value of h is exposed to a wide range of spreading gain or chip rate (N_k) and vice versa. For $h = 2$, the construction validates its feasibility for *arbitrary values* of code length $N_k = (k+1)$ for $k \in \mathbf{Z}^+$ (see Figure 5.1). In other words, it

further optimizes the *rate-capacity trade off*[1].

• If two different matrices $\mathbf{C}^{k_1}$ and $\mathbf{C}^{k_2}$ carry identical values of M_k (5.5) e.g., M_{k_1}=M_{k_2}, then for $h_1 > h_2$, the outcome $k_1 < k_2$ is verified resulting in $N_{k_1} < N_{k_2}$ and $\beta_{k_1} < \beta_{k_2}$.

$$M_k = \left(\frac{h}{h-1}\right)(N_k - 1) \tag{5.5}$$

• To achieve $\beta > 1$, the required criterion of $^{h}/_{(h-1)} > 1$ can be verified from (5.5). As evident, its impact varies inversely with the values of h ($h << N_k$) i.e., for the smallest value of h ($= 2$), the highest value of $\beta \approx 2$ can be attained. Similarly, the higher value of h ($\approx N_k$) results in the value of $\beta \approx 1$. So, the maximum achievable value of β in this case is two i.e.; $1 \leq \beta \leq 2$, which can be considered as satisfactory, provided, the decoder's design leading to the efficient recovery over noisy transmission is practically realizable. In Section 5.3, we show the proposed decoder to be simplified and hence, implementable in design.

5.2.2 Basis Set and its Generalization

For the tensor product based constructions [32, 71, 73, 75] of the large suboptimal UD sets from the smaller optimal counterparts (core set), the only necessary, and sufficient criterion to be met for the basis set is its UD nature. On the contrary, for the proposed generalized construction, it does not suffice for the selection of the basis set. In order to derive the specific criterion for its selection, first, we present Theorem 1 to validate the UD nature of the proposed construction over a set of M input symbols $\psi = \{\xi_1, \xi_2, \cdots \xi_M\}$, such that $\psi \subset \{\alpha_1, \alpha_2, \cdots, \alpha_N, \bar{\alpha}\}$ for $\bar{\alpha}$ being the linear combination over the set of algebraically independent numbers (AIN) $\{\alpha_1, \alpha_2, \cdots, \alpha_N\}$. For an algebraically independent set, the linear combinations of the numbers with integer coefficients become zero. For the proof, we take the construction of (5.1), where the Hadamard set (both orthogonal, and UD) has been considered as the basis set. Later, from the analysis of the proof, we derive a generalized criterion for selection of the basis matrix in Corollary-1.

Theorem 1: For $\mathbf{H}_h$ being the basis set of construction, the proposed matrix $\mathbf{C}^k$ in (5.1) is uniquely decodable over ψ.

Proof : To prove the one-to-one transformation of $\mathbf{C}^k$, we follow the contradictory

[1]rate-capacity trade off refers to the proportional reduction in transmission rate incurred due to the selection of code matrix with higher spreading gain (N_k) for enhanced user capacity (M_k).

approach i.e.; for $\mathbf{C}^k\mathbf{A}\mathbf{x} = 0$, we aim to show $\mathbf{x} = [\mathbf{x}_1\ \mathbf{x}_2\ \cdots\ \mathbf{x}_k]^T = \mathbf{0}_{M_k \times 1}$, where $\mathbf{x}_a = [x_{a1}\ x_{a2}\ \cdots\ x_{ah}]^T \in \{\psi\}^h$ (for $a = 1, 2, ..., k$) denotes the input vector corresponding to $\mathbf{C}_a$.

The proof below includes k sequential steps, where the decision of $\mathbf{x}_a = \mathbf{0}_{h\times 1}$ derived in step-a is the collective outcome of the results derived from previous $(a-1)$ steps. Now, to show $\mathbf{x}_a = \mathbf{0}_{h\times 1}$ in step-a, it is essential to consider the vector comprising the first N_a chips of $\mathbf{r}_k = [r_1 r_2 \cdots r_{N_k}]$ as the input, since for class $\mathbf{C}_a^k$, $N_{ef} = N_a$.

Start with $a = 1$, for which $N_1 = h$. So, $[r_1\ r_2\ \cdots\ r_{N_1}]^T = \mathbf{0}_{N_1\times 1}$ corresponding to the resultant sum vector $\sum_{a=1}^{k} \mathbf{C}_a\mathbf{x}_a = 0$ can be expanded as

$$\mathbf{H}_h\mathbf{x}_1 = -\mathbf{1}_{h\times(M_k-h)}\left[\mathbf{x}_2\ \mathbf{x}_3\ \cdots\ \mathbf{x}_k\right]. \tag{5.6}$$

Likewise, for another set of input $\mathbf{x}^* = [\mathbf{x}_1^*\mathbf{x}_2 \cdots \mathbf{x}_k]^T$ for $\mathbf{x}_1^* \neq \mathbf{x}_1$, we can rewrite (5.6) as

$$\mathbf{H}_h\mathbf{x}_1^* = -\mathbf{1}_{h\times(M_k-h)}\left[\mathbf{x}_2\ \mathbf{x}_3\ \cdots\ \mathbf{x}_k\right] \tag{5.7}$$

So, (5.6) and (5.7) collectively results in the equality $\mathbf{H}_h\mathbf{x}_1 = \mathbf{H}_h\mathbf{x}_1^*$ implying $\mathbf{x}_1 = \mathbf{x}_1^*$ that is possible only if $\mathbf{x}_1 = \mathbf{x}_1^* = \mathbf{0}_{h\times 1}$. This completes the first step.

Now, for $a = 2$, $N_2 = (2h-1)$ and $[r_1\ r_2\ \cdots\ r_{2h-1}]^T = \mathbf{0}_{(2h-1)\times 1}$ exposed to the substitution of $\mathbf{x}_1 = \mathbf{x}_1^* = \mathbf{0}_{h\times 1}$ (from previous step) have the following expansion

$$\left[\mathbf{1}_{(h-1)\times h}|\mathbf{H}_h\right]^T\mathbf{x}_2 + \left[\mathbf{1}_{(h-1)\times h}|\mathbf{1}_{h\times h}\right]^T\mathbf{x}_3 + \cdots + \left[\mathbf{1}_{(h-1)\times h}|\mathbf{1}_{h\times h}\right]^T\mathbf{x}_k = \mathbf{0}_{N_2\times 1}.$$

The above expression can also be rewritten as

$$\mathbf{H}_h\mathbf{x}_2 = -\mathbf{1}_{h\times(M_k-2h)}\left[\mathbf{x}_3\ \mathbf{x}_4\ \cdots\ \mathbf{x}_k\right] \tag{5.8}$$

Hence, the expression in (5.8) has the similar structure to that of (5.6), thus reflects the uniformity in analysis to be undertaken afterwards. For another set of input $\mathbf{x}^* = [\mathbf{x}_2^*\ \mathbf{x}_3\ \cdots\ \mathbf{x}_k]^T$ with $\mathbf{x}_2^* \neq \mathbf{x}_2$, it is easy to have the equivalent expression corresponding to (5.7). Next, these two expression also will jointly approve for the equality $\mathbf{H}_h\mathbf{x}_2 = \mathbf{H}_h\mathbf{x}_2^*$ in the same way, that has been achieved involving (5.6) and (5.7). It validates for $\mathbf{x}_2 = \mathbf{x}_2^* = \mathbf{0}_{h\times 1}$, and completes the second step.

Sequentially, similar approach is to be incorporated till $a = k$ where for $\mathbf{x}_1 = \mathbf{x}_2 = \cdots = \mathbf{x}_{k-1} = \mathbf{0}_{h\times 1}$, the expression $[r_1\ r_2\ \cdots\ r_{n_k}]^T = \mathbf{0}_{n_k\times 1}$ results in $\mathbf{H}_h\mathbf{x}_k = \mathbf{0}_{h\times 1}$. Later, it approves for the equality: $\mathbf{H}_h x_k = \mathbf{H}_h\mathbf{x}_k^*$ and proves $\mathbf{x}_k = \mathbf{x}_k^* = \mathbf{0}_{h\times 1}$. Finally, combining the decisions on $\mathbf{x}_a$ from all k-steps, the desired criterion $\mathbf{x} = [\mathbf{x}_1\ \mathbf{x}_2\ \cdots\ \mathbf{x}_k]^T = \mathbf{0}$ is proved for the initial assumption of $\mathbf{C}^k\mathbf{A}\mathbf{x} = \mathbf{0}$. ■

Corollary 1 *(Generalized Criterion for Selection of the Basis Set):*

From Theorem 1, in step-a of the proof, the design specific presence of the matrix $\mathbf{1}_{h\times(M_k-ah)}$ plays the vital role in achieving the equality $\mathbf{H}_h\mathbf{x}_a = \mathbf{H}_h\mathbf{x}_a^*$, which further validates for $\mathbf{x}_a$ to be a zero vector. In particular, the overlapping of the row of $\mathbf{H}_h$ having all 1s in $\mathbf{C}_{a+1}$ with the trailing row of that in $\mathbf{C}_a$ directly contributes to the existence of $\mathbf{1}_{h\times(M_k-ah)}$, as shown by (5.6),(5.7), and (5.8). Therefore, besides UD nature, the presence of *at least an end row with all 1s* is the necessary criterion to be satisfied by any existing matrices to be considered as the basis set for the proposed construction. Interestingly, our further retrospective study shows that most of the existing UD matrices [8–10, 13–16, 32, 71, 73, 81, 92, 99] with high value of β qualifies the above criterion and thus, our objective of proposing a new approach generalized construction is fulfilled. ■

Note 2: Besides the recursive construction in (5.4), we may also follow the *tensor product rule* [71] to generate the proposed UDC sets of larger dimensions i.e.; $\left(\mathbf{H}\otimes\mathbf{C}^k\right)$ of size $(hN_k \times hM_k)$. For its decoding, the received (decoding) vector is to be multiplied by $(\mathbf{H}^{-1}\otimes\mathbf{I})$ to split the overall recovery problem into h parallel stages, each of which contributes to the detection of M_k users. Under such condition, the proposed matrix $\mathbf{C}^k$ also plays the role of the so called *core matrix* in context of the tensor product based construction, as described in [32]. Now, comparing both the approaches, it is easy to decipher that our approach of construction offers a higher value of β than that of the tensor product based construction [71, 73, 74, 76], *provided* the *basis matrix* (proposed construction), and *core matrix* [32] (later one) remains the same. As the reason, the reduction in value of N_k due to the overlapping along the spreading dimension (Corollary 1) is to be held responsible. ■

5.3 MUD using DVS

5.3.1 Hierarchy of MAI

Following (5.4), the zero matrix $\mathbf{0}_{(N_k-N_{k-1})\times M_{k-1}}$ adjoined to $\mathbf{C}_{k-1}^k$ for construction of $\mathbf{C}^k$ splits $\mathbf{r}_k$ into two sections of unequal length. Its first N_{k-1} chips carries the data of the M_{k-1} users common to $\mathbf{C}^k$ and $\mathbf{C}^{k-1}$, whereas the last $(N_k - N_{k-1}) = (h-1)$ chips have the spread data of the users of $\mathbf{C}_k^k$ only. Equivalently, a section of the spread

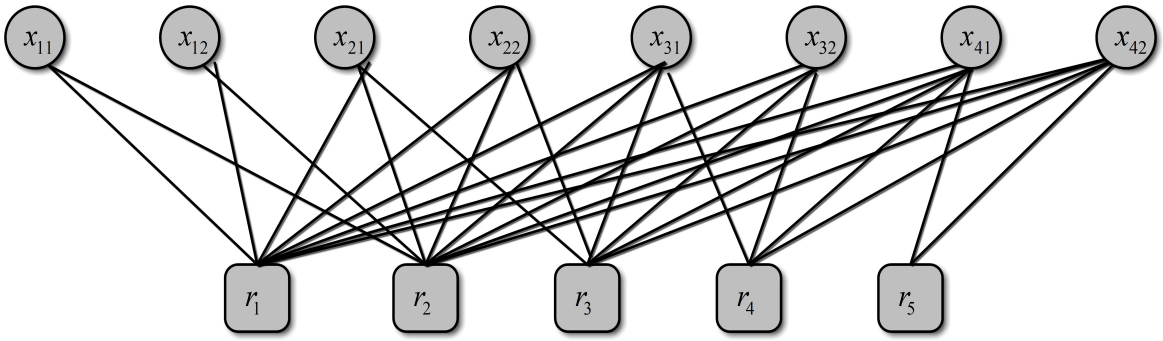

Figure 5.2: Factor Graph representation of the HLDS $\mathbf{C}(5, 8, \mathbf{H}_2)$ (Figure 5.1 (d)).

data of $\mathbf{C}_k^k$ exists in the last $(h-1)$, and first $N_{k-1} = (N_k - h + 1)$ chips of $\mathbf{r}_k$ with *zero MAI* and *MAI from* $\mathbf{C}^{k-1}$ respectively. Recursively, similar logic also holds for the lower indexed matrices $\mathbf{C}^a$ for $1 < a \leq (k-1)$.

For better realization of the pattern of MAI, let us take a look at the factor graph [80] presentation of the matrix $\mathbf{C}(5, 8, \mathbf{H}_2)$ or $\mathbf{C}^4$ in Figure 5.2, where $\mathbf{x} = [x_{11}\ x_{12}\ x_{21}\ x_{22}\ x_{31}\ x_{32}\ x_{41}\ x_{42}]$ and $\mathbf{r} = [r_1\ r_2\ r_3\ r_4\ r_5]$. As evident, the level of MAI on the transmitted vector $\mathbf{r}$ is the least at the right most chip (i.e.; $\mathbf{r}_5$) and manifests an incremental growth towards the left. For $\mathbf{r}_1$ and $\mathbf{r}_2$, the MAI is maximum and at equal level with each other. Under such pattern of distribution of MAI, the most favorable approach to start the process of decoding is to attempt to recover the input vector corresponding to $x_4 = [x_{41}\ x_{42}]$ from the chips under relatively low MAI i.e.; $\mathbf{r}_4$ and $\mathbf{r}_5$. Exploiting the recurrent construction, identical interpretation can be made for the recovery of $x_3 = [x_{31}\ x_{32}]$, $x_2 = [x_{21}\ x_{22}]$, and $x_1 = [x_{11}\ x_{12}]$ from $\mathbf{C}(4, 6, \mathbf{H}_2)$, $\mathbf{C}(3, 4, \mathbf{H}_2)$, and $\mathbf{C}(2, 2, \mathbf{H}_2)$ respectively.

5.3.2 Principle of Design

Consider the CDMA system with orthogonal Hadamard matrix, that is also the basis set for our proposed construction (5.1). Assuming the channel to be noiseless, and the input symbols to be binary ($\psi \subset \{1, -1\}$), the decoding of all 2^h combinations of X becomes errorless, which is best explained by

$$\hat{\mathbf{x}} = \text{sign}\left(\mathbf{H}_{h\times h}\mathbf{x}_{h\times 1}\mathbf{H}_{h\times h}\right) = \mathbf{x}_{h\times 1} \tag{5.9}$$

where $\hat{\mathbf{x}}$ is the decoded (estimated) version of $\mathbf{x}$, and sign( ) denotes the hard limiter. Now, we propose the *design statement* of the decoder through the following (Question-Answer) logic in Table 5.3.

Table 5.3: Defining the Design Principle.

Question. What if, instead of all the h rows of $\mathbf{H}_{h\times h}$ in CDMA, the matrix comprising only the last $(h-1)$ rows (all rows except the one with all 1's (Corollary 1)) $\mathbf{H}_{(h-1)\times h}$ is considered for decoding in (5.9).

Answer. Although application of this logic of decoding is successfully verified for majority of the 2^h combinations of $\mathbf{x}$, but not for all. In particular, for the combination $\mathbf{x} = \mathbf{1}_{h\times 1}$ and $-\mathbf{1}_{h\times 1}$, the decision $\hat{\mathbf{x}}$ goes ambiguous, since $\left(\mathbf{H}_{(h-1)\times h}\mathbf{x}_{h\times 1}\mathbf{H}^T_{(h-1)\times h}\right) = \mathbf{0}_{h\times 1}$ (see **Appendix A**).

The explanation in Table 5.3 clearly mentions the challenge associated to recover all possible input combinations of $\mathbf{x}$, provided, we consider the last $(h-1)$ instead of h rows for MF decoding (5.9). Hence, this approach becomes unfavorable for conventional CDMA. However, the ambiguity raised for the particular minority input combinations ($\mathbf{x} = \mathbf{1}_{h\times 1}$, and $\mathbf{-1}_{h\times 1}$), if somehow resolved will absolutely facilitate the errorless decoding, and we take this probable logic to build the layout of the MUD. Afterwards, the term "ambiguity" strictly refers to the imperfect decision, when only last $(h-1)$ rows are considered for decoding.

5.3.3 DVS Algorithm

From our discussion on the hierarchy of MAI corresponding to the factor graph (Figure 5.2) in subsection 5.3.1, the only class in $\mathbf{C}^k$ that justifies its strongest candidature for being recovered at the most initial stage of decoding is the last class $\mathbf{C}^k_k$. It is due to the availability of no MAI on it during the last $(h-1)$ chips of $\mathbf{r}_k$. Since, the last $(h-1)$ rows of $\mathbf{C}^k_k$ completely matches with that of the Hadamard matrix i.e., $\mathbf{C}^k_{k_{(h-1)\times h}} = \mathbf{H}_{(h-1)\times h}$, now, our decoding problem for $\mathbf{C}^k_k$ has gained full resemblance to the design statement. Despite this similarity, the only thing that still affects the errorfree decoding of $\mathbf{C}^k_k$ is the condition of ambiguity for $\mathbf{x}_k = \mathbf{1}_{h\times 1}$ and $\mathbf{-1}_{h\times 1}$, where $\mathbf{x}_k \subset \mathbf{x}$.

One probable approach to overcome this ambiguity is to verify the decision of $\hat{\mathbf{x}}_k$ for all possible combinations of the received sub-vectors derived from $\mathbf{r}_k = [r_1\ r_2\ \cdots\ r_{n_k}]$. Note that for the received vector $\mathbf{r}_k$ with N_k elements, there exists N_k possible sub-vectors of different length such that each of them has a common end element (r_{N_k}). A *sub-vector* of length l from $\mathbf{r}_k$ simply refers to the last l chips of $\mathbf{r}_k$. In overall,

Table 5.4: DVS Algorithm.

Step 1: For $i \in \{1, 2, \cdots, k-1\}$, initialize $l = (h-1)$ and evaluate
$$\mathbf{z} = (\mathbf{r}_{k-i+1})_{l\times 1} \left(\mathbf{C}^k_{k-i+1}\right)^T_{h\times l}$$
where $(\mathbf{r}_{k-i+1})_{l\times 1}$ represents the last l chips of $\mathbf{r}_k$ and $\left(\mathbf{C}^k_{k-i+1}\right)_{h\times l}$ represents the last l rows of class $\mathbf{C}^k_{k-i+1}$.

Step 2: If $\mathbf{z} \neq \mathbf{0}_{h\times 1}$, then $\hat{\mathbf{x}}_{k-i+1} = \text{sign}\ (\mathbf{z})$,
Else modify l as per the following rule and subject $\mathbf{z}$ to sign ( ) to have the final decision.
- For $h > 2$: Assign $l = (h+1)$ to have $\mathbf{z} \neq 0_{h\times 1}$
- For $h = 2$: Assign $l = \{h, h+1, h+2, \cdots, N_{k-i+1}\}$ in sequence till $\mathbf{z} \neq \mathbf{0}_{h\times 1}$ is achieved.

out of N_k different combinations of sub-vectors, the present analysis gets limited to the remaining $(N_k - h + 2)$ number of combinations only i.e.; $h \leq l \leq N_k$. Now, our strategy is to consider each of them sequentially (from $l = h$ to N_k) with an aim to discover that specific sub-vector for which the existing ambiguity will vanish, and the correct decision of $\hat{\mathbf{x}}_k$ can be achieved. That particular sub-vector, therefore, can be termed as the decision vector (DV) for class $\mathbf{C}_k$.

In Lemma 1, we explain the overall approach of searching for the DV with a better insight into the role of the active cross-correlation matrix corresponding to class $\mathbf{C}_k$. This method can be extrapolated to any other class $\mathbf{C}_a$, for $1 < a \leq k-1$, *provided*, the received vector $\mathbf{r}_a$ corresponding to the decoding matrix $\mathbf{C}^a$ is known. The generalized version of this approach is presented in Table 5.4, and termed as the *Decision Vector Search* algorithm.

Lemma 1: Consider $\mathbf{C}^k$ in (5.1) as the decoding matrix with $\mathbf{H}_{h\times h}$ as the basis set, and $\mathbf{x} \in \{1, -1\}^{M_k}$. For detection of the last class $\mathbf{C}^k_k$, there always exists a DV $\subseteq \mathbf{r}_k$ of length l for $1 \leq l \leq N_k$, corresponding to each of the 2^{M_k} combinations of $\mathbf{x}$.

For the proof, please refer to **Appendix A**.

5.3.4 Design of MUD (DVS)

The overall design of the MUD (DVS) followed by the proof of its errorless feature (in Theorem 2) are discussed below.

Theorem 2: For $\mathbf{C}^k$ denoting the k^{th} indexed matrix of the proposed HLDS matrix in (5.1), the decoding of $\mathbf{x} \in \{1, -1\}^{M_k}$ from $\mathbf{r}_k$, using the DVS algorithm is errorless.

Table 5.5: l versus *Number of Combinations* for decoding of $\mathbf{C}_k$, where $s = 2^{M_k-1} - 2^{(2N_k-5)}$, $h = 2$.

l	1	2	3	4	...	$N_k - 1$	N_k
Number of Combinations	2^{N_k-1}	s	$s/4$	$s/16$	...	6	2

Proof : The proof is simple and based on induction on k. From (5.3) and (5.4), $\mathbf{r}_k$ as the summed contribution of the received vectors from k different classes of $\mathbf{C}^k$ can be expressed as

$$\mathbf{r}_k = \sum_{a=1}^{k} \mathbf{r}_{N_a} \quad \text{for} \quad \mathbf{r}_{N_a} = \mathbf{C}_a^k \mathbf{A}_a \mathbf{x}_a \tag{5.10}$$

where $\mathbf{A}_a = \mathbf{I}_{h\times h}$, $\mathbf{x}_a \in \mathbf{x} = [\mathbf{x}_1 \mathbf{x}_2 \cdots \mathbf{x}_k]^T$. In Lemma 1, we have already shown that subset-$\mathbf{C}_k^k$ can be extracted from $\mathbf{r}_k$ without any error ($\hat{\mathbf{x}}_k = \mathbf{x}_k$), which can be considered as the first stage of decoding ($i = 1$). Next, its IE on other existing classes is evaluated as $\mathbf{i} = \mathbf{C}_k^k \hat{\mathbf{x}}_k$. The estimated interference $\mathbf{i}$ is then subtracted from $\mathbf{r}_k$ to produce $\mathbf{r}_{k-1}$ such that

$$\left[\mathbf{r}_{k-1} \mathbf{0}_{(h-1)\times 1}\right] = \left[\mathbf{r}_k - \mathbf{i}\right].$$

Now, following the recursive structure in (5.4), $\mathbf{r}_{k-1}$ denotes the received vector for $\mathbf{C}^{k-1}$ i.e.; $\mathbf{r}_{k-1} = \mathbf{C}^{k-1} \mathbf{A}_{k-1} \mathbf{x}_{(M_k-h)\times 1}$, whose last class is $\mathbf{C}_{k-1}^k$. Hence, $\mathbf{r}_{k-1}$ if exposed to the proposition of Lemma 1 results in the errorless decoding of $\mathbf{x}_{k-1}$. This becomes the second stage of decoding ($i = 2$). Without loss in generality, this sequence of Detection (of a class)-Estimation (of its MAI on other classes)-Cancellation (of the estimated MAI) is continued until class-$\mathbf{C}_1^k$ gets retrieved from the respective decoding vector $\mathbf{r}_1 = \mathbf{C}^1 \mathbf{A}_1 \mathbf{x}_1$ in the k^{th} stage (i.e.; $i = k$). This completes the proof. For better organization of the above analysis, i is used to indicate the decoding stage, and hence termed as *decoding index*. ■

From the proof of Theorem 2, the length of the decoding vector $\mathbf{r}_{k-i}$ or *Rank* of the decoding matrix $\mathbf{C}^{k-i}$, after stage-i gets reduced by $(h-1)$. In general, for decoding of $\mathbf{C}_{k-i+1}^k$ in stage-i, the dimension in terms of the length of the decoding vector becomes $L_i = N_k - (i-1)(h-1) = N_{k-i+1}$. Thus, $L_1 > L_2 > \cdots > L_k$, for $i = 1, 2, ..., k$.

In Table 5.5, we present the l versus *Number of Combinations* layout for $\mathbf{C}_k^k$ that we will use for deriving the expression for the upper bound of the BER in the next section.

Corollary 2 Availability of Enhanced Diversity for $h > 2$: From step 2 of DVS,

Table 5.6: MUD (DVS) for AWGN Channel.

Step 1: Allow $\mathbf{y}$ in (1) to pass through a (M_k+1)-ary ADC to deliver

$$\mathbf{y}_{AD} = [y_1 \; y_2 \; \cdots \; y_{N_k}]$$

where the *Range* of constellation of the ADC is $[0, \pm 2, \pm 4, \cdots, \pm\,(k-j)\,h]$

- for $y_{((j+1)h-j)-(h-2)}$ to $y_{((j+1)h-j)}$, when j=1,2,...,(N_k-1)
- for $y_{((j+1)h-j)-(h-1)}$ to $y_{((j+1)h-j)}$,when j=0.

Step 2: For stage-i $(1 < i \leq k-1)$, determine

- $\mathbf{i}^i = \mathbf{C}_{k-i+2}\hat{\mathbf{x}}_{k-i+2}$
- $\mathbf{y}^i_{AD} = \left[y^i_1 \; y^i_2 \; \cdots \; y^i_{N_{k-i+1}}\right]$, such that $\left[\mathbf{y}^i_{AD} \; \mathbf{0}_{(h-1)\times 1}\right] = \left[\mathbf{y}^{i-1}_{AD} - \mathbf{i}^i\right]$

(For $i = 1$, $\mathbf{y}^1_{AD} = \mathbf{y}_{AD}$, $\mathbf{i}_1 = \mathbf{0}_{N_k \times 1}$)

Step 3: For stage-i, $\hat{\mathbf{x}}_{k-i+1}$ for $\mathbf{C}^k_{k-i+1}$ is recovered by application of DVS algorithm, where $\mathbf{r}_k$ is to replaced by $\mathbf{y}^i_{AD}$.

Step 4: Go to step-2, and repeat the sequence till ***Setp 3***, for $i = i+1$.

(As an exception, for $i = k$, $\hat{\mathbf{x}}_k = \mathbf{y}^k_{AD}\mathbf{C}^k_1$, where $\mathbf{C}^k_1 = \mathbf{H}_h$.

Finally, $\hat{\mathbf{x}} = [\hat{\mathbf{x}}_1 \; \hat{\mathbf{x}}_2 \; \cdots \; \hat{\mathbf{x}}_k]^T$ is the decoded input vector

for $h > 2$, the value of l required to resolve the ambiguity in the worst possible case is $(h+1)$. However, our further investigation also verifies the existence of values of DV with l beyond $(h+1)$. It is because, the factor that notably controls the decision of $l_{\max(ambg.)}$ $(> l_{\min(ambg.)} = (h+1))$ is, in fact, the level of MAI from more number of classes (unlike only one class for $l_{\min(ambg.)}$ i.e.; $\mathbf{C}^k_{k-1}$). Since with the increase in l $(> l_{\min(ambg.)})$, the number of classes contributing to r_k also increases. Under such conditions, a particular value of l is reached at which the overall MAI becomes dominant enough to affect the decision of $\hat{\mathbf{x}}_{k-i+1}$, subtracting unity (i.e.; 1) from which gives the value of $l_{\max(ambg.)}$. For $\mathbf{C}\,(N_k, M_k, \mathbf{H}_h)$ with k approaching to infinity, having $l_{\max(ambg.)} < N_k$ is obvious. Finally, for h=4 and 8, $l_{\max(ambg.)}$= 10 and 26 respectively, and for $h > 8$, $l_{\max(ambg.)} = (4h-7)$. ■

So, implementation of the DVS algorithm with $l_{\max(ambg.)}$ offers better diversity (degree of freedom) in terms of more number of chips involved for decision making. It becomes advantageous in enhancing the overall BER performance, as shown in Figure 5.11.

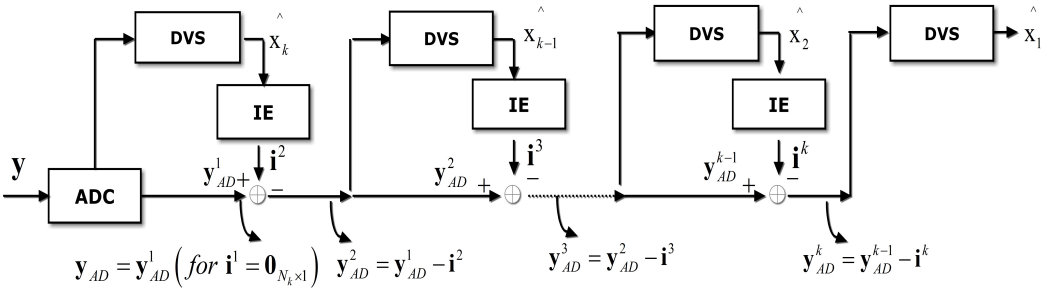

Figure 5.3: Block Diagram of the Proposed MUD (DVS).

So far, our discussion on decoding was limited to the noiseless transmission. The steps in Table 5.6 in correspondence with Figure 5.3 reveals the sequential steps devised for detection over AWGN channel.

5.3.5 Performance Analysis

5.3.5.1 Bit Error Rate

In this section, we analyze the error performance of the decoder for AWGN channel. The input system is considered to be binary, and the proposed code sets (5.1) as the encoding matrices. While for noiseless applications, the decoder offers errorless recovery (Theorem 2), the loss in this behavior for noisy environment is only due to the error (for $\mathbf{y}_{AD} \neq \mathbf{r}_k$) induced during the analog to digital conversion in step-1 of the decoder in Table 5.6. Due to the sequential nature of decoding (the class with lower N_{ef} is recovered only after decoding of that with higher N_{ef}), the BER performance of the latter being improved than that of the former is easily predictable e.g.;

$$P_e^1 < P_e^2 < \cdots < P_e^k \tag{5.11}$$

where P_e^i denotes the average BER for stage-i. Assuming the system to be fully loaded, we derive the following upper bound (UB) for the average BER of $\mathbf{C}^k$ e.g.,

$$P_{e(avg)} \leq \left(1/k\right)\left(P_e^1 + \sum_{i=1}^{k-1} P_e^i + P_e^1\left((k-1) - \sum_{i=1}^{k-1} P_e^i\right)\right) \tag{5.12}$$

where P_e^1 denotes the BER for stage-1 or $\mathbf{C}_k$ that is shown to be the minimum value, according to (5.12). Subsequently, the worst case BER upper bound for the stage-i (P_e^i) in terms of that of the stage-$(i-1)$ (P_e^{i-1}) can be expressed as

$$P_e^i \leq P_e^{i-1} + \left(1 - P_e^{i-1}\right) P_e^1. \tag{5.13}$$

For $h > 2$

$$P_e^1 = {}^1\!/\!_h \left(2^{-M_k}\right) E(z) \left(h2^{(M_k-h)} \left(1 - P(z)^{h+1}\right) + 2^{M_k} \left(1 - h2^{-h}\right) \left(1 - P(z)^{h-1}\right)\right), \tag{5.14}$$

for $h = 2$

$$P_e^1 = 2^{-(M_k+1)} E(z) \begin{bmatrix} 2^{\left(s+2^{2N_k+5}\right)} \left(1 - P\left(z\right)\right) + \\ 2^{S}\!/\!_{2^0} \left(1 - P(z)^2\right) + 2^{S}\!/\!_{2^2} \left(1 - P(z)^3\right) + 2^{S}\!/\!_{2^4} \left(1 - P(z)^4\right) + \cdots \\ +2 \left(1 - P(z)^{N_k}\right) \end{bmatrix} \tag{5.15}$$

In (5.14), and (5.15), $E(z) = \left(\frac{P(z)}{1-P(z)}\right)$, $j = (2^{M_{k-1}} - 2^{2N_k-5})$, and $P\left(z\right) = 2Q\left({}^1\!/\!_\sigma\right) - Q^2\left({}^1\!/\!_\sigma\right)$ represents the probability of error associated with each of the participating chips in decision making for $Q\left(x\right) = \int_0^x {}^1\!/\!_{\sqrt{2\pi}} e^{-\left({}^{t^2}\!/\!_2\right)} dt$. In (5.15), the first and second term relates to the decision of $\mathbf{C}_k^k$ from $l = (h+1)$ and $(h-1)$ respectively. Similarly, each term in (5.16) corresponds to $l = 1, 2, 3, ..., N_k$ with reference to Table 5.5. For derivation of (5.15) and (5.16), please refer to **Appendix B**.

5.3.5.2 Complexity

To evaluate the complexity for $\mathbf{C}^k$, we take the maximum loading conditions (i.e.; $h = 2$), and define complexity in terms of multiplications (S_{mul}), additions (S_{add}), and comparisons (S_{cmp}). First, following Table 5.6, we divide the process of decoding in each stage ($1 \leq i \leq k$) of MUD into two major steps i.e.; DVS algorithm, and interference estimation and cancellation (IEC). For each stage (stage-i), we calculate the number of multiplications (S_{mul}^i), additions (S_{add}^i), and comparisons (S_{cmp}^i) involved with respect to all possible input combinations e.g.; $S_{mul}^i = S_{mul(DVS)}^i + S_{mul(IEC)}^i$, $S_{add}^i = S_{add(DVS)}^i + S_{add(IEC)}^i$, $S_{cmp}^i = S_{mul}^i$ (as $S_{cmp(IEC)}^i = 0$, and it is trivial to show $S_{cmp_i}^i = S_{mul_i}$). Then, we average their (S_{mul}^i or S_{add}^i or S_{cmp}^i) whole sum of over k (number stages) to reach a suitable value that describes the corresponding average complexity of the whole system i.e.; $S_{mul}^{avg} = \sum_{i=1}^{k} S_{mul}^i$, $S_{add}^{avg} = \sum_{i=1}^{k} S_{add}^i$, $S_{cmp}^{avg} = \sum_{i=1}^{k} S_{cmp}^i$.

In Table 5.7, we illustrate the l versus *Number of Combinations* layout for the decoding of the whole matrix $\mathbf{C}^k$, where each row corresponds to a specific class (Table 5.5). For example, the first, and last row represent the decoding of $\mathbf{C}^k$ (Table 5.5),

Table 5.7: l versus *Number of Combinations* for decoding of $\mathbf{C}^k = \left[\mathbf{C}_1^k|\mathbf{C}_2^k|\ldots|\mathbf{C}_k^k\right]$, where $s = 2^{M_k-1} - 2^{(2M_k-5)}$, $h = 2$, and "-" stands for "Not Applicable".

l	1	2	3	...	$N_k - 1$	N_k	i
No of comb.	2^{M_k-1}	s	$\frac{s}{2^2}$	...	$\frac{s}{2^{M_k-4}}$	2	1
	2^{M_k-3}	$\frac{s}{2^2}$	$\frac{s}{2^4}$	...	2	-	2
	2^{M_k-5}	$\frac{s}{2^4}$	$\frac{s}{2^8}$	...	-	-	3
	$\vdots$	$\vdots$	$\vdots$	$\vdots$	$\vdots$	$\vdots$	$\vdots$
	2^3	$\frac{s}{2^{M_k-4}}$	2	-	-	-	$k-1$
	2^1	2	-	-	-	-	k

and $\mathbf{C}^1$ respectively. Finally, following the layout of Table 5.7, the value of $S_{muli(DVS)}$, and $S_{addi(DVS)}$ can be estimated by the following expression.

$$S^i_{mul_{(DVS)}} = 2^{M_k-i+1} \sum_{l=1}^{N_k-i+1} (No\ of\ comb.)_l\ l$$

$$S^i_{add_{(DVS)}} = 2^{M_k-i+1} \sum_{l=1}^{N_k-i+1} (No\ of\ comb.)_l\ (l-1)$$

Likewise, the number of multiplications, and additions involved in IEC for iteration-i are estimated to be

$$S^i_{mul_{(IEC)}} = S^i_{add_{(IEC)}} = N_{k-i+1} \text{ for } i < k$$

Lastly, combining all the terms (above), the value of S^{avg}_{mul}, and S^{avg}_{add} are derived to be

$$S^{avg}_{mul} = \left[\begin{array}{l} \left(k/2\right) + \\ \left(1-2^{-3}\right)\left(\frac{2(k-1)}{2^0} + \frac{3(k-2)}{2^2} + \cdots + \frac{N_{k-1}(1)}{2^{M_k-4}}\right) + \\ 2\sum_{i=2}^{N_k} \frac{i}{2^{2i-2}} + \sum_{i=3}^{N_k} i \end{array}\right] \tag{5.16}$$

and

$$S^{avg}_{add} = \left[\begin{array}{l} \left(1-2^{-3}\right)\left(\frac{2(k-1)}{2^0} + \frac{3(k-2)}{2^2} + \cdots + \frac{N_{k-2}(1)}{2^{M_k-4}}\right) + \\ 2\sum_{i=2}^{N_{k-1}} \frac{i}{2^{2i-2}} + \sum_{i=3}^{N_k} i \end{array}\right] \tag{5.17}$$

Note that the above expressions are derived for the noiseless case only. For noisy scenario, the variation in their final value is random, but marginal depending on the error introduced at ADC (in step-1) for $\mathbf{y}_{AD} \neq \mathbf{r}_k$.

Note 3: Following Figure 5.1, for the maximum loading condition (for $h = 2$), it is easy to estimate the interference vector $\mathbf{i}^i$ in Table 5.6 directly from the pattern

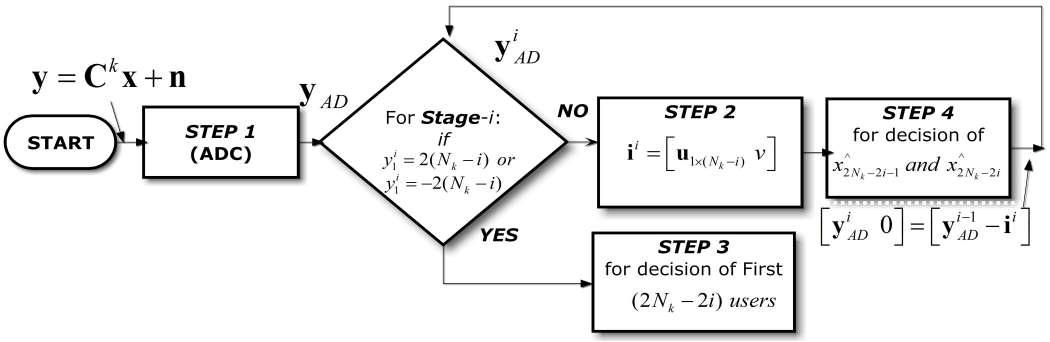

Figure 5.4: Sequential Flow Diagram for MUD (CAD) (Table 5.8).

of the signature elements (1,-1, 0) of class-i, provided the value of $\mathbf{x}_{k-i+2}$ is known. Therefore, the demand for computing $S^i_{mul_{(IEC)}}$, and $S^i_{add_{(IEC)}}$ no more exists, and it adds further simplification to the MUD's design.

Note 4: While design the structure of the DVS algorithm (Table 5.4), we have assumed the system to be fully loaded i.e., $\mathbf{x} \in \{1, -1\}^{M_k}$. However, the possibility of at least one of the h users in a class becoming inactive still exists. In such case, the decoding even gets further simplified, as $l = (h - 1)$ (in step 1) suffices for the recovery with no case of ambiguity raised. In other words, no further demand of step 2 (in DVS) is required.

5.4 MUD using CAD

5.4.1 Principle of Design

In this section, we present the structure of another type MUD for the proposed construction for $\mathbf{H}_2$ as the basis. The DVS based MUD discussed in Section-5.3 exploits the available hierarchy of MAI advantageously to facilitate the MF blocks to decode the input bits of each class with no error for noiseless applications. Our further study reports that there also resides a particular pattern in the constellation values of the chips associated with the transmitted sum vector (i.e.; $\mathbf{r}_k$ in (5.1)), which if suitably leveraged will translate the decoding logic of each class into a comparison driven one. Accordingly, it is named as comparison aided decoding and subsequently, we call the overall process of decoding as MUD (CAD). Prior to proposing the decoding algorithm for noisy transmission in Table 5.8, we present the following theorem to prove errorless behavior of the decoder in absence of noise. First, we propose Lemma 2 to supplement

Table 5.8: MUD (CAD) Algorithm for AWGN channel.

Step 1: Allow $\mathbf{y}$ in (1) to pass through a (M_k+1)-ary ADC to deliver

$$\mathbf{y}_{AD} = [y_1 \ y_2 \ \cdots \ y_{N_k}]^T$$

where $y_j \in \{0, \pm 2, \pm 4, \cdots, \pm(2N_k - 2j + 2)\}$ for $1 < j \leq N_k$

and

$$Range(y_1) = Range(y_2)$$

Step 2: For stage-i $(1 < i \leq k)$, Find

- $\mathbf{i}^i = \mathbf{C}^k_{k-i+2}\hat{\mathbf{x}}_{k-i+2} = \left[\mathbf{u}_{1\times(N_k-i)}\, v\right]^T$

where $\mathbf{u}_{1\times(N_k-i)} = [u \ u \cdots u]_{1\times(N_k-i)}$ for $u = (\hat{x}_{2N_k-2i-1} + \hat{x}_{2N_k-2i})$, and $v = (\hat{x}_{2N_k-2i-1} - \hat{x}_{2N_k-2i})$, where $\hat{\mathbf{x}}_{k-i+2} = [\hat{x}_{2N_k-2i-1} \ \hat{x}_{2N_k-2i}]^T$ and

- $\mathbf{y}^i_{AD} = \left[y^i_1 y^i_2 \cdots y^i_{N_{k-i+1}}\right]^T$ e.g., $\left[\mathbf{y}^i_{AD} \ \ \mathbf{0}_{(h-1)\times 1}\right] = \left[\mathbf{y}^{i-1}_{AD} - \mathbf{i}^i\right]$

(For $i = 1$, $\mathbf{y}^1_{AD} = \mathbf{y}_{AD}$, $\mathbf{i}_1 = \mathbf{1}_{N_k\times 1}$)

Step 3: For $\mathbf{y}^i_{AD}$

If $y^i_1 = 2(N_k - i)$ **then** $[\hat{x}_1, \hat{x}_2 \cdots \hat{x}_{2N_k-2i-1}, \hat{x}_{2N_k-2i}]^T = [1]_{2N_k-2i\times 1}$,
Else If $y^i_1 = -2(N_k - i)$ **then** $[\hat{x}_1, \hat{x}_2 \cdots \hat{x}_{2N_k-2i-1}, \hat{x}_{2N_k-2i}]^T = [-1]_{2N_k-2i\times 1}$.
(Thus, $\mathbf{x}_k$ is completely decoded and no need of any further stages.
Otherwise, follow ***Step 4***).

Step 4: For $\mathbf{y}^i_{AD}$, traverse from its $chip - (N_k - i + 1)$ to $chip - 1$ and decipher $chip - p$, such that $\mathbf{y}^i_{AD}(p) \neq 0$ and verify the following.
If $y^p_1 = 2$ *or* 4 **then** $(\hat{x}_{2N_k-2i-1}, \hat{x}_{2N_k-2i}) = (1, 1)$
Else if $y^p_1 = -2$ *or* -4 **then** $(\hat{x}_{2N_k-2i-1}, \hat{x}_{2N_k-2i}) = (-1, -1)$

Go to ***Step 2*** and repeat the sequence of steps for stage-$(i+1)$.
(Finally, $\hat{\mathbf{x}} = [\hat{\mathbf{x}}_1\hat{\mathbf{x}}_2 \cdots \hat{\mathbf{x}}_k]^T$ is the decoded input vector)

the proof in Theorem 2 (in 5.3.4).

Lemma 2: The first non-zero element encountered during the traversal from chip-N_k to chip-1 of the transmitted total sum vector $\mathbf{r}_k$ suffices for the errorfree decoding of the last class in $\mathbf{C}^k$ i.e., $\mathbf{C}_k$.

For the proof, please refer to **Appendix C**

5.4.2 Complexity

From step-2 of CAD, the prevailing pattern among the signatures of each class can be exploited to make the estimation of $\mathbf{i}^i$ void of multiplications. Therefore, the overall

complexity gets limited to comparisons and additions only. Here, we consider the noiseless case for estimation of the complexity. For noisy scenario, the variation is highly marginal depending on the error introduced at ADC (in step-1) for $\mathbf{y}_{AD} \neq \mathbf{r}_k$.

For calculation of the total number of comparisons (P_X), the input vector $\mathbf{x}$ can be split based on the decision making steps i.e.; $\mathbf{x} = \{\mathbf{x}_{step-3}|\mathbf{x}_{step-4}\}$. In other way, $k = p+q$, where p and q indicate the number of classes included in $\mathbf{x}_{step-3}$ and $\mathbf{x}_{step-4}$ respectively. Thus,

$$(S_{cmp})_{\mathbf{x}} = (S_{cmp})_{\mathbf{x}_{step-3}} + (S_{cmp})_{\mathbf{x}_{step-4}}. \tag{5.18}$$

In (5.18), $(S_{cmp})_{\mathbf{x}_{step-3}} = 1$, if and only if $\mathbf{x}$ contains a series of 1 or -1 for consecutive classes starting from $\mathbf{x}_1$ i.e., $\mathbf{x}_1 = \mathbf{1}_{2\times1}or-1_{2\times1}$, $[\mathbf{x}_1\ \mathbf{x}_2] = 1_{4\times1}or-1_{4\times1}$, $[\mathbf{x}_1\ \mathbf{x}_2\ \mathbf{x}_3] = 1_{6\times1}or-1_{6\times1}$, $\ldots$, $[\mathbf{x}_1\ \mathbf{x}_2\ \mathbf{x}_3 \cdots \mathbf{x}_k] = 1_{M_k\times1}or-1_{M_k\times1}$ for which $p = 1, 2, 3, \ldots, k$ respectively. Otherwise, $(S_{cmp})_{\mathbf{x}_{step-3}} = 0$. Unlikely, the value of $(S_{cmp})_{\mathbf{x}(step-4)}$ is the sum of all the comparisons needed for each stage individually, where step-4 is required for decoding. So, inclusion of more classes to $\mathbf{x}_{step-3}$ in turn minimizes the number of calls made to step-4 (i.e., q) and thus simplifies the overall decoding. Interestingly, for $\mathbf{x}_{step-3} = \mathbf{x}$ i.e., $(S_{cmp})_{\mathbf{x}} = 1$, which implies that only a comparison decides for the input vector $\hat{\mathbf{x}}$.

Similar to $(S_{cmp})_{\mathbf{x}}$, total number of additions $(S_{add})_{\mathbf{x}}$ is also input combination variant. However, the noteworthy point is that addition operation is demanded only for the decoding of the q consecutive classes of $\mathbf{x}_{step-4}$. As evident from Table 5.8, decoding in such case is achieved by the joint contribution of step-2 and step-4. Where step-2 is meant for estimation and cancellation of the interference, step-4 process the outcome of step-2 to offer the final decision. Thus, we can express $(S_{add})_{\mathbf{x}}$ as

$$(S_{add})_{\mathbf{x}} = (S_{add})_{IE} + (S_{add})_{IC} \tag{5.19}$$

where $(S_{add})_{IE}$=$2q$= number of additions for IE and $(S_{add})_{IC} = \sum_{e=1}^{q} N_{k-e+1}$= number of additions involved in q stages of IC. For better perception of the overall simplicity of CAD, a comparative study of complexity with respect to optimum MLD is presented in Table .

Table 5.9: Complexity Analysis: MUD (CAD) versus MUD (DVS) versus Optimum MLD.

MUD Type	Size	S_{mul}^{avg}	S_{add}^{avg}	S_{cmp}^{avg}
MUD (CAD)	4x6	Nil	2.3	6.5
	8x14	Nil	10.4	17.2
MUD (DVS)	4x6	9.69	3.7	7.36
	8x14	24.66	14.09	19.95
Optimum MLD	4x6	$2^6(4 \times 6)$	$2^6(4 \times 6)$	2^7
	8x14	$2^{14}(8 \times 14)$	$2^{14}(8 \times 14)$	2^{15}

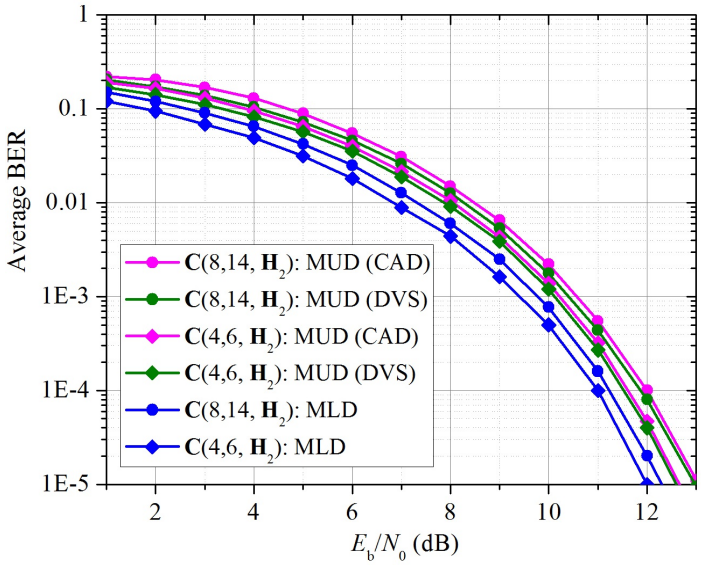

Figure 5.5: BER versus (E_b/N_o) performance for $\mathbf{C}(4, 6, \mathbf{H}_2)$, $\mathbf{C}(8, 14, \mathbf{H}_2)$: Optimum MLD versus MUD (DVS) versus MUD (CAD).

5.5 Simulation Results

Here, we discuss the BER versus (E_b/N_0) performance of the system, assuming the channel to be AWGN. Also, the system is assumed to be BPSK modulated and perfectly power controlled.

Figure 5.5 offers an overview of the performance of proposed MUD (DVS) as compared to that of optimum MLD [41]. For simulation, the code sets $\mathbf{C}(4, 6, \mathbf{H}_2)$, $\mathbf{C}(8, 14, \mathbf{H}_2)$ ($\beta = 1.5$ and 1.75) are chosen. The observation shows the BER degradation of the proposed decoder to be nominal, and worthy to be overlooked due to the prominent advantage achieved in terms of its design simplicity (Table 5.9). Moreover, the degradation in error performance of the proposed MUD (CAD) (in

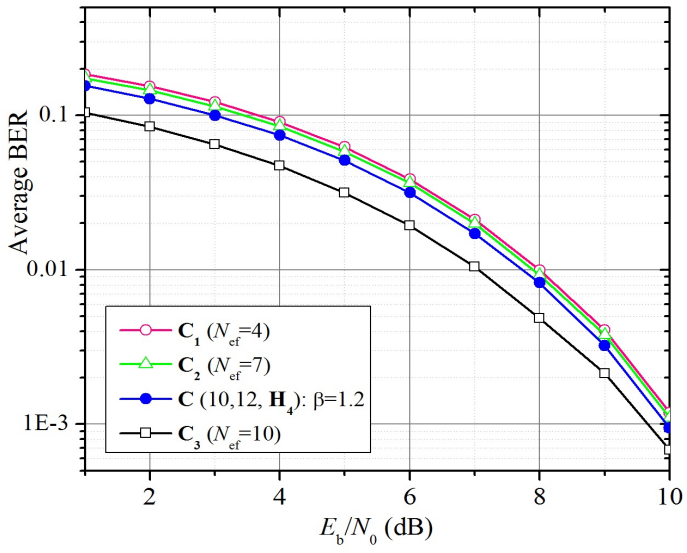

Figure 5.6: BER versus (E_b/N_o) performance for individual classes in $\mathbf{C}(10, 12, \mathbf{H}_4) = [\ \mathbf{C}_1^3 \mid \mathbf{C}_2^3 \mid \mathbf{C}_3^3\ ]$ (9), using MUD (DVS).

Section 5.4) is found to be negligible, while its simplicity over the former counterpart is easily realizable from Table 5.9.

Figure 5.6 illustrates the BER response of different classes of $\mathbf{C}(10, 12, \mathbf{H}_4)$. The intention is to study the variation in error performance with the change in average transmission power. From the observation, even if the class with lower value of N_{ef} is less error protected than that with higher value (5.11), the deviation is found to be acceptable.

In Figure 5.7, the error performance of the decoder subjected to different loading conditions is analyzed by continuously varying β, while keeping h fixed. To ensure the maximum loading condition, $h = 2$ is set (Note 1). Four different code sets $\mathbf{C}(2, 2, \mathbf{H}_2)$, $\mathbf{C}(4, 6, \mathbf{H}_2)$, $\mathbf{C}(13, 24, \mathbf{H}_2)$, $\mathbf{C}(64, 126, \mathbf{H}_2)$ $(\beta = 1, 1.5, 1.84, 1.97)$ are chosen for simulation. Also in each case, the derived upper bound is plotted for the comparison purpose. Besides, the case of $\mathbf{C}(2, 2, \mathbf{H}_2)$ $(\beta = 1)$ is included as the performance bound (benchmark). Following the observations, with increase in value of β, although there exists a rise in the level of BER, the degradation is found to be negligible. At high loading condition $(\beta = 1.96)$, the sacrifice in (E_b/N_0) as compared to $\beta = 1$ (performance benchmark) remains < 1 dB only. Also, with the lowering of β (or k), the theoretical upper bound approaching close to that of simulation is also traced resulting in a complete overlap for $\beta = 1$. In contrast, for higher values of β, this deviation is significant for which the worst case assumptions during the

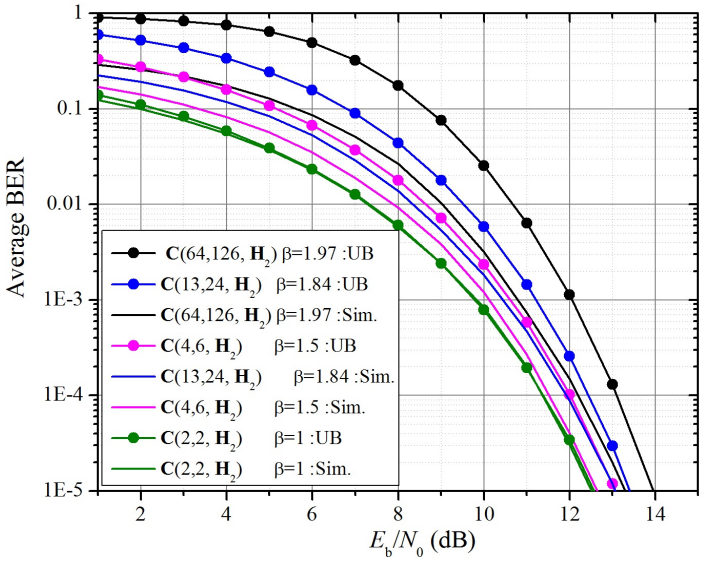

Figure 5.7: BER versus (E_b/N_o) performance variation with change in β, for $\mathbf{H}_2$ as the basis set, using MUD (DVS)

formulation of the upper bound in (5.13) is to be held responsible.

Figure 5.8 reflects the BER versus (E_b/N_0) behavior for MUD (DVS), when a specific value of M_k is to be attained for different values of h. To have $M_k = 16$, the matrices $\mathbf{C}(16, 16, \mathbf{H}_{16})$, $\mathbf{C}(15, 16, \mathbf{H}_8)$, $\mathbf{C}(13, 16, \mathbf{H}_4)$, $\mathbf{C}(9, 16, \mathbf{H}_2)$ $(\beta = 1, 1.06, 1.23, 1.77)$ are constructed. The intention of appointing $\mathbf{C}(16, 16, \mathbf{H}_{16})$ is to establish the *performance bound* for comparison. For fixed M_k, the higher values of h leading the construction results in lowering of k, and hence β. Subsequently, the gradual enhancement in the error performance is visualized due to the rise in spreading diversity.

In Figure 5.9, three different systems: the proposed system, GCO with SMLD [71], and logical signature matrix (LSM) [81] with LD [100] are subjected to comparison. All the matrices are of ternary type, and size (8×14) i.e; $\beta = 1.75$. For comparison, we also plot the performance of the proposed system for $\mathbf{C}(64, 126, \mathbf{H}_2)$ (i.e.; $\beta = 1.97$), using MUD (DVS). It is observed that for lower values of $(\mathrm{E}_b/N_0) \leq 5$dB, the BER level of the proposed system behaves close to that of GCO. However, at higher levels of (E_b/N_0), the proposed system outsmarts that of GCO. For the better error performance, the efficiency of the DVS in exploiting the orthogonality of the basis sets, and implementation of ADC to preserve the received constellation plays the major role. As compared to LSM, the proposed system consistently maintains its superiority in BER throughout the scale of (E_b/N_0) at the cost of rise in complexity by acceptable

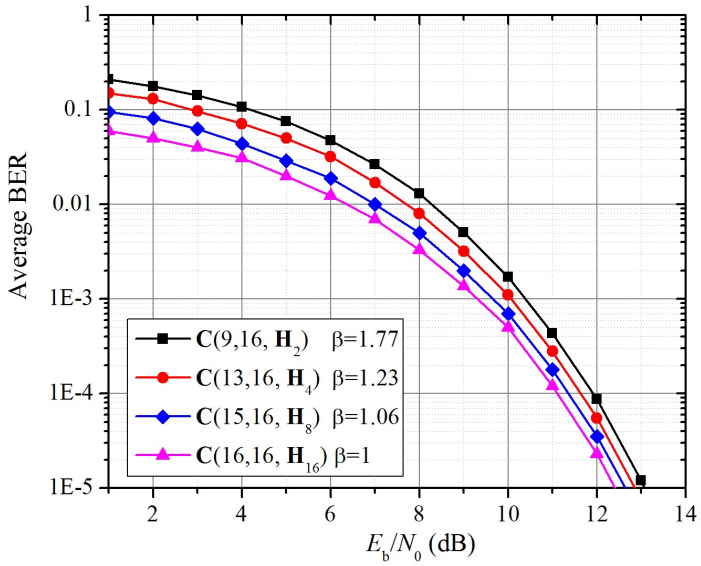

Figure 5.8: BER versus (E_b/N_0) performance comparison for $M_k = 16$ realized through $\mathbf{H}_4$, $\mathbf{H}_2$, $\mathbf{H}_8$, and $\mathbf{H}_{16}$ as the basis set, using MUD (DVS).

margin. Besides, the convergence in BER for the proposed system is also observed for higher values of (E_b/N_0), even at high loading condition ($\beta = 1.97$). It is due to the use of ADC for which at high value of (E_b/N_0), the system behaves close to that of the noiseless case ($\mathbf{y}_{AD} \approx \mathbf{r}_k$).

In Figure 5.10, the BER performance of the extended code sets (Note 2) is analyzed while keeping the system capacity fixed. To have equal capacity ($hM_k = 96$), the proposed code sets $\mathbf{C}(4, 6, \mathbf{H}_2)$, $\mathbf{C}(7, 12, \mathbf{H}_2)$, $\mathbf{C}(13, 24, \mathbf{H}_2)$ are indulged corresponding to $\mathbf{H}_{16}$, $\mathbf{H}_8$, $\mathbf{H}_4$ respectively. For hM_k being fixed, having the smaller $\mathbf{H}_h$ (larger $\mathbf{C}^k$) results in rise of β, costing the level of (E_b/N_0) by small margin. In addition, it is observed that the target capacity being fixed, the system realization through the extended matrices [71] offers better scope for BER over the proposed system with $\mathbf{C}(49, 96, \mathbf{H}_2)$, using MUD (DVS).

In Figure 5.11, the simulation study shows the impact of the enhanced diversity (Corollary 2) on the overall BER performance. We consider $\mathbf{C}(10, 12, \mathbf{H}_4)$, and $\mathbf{C}(13, 16, \mathbf{H}_4)$ for simulation and MUD (DVS) at the receiver. For the improvement, we have considered the maximum allowable diversity $l = l_{\max(ambg.)} = 10$, and results are compared with that of the regular one ($l = l_{\min(ambg.)} = 5$ for $\mathbf{H}_4$). To our expectation, the respective gain in recovery performance is observed for $l = l_{\max(ambg.)}$.

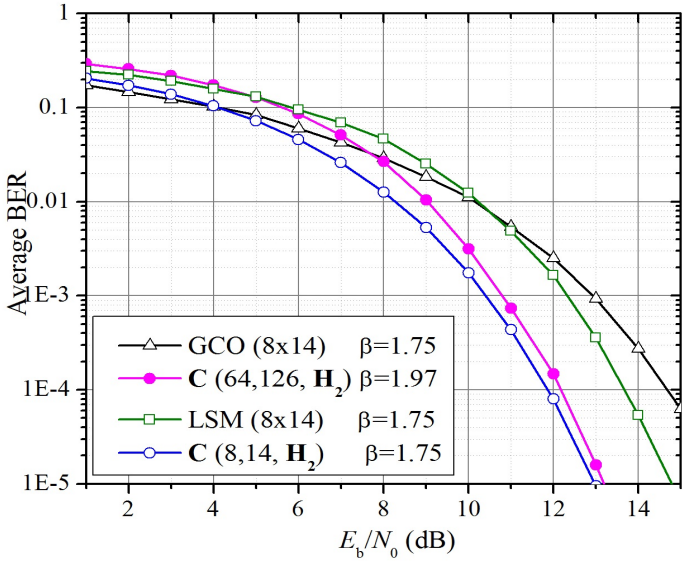

Figure 5.9: BER versus (E_b/N_0) performance for the systems with Ternary UD Matrices of size (8×14): HLDS (MUD (DVS)), GCO (SMLD) and LSM (LD).

5.6 Summary

In this chapter, we investigated the problem of design a new family of generalized ternary matrices for overloaded CDMA. First, we introduced the method of construction both recursive, and non-recursive. We proved its uniquely decodable nature, and derived the generalized criterion for selection of the basis sets. Later, we showed the qualifying nature of most of the existing UDC sets to meet this specified criterion. The overall method of construction was driven by an overlapped hierarchy involving the basis sets, and has faster implementation over other available approaches. For orthogonal hadamard sets $\mathbf{H}_h$ as the basis of construction, we introduced the MUD (DVS), whose operation in each stage was supervised by the proposed DVS algorithm. In fact, it was the advantageous cross-correlation hierarchy generated due to the unique encoding feature of the Hadamard sets (besides orthogonality), which granted the errorless nature of the decoder in the absence of noise. Also, we validated its proof, mathematically. The expressions to estimate the complexity, and BER upper bound were derived. For $\mathbf{H}_2$ as the basis, the system presented the maximum loading condition ($\beta \approx 2$), and feasibility of construction for arbitrary values of code length ($N_k \in \mathbf{Z}^+$). From the derived expressions, we found the complexity of the proposed MUD (DVS) to be highly insignificant as compared to the optimum MLD. Yet, any significant deviation in the error performance was hard to observe. Simulation results

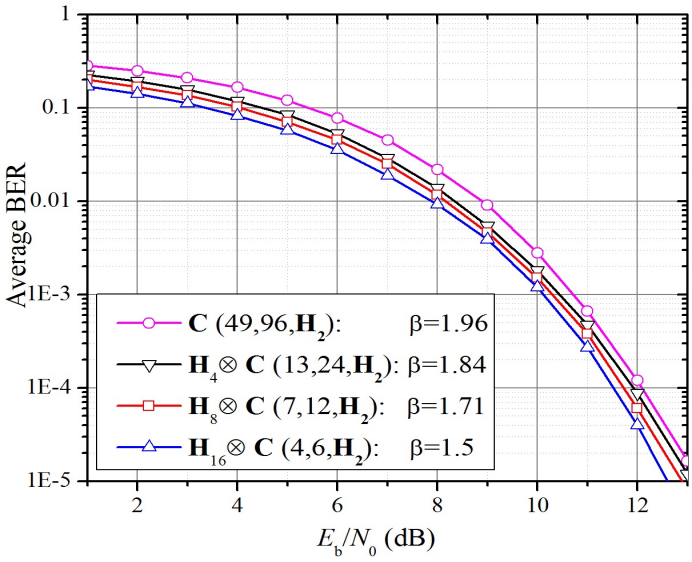

Figure 5.10: BER versus (E_b/N_0) performance of the extended matrices of uniform capacity $hM_k = 96$: $\mathbf{H}_4 \otimes \mathbf{C}(13, 24, \mathbf{H}_2)$, $\mathbf{H}_8 \otimes \mathbf{C}(7, 12, \mathbf{H}_2)$, $\mathbf{H}_{16} \otimes \mathbf{C}(4, 6, \mathbf{H}_2)$ (Note 2).

validated for its superiority in BER over other equivalent systems using the ternary code sets: LSM (LD), and GCO (SMLD). Also, the complexity analysis showed the decoder to be more favorable over SMLD. For $h > 2$, the scope of maximum available diversity for BER improvement was verified through simulation. Lastly, we proposed the MUD (CAD) algorithm which despite of its simplicity regarding the comparison driven logic achieves the BER performance, very close to that of the proposed MUD (DVS).

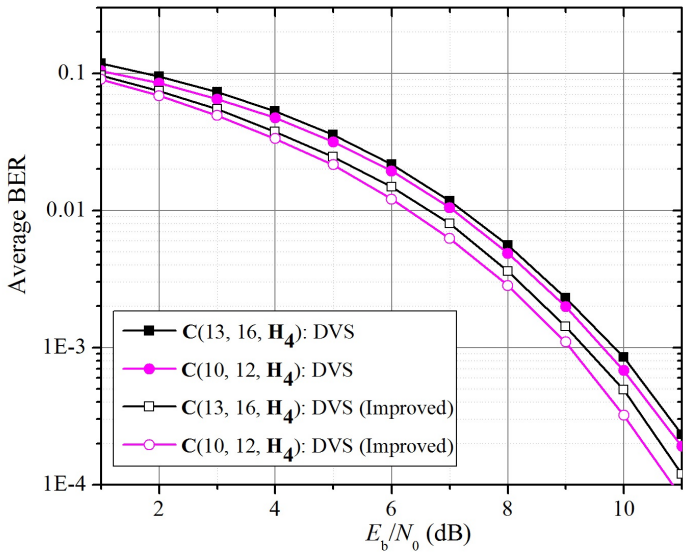

Figure 5.11: BER versus (E_b/N_0) performance improvement for $l_{\max(ambg.)}$ using MUD (DVS), for $\mathbf{H}_4$ as the basis set (Corollary 2).

Chapter 6
Conclusions

In this chapter, we summarize the overall contribution followed by presenting the limitations and possible scope of future work.

Chapter 1 emphasized on the background study on overloaded CDMA where the existing literature associated with the relevant constructions of UD matrices, role of TSC and it's bounds, existing MUD designs and challenges associated with their implementation, and moreover, the construction and decoding of LDS matrices were discussed. This analysis, later on, led to the formation of the problem statement followed by listing down of the objectives.

Chapter 2 presented the variants of ternary signature matrices for overloaded CDMA (i.e.; TSMOS (Type I, Type II, Type III, and their mixed counterparts) which projected a hierarchy based correlation pattern. The recursive construction of the matrix was fundamentally guided by the structure of the basis set, which was carefully chosen from the existing literature. At the cost of sacrificing the asymptotic equality, the final matrix generated (with a capacity to achieve $\beta \approx 2$) was shown to produce a twin tree hierarchical correlation pattern among its subsets. The equality in the level of MAI for both left and right child delivered a uniform structure to the overall tree hierarchy, which consistently approved the necessary condition (i.e.; PA $>$ TPC) for the errorfree decoding of each subset using MF. As a result, the overall design of the MUD using MF as the core block of design became simplified leading to the recovery of each subset with no error for noiseless transmission. Further, we uncovered the complementary nature of the 50% signatures of the binary (Hadamard) subset, which further led to their optimality for transmission delay of $t_d = 0.5T_c$, between the binary and ternary subsets. Also, we verified the periodic nature of occurrence of the optimal behavior and existence of EDP. For noisy transmission, the BER performance of the

TSMOS was observed to outperform that of the WBE, and random binary sequence set with an improved design of MUD. Besides, due to the optimized control over the MAI, the improvement in its average error performance over that of the O/O CDMA was also easy to speculate. As compared to the binary GCO set using SMLD, the degradation in BER performance of the TSMOS was found to be acceptable when compared with the gain rendered in the proposed MUD concerning its simplicity. Our intention to analyze the error performance of individual subset provided us a more accurate study of their performance. By and large, the overall design of the MUD was found to be far simplified over the existing iterative architecture involving SIC, PIC, HIC, and SMLD. Therefore, the outcome of discussion of the whole system was interesting, as it validated the fact that design of signature matrices with improved cross-correlation pattern can be an efficient alternative to overcome the excessive complexity of the MUD for overloaded CDMA system and achieving acceptable quality of recovery at the same time.

Chapter 3 focused on the non-ternary version of SMOS, also known as $2k$-ary SMOS or $2k$-SMOS. Unlike TSMOS, twin tree hierarchy correlation pattern involving the binary subsets were nonuniform in nature. As a result, the left and right child at each level was exposed to different levels of MAI, thus leading to the classification of the BER analysis of each of its individual subsets into two sections. Moreover, with no complementary feature, the construction allowed the existence of $\frac{N_k}{2}$ number of optimal users in the largest (Hadamard) subset. Using the concept of suitable anomalies and trade-off, we reasonably validated the difference between the performance of the ternary and $2k$-ary. Despite the prominent edge regarding optimality of the specific users, proclaiming the $2k$-ary to be superior over ternary appeared to be illogical, since the outcome of our attempt for recognizing either of them as superior was later found not to be mutually exclusive. This inference became more vivid from our observations when for a fixed loading condition, the superiority of any of them hardly retained the uniformity for all the constituent subsets. Therefore, evidently enough, superiority in this context became a conditional entity. However, with a difference, for the maximization in loading capacity to be 150% ($\beta = 1.5$ i.e.; the first two subsets being active), the superiority was found to be exclusively possessed by the $2k$-ary.

Chapter 4 , can be considered as an overall generalization to the concept of SMOS. The idea of proposing the HSMOS, as a combination of the TSMOS and $2k$-SMOS, resulted in variety of structures following the $top-to-bottom$ and $bottom-to-top$ approach. For each case, for the construction of SMOS with k subsets, k different structures were found to exist. Each of them (including TSMOS and $2k$-SMOS) projects a different level of BER for the individual subsets and the variation observed was straight due to the change in the status of the inequality (PA >TPC) controlling the quality of detection of the proposed MUD using MF. The transition in the status the inequality for the left and right child, for each configuration, was offered an in-depth analysis. Also, the observation from the analysis of the inequality were found to be matched with that of the simulation results.

Chapter 5 was about a new family of generalized LDS matrices for overloaded CDMA. First, we introduced the method of its construction, mathematically proved its UD nature and derived the generalized criterion for selection of the basis sets. Later, we showed the qualifying nature of most of the existing UD sets to meet this specified criterion. The overall method of construction was driven by an overlapped hierarchy involving the basis sets and has faster implementation over other available approaches. For orthogonal Hadamard sets $\mathbf{H}_h$ as the basis of construction, we introduced a MUD, whose operation in each stage was supervised by the proposed DVS algorithm. In fact, it was the advantageous cross-correlation hierarchy generated due to the unique encoding feature of the Hadamard sets (besides orthogonality), which granted the errorless nature of the MUD (DVS) in the absence of noise. Also, we validated its proof, mathematically. The expressions to estimate the complexity and BER upper bound were derived. For $\mathbf{H}_2$ as the basis, the system presented the maximum loading condition ($\beta \approx 2$), and feasibility of construction for arbitrary values of code length ($N_k \in \mathbf{Z}^+$). From the derived expressions, we found the complexity of the decoder to be highly insignificant as compared to the optimum MLD and SMLD. Any significant deviation in the error performance was hard to observe. Simulation results validated for its superiority in BER over other equivalent systems using the ternary code sets i.e.; LSM (using LD), and GCO (using SMLD). For $h > 2$, the scope of maximum available diversity for BER improvement was verified through simulation. Lastly, we further transformed the structure of the MUD (DVS) to a more simplified one (i.e.;

MUD (CAD)), where mere comparisons were found to suffice for the recovery of the input vector with marginal degradation in error performance as compared to the MUD (DVS).

Limitations: The limitations of our contribution in this thesis can be listed down as follows.

- The degradation in the error performance of the variants of SMOS matrices for multi-path fading channels is apparent.
- Likewise, the deterioration in the error performance is also expected under imperfect power control transmission condition.
- Also, expecting the rise in the error performance for fully asynchronous transmission is inevitable.
- Particularly, for HLDS construction under multi-path fading channel, the efficiency of the use of ADC to restore the transmitted symbols at the receiver is prone to destruction, which, subsequently, will lead to BER degradation.

Future Work: As a part of the future works, we consider the following.

- To study the performance of the proposed UD matrices (SMOS, HLDS) for non-ideal channel conditions e.g.; imperfect power control conditions, multi-path fading channel, etc..
- To analyze the impact of HLDS towards the PAPR reduction in OFDM architecture.
- To study the performance of HLDS based overloaded CDMA with that of the LDPC based CDMA system and compare under OFDM platform.
- To construct improved code designs and MUD for SCMA applications.

Chapter A
Appendix A: Proof of Errorless nature of DVS Algorithm

We divide the proof into two sections i.e., for $h > 2$ and $h = 2$, since there exists a variation in the pattern of their cross-correlation matrices.

A.0.1 For $h > 2$

In order to have the cross-correlation matrices of the lowest dimension for analysis, we keep the proposed matrix simple ($k = 1$) i.e.; $\mathbf{C}(7, 8, \mathbf{H}_4)$. Later, we reveal that for higher values of k, the analysis also produces the similar outcome. Since, we access the orthogonality of the generalized Hadamard construction $\mathrm{H}_{2^{k+1}} = \begin{bmatrix} \mathrm{H}_{2^k} & \mathrm{H}_{2^k} \\ \mathrm{H}_{2^k} & -\mathrm{H}_{2^k} \end{bmatrix}$ for $k \in \mathbf{Z}^+$, application of the following method to other values of h (> 4) is obvious.

Table A.1 presents the cross-correlation matrices involved in decoding. Correspondingly, Table A.2 shows the decision logic involving the cross-correlation matrices in Table A.1. We intend to show the decoding of $\mathbf{C}_k^k$ to be errorless. So, following Table 5.4, our approach is to start the analysis from $l = (h - 1)$, and continuously increment l by 1, till all possible combinations of $\mathbf{x}_k$ are determined.

• For $l = (h-1)$, decoding of $\mathbf{C}_k^k$ can be achieved by multiplication of $(\mathbf{C}^k_{k_{(h-1\times h)}})^T$ with $\mathbf{r}_{k_{(h-1\times 1)}} = \mathbf{C}^k_{k_{(h-1\times h)}}\mathbf{x}_{k_{(h\times 1)}}$ (Table A.2 (E11)). Onwards, simply (E11) will be used instead. The same also holds for all other rows in Table A.2. $\boldsymbol{\rho}_{h-1}$ denotes the peak auto correlation matrix for $\mathbf{C}^k_{k_{(h-1\times h)}}$. Substitution of $\boldsymbol{\rho}_{h-1}$ from Table A.1 in (E11) gives decision for $\hat{\mathbf{x}}_k$. Due to the symmetry among the elements of $\boldsymbol{\rho}_{h-1}$, any of the h elements of $\hat{\mathbf{x}}_k = [\hat{\mathbf{x}}_k(1)\ \hat{\mathbf{x}}_k(2)\ \cdots\ \hat{\mathbf{x}}_k(h)]$ in (E11) can be considered to test the impact. We choose $\hat{\mathbf{x}}_k(1)$ for this purpose, whose expanded view is presented in (E12). Afterwards, for other values of $l > (h-1)$, we incorporate the similar approach.

From (E12), decoding of $\hat{\mathbf{x}}_k(1)$ is unambiguous for all 2^{M_k} combinations of $\mathbf{x}$ except when $\mathbf{x}_k(1) = \mathbf{x}_k(2) = \cdots = \mathbf{x}_k(h)$. It is because, for these combinations, the input

Table A.1: Cross Correlation Matrix with respect to class $\mathbf{C}_k^k$ for $h = 4$

$$\boldsymbol{\rho}_{h-1} = \left((\mathbf{C}^k_{k_{(h-1\times h)}})^T \mathbf{C}_{k_{(h-1\times h)}}\right)$$

$$= (h-1)\begin{bmatrix} u_{h-1} & v_{h-1} & v_{h-1} & v_{h-1} \\ v_{h-1} & u_{h-1} & v_{h-1} & v_{h-1} \\ v_{h-1} & v_{h-1} & u_{h-1} & v_{h-1} \\ v_{h-1} & v_{h-1} & v_{h-1} & u_{h-1} \end{bmatrix}$$

$$\boldsymbol{\rho}_{h} = \left((\mathbf{C}^k_{k_{(h\times h)}})^T \mathbf{C}_{k_{(h\times h)}} \mid (\mathbf{C}^k_{k-1_{(h\times h)}})^T \mathbf{C}_{k_{(h\times h)}})\right)$$

$$= h\left[\begin{array}{c|cccc} \mathbf{I} & u_h & -u_h & -u_h & u_h \\ & u_h & -u_h & -u_h & u_h \\ & u_h & -u_h & -u_h & u_h \\ & u_h & -u_h & -u_h & u_h \end{array}\right]$$

$$\boldsymbol{\rho}_{h+1} = \left((\mathbf{C}^k_{k_{(h+1\times h)}})^T \mathbf{C}_{k_{(h+1\times h)}} \mid (\mathbf{C}^k_{k-1_{(h+1\times h)}})^T \mathbf{C}_{k_{(h\times h)}})\right)$$

$$= (h+1)\left[\begin{array}{cccc|cccc} u_{h+1} & v_{h+1} & v_{h+1} & v_{h+1} & 2v_{h+1} & 0 & -2v_{h+1} & 0 \\ v_{h+1} & u_{h+1} & v_{h+1} & v_{h+1} & 2v_{h+1} & 0 & -2v_{h+1} & 0 \\ v_{h+1} & v_{h+1} & u_{h+1} & v_{h+1} & 2v_{h+1} & 0 & -2v_{h+1} & 0 \\ v_{h+1} & v_{h+1} & v_{h+1} & u_{h+1} & 2v_{h+1} & 0 & -2nv_{h+1} & 0 \end{array}\right]$$

where $\mathbf{x}_{h-1} = \mathbf{x}_k$ and $\mathbf{x}_{h+1} = \mathbf{x}_h = [\mathbf{x}_k \mathbf{x}_{k-1}]^T$

Table A.2: Decision logic for $h = 4$ (derived from Table A.1)

(E11) $\hat{\mathbf{x}}_k = \text{sign}\left(\boldsymbol{\rho}_{h-1}\mathbf{x}_{h-1}\right)$
(E12) $\hat{\mathbf{x}}_k(1) = \text{sign}\left(3\mathbf{x}_k(1) - (\mathbf{x}_k(2) + \mathbf{x}_k(3) + \mathbf{x}_k(4))\right)$

(E21) $\hat{\mathbf{x}}_k = \text{sign}\left(\boldsymbol{\rho}_{h}\mathbf{x}_{h}\right)$
(E22) $\hat{\mathbf{x}}_k(1) = \text{sign}\left(4\mathbf{x}_k(1) - (\mathbf{x}_k(3) - \mathbf{x}_k(4) - \mathbf{x}_{k-1}(1) + \mathbf{x}_{k-1}(2))\right)$

(E31) $\hat{\mathbf{x}}_k = \text{sign}\left(\boldsymbol{\rho}_{h+1}\mathbf{x}_{h+1}\right)$
(E32) $\hat{\mathbf{x}}_k(1) = \text{sign}\left(5\mathbf{x}_k(1) + (\mathbf{x}_k(2) + \mathbf{x}_k(3) + \mathbf{x}_k(4)) + 2\left(\mathbf{x}_{k-1}(1) - \mathbf{x}_{k-1}(3)\right)\right)$

where $\mathbf{x}_{h-1} = \mathbf{x}_k$ and $\mathbf{x}_{h+1} = \mathbf{x}_h = [\mathbf{x}_k \mathbf{x}_{k-1}]^T$

element to sign ( ) becomes zero producing decision ambiguity. To overcome this, let us consider for $l > (h-1)$.

• For $l = h$, $\mathbf{r}_{k_{(h\times 1)}} = \mathbf{C}^k_{k_{(h\times h)}}\mathbf{x}_k + \mathbf{C}^k_{k-1_{(h\times h)}}\mathbf{x}_{k-1}$. So, the equivalent expression for $\hat{\mathbf{x}}_k$ is given by (E21). Replacing $\boldsymbol{\rho}_h$ from Table VII in expression for $\hat{\mathbf{x}}_k$ in (E22) reveals that the presence of interference from $\mathbf{C}^k_{k-1}$ as $\mathbf{x}_{k-1}(1)$ and $\mathbf{x}_{k-1}(2)$, in deed, makes the decision ambiguous.

• For $l = (h+1)$, repeating the similar approach finally resolves the problem of ambiguity completely. We can verify it from the expression of $\hat{\mathbf{x}}_k(1)$ in (E32) corresponding to $\boldsymbol{\rho}_{h+1}$ in Table A.1.

So, it confirms that selecting the DV with $l = (h-1)$, and $(h+1)$ can lead to errorless decoding, for $h > 2$.

• From the aforementioned process of decision making of $\mathbf{C}^k_k$, role of any other class besides $\mathbf{C}^k_{k-1}$ does not come into picture, which implies that considering the matrix with even more number of classes ($k > 2$) will neither affect our analysis nor its outcome. Thus, it justifies the selection of $\mathbf{C}(7, 8, \mathbf{H}_4)$ for the proof. ■

A.0.2 For $h = 2$

Similar to the case of $h > 2$, the problem of ambiguity also persists for $l = (h-1)$, when $\mathbf{x}_k(1) = \mathbf{x}_k(2)$. It indicates that decoding for 50% of the total input combinations of $\mathbf{x}_k$ are resolved for $l = (h-1)$ only, whereas for rest of the combinations, our search for DV starts with $l = h$ and ends at $l = N_k$. Following Figure 5.1, for $h \le l \le (N_k - 1)$, there exists $2l$ distinct signatures. So, ρ_l becomes a $(2l \times l)$ matrix, and can be defined as

$$\boldsymbol{\rho}_{l_{(1j)}}{}^T = \begin{pmatrix} l & j=1 \\ l-2 & j=2 \\ l-3 & j=3 \\ l-1 & j=4 \\ l-4 & j=5 \\ l-2 & j=6 \\ \vdots & \vdots \\ -1 & j=2l-1 \\ 1 & j=2l \end{pmatrix} \quad \boldsymbol{\rho}_{l_{(2j)}}{}^T = \begin{pmatrix} l-2 & j=1 \\ l & j=2 \\ l-3 & j=3 \\ l-1 & j=4 \\ l-4 & j=5 \\ l-2 & j=6 \\ \vdots & \vdots \\ -1 & j=2l-1 \\ 1 & j=2l \end{pmatrix} \tag{A.1}$$

where $\boldsymbol{\rho}_{l_{(1j)}}$ and $\boldsymbol{\rho}_{l_{(2j)}}$ represent the level of the peak cross correlation of user-j on user-1 and 2 respectively. Now, for $\boldsymbol{\rho}_l = [\boldsymbol{\rho}_{l_{(1j)}}\boldsymbol{\rho}_{l_{(2j)}}]$, and the input combination $\mathbf{x}_l$=$[\mathbf{x}_k\ \mathbf{x}_{k-1}\ \mathbf{x}_{k-2}\ \ldots\ \mathbf{x}_{k-l+1}]$, the perfect decision is offered by $\hat{\mathbf{x}}_k = \text{sign}\,(\boldsymbol{\rho}_l\mathbf{x}_l)$.

For the specific cases where $l = (N_k - 1)$ fails to detect, $l = N_k$ is to considered. This is apprehended as the worst case as it consumes all the N_k chips for decoding i.e.; length of DV = length of decoding vector $\mathbf{r}_k$. To test the validity of our algorithm for the worst case, consider one such input combination $\mathbf{x} = [-+ \quad -+ \quad \cdots \quad -+ \quad ++]$, for which the ambiguity still exists for $l = N_{k-1}$ i.e., $(\boldsymbol{\rho}_{N_{k-1}} \mathbf{x}_{N_k - 1}) = \mathbf{0}_{2\times 1}$. To resolve, we replace the last two elements in (A.1) corresponding to $j = (2l - 1)$ and $2l$ to produce $\boldsymbol{\rho}_{N_k}$, such that for $l = N_k$

$$\rho_{l_{1(2l-1)}} = \rho_{l_{2(2l-1)}} = 2 \text{ and } \rho_{l_{1(2l)}} = \rho_{l_{2(2l)}} = 0.$$

Further, solving for $\hat{\mathbf{x}}_k = \text{sign}\,(\boldsymbol{\rho}_{N_k} \mathbf{x}_k)$ results in the decoded vector $\hat{\mathbf{x}}_k = [++]$, and justifies the errorless attribute of the proposed approach for $h = 2$. Similar inference can be drawn for the second worst case combination $\mathbf{x} = [+- \quad +- \quad \cdots \quad +- \quad --]$, for which $\hat{\mathbf{x}}_k = [--]$ can be easily verified. Thus, for $\mathbf{C}^k$ with $h = 2$, decoding of $\mathbf{x}_k$ is errorfree. Also, this completes the proof for all values of h $(h > 2 \text{ and } h = 2)$. ■

Chapter B
Appendix B: BER Upper Bound for HLDS using MUD (DVS)

Here, we derive the expression for P_e^1 for (5.14), and (5.15) that denotes the average probability of error associated with decoding of $\mathbf{C}_k^k$. From Section 5.3.5.1, we recall that for noisy transmission, the error introduced in decoding of $\mathbf{C}_k$ is due to the occurrence of error in the elements of the DV during the analog to digital conversion. Hence, for l denoting the length of DV=$[z_1 z_2 \cdots z_l] \subseteq \mathbf{y}_{AD}$, the probability of having at least one of its element with error (i.e.; $P_{e(l)}$) can be expressed as

$$P_{e(l)} = P_e(z_1) + P_e(z_1 z_2) + \cdots + P_e(z_1 z_2 \cdots z_l).$$

Since the availability of error with one element is independent of the other: $P_e(z_1 z_2 \cdots z_l) = P_e(z_1)\ P_e(z_2)\ \cdots\ P_e(z_l)$, and equal likely: $P_e(z_1) = P_e(z_2) = \cdots P_e(z_l) = P_e(z)$, $P_{e(l)}$ in terms of $P_e(z)$ can be rewritten as $P_{e(l)} = P_e(z) + (P_e(z))^2 + \cdots + (P_e(z))^l$. This series being a geometric progression can further be simplified to $P_{e(l)} = \left(\frac{P_e(z)}{1-P_e(z)}\right)\left(1 - (P_e(z))^l\right)$. As the distance between the two nearest points in the constellation of the proposed ADC (see Table 5.6) is always 2 (two), the expression for $P_e(z)$ subjected to the noise with standard deviation σ, and mean $\mu = 0$ can be written as

$$\begin{aligned} P_e(z) &= P\left(\sigma > 1 \ \text{ or } \ \sigma < -1\right) \\ &= P(\sigma > 1) + P(\sigma < -1) - P(\sigma > 1)P(\sigma < -1) \\ &= 2Q\left(\tfrac{1}{\sigma}\right) - Q^2\left(\tfrac{1}{\sigma}\right). \end{aligned}$$

Due to the symmetry of Gaussian distribution about mean μ, $P(\sigma > 1) = P(\sigma < 1) = Q\left(\frac{1}{\sigma}\right)$ for $Q(x) = \int_0^x {}^1\!/\!_{\sqrt{2\pi}} e^{-\left(t^2/2\right)} dt$. According to DVS algorithm (in Table 5.4), for basis matrices with $h > 2$, the available values of l are $(h-1)$, and $(h+1)$. So, the final expression for P_e^1 (for $h > 2$) becomes

$$P_e^1 = (1/h)2^{-m_k}\left(w_{h-1}P_{e(h-1)} + w_{h+1}P_{e(h+1)}\right),$$

which on further simplification results in (5.14). w_{h-1}, and w_{h+1} denote the number of combinations out of 2^{M_k} demanding the DV with $l = (h-1)$, and $(h+1)$ respectively, where $(w_{h-1} + w_{h+1}) = 2^{M_k}$, $P_{e(h-1)}$ and $P_{e(h+1)}$ represents the value of $P_{e(l)}$ for $l = (h-1)$, and $(h+1)$ respectively.

Similarly, to have the expression for P_e^1 for $h = 2$, all we need to know is the value of l for different possible combinations of $\mathbf{x}$, that is already available in Table 5.7. So, for $h = 2$,

$$P_e^1 = 2^{-(m_k+1)} \sum_{l=1}^{N_k} w_l P_{e(l)}$$

leads to the expression in (5.15) for $\sum_{l=1}^{N_k} w_l = 2^{M_k}$, where $P_{e(l)}$, and w_l denote the probability of error and the number of input combinations corresponding to the DV with $l = 1, 2, ..., N_k$ respectively. ■

Chapter C
Appendix C: Proof of Errorless nature of CAD

According to (5.10), the following expressions can be explicitly inferred for $\mathbf{r}_{N_a} \in \{\pm 2, 0\}^{N_a}$ corresponding to class $\mathbf{C}_a^k$.

$$\mathbf{r}_{N_a}(N_a) = \mathbf{x}_a(1) - \mathbf{x}_a(2) \tag{C.1}$$

$$\mathbf{r}_{N_a}(N_a) = \mathbf{x}_a(1) + \mathbf{x}_a(2) \tag{C.2}$$

where $1 \leq a \leq k$ and $\mathbf{x}_a(b)$ for $b = 1, 2$ represents the input symbols of the two users of $\mathbf{C}_a^k$ and $\mathbf{r}_{N_a}(N_a)$ refers to the last non-zero chip of the sum vector for $\mathbf{C}_a^k$ for N_a denoting the length of the non-zero sequence of the signatures in $\mathbf{C}_a^k$. For remaining $(N_a - 1)$ number of chips of $\mathbf{r}_{N_a}$ with non-zero signal levels, we find the constellation pattern predictable structured, such that

$$\begin{aligned} \mathbf{r}_{N_a}(N_a) = 0 \quad &\Rightarrow \quad \mathbf{r}_{N_a}(c) = 2 \text{ or } -2 \\ \mathbf{r}_{N_a}(N_a) = 2 \text{ or } -2 \quad &\Rightarrow \quad \mathbf{r}_{N_a}(c) = 0 \end{aligned} \tag{C.3}$$

where $c = 1, 2, ..., (N_a - 1)$.

With these preliminaries, our intention is to trace the variation in constellation values among all the N_k non-zero chips of the sum vector $\mathbf{r}_k$. Note that we focus to correctly decode the last class only i.e., $\mathbf{C}_k^k$. We deduce the following relation in (C.4) to define the constellation value at chip-$(N_k - s)$ of $\mathbf{r}_k$, which is a function of the sum vectors of the participating classes i.e.;

$$\mathbf{r}_k(N_k - s) = \sum_{t=0}^{s} \mathbf{r}_{(N_k - t)}(N_k - s) \tag{C.4}$$

Onwards, the proof to show $\hat{\mathbf{x}}_k = \mathbf{x}_k$ is based on induction on s. So, we present Table C.1 as an expanded overview of the expression in (C.4). Our intention is to study the pattern of constellation of $\mathbf{x}_k$ subjected to all possible combinations of the sum

vectors of constituent classes, for specific values of s. Following an uniform approach of analysis, we start with $s = 0$ and proceed till $s = k$. However, the information in Table C.1 covers for the first four values of s ($0 \leq s \leq 3$) in a top to bottom chronology. This is because, our objective is just to study the pattern of the constellation for different values of s. To accomplish this consideration of the first four values of s are sufficient, since similar behavior in the pattern can be expected for higher values of s too.

In Table C.1, the rows corresponding to a particular value of s carry all possible combinations of the sum vector from $(s+1)$ classes contributing to the level of $\mathbf{r}_k(N_k - s)$. The contents of the last (rightmost) column indicates the status of decoding: unambiguous or ambiguous, denoted by "Y" or "N" respectively. The symbol (-) indicates the specific classes, not contributing to the final sum $\mathbf{r}_k(N_k - s)$.

With the increase in value of s the number of classes or class wise sum vectors leading to $\mathbf{r}_k$ increases. Following a possible approach, the decoding analysis for "Y" or "N" can be switched to a next value of s, if and only if there appears an ambiguity ("N" in Table C.1) with respect to its present value. Below, we explain the proposed analysis to be incorporated for each value of s.

For $s = 0$, if $\mathbf{r}_k(N_k) = \mathbf{r}_{N_k}(N_k) = 2$ and -2 then $(\mathbf{x}_k(1), \mathbf{x}_{N_k}(2)) = (1, -1)$ and $(-1, 1)$. Thus, decoding is errorless (unambiguous), as shown by "Y" in first row of for $s = 0$. In contrast, For $s = 0$, if $\mathbf{r}_k(N_k) = 0$ then there exists an ambiguity for $(\mathbf{x}_k(1), \mathbf{x}_k(2)) = (1, 1)$ or $(-1, -1)$, shown by "N" in second row for $s = 0$. To resolve this, s is to be incremented by 1, such that for $s = 1$ and $\mathbf{r}_k(N_k) = 0$

$$\mathbf{r}_k(N_k - 1) = \mathbf{r}_{N_k}(N_k - 1) + \mathbf{r}_{N_k - 1}(N_k - 1) \tag{C.5}$$

According to (C.5), the value of $\mathbf{r}_{N_k}(N_k - 1) = 2$ *or* -2, since $\mathbf{r}_k(N_k) = 0$. Under such conditions, if $(\mathbf{r}_{N_k}(N_k - 1), \mathbf{r}_{N_k - 1}(N_k - 1))$ becomes (2, 0), (2, 2), (-2, 0), (-2, -2) further leading to $\mathbf{r}(N_k - 1)$= 2, 4, -2, -4, then $(\hat{\mathbf{x}}_{N_k}(1), \hat{\mathbf{x}}_{N_k}(2))$ = (1,1), (1,1), (-1,-1) and (-1,-1) respectively, shown by "Y", where as for $(\mathbf{r}_{N_k}(N_k - 1), \mathbf{r}_{N_k - 1}(N_k - 1))$ = (2,-2) and (-2,2), $\mathbf{r}(N_k - 1) = 0$ asserts an ambiguity, reported by "N" (see Table C.1, $s = 1$). To overcome this, s is again incremented by 1, such that for $s = 2$ and $\mathbf{r}_k(N_k) = \mathbf{r}_k(N_k - 1) = 0$

$$\mathbf{r}_k(N_k - 2) = \mathbf{r}_{N_k}(N_k - 2) + \mathbf{r}_{N_k - 1}(N_k - 2) + \mathbf{r}_{N_k - 2}(N_k - 2) \tag{C.6}$$

Following (C.5), since $\mathbf{r}_{N_{k-1}}(N_k - 1) = 2$ or -2 implies $\mathbf{r}_{N_{k-1}}(N_k - 2) = 0$ (also see

Table C.1, $s = 2$), the expression in (C.6) becomes

$$\mathbf{r}_k(N_k - 2) = \mathbf{r}_{N_k}(N_k - 2) + \mathbf{r}_{N_k-2}(N_k - 2) \tag{C.7}$$

The resulting expression in (C.7) has complete similarity to that of (C.5). Hence it is trivial to expect the analysis for decoding from (C.7) to be identical to that of (C.5).

From Table C.1, we note that for higher values of $s(> 1)$, the analysis aiming for the unambiguous decoding although involves more number of classes (> 2), the final sum element of $\mathbf{r}_k$ carries a value equal to the addition of sum vectors of two class only, one of which is always the last class $\mathbf{C}_k^k$, by default. Therefore, for a given transmitted vector $\mathbf{r}_k$, this is feasible to decipher the input vector of the last class ($\hat{\mathbf{x}}_k$) following the construction and analysis of equations similar to (C.5) and (C.7). Furthermore, this process continues till $s = (N_k - 1)$, unless a non-zero level of constellation is found for $\mathbf{r}_k(N_k - s)$ i.e., $\hat{\mathbf{x}}_k$ is decoded. In particular, when all last $(N_k - 1)$ chips of $\mathbf{r}_k$ fails to offer the unambiguous recovery due to the absence of non-zero elements i.e., for $s = N_k - 2$ and $\mathbf{r}_k(N_k) = \mathbf{r}_k(N_k - 1) = \cdots = \mathbf{r}_k(2) = 0$, there always exists a non-zero element at $\mathbf{r}_k(1)$ that leads to the correct decoding. Thus, feasibility of the errorless decoding for the last class of $\mathbf{C}^k$ (i.e.; $\mathbf{C}_k^k$) is verified. ■

Table C.1: Study of constellation pattern of the total sum vector $\mathbf{r}_k(N_k - s)$ in (C.4), as a function of the sum vector of the individual constituent classes, subjected to variation in value of s $(0 \leq s \leq 3)$

s	$\mathbf{r}_{N_k}(N_k - s)$	$\mathbf{r}_{N_{k-1}}(N_k - s)$	$\mathbf{r}_{N_{k-2}}(N_k - s)$	$\mathbf{r}_{N_{k-3}}(N_k - s)$	$\mathbf{r}_k(N_k - s)$	Status of Decoding
0	2 / -2	-	-	-	2 / -2	Y
	0	-	-	-	0	N
1	2	0 / 2	-	-	2 / 4	Y
	-2	0 / -2	-	-	-2 / -4	Y
	2	-2	-	-	0	N
	-2	2	-	-	0	N
2	2	0	0 / 2	-	2 / 4	Y
	-2	0	0 / -2	-	-2 / -4	Y
	2	0	-2	-	0	N
	-2	0	2	-	0	N
3	2	0	0	0 / 2	2 / 4	Y
	-2	0	0	0 / -2	-2 / -4	Y
	2	0	0	-2	0	N
	-2	0	0	2	0	N

References

[1] Hosein Nikopour and Hadi Baligh. Sparse code multiple access. In *Personal Indoor and Mobile Radio Communications (PIMRC), 2013 IEEE 24th International Symposium on*, pages 332–336. IEEE, 2013.

[2] Hosein Nikopour, Eric Yi, Alireza Bayesteh, Kelvin Au, Mark Hawryluck, Hadi Baligh, and Jianglei Ma. SCMA for downlink multiple access of 5g wireless networks. In *Global Communications Conference (GLOBECOM), 2014 IEEE*, pages 3940–3945. IEEE, 2014.

[3] Lei Wen, Razieh Razavi, Muhammad Ali Imran, and Pei Xiao. Design of Joint Sparse graph for OFDM system. *Wireless Communications, IEEE Transactions on*, 14(4):1823–1836, 2015.

[4] NGMN Alliance. 5g white paper. *Next Generation Mobile Networks, White paper*, 2015.

[5] Staffan Soderberg and Harold S Shapiro. A combinatory detection problem. *American Mathematical Monthly*, pages 1066–1070, 1963.

[6] Bernt Lindström. On a combinatory detection problem. *I. Magyar Tud. Akad. Mat. Kutató Int. Közl*, 9:195–207, 1964.

[7] David G Cantor and WH Mills. Determination of a subset from certain combinatorial properties. *Can. J. Math*, 18:42–48, 1966.

[8] Shih-Chun Chang and E Weldon. Coding for t-user multiple-access channels. *Information Theory, IEEE Transactions on*, 25(6):684–691, 1979.

[9] T Ferguson. Generalized T-user codes for multiple-access channels (corresp.). *Information Theory, IEEE Transactions on*, 28(5):775–778, 1982.

[10] Shih-Chun Chang. Further results on coding for T-user multiple-access channels. *IEEE transactions on information theory*, 30(2):411–415, 1984.

[11] GK Khachatrian and SS Martirossian. Codes for T-user noiseless adder channel. *PROB. CONTROL INF. THEORY.*, 16(3):187–192, 1987.

[12] SS Martirosyan and GG Khachatryan. Construction of signature codes and the coin weighing problem. *Problemy Peredachi Informatsii*, 25(4):96–97, 1989.

[13] Wai Ho Mow. Recursive constructions of detecting matrices for multiuser coding: A unifying approach. *Information Theory, IEEE Transactions on*, 55(1):93–98, 2009.

[14] Gurgen H Khachatrian and Samvel S Martirossian. A new approach to the design of codes for synchronous-CDMA systems. *Information Theory, IEEE Transactions on*, 41(5):1503–1506, 1995.

[15] Ying-Wah Wu and Shih-Chun Chang. Coding scheme for synchronous-CDMA systems. *Information Theory, IEEE Transactions on*, 43(3):1064–1067, 1997.

[16] Wai Ho Mow. Multiuser coding based on detecting matrices for synchronous-CDMA systems. In *Crytography and Coding*, pages 251–257. Springer, 1997.

[17] Sennur Ulukus and Roy D Yates. Iterative construction of optimum signature sequence sets in synchronous CDMA systems. *Information Theory, IEEE Transactions on*, 47(5):1989–1998, 2001.

[18] Christopher Rose, Sennur Ulukus, and Roy D Yates. Wireless systems and interference avoidance. *Wireless Communications, IEEE Transactions on*, 1(3):415–428, 2002.

[19] Pramod Viswanath and Venkat Anantharam. Optimal sequences and sum capacity of synchronous CDMA systems. *IEEE Transactions on Information Theory*, 45(6):1984–1991, 1999.

[20] Pramod Viswanath and Venkat Anantharam. Optimal sequences for CDMA under colored noise: A schur-saddle function property. *Information Theory, IEEE Transactions on*, 48(6):1295–1318, 2002.

[21] Joel A Tropp, Inderjit S Dhillon, and Robert W Heath Jr. Finite-step algorithms for constructing optimal CDMA signature sequences. *IEEE transactions on information theory*, 50(11):2916–2921, 2004.

[22] Otilia Popescu and Christopher Rose. Sum capacity and TSC bounds in collaborative multibase wireless systems. *Information Theory, IEEE Transactions on*, 50(10):2433–2440, 2004.

[23] Gowri S Rajappan and Michael L Honig. Signature sequence adaptation for DS-CDMA with multipath. *Selected Areas in Communications, IEEE Journal on*, 20(2):384–395, 2002.

[24] Cunsheng Ding and Tao Feng. A generic construction of complex codebooks meeting the Welch bound. *Information Theory, IEEE Transactions on*, 53(11):4245–4250, 2007.

[25] Pengfei Xia, Shengli Zhou, and Georgios B Giannakis. Achieving the Welch bound with difference sets. *Information Theory, IEEE Transactions on*, 51(5):1900–1907, 2005.

[26] George N Karystinos and Dimitrios A Pados. New bounds on the total squared correlation and optimum design of DS-CDMA binary signature sets. *Communications, IEEE Transactions on*, 51(1):48–51, 2003.

[27] Cunsheng Ding, Mordecai Golin, and Torleiv Kløve. Meeting the Welch and Karystinos-pados bounds on DS-CDMA binary signature sets. *Designs, Codes and Cryptography*, 30(1):73–84, 2003.

[28] Valery P Ipatov. On the Karystinos-Pados bounds and optimal binary DS-CDMA signature ensembles. *IEEE communications letters*, 8(2):81–83, 2004.

[29] George N Karystinos and Dimitris A Pados. The maximum squared correlation, sum capacity, and total asymptotic efficiency of minimum total-squared-correlation binary signature sets. *Information Theory, IEEE Transactions on*, 51(1):348–355, 2005.

[30] Harish Ganapathy, Dimitris A Pados, and George N Karystinos. New bounds and optimal binary signature sets—part I: periodic total squared correlation. *Communications, IEEE Transactions on*, 59(4):1123–1132, 2011.

[31] James L Massey and Thomas Mittelholzer. Welch's bound and sequence sets for code-division multiple-access systems. In *Sequences II*, pages 63–78. Springer, 1993.

[32] Ming Li. Fast code design for Overloaded Code-Division Multiplexing Systems. 2015.

[33] Frederik Vanhaverbeke and Marc Moeneclaey. Sum capacity of binary signatures that minimize the total squared correlation. In *IEEE International Symposium on Information Theory*, 2004.

[34] Frederik Vanhaverbeke and Marc Moeneclaey. Sum capacity of the OCDMA/OCDMA signature sequence set. *Communications Letters, IEEE*, 6(8):340–342, 2002.

[35] Frederik Vanhaverbeke and Marc Moeneclaey. Binary signature sets for increased user capacity on the downlink of CDMA systems. *Wireless Communications, IEEE Transactions on*, 5(7):1795–1804, 2006.

[36] Panayiotis D Papadimitriou and Costas N Georghiades. Code-search for optimal TSC binary sequences with low cross-correlation spectrum. In *Military Communications Conference, 2003. MILCOM'03. 2003 IEEE*, volume 2, pages 1071–1076. IEEE, 2003.

[37] Cunsheng Ding. Complex codebooks from combinatorial designs. *Information Theory, IEEE Transactions on*, 52(9):4229–4235, 2006.

[38] Aixian Zhang and Keqin Feng. Two classes of codebooks nearly meeting the Welch bound. *Information Theory, IEEE Transactions on*, 58(4):2507–2511, 2012.

[39] Seokbeom Hong, Hosung Park, Jong-Seon No, Tor Helleseth, and Young-Sik Kim. Near-optimal partial hadamard codebook construction using binary sequences obtained from quadratic residue mapping. *Information Theory, IEEE Transactions on*, 60(6):3698–3705, 2014.

[40] Honggang Hu and Jinsong Wu. New constructions of codebooks nearly meeting the welch bound with equality. *Information Theory, IEEE Transactions on*, 60(2):1348–1355, 2014.

[41] Sergio Verdu. *Multiuser detection*. Cambridge university press, 1998.

[42] Shimon Moshavi. Multi-user detection for DS-CDMA communications. *Communications Magazine, IEEE*, 34(10):124–136, 1996.

[43] Alexandra Duel-Hallen. Decorrelating decision-feedback multiuser detector for synchronous code-division multiple-access channel. *Communications, IEEE Transactions on*, 41(2):285–290, 1993.

[44] Alexandra Duel-Hallen, Jack Holtzman, and Zoran Zvonar. Multiuser detection for CDMA systems. *Personal Communications, IEEE*, 2(2):46–58, 1995.

[45] Wei Zha. *Multiuser Receiver Structures for CDMA*. PhD thesis, Citeseer, 2002.

[46] Ruxandra Lupas and Sergio VerdŰ. Linear multiuser detectors for synchronous code-division multiple-access channels. *Information Theory, IEEE Transactions on*, 35(1):123–136, 1989.

[47] Michail K Tsatsanis. Inverse filtering criteria for CDMA systems. *Signal Processing, IEEE Transactions on*, 45(1):102–112, 1997.

[48] Upamanyu Madhow and Michael L Honig. MMSE interference suppression for direct-sequence spread-spectrum CDMA. *Communications, IEEE Transactions on*, 42(12):3178–3188, 1994.

[49] Vincent H Poor and Sergio Verdü. Probability of error in MMSE multiuser detection. *Information Theory, IEEE Transactions on*, 43(3):858–871, 1997.

[50] Mahesh K Varanasi. Group detection for synchronous Gaussian code-division multiple-access channels. *Information Theory, IEEE Transactions on*, 41(4):1083–1096, 1995.

[51] Stefano Buzzi, Marco Lops, and Giuseppe Ricci. A new group detection strategy for DS/CDMA systems. In *Information Theory, 2000. Proceedings. IEEE International Symposium on*, page 357. IEEE, 2000.

[52] Ateet Kapur and Mahesh K Varanasi. Multiuser detection for overloaded CDMA systems. *Information Theory, IEEE Transactions on*, 49(7):1728–1742, 2003.

[53] Mahesh K Varanasi. Decision feedback multiuser detection: A systematic approach. *Information Theory, IEEE Transactions on*, 45(1):219–240, 1999.

[54] Hikmet Sari, Frederik Vanhaverbeke, and Marc Moeneclaey. Multiple access using two sets of orthogonal signal waveforms. *Communications Letters, IEEE*, 4(1):4–6, 2000.

[55] Frederik Vanhaverbeke, Marc Moeneclaey, and Hikmet Sari. DS/CDMA with two sets of orthogonal spreading sequences and iterative detection. *Communications Letters, IEEE*, 4(9):289–291, 2000.

[56] Simone Morosi, Romano Fantacci, Enrico Del Re, and Angela Chiassai. Design of Turbo-MUD receivers for overloaded CDMA systems by density evolution technique. *Wireless Communications, IEEE Transactions on*, 6(10):3552–3557, 2007.

[57] Preetam Kumar and Saswat Chakrabarti. An analytical model of iterative interference cancellation receiver for orthogonal/orthogonal overloaded DS-CDMA system. *International Journal of Wireless Information Networks*, 17(1-2):64–72, 2010.

[58] S Sasipriya and CS Ravichandran. Performance analysis of overloaded CDMA system under imperfect synchronization using Parallel/Successive Interference Cancellation. *Telecommunication Systems*, 56(4):509–518, 2014.

[59] Andrew J Viterbi. Very low rate convolution codes for maximum theoretical performance of spread-spectrum multiple-access channels. *Selected Areas in Communications, IEEE Journal on*, 8(4):641–649, 1990.

[60] Lars K Rasmussen, Teng J Lim, and A-L Johansson. A matrix-algebraic approach to successive interference cancellation in CDMA. *Communications, IEEE Transactions on*, 48(1):145–151, 2000.

[61] Dariush Divsalar, Marvin K Simon, and Dan Raphaeli. Improved parallel interference cancellation for CDMA. *Communications, IEEE Transactions on*, 46(2):258–268, 1998.

[62] Guoqiang Xue, Jianfeng Weng, Tho Le-Ngoc, and Sofiène Tahar. Adaptive multistage parallel interference cancellation for CDMA. *Selected Areas in Communications, IEEE Journal on*, 17(10):1815–1827, 1999.

[63] Jie Luo, Krishna R Pattipati, Peter K Willett, and Fumihiro Hasegawa. Near-optimal multiuser detection in synchronous CDMA using probabilistic data association. *Communications Letters, IEEE*, 5(9):361–363, 2001.

[64] Frederik Vanhaverbeke and Marc Moeneclaey. An improved OCDMA/OCDMA scheme based on displaced orthogonal user sets. *Communications Letters, IEEE*, 8(5):265–267, 2004.

[65] Dilip V Sarwate. Meeting the Welch bound with equality. In *Sequences and their Applications*, pages 79–102. Springer, 1999.

[66] Ha H Nguyen and Ed Shwedyk. A new construction of signature waveforms for synchronous CDMA systems. *Broadcasting, IEEE Transactions on*, 51(4):520–529, 2005.

[67] Frederik Vanhaverbeke and Marc Moeneclaey. Optimal signature sets for oversaturated quasi-scalable direct-sequence spread-spectrum systems. *Information Theory, IEEE Transactions on*, 51(3):1136–1139, 2005.

[68] Falah H Ali and Indu Shakya. Collaborative spreading for the downlink of overloaded CDMA. *Wireless Communications and Mobile Computing*, 10(3):383–393, 2010.

[69] F Ali and B Honary. Collaborative coding and decoding techniques for multiple access channel. In *Communications, IEE Proceedings-*, volume 141, pages 56–62. IET, 1994.

[70] Yaseen H Tahir, Chee Kyun Ng, Nor K Noordin, Borhanuddin Mohd Ali, and Sabira Khatun. Superposition coding with unequal error protection for the uplink of overloaded DS-CDMA system. *Wireless Personal Communications*, 65(3):567–582, 2012.

[71] Pedram Pad, Farokh Marvasti, Kasra Alishahi, and Saieed Akbari. A class of errorless codes for overloaded synchronous wireless and optical CDMA systems. *Information Theory, IEEE Transactions on*, 55(6):2705–2715, 2009.

[72] Pedram Pad, Ali Mousavi, Ali Goli, and Farokh Marvasti. Simplified MAP-MUD for active user CDMA. *Communications Letters, IEEE*, 15(6):599–601, 2011.

[73] Kasra Alishahi, Sh Dashmiz, Pedram Pad, and Farokh Marvasti. Design of signature sequences for overloaded CDMA and bounds on the sum capacity with arbitrary symbol alphabets. *Information Theory, IEEE Transactions on*, 58(3):1441–1469, 2012.

[74] Mohsen Heidari Khoozani, Farokh Marvasti, Masoumeh Azghani, and Mona Ghassemian. Finding sub-optimum signature matrices for overloaded code division multiple access systems. *IET Communications*, 7(4):295–306, 2013.

[75] Kasra Alishahi, Farokh Marvasti, Vahid Aref, and Pedram Pad. Bounds on the sum capacity of synchronous binary CDMA channels. *Information Theory, IEEE Transactions on*, 55(8):3577–3593, 2009.

[76] Shayan Dashmiz, Mohammad Reza Takapoui, Sajjad Moazeni, Mehrdad Moharrami, Melika Abolhasani, and Farokh Marvasti. Generalisation of code division multiple access systems and derivation of new bounds for the sum capacity. *IET Communications*, 8(2):153–162, 2014.

[77] Rachel E Learned, Alan S Willsky, and Don M Boroson. Low complexity optimal joint detection for oversaturated multiple access communications. *Signal Processing, IEEE Transactions on*, 45(1):113–123, 1997.

[78] Li Ping. Interleave-division multiple access and chip-by-chip iterative multi-user detection. *Communications Magazine, IEEE*, 43(6):S19–S23, 2005.

[79] Anderson Fergus John Ross. Multiple-user communications with nonorthogonal signalling. 1994.

[80] Reza Hoshyar, Ferry P Wathan, and Rahim Tafazolli. Novel low-density signature for synchronous CDMA systems over AWGN channel. *Signal Processing, IEEE Transactions on*, 56(4):1616–1626, 2008.

[81] Omid Mashayekhi and Farokh Marvasti. Uniquely decodable codes with fast decoder for overloaded synchronous CDMA systems. *Communications, IEEE Transactions on*, 60(11):3145–3149, 2012.

[82] Paeiz Azmi and Tahereh Shojaee Zand. An iterative multiuser detector for overloaded LDPC coded CDMA systems. *Wireless Personal Communications*, 66(1):41–56, 2012.

[83] Andrea Montanari and David Tse. Analysis of belief propagation for non-linear problems: The example of CDMA (or: How to prove Tanaka's formula). In *Information Theory Workshop, 2006. ITW'06 Punta del Este. IEEE*, pages 160–164. IEEE, 2006.

[84] Reza Hoshyar, Razieh Razavi, and Mohammed Al-Imari. LDS-OFDM an efficient multiple access technique. In *Vehicular Technology Conference (VTC 2010-Spring), 2010 IEEE 71st*, pages 1–5. IEEE, 2010.

[85] Razieh Razavi, Mohammed Al-Imari, Muhammad Ali Imran, Reza Hoshyar, and Dageng Chen. On receiver design for uplink low density signature OFDM (LDS-OFDM). *Communications, IEEE Transactions on*, 60(11):3499–3508, 2012.

[86] Dongning Guo, Lars K Rasmussen, Sumei Sun, and Teng J Lim. A matrix-algebraic approach to linear parallel interference cancellation in CDMA. *Communications, IEEE Transactions on*, 48(1):152–161, 2000.

[87] Kelvin Au, Liqing Zhang, Hosein Nikopour, Eric Yi, Alireza Bayesteh, Usa Vilaipornsawai, Jianglei Ma, and Peiying Zhu. Uplink contention based SCMA for 5G radio access. In *Globecom Workshops (GC Wkshps), 2014*, pages 900–905. IEEE, 2014.

[88] Mahmoud Taherzadeh, Hosein Nikopour, Alireza Bayesteh, and Hadi Baligh. SCMA codebook design. In *Vehicular Technology Conference (VTC Fall), 2014 IEEE 80th*, pages 1–5. IEEE, 2014.

[89] Baicen Xiao, Kexin Xiao, Shutian Zhang, Zhiyong Chen, Bin Xia, and Hui Liu. Iterative detection and decoding for SCMA systems with LDPC codes. In *Wireless Communications & Signal Processing (WCSP), 2015 International Conference on*, pages 1–5. IEEE, 2015.

[90] Dongning Guo and Chih-Chun Wang. Multiuser detection of sparsely spread CDMA. *Selected Areas in Communications, IEEE Journal on*, 26(3):421–431, 2008.

[91] Yiqun Wu, Shunqing Zhang, and Yan Chen. Iterative multiuser receiver in sparse code multiple access systems. In *Communications (ICC), 2015 IEEE International Conference on*, pages 2918–2923. IEEE, 2015.

[92] GH Khachatrian and SS Martirossian. Code construction for the T-user noiseless adder channel. *Information Theory, IEEE Transactions on*, 44(5):1953–1957, 1998.

[93] Hikmet Sari, Frederik Vanhaverbeke, and Marc Moeneclaey. Extending the capacity of multiple access channels. *Communications Magazine, IEEE*, 38(1):74–82, 2000.

[94] Frederik Vanhaverbeke and Marc Moeneclaey. Sequences for oversaturated cdma channels. In *Spread Spectrum Techniques and Applications, 2008 IEEE 10th International Symposium on*, pages 735–739. IEEE, 2008.

[95] Farokh Marvasti, Pedram Pad, and Mahmood Ferdosy Naeiny. Iterative synchronous and asynchronous multi-user detection with optimum soft limiter, May 17 2008. US Patent App. 12/122,668.

[96] Robert G Gallager. Low-density parity-check codes. *Information Theory, IRE Transactions on*, 8(1):21–28, 1962.

[97] Michel Kulhandjian and Dimitrios A Pados. Uniquely decodable code-division via augmented sylvester-hadamard matrices. In *Wireless Communications and Networking Conference (WCNC), 2012 IEEE*, pages 359–363. IEEE, 2012.

[98] Frederik Vanhaverbeke, Marc Moeneclaey, and Hikmet Sari. Increasing CDMA capacity using multiple orthogonal spreading sequence sets and successive interference cancellation. In *Communications, 2002. ICC 2002. IEEE International Conference on*, volume 3, pages 1516–1520. IEEE, 2002.

[99] Kasra Alishahi, Sh Dashmiz, Pedram Pad, Farrokh Marvasti, MH Shafinia, and M Mansouri. The Enigma of CDMA revisited. *arXiv preprint arXiv:1005.0677*, 2010.

[100] Omid Mashayekhi and Farokh Marvasti. Uniquely decodable codes and decoder for overloaded synchronous CDMA systems, November 12 2013. US Patent 8,582,604.

Dissemination

Journals:

- 1 **A. Singh**, A Amini, P Singh, F Marvasti, "Set of Codes with Low Complex Decoder for Overloaded Synchronous CDMA," *IET Communications*, 10 (10), 1236-1245, 2016. **(Published)**
- 2 **A. Singh**, P Singh, A Amini, F Marvasti, "Twin Tree Hierarchy: A Regularized Approach to Construction for Signature Matrices for Overloaded CDMA," *Wireless Communication and Mobile Computing* (Willey), 16 (17), 3070-3088, 2016. **(Published)**
- 3 **A. Singh**, A Amini, P Singh, F Marvasti, "Generalized Construction of Codes with Fast Decoder for Overloaded Synchronous CDMA," *Physical Communications* (Elsevier). **(Under review)**
- 4 **A. Singh**, P Singh, A Amini, F Marvasti, "Unified approach to the Construction of Signature Matrices with Orthogonal Subsets for Overloaded CDMA," *Telecommunication Systems* (Springer). **(Under review)**

Conference:

- 1 **A. Singh**, P Singh, "On the Complementary Nature of the Signature Matrices with Orthogonal Subsets for Overloaded CDMA," *IEEE TENCON 2016*, Singapore.
- 2 **A. Singh**, P Singh, A Amini, F Marvasti, "Comparison Aided Decoding (CAD) for a New Set of Codes for Overloaded Synchronous CDMA," 22^{th} *IEEE NCC*, IIT Guwahati, March. 2016.
- 3 **A. Singh**, P Singh, "Uniquely Decodable Codes for Overloaded CDMA with Two sets of Orthogonal Signatures," 11^{th} *IEEE INDICON* , Pune, Nov. 2014.
- 4 **A. Singh**, P Singh, "Overloading the capacity of Multiple Access Channel," *In Proceedings of ICACACT*, Mumbai, Aug. 2013.
- 5 **A. Singh**, P Singh, "Effect of Erroneous Power Control on the performance of Overloaded Cellular UCDS-CDMA," *In Proceedings of IEEE International Conference on Electronics, Computing and Communication Technologies (CONECCT)*, Bangalore, Jan. 2013.
- 6 **A. Singh**, P Singh, "Synchronous Overloaded system for the uplink of cellular CDMA with unequal chip delay spreading," *In Proceedings of 5th IEEE International Conference on computers and devices for communication (CODEC)* , Kolkata, Dec. 2012.

Author's Biography: Amiya Singh is from a small village (Tarakote) in Jajpur district, Odisha. In 2002, he completed his matriculation from R.S. High School, Tarakote. He moved to Ravenshaw Junior College, Cuttack and passed the Higher Secondary Examination in 2004. In 2005, he started his engineering career in Electronics and Telecommunication Engineering at Institute of Technical Education and Research (ITER), Bhubaneswar, under Biju Pattnaik University of Technology (BPUT). After completion of engineering, he joined the Centurion Institute of Technology (CIT) as a lecturer in August 2009 and had taught the subjects like, Basic Electronics, Analog Electronics, Digital Electronics, Communication Systems, Physics of Semiconductor Devises, etc. During this phase of teaching, he developed his interest towards research. In January 2012, after qualifying the Graduate Aptitude Test in Engineering (GATE) Examination, he enrolled for the Ph. D programme in the Department of Electronics and Communication Engineering. During December 2014 to January 2015, he was with the Advanced Communication Research Institute (ACRI) of Sharif University of Technology (SUT) for pursuing collaborative research. His area of research interests are Overloaded CDMA, Multiuser detection, Multi Carrier Communications, and Sparse signal processing for communication. He can be contacted at amiyasingh87@gmail.com.